Project Number: 248267
Project acronym: BuNGee
Project title: Beyond Next Generation Mobile Networks

BuNGee Deliverable: D2.3

Final Report on Advanced MIMO Techniques

Submission date: 4th July 2012

Start date of project: January 1, 2010	**Duration**: 30 months
Lead Participant: Alister Burr, University of York **Contributors:** See page 3 **Release number:** 1.0 **Keywords:** MIMO, MBA-MIMO, Network-enabled MIMO, MIMO-TSB, CSI transmission, Gram matrix, physical layer network coding (PLNC), precoding, dual polarisation	
Project co-funded by the European Commission within the Seventh Framework Programme (2007-2013)	
Dissemination Level: Public **Restricted to other programme participants (including the Commission Services),** **Restricted to a group specified by the consortium (including the Commission Services)Confidential, only for members of the consortium (including the Commission Services)**	

The research leading to these results has received funding from the European Community's Seventh Framework Programme (FP7/2007-2013) under grant agreement n 248267

Executive Summary

This report describes work carried out within Task 2.3 “Collaborative, Networked and Multibeam MIMO” of the BuNGee (“Beyond Next Generation Mobile Broadband”) project. The focus of the work is therefore on the use of advanced MIMO techniques to increase the capacity of the BuNGee wireless access network, including investigate *multibeam assisted MIMO* (MBA-MIMO) for the backhaul segment of the network, where the BuNGee multibeam antenna is used, and *network-enabled MIMO* on the access segment.

It is shown that the MBA-MIMO approach, employing joint beam processing at the HBS, can increase capacity by a factor of around 6 to 8 compared with conventional single beam processing, in which signals received by other beams are treated as interference. This is further increased by a further factor of nearly two by the use of dual polarisation on the backhaul links. This contributes to nearly doubling the overall capacity available from the BuNGee network, as demonstrated by the BuNGee network-level simulator.

In the access segment the value of network-enabled MIMO is investigated, and shown to increase capacity by at least a factor of 4 compared to the baseline frequency-planning scheme used in BuNGee, because it enables the whole access segment bandwidth to be used by all ABSs. However this results potentially in a large increase in the backhaul load.

In view of this the application of physical layer network coding is also investigated, and found to be a promising approach to reduce backhaul load while providing most of the benefit of network-enabled MIMO. It also allows the resources of backhaul and access network to be more readily shared, helping to overcome the restrictions resulting from the duplexing constraint upon the ABSs.

On both backhaul and access segments it is assumed that precoding techniques will be used, as prescribed by wireless access standards such as WiMAX and LTE. Aspects of precoder selection are discussed, and an iterative interference cancellation approach is proposed to the implementation of ML detection. It is shown that this gives rise to significant gain compared to the more usual linear detectors, as well as making the task of precoder selection less critical. A more robust and efficient method than conventional techniques is developed for the transmission of channel state information (CSI) between receiver and transmitter, as required for the implementation of precoding. This enables significant reduction in the number of feedback bits required.

Task 2.3 also supports the system-level simulation carried out in Task 4.1, as part of WP4, “Proof of Concept”. The concept of the *truncated Shannon bound* (TSB) is introduced in this context to provide a simple means of modelling link throughput as a function of signal to interference plus noise ratio. This is further extended to MIMO links, and also to the MBA-MIMO concept, and this approach has been widely used in T4.1.

This document was issued in a much earlier form in M8 of the project, as Interim Report IR2.3. The present deliverable report is an updated and greatly expanded version of that report, reflecting the work done in the remainder of the project.

Contributors

Participant #	Participant short name	Name of the Contributor	E-mail
5	UOY	Alister Burr	alister.burr@york.ac.uk
3	CTTC	Miquel Payaró Llisterri	miquel.payaro@cttc.es
5	UOY	Agisilaos Papadogiannis	agisilaos.papadogiannis@chalmers.se
3	CTTC	Antonio Pascual Iserte	toni.pascual@cttc.es
3	CTTC	Daniel Sacristán Murga	daniel.sacristan@cttc.es
5	UOY	Peng Li	peng.li@york.ac.uk
5	UOY	Yi Wang	yi.wang@york.ac.uk
5	UOY	Chunshan Liu	chunshan.liu@york.ac.uk
5	UOY	Dong Fang	dong.fang@york.ac.uk

Table of Contents

List of Tables

List of Figures

List of Acronyms

Abbreviation / acronym	Description
3GPP	3rd Generation Partnership Project
8PSK	Eight Phase-Shift Keying
ABS	Acess Base Station
AC	Access Network
AF	Amplify-and-Forward
AF-LMMSE	Amplify-and-Forward Linear Minimum Mean Square Error
APP	A Posteriori Probability
AWGN	Additive White Gaussian Noise
BC	Broadcast Channel
BD	Block Diagonalization
BER	Bit Error Rate
BH	Backhaul Network
BICM	Bit-Interleaved Coded Modulation
BSA	Binary Switching Algorithm
B-TDL	BuNGee Tappled Delay Line
CCI	Co-channel Interference
CDF	Cumulative Distribution Function
CF	Compress-and-Forward
CSI	Channel State Information
C-SI	Complementary Side Information
DAS	Distributed Antenna System
DF	Decode-and-Forward
DID	Distributed Iterative Decoding
DIDRMP	Distributed Iterative Detection and Decoding with Reduced Message Passing
DPC	Dirty Paper Coding
DPCM	Differential Pulse Code Modulation
DS-CDMA	Direct Sequence - Code Division Multiple Access
EXIT	Extrinsic Information Transfer
FDMA	Frequency Division Multiple Access
HBS	Hub Base Station
HDF	Hierarchical Decode and Forward
HSS	Hub Subscriber Stations
HWN	Hierarchical Wireless Network
IAI	Inter Antenna Interference
ICI	Inter Cell Interference
i.i.d	Independent Identically Distribution
INR	Interference to Noise Ratio
JCC	Joint Coding and Decoding
LLR	Log Likelihood Ratio
LOS	Line-Of-Sight
LTE	Long Term Evolution
MAC	Multiple Access Channel
MAP	Maximum a Posteriori

MBA	Multi-Beam Assisted
MIMO	Multiple Input Multiple Output
ML	Maximum Likelihood
MMSE	Minimum Mean Square Error
MRC	Maximum Ratio Combining
MS	Mobile Station
MSE	Mean Square Error
NNUB	Nearest Neighbout Union Bound
OFDM	Orthogonal Frequency Division Multiplexing
OSIC	Ordered Successive Interference Cancellation
PDP	Power Delay Profile
PLNC	Physical Layer Network Coding
PSK	Phase-Shift Keying
QAM	Quadrature Amplitude Modulation
QPSK	Quadrature Phase-Shift Keying
RF	Radio Frequency
SIC	Successive Interference Cancellation
SINR	Signal to Interference plus Noise Ratio
SIR	Signal to Interference Ratio
SISO	Single-Input Single Output
SfISfO	Soft input, soft output
SNR	Signal to Noise Ratio
STBC	Space Time Block Codes
TDL	Tapped Delay Line
TDMA	Time Division Multiple Access
TSB	Truncated Shannon Bound
UE	User Equipment
UEP	Unequal Error Protection
VS	Virtual Station
VSER	Vector Symbol Error Rate
WiMAX	Worldwide Interoperability for Microwave Access
ZF	Zero Forcing

1. Introduction

This report describes work carried out within Task 2.3 “Collaborative, Networked and Multibeam MIMO” of the BuNGee (“Beyond Next Generation Mobile Broadband”) project. The focus of the work is therefore on the use of advanced MIMO techniques to increase the capacity of the BuNGee wireless access network. In this report we focus on one of the network architectures BuNGee has investigated: *in-band wireless backhauling* or *self-backhauling*. Deliverable report [BunD24] has covered other architectures, especially 60 GHz unlicensed backhauling.

In this case the network can be partitioned into two segments: *access* and *backhaul*. In the access segment approaches based on *network-enabled MIMO* are considered: these are discussed in section 8. In the backhaul segment, for in-band backhauling at UHF frequencies, the BuNGee multibeam antenna is used (as described in deliverable report [BunD22]), and hence for the backhaul segment we investigate *multibeam assisted MIMO* (MBA-MIMO), as described in section 5.

On both backhaul and access segments it is assumed that precoding techniques will be used, as prescribed by wireless access standards such as WiMAX [IEE05, IEE06] and LTE [3GP07]. Section 7 discusses some aspects of precoder selection, proposing an iterative interference cancellation approach to the implementation of ML detection, and showing that this gives rise to significant gain compared to the more usual linear detectors, as well as making the task of precoder selection less critical. Section 6 discusses the transmission of channel state information (CSI), as required for the implementation of precoding, between receiver and transmitter, describing a more robust and efficient method than conventional techniques.

A second goal of Task 2.3 has been to support the system-level simulation carried out in Task 4.1, as part of WP4, “Proof of Concept”. System-level simulation requires a low complexity but accurate (in a statistical sense) means of determining the throughput of individual links, given their signal to interference plus noise ratio (SINR). For this purpose we draw upon the concept of the *truncated Shannon bound* (TSB) described in [3GP10]. In Section 3 we describe the principle of the TSB, and consider the optimisation of its parameters for the BuNGee scenario, while in Section 4 we extend the approach to fading links, where the link throughput is a stochastic rather than deterministic function of SINR, and specifically to MIMO links where the throughput depends on the channel matrix which is in general a random matrix.

Much of this work depends on the use of appropriate stochastic models for the propagation channel. This work has largely been carried out in T2.1, on “Multidimensional channel models”, and reported in [BunD21]. In section 2 of this deliverable report we summarise material from that report in order to define a set of channel models which can be used for both access and backhaul links. It models frequency selectivity in terms of a tapped delay line model, and the dual polarised antennas in terms of a 2×2 MIMO model, with defined correlation matrices.

One challenge for the self-backhauling approach is that the duplex constraint of wireless terminals prevents the same resources being used on the access and backhaul segments of the network. This then either requires that the segments are separated in two different parts of the spectrum, or that careful frequency planning is needed. An interesting method which overcomes this backhaul constraint, allowing the same resources to be used simultaneously on access and backhaul at the same ABS, is *physical layer network coding* (PLNC). In section 9 a WNC technique based on the two-way relay channel (TWRC) is described. In this case however there is interference between the two relays, which has the potential to degrade performance. However we show that in fact with the appropriate network coding approach it is possible even to benefit from this interference, gaining a benefit analogous to that of Network MIMO. In Section 9 a related approach is described, in this case providing communication between two ABSs.

This document was issued in a much earlier form in M8 of the project, as Interim Report IR2.3. The present deliverable report is an updated and greatly expanded version of that report, reflecting the work done in the remainder of the project. Specifically:

- Section 2 is largely new (though incorporating an update of Section 3 of IR2.3), reflecting work carried out in D2.1 and the updating of the channel models used in T2.3 to more accurately model the BuNGee scenario;
- Section 3 has been greatly expanded, and now includes a new general methodology to choose parameters for the TSB, as well as a new choice of parameters for the BuNGee scenario;
- Section 4 is new, containing a description of the methodology for link modelling for stochastic (i.e. fading) channels in general, and specifically a MIMO version of the TSB;
- Section 5 has been significantly updated and expanded, to include the new BuNGee deployment scenario defined in [BunD12] and the corresponding backhaul path loss modelling carried out in T2.1 (reported in [BunD21]). Also it is expanded to consider the effect of the frequency-selective channel, the dual polarised channel, and the effect of interference from other HBSs on the backhaul capacity;

- Section 6 has been greatly expanded to include a transceiver design framework for the BuNGee system based on channel Gram matrix feedback.
- Section 8 is new, describing the work done in T2.3 on network-enabled MIMO;
- Section 10 is new; it describes the work in T2.3 applying wireless network coding to multiple interfering two-way relay channels, allowing resource sharing between access and backhaul segments.

Note that it has not been necessary to significantly amend section 7 or 9. Note also that in place of a separate section describing the 'state of the art' in advanced MIMO (section 2 of IR2.3), there are sub-sections in several of the other sections describing work prior or external to BuNGee.

2. Channel modelling

Since knowledge of the channel is essential to determining the performance of the physical layer of a wireless system, in this section we review the characteristics of the wireless propagation channels involved in the BuNGee network, and describe the models that will be used to describe them in the work described in this report. This characterisation and model definition is the responsibility of Task 2.1 "Multidimensional Channel Modelling" in BuNGee, and is described in detail in [BunD21]: here we extract and summarise the models needed for physical layer performance evaluation.

In BuNGee, at least for the in-band backhauling scenario upon which most of the work described in this report is based, the network can be divided between the *backhaul segment* and the *access segment*. The backhaul segment, between the ABS (or specifically that part of the ABS involved in the backhaul, referred to at some points as the HSS) and the HBS. Because the ABS is placed at around 5 m height within a street canyon, and the HBS is at around 25 m, with narrow beam-widths, the propagation on this link does not fit well with any standardised channel models, and for this reason this segment receives the most attention in the section. Its characteristics have largely been determined using a ray-tracing tool developed at UCL [BunD21], and are described in section 2.1 for the SISO case and in section 2.2, which discusses models for dual polarised antennas. The access segment, on the other hand, is similar to more standard scenarios, and hence a standard model can be used. This is discussed briefly in section 2.3.

2.1 Backhaul SISO model based on ray-tracing

2.1.1 Path loss modelling

The path loss is obtained using the ray-tracing tool of [BunD21]. Since the ABSs in each deployment scenario (as defined in [BunD12]) are located in defined positions, it is possible for the backhaul segment to tabulate the path gain between the HBS and each ABS. Note that there is of course a propagation loss on this link, but we prefer to express it as a negative path gain (in dB) rather than a positive path loss. The HBS in the in-band backhauling scenario is a multi-beam antenna [BunD22], and hence we must in principle calculate the path gain between each ABS and each beam of each HBS which may contribute to, or interfere with, the ABS signal. Examples of these tables are included in [BunD21].

The ray-tracing tool works by determining specular reflections based on a building database, in this case defined by the "square" deployment scenario of [BunD21] (we do not in this case attempt to model deployment in a real city). However its accuracy is enhanced by including diffuse multipath signals, as well as the specular reflections. Diffraction and penetration are also included. Comparison with measurements taken in a scenario similar to the BuNGee case show that inclusion of diffuse scattering greatly improves the accuracy of the ray tracing, giving an average error of 2.8 dB [BunD21].

2.1.2 Frequency-selective model

The project assumes frequency-selective fading on BuNGee's HBS-to-HSS backhaul link. Hence a tapped delay line model has been developed in order to investigate the most suitable transmission schemes in the BuNGee system. An important parameter of the tapped delay line model is the Power Delay Profile (PDP), which gives the intensity of a signal received through a multipath channel as a function of time delay. The PDP of a given channel consists of a number of multipath components or taps. Each tap is defined by its

power and relative delay. The averaged PDP was estimated by taking the spatially averaged impulse response of a multipath channel over a square grid area [BunD12].

Figure 2-1 (marked with 7 blue circles) gives the tapped delay line model for the HBS-to-HSS link. Averaged powers and delays (over square grid) are normalized to the power and delay of the first tap respectively; thus removing the effects of path loss and shadowing. This tapped delay model was obtained on the basis of a 20 MHz system bandwidth (that envisaged for BuNGee). A threshold level of -30 dB (relative to the first tap) is applied, so that any tap powers below this level are excluded, as this would correspond to a typical system dynamic range [BunD21]. In most tapped delay models present in the literature, the tap amplitude are assumed to be Rayleigh-distributed random variables, except the first tap which is normally considered as a Ricean-distributed random variable if a strong Line-Of-Sight (LOS) component exists. In the BuNGee tapped delay line model, however, in [BunD21] it was found that amplitudes of all taps are Ricean-distributed instead of Rayleigh, with high K-factors. This is believed to be because the narrow-beamwidth antennas mean that the multipath received in each tap tends to be dominated by one large reflected component, which leads to a Ricean amplitude distribution. The results obtained show that the K-factors are almost the same after the first three taps (see Table 2-1).

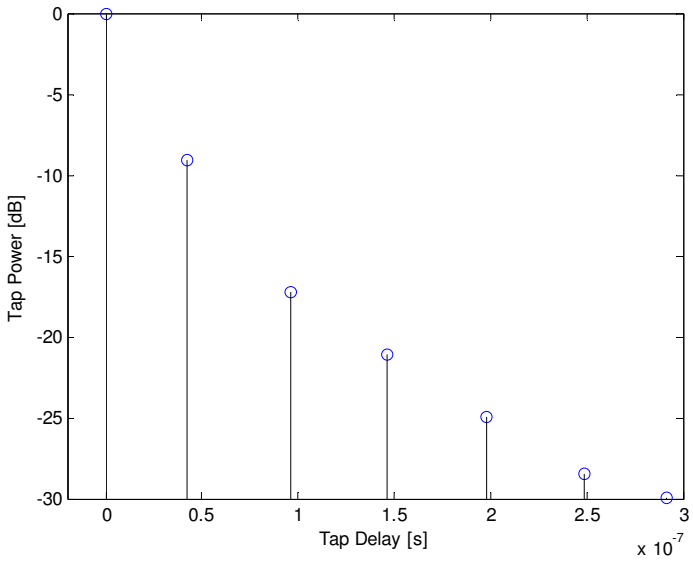

Figure 2-1 PDP of the tapped delay line for BuNGee's backhaul.

Tap Number	Delay [ns]	Power [dB]	K-factor [dB]
1	0	0	14.9
2	42.2	-9.06	19.8
3	95.8	-17.22	17.3
4	146.6	-21.07	29.8
5	198.1	-24.95	25.2
6	248.4	-28.49	26.5
7	291.4	-29.93	25.7

Table 2-1 Parameters of the tapped delay line model for HBS-HSS link.

In addition, since the uncertainty in the path length between HBS and HSS is much more than one wavelength, the phases of the LOS components for all taps are assumed to be identically and independently distributed random variables over the range $[0,2\pi]$. The RMS delay spread is calculated as:

$$\sigma_\tau = \sqrt{\frac{\sum_i \tau_i^2 P(\tau_i)}{\sum_i P(\tau_i)} - \left(\frac{\sum_i \tau_i P(\tau_i)}{\sum_i P(\tau_i)}\right)^2} \tag{2.1}$$

where τ_i and $\mathrm{P}(\tau_i)$ refer to the delay of the i^{th} tap and the corresponding power, respectively. Hence this multipath model has a RMS delay spread:

$$\sigma_\tau = 26 \text{ ns} \tag{2.2}$$

Based on the aforementioned tapped delay line model, we also show in Figure 2-2 the results (black lines) obtained from the developed channel simulator, which well match the given PDP (blue circles). Some frequency responses obtained using this model are shown in Figure 2-2 where 4 instances are given as examples.

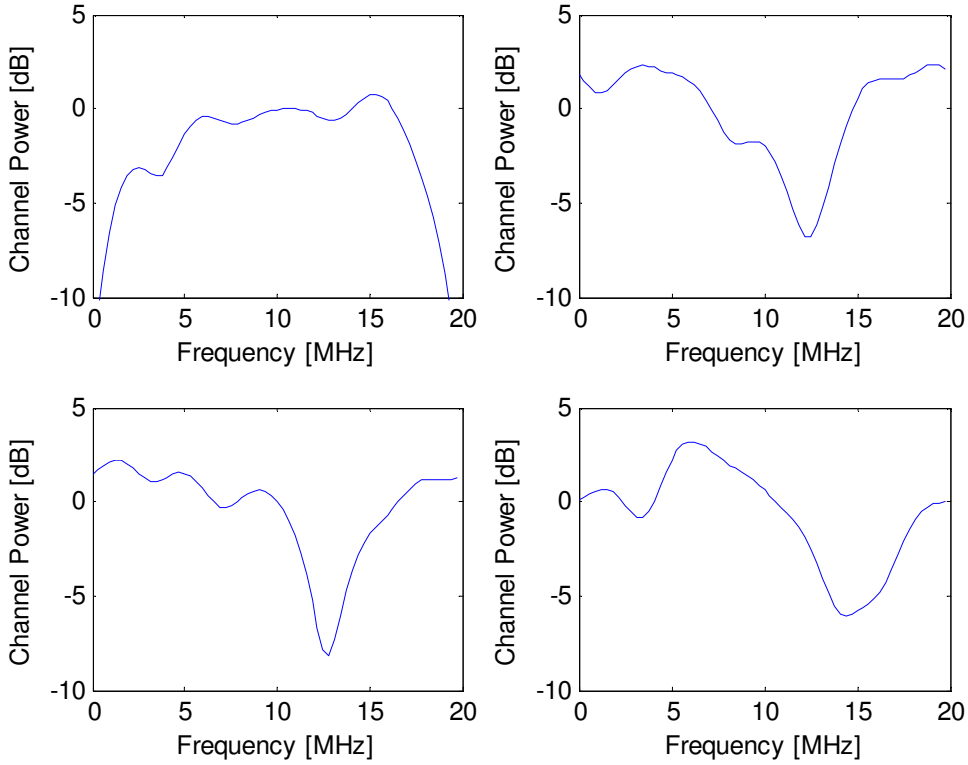

Figure 2-2 Frequency response of the tapped delay line model for 4 instances.

2.2 Backhaul dual polarised model

The use of dual-polarized antennas at both the HSSs and the HBS further increases the dimension of the MIMO channel matrix. In this section, the method used to model the backhaul link channels using existing parameters as well as the process of generating channel realizations will be presented.

2.2.1 Dual-Polarization

In BuNGee, $\pm 45^{\circ}$ dual-polarized antennas are used both at the transmitter (HSSs for uplink) and receiver end (HBS for uplink) to increase the system throughput.

It is important to note that although we have only one physical transmit antenna and one physical receive antenna [Nab02], the resulting channel is equivalent to that of a 2×2 MIMO system, since each antenna has two ports. In ideal signal propagation conditions in which the two polarizations are orthogonal to each other, the 2×2 channel matrix is a diagonal matrix. In reality, however, due to the complicated propagation environment including rich scattering, some of the energy of one polarization may leak into the other. Denoting the 2×2 channel matrix $\mathbf{H}$ as:

$$\mathbf{H} = \begin{bmatrix} h^{++} & h^{+-} \\ h^{-+} & h^{--} \end{bmatrix} \tag{2.3}$$

where the first and second upper indices '+/-' and '+/-' correspond to the polarization direction at the transmitter and receiver, respectively, the correlation between different channel elements can be defined using a 4×4 covariance matrix $\mathbf{R}$ given as:

$$\mathbf{R} = \mathrm{E}\{vec\{\mathbf{H}\} \bullet vec\{\mathbf{H}\}^{H}\} \tag{2.4}$$

The operator $vec\{\mathbf{H}\}$ puts the columns of matrix $\mathbf{H}$ into one column as $vec\{\mathbf{H}\} = [h^{++}\ h^{-+}\ h^{+-}\ h^{--}]^{T}$. Operators $(\cdot)^{T}$ and $(\cdot)^{H}$ are the transpose and complex conjugate transpose, respectively.

The cross polarization discrimination [Jan04] can be defined as:

$$\Lambda = \begin{bmatrix} \alpha^{++} & \alpha^{+-} \\ \alpha^{-+} & \alpha^{--} \end{bmatrix} = \frac{1}{\left|h^{++}\right|^{2}} \begin{bmatrix} \left|h^{++}\right|^{2} & \left|h^{+-}\right|^{2} \\ \left|h^{-+}\right|^{2} & \left|h^{--}\right|^{2} \end{bmatrix} \tag{2.5}$$

Accounting for the correlation and the cross polarization discrimination, the channel matrix for the dual-polarized antennas can then be generated based on independently fading coefficients:

$$vec\{\mathbf{H}\} = vec\{\Lambda\} \odot \left(\mathbf{R}^{\frac{1}{2}} vec\{\mathbf{H}_{\omega}\}\right) \tag{2.6}$$

where $\mathbf{H}_{w}$ is a 2×2 matrix with elements independently drawn from the same small-scale fading distribution and $\odot$ is the Hadamard product.

The 2×2 correlated channel model for a single dual-polarized antenna at both the transmitter and the receiver end can be conveniently extended to more complicated cases with more antennas. However, as the number of antennas increases, fully characterizing the covariance matrix $\mathbf{R}$ may be difficult. It requires measuring the channel correlation coefficients of all possible transmitter and/or receiver combinations. In fact, since channels with antennas that are separated with sufficient distances can be treated as uncorrelated, it is reasonable to assume that channels associated with different transmitter/receiver pairs are uncorrelated regardless of the polarization. For the backhaul link in BuNGee, this assumption becomes that channels of different beam pairs are considered as uncorrelated with each other.

2.2.2 Generation of channel realizations for the backhaul link

For the link of each transmitter/receiver pair, the frequency-selective channel is characterized by a tapped-delay line, where the L taps of the channel are assumed independent of each other. As described in Section 2.1.2, all the taps are Rician fading, each with a different spatial K factor and a different power loss. The channel can be generated in a tap-by-tap manner.

For each tap of the channel:

1. For the link between the i^{th} HSS (transmitter for uplink) and the j^{th} beam (receiver for uplink), the elements of the 2×2 matrix $\mathbf{H}_{w}$ are independently drawn from a Ricean distribution with K-factor given by the spatial K factor of this tap.
2. Compute the cross polarization discrimination $\mathbf{\Lambda}$ according to equation (2.5) and the covariance matrix $\mathbf{R}$. In this work, the ratios between $|h^{++/--}|^{2}$ and $|h^{\pm/-+}|^{2}$ are found according to the

parameters provided in [BunD21]. The covariance matrix $\mathbf{R}$ for different transmitter/receiver can also be found in [BunD21].

3. Use equation (2.6) so that the effect of polarization is taken into account:

$$vec\{\mathbf{H}_{ij}\} = vec\{\mathbf{\Lambda}\} \left(\mathbf{R}^{\frac{1}{2}} vec\{\mathbf{H}_{\omega}\} \right)$$

4. Take account the path loss for different transmitter/receiver pairs: denoting the path loss of the i^{th} transmitter and the j^{th} receiver as $G_{i,j}$, the channel matrix becomes: $\mathbf{H}_{i,j} = G_{i,j}\mathbf{H}_{i,j}$.
5. Repeat Step1 to Step3 for all possible transmitter/receiver pairs.
6. The resulting channel coefficients of this tap are further scaled according to its power loss.

The channel coefficients for different transmitter/receiver pairs $\mathbf{H}_{i,j}$ are stacked together to form the overall channel matrix $\mathbf{H}$ for the whole multi-beam system.

Assuming the number of beams of an HBS is *N* and the number of HSSs served by this HBS is *K*, $\mathbf{H}$ is of dimension $2N \times 2K$, with

$$\mathbf{H} = \begin{bmatrix} \mathbf{H}_{11} & \cdots & \mathbf{H}_{1K} \\ \cdots & \mathbf{H}_{ij} & \cdots \\ \mathbf{H}_{N1} & \cdots & \mathbf{H}_{NK} \end{bmatrix} \quad (2.7)$$

The above operations are repeated for all the channel taps to characterize the frequency selective channels. In BuNGee, OFDM signals are adopted in the backhaul link. Therefore, the obtained frequency-selective channel matrices are Fourier transformed to form a set of narrow-band channel matrices $\mathbf{H}_q$ $(q = 1,2,\cdots,Q)$ for Q subcarriers.

2.3 Access channel modelling

For the ABS to MS link, the BuNGee scenario assumes that a directional antenna is used at the ABS, at approximately 5 m height, pointing along the street in a Manhattan-type grid street layout. This is sufficiently similar to the WINNER B1 model [Kyo07] (except for the precise ABS height and antenna beamwidth) for that model to be directly usable. Its use to determine path losses for the purpose of system-level simulation is also described in [BunD412].

3. The Truncated Shannon Bound (TSB)

3.1 Principle of TSB

It is useful to have a simple means of relating link throughput to signal to interference plus noise ratio (SINR). The Shannon bound as it applies to a white Gaussian noise channel is sometimes used for this purpose, but is not accurate in practical systems for (at least) four reasons:

1. It is an upper bound on throughput, and practical modulation and coding schemes do not attain it;
2. It gives unlimited throughput for unlimited SINR, whereas practical schemes have an upper limit corresponding to the highest modulation/code rate provided;
3. It indicates non-zero throughput for any SINR, whereas practical schemes have a minimum SINR below which no data can be transmitted;
4. Practical schemes have a finite granularity, which reduces the average throughput over a range of SINR.

The TSB has been defined in [3GP10] so as to overcome these issues. In this version (1) and (4) are dealt with by multiplying the throughput by a scaling factor $\alpha < 1$; (2) by setting a maximum SINR above which throughput does not increase further (at which the predicted throughput equals the maximum throughput of the modulation/coding scheme), and (3) by similarly setting a minimum SINR below which throughput is set to zero. This definition can be summarised as follows:

$$Throughput, Thr, bps/Hz = \begin{cases} Thr = 0 & \text{for SNIR} < \text{SNIR}_{MIN} \\ Thr = \alpha.S(SNIR) & \text{for SNIR}_{min} < \text{SNIR} < \text{SNIR}_{MAX} \\ Thr = Thr_{MAX} & \text{for SNIR} > \text{SNIR}_{MAX} \end{cases}$$

Where: S(SNIR) is the Shannon bound: $S(SNIR) = \log_2(1+SNIR)$ bps/Hz

α	Attenuation factor, representing implementation losses
SNR_{MIN}	Minimum SNIR of the codeset, dB
Thr_{MAX}	Maximum throughput of the codeset, bps/Hz
$SNIR_{MAX}$	SNIR at which max throughput is reached $S^{-1}(Thr_{MAX})$, dB

In this report we further generalise this as follows [Bur12]:

$$C_{TSB}(\gamma) = \begin{cases} 0 & \gamma < \gamma_0 \\ W\alpha \log_2(1+\gamma/\gamma_{sh}) & \gamma_0 \le \gamma < \gamma_{max} \\ C_{max} & \gamma_{max} < \gamma \end{cases} \quad (3.1)$$

where γ_{sh} denotes the shift, which we introduce here in addition to the scaling factor α described in [3GP10]. This is because there is in practice an irreducible 'gap from Shannon' between the Shannon bound and the performance of practical schemes, which results in a right-ward shift of the throughput *versus* SINR characteristic. The gap also tends to be larger for higher modulation rate, because the dominant form of coded modulation, bit interleaved coded modulation (BICM) does not approach the Shannon bound so closely. This has the effect of also scaling the throughput characteristic.

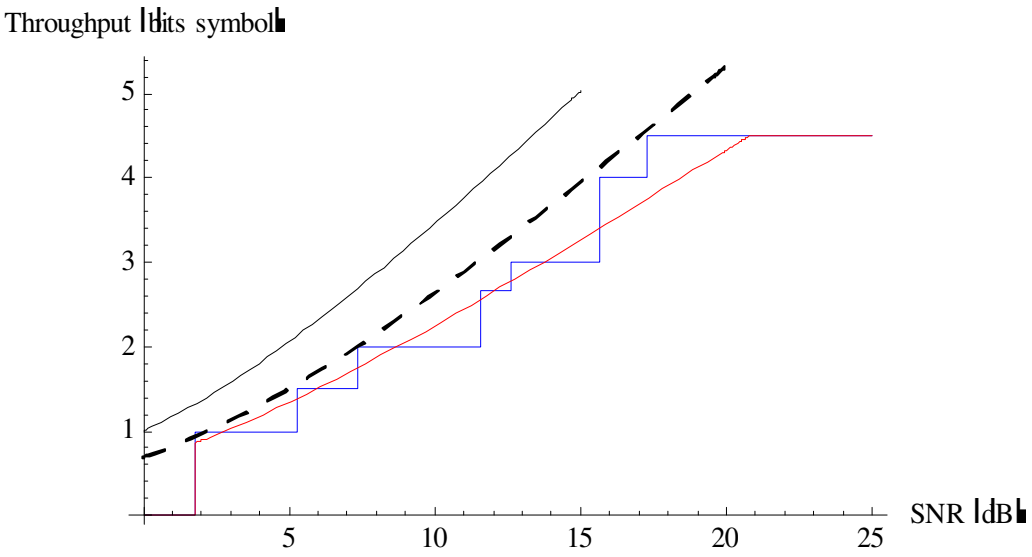

Figure 3-1 Throughput function of a set of coding/modulation schemes (stepped blue) compared with Shannon bound (solid black), shifted/scaled Shannon bound (dashed black), and truncated Shannon bound (red)

This is illustrated in Figure 3-1, which compares the Shannon bound to the throughput of the set of practical modulation and coding schemes described in [BunD21]. The dashed line shown is the Shannon bound shifted by 1.2 dB and scaled by 0.82, giving a good match to the throughputs of the schemes. However this approximation does not take into account the granularity of the discrete set of schemes employed, which means that the true throughput function is stepped, as shown. This will further reduce the throughput achieved on average. The true throughput, including all the effects mentioned above, is better approximated by the red line, which denotes the truncated Shannon bound as used in BuNGee.

3.2 TSB parameter matching

A question then arises of what shift and scaling parameters should be used in the TSB to optimally approximate the actual throughput function for an arbitrary set of coding/modulation schemes. In our context we wish to ensure that the average throughput given by the TSB is as close as possible to the average throughput using the true throughput function, given that the link SNR is random, so that the average should be taken over its distribution. Mathematically we can therefore write:

$$\int_{s_0}^{\infty} C_{TSB}(s)\, p(s,\bar{s})\, ds \equiv \int_{s_0}^{\infty} C_{thr}(s)\, p(s,\bar{s})\, ds = \bar{C}(\bar{s}) \tag{3.2}$$

where C_{TSB} denotes the TSB function, $s = 10\log_{10}(\gamma)$ and $\bar{s}$ denote respectively the instantaneous SNR and the average SNR, both in dB, $p(s,\bar{s})$ denotes the probability density function of the instantaneous SNR (in dB) on a given link, C_{thr} denotes the true throughput function, and $\bar{C}(\bar{s})$ denotes the average throughput as a function of average SNR. The parameters of the TSB are to be chosen to fulfil this identity, as far as possible with any likely SNR distribution.

We can approximate the PDF $p(s,\bar{s})$ with arbitrary accuracy as the sum of a set of rectangular functions: that is, the distribution can be treated as a mixture distribution of uniform distributions, provided the range δ of the support of these PDFs is less than that of the actual distribution. We write:

$$p_{ap}(s,\bar{s}) = \sum_{i=1}^{n_p} a_i u(s,\bar{s}_i,\delta_i) \tag{3.3}$$

where:

$$u(s,\bar{s},\delta) = \begin{cases} 0 & s \le \bar{s} - \delta/2 \\ \dfrac{1}{\delta} & \bar{s} - \delta/2 < s < \bar{s} + \delta/2 \\ 0 & s \ge \bar{s} + \delta/2 \end{cases} \tag{3.4}$$

Then:

$$\begin{aligned} \bar{C}(\bar{s}) &= \int_0^{\infty} \sum_{i=1}^{n_p} a_i u(s,\bar{s}_i,\delta) C_{TSB}(s) ds \equiv \int_0^{\infty} \sum_{i=1}^{n_p} a_i u(s,\bar{s}_i,\delta) C_{thr}(s) ds \\ &= \sum_{i=1}^{n_p} a_i \int_{\bar{s}_i-\delta/2}^{\bar{s}_i+\delta/2} C_{TSB}(s)\, ds \equiv \sum_{i=1}^{n_p} a_i \int_{\bar{s}_i-\delta/2}^{\bar{s}_i+\delta/2} C_{thr}(s)\, ds \end{aligned} \tag{3.5}$$

and hence capacities will match provided:

$$\int_{\bar{s}_i-\delta/2}^{\bar{s}_i+\delta/2} C_{TSB}(s)\, ds \equiv \int_{\bar{s}_i-\delta/2}^{\bar{s}_i+\delta/2} C_{thr}(s)\, ds, \forall \bar{s}_i \tag{3.6}$$

Hence we plot the average of C_{thr} (r.h.s. of equation (3.6)) for some value of δ which is less than the likely range of values of SNR encountered in the system, and similarly plot C_{TSB} (l.h.s. of equation (3.6)), choosing α and γ_{sh} to provide the closest match between the two over the full range of average SNR. Figure 3-2 shows this plot for two sets of values of α and γ_{sh} which have been used in BuNGee. It shows that α = 0.77 and γ_{sh} = 2 dB gives the best match, but the values α = 0.65 and γ_{sh} = 0 dB, as used in [IR2.3] also give a reasonable match.

Figure 3-3 then shows the average throughput for the actual throughput function and the truncated Shannon bound (with α = 0.77 and γ_{sh} = 2 dB) for a log-normal SNR distribution, with standard deviation 6 dB. We note that the average throughputs match very closely.

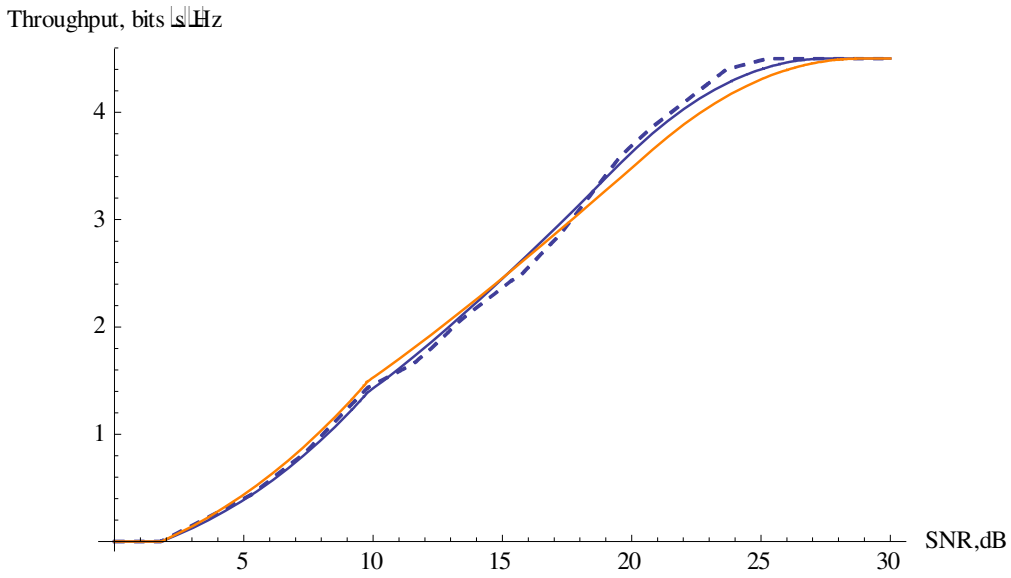

Figure 3-2 Average throughput versus average signal to noise ratio for uniform distribution with δ = 8 dB, for actual throughput function C_{thr}(SNR) (dashed line), for the truncated Shannon bound with α = 0.65 and zero shift (orange line), and for the truncated Shannon bound with α = 0.77 and shift 2 dB (solid blue line)

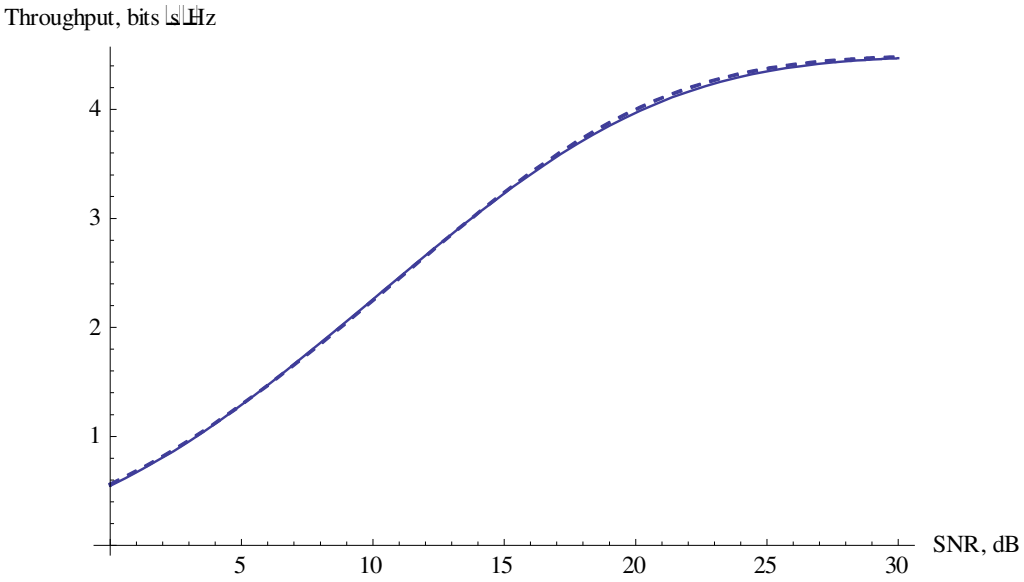

Figure 3-3 Average throughput versus average signal to noise ratio for log-normal distribution with σ = 6 dB, for actual throughput function C_{thr}(SNR) (dashed line), and for the truncated Shannon bound with α = 0.77 and 2 dB shift (solid line).

4. Link throughput modelling

For a system like the BuNGee network which may contain many nodes (many HBSs, ABSs and MSs), the number of channel links rapidly becomes very large. It is thus clearly not feasible to carry out a full-scale, bit level Monte Carlo simulation to evaluate the throughput of every link in the system.

In order to address this problem, similar to [Bur94], in BuNGee, we use a two -step process: a system-level simulation to evaluate the signal-plus-noise ratio (SINR) of each link and taking into account path loss, shadowing and slow fading on the signal. Thereupon a link-level function is applied to evaluate the capacity of each link. This could be based on the (1) Shannon bound, or on (2) closed-form expressions for BER *versus* SNR, or (3) a look-up table obtained by simulation. In a single-input, single-output (SISO) link, assuming that slow Rayleigh fading is included in the calculation of the SINR, this function can be treated as

deterministic. (Fast Rayleigh fading could be included in the average BER function). As discussed in section 3, in BuNGee we have developed the truncated Shannon bound (TSB) for this purpose.

The introduction of multiple antenna elements at both transmitter and receiver has made this process significantly more complicated. First, it is no longer sufficient simply to consider the aggregate interference experienced by a specific link and quantify it as a simple SINR, since the direction of the interference becomes important. Secondly, the link capacity can no longer be treated as a deterministic function of any SINR, even in the absence of interference, since capacity is a function of the channel matrix **H**, which must be treated as random.

4.1 Stochastic throughput model

In order to reduce our simulator's complexity we have therefore developed a stochastically based methodology, which maps each value of average link SINR to a statistical distribution of achievable rates. Our simulator tracks the average SINR value for each considered wireless link; the average SINR does not depend on the coefficients of the MIMO channel (the entries of **H**), but solely on the path loss and shadowing realization of the useful and the interfering links. In BuNGee these parameters can be obtained from the ray-tracing propagation models described in [BunD21], and therefore do not need to be treated as random.

The effect of Rayleigh fading, however, cannot reliably be predicted by ray-tracing, and must be treated as random. (Note that this applies to SISO as well as MIMO channels, although the issue is much more complex in MIMO channels). The link level throughput function is therefore stochastic, consisting of a throughput distribution which is in turn a function of link SINR.

While for some channels it may be possible to define such a distribution in closed form, in general this is not possible, and hence we have used an empirical approach. For a useful range of average SINR values we have obtained offline the empirical distributions of the achievable capacity by means of link level simulations. Such an empirical distribution has been obtained for each of a range of SINR values, sufficiently closely spaced to allow accurate interpolation. Therefore in our actual simulation for every generated value of average SINR, the attained throughput takes a value from the corresponding empirical throughput distribution. This accelerates and simplifies the general numerical evaluation of the throughput of the BuNGee wireless links. In order to guarantee highly accurate results we need to ensure that the empirical throughput distributions, that are generated offline for a range of average SINR values, are truly representative of the achievable throughput.

These empirical distributions must be stored as some form of look-up table. A convenient format for this look-up table is the cumulative distribution function (CDF) of throughput, defined as:

$$F_C\left(\tilde{C},\bar{s}\right)=\Pr\left[C\le\tilde{C}\middle|\bar{s}\right]=\int_0^{\tilde{C}}p_C\left(C,\bar{s}\right)dC \tag{4.1}$$

where $\bar{s}$ denotes the average SINR in dB. This is a monotonically increasing function within the range [0, 1]. In the system-level simulation we may then generate a random variable $f\in[0,1]$ with uniform distribution, and use it to look up $\tilde{C}$ such that $F_C\left(\tilde{C},\bar{s}\right)=f$. The PDF of $\tilde{C}$ is then given by:

$$\begin{aligned}p_{\tilde{C}}\left(\tilde{C}\right)&=\underset{\delta C\to 0}{\mathrm{Lt}}\left[\frac{\Pr\left[\tilde{C}\in\delta C\right]}{\delta C}\right]=\underset{\delta C\to 0}{\mathrm{Lt}}\left[\frac{\Pr\left[F_C\in\delta F_C\right]}{\delta C}\right]\\&=\underset{\delta C\to 0}{\mathrm{Lt}}\left[\frac{\delta F_C\,p\left(F_C\right)}{\delta C}\right]=\frac{dF_C}{d\tilde{C}}=p_C\left(C\right)\end{aligned} \tag{4.2}$$

Hence the random variable $\tilde{C}$ has the required distribution. Since this CDF is in general also a function of the average SINR $\bar{s}$, a two-dimensional look up table is required. It is in principle possible to interpolate between values of this function, both in terms of $\bar{s}$ and of f, reducing the number of values that need to be stored. If other factors such as interference to noise ratio (INR), etc, are also significant, then a larger

number of dimensions may be required. However if the effect of such factors is not large, or if their distributions are separable from that of SINR, a good approximation is obtained by averaging over them.

We give an example of such a look-up table and its use in a system-level simulator in section 4.2.3 below.

4.2 MIMO TSB

As mentioned above MIMO systems raise particular problems for link level capacity modelling, since the link capacity is necessarily a function of the channel coefficients (entries of **H**), which must in practice be treated as random. In addition link capacity cannot be treated as a function of a simple SINR, but may also be affected by the interference to noise ratio (INR), the directional spectrum of the interference, etc. In this section we describe the BuNGee approach to stochastic modelling of MIMO links, using the stochastic approach described in section 4.1 and the truncated Shannon bound of section 3.

Our general approach applies to MIMO schemes in which multiple sub-channels are provided by appropriate signal processing, over which one or more independent data streams may be transmitted. This applies to a wide class of MIMO schemes, including all those used in current wireless standards, such as space time block codes (STBC), spatial multiplexing, linear precoding, etc. The TSB can then be applied to calculate the throughput of each sub-channel, leading to a total link throughput value which will be used to provide throughput CDFs for the look-up table.

4.2.1 MIMO signal processing

In our present evaluation we focus on the uplink (MS-ABS, ABS-HBS link), although similar concepts can be applied in the downlink. In order to exploit MIMO channels for increasing throughput through spatial multiplexing we consider some well-known signal processing techniques, namely, linear detection and successive interference cancellation (SIC) detection.

In the case of linear detection, a beamforming matrix $\mathbf{\Omega}$, which is a form of channel matrix inverse, is applied to the received signal vector **r** in order to minimize the interference between the transmitted data streams. Then the symbol estimates are obtained via

$$\hat{\mathbf{s}} = Q(\mathbf{\Omega}^H \mathbf{r}), \tag{4.3}$$

where $Q(\square)$ denotes the quantization operation. The beamforming matrix can be designed according to either the Zero-Forcing (ZF) or the Minimum Mean Square Error (MMSE) criteria. ZF completely eliminates inter-stream interference, and the beamforming matrix takes the form of the Moore-Penrose pseudoinverse of the channel matrix. The ZF beamforming matrix is given by:

$$\begin{aligned} \mathbf{\Omega}_{ZF} &= \arg\min_{\Omega}\{\mathbf{s} - \mathbf{\Omega}^H \mathbf{H}\mathbf{s}\} \\ &= \left(\mathbf{H}^H \mathbf{H}\right)^{-1} \mathbf{H}^H \end{aligned} \tag{4.4}$$

where **s** is the transmitted vector, **H** is the channel matrix and $\mathbf{\Omega}_{ZF}$ is ZF filter. Although ZF can eliminate interference, it gives rise to noise enhancement when the channel matrix is ill-conditioned. MMSE beamforming, on the other hand, allows some inter-stream interference, but achieves an optimal trade-off between noise enhancement and interference and results in higher performance than ZF. The cost function of MMSE filtering is given as follows:

$$\begin{aligned} \mathbf{\Omega}_{\mathrm{MMSE}} &= \arg\min_{\mathbf{\Omega}} \{\mathbf{s} - \mathbf{\Omega}^H \mathbf{r}\} \\ &= \left(\mathbf{H}^H \mathbf{H} + \sigma^2 \mathbf{I}\right)^{-1} \mathbf{H}^H \end{aligned} \tag{4.5}$$

where **r** is the received vector, σ^2 is the noise variance and $\mathbf{\Omega}_{\mathrm{MMSE}}$ is MMSE filter.

Detection performance can be further improved if it is performed in a successive fashion, i.e., the detected symbols are successively stripped off from the remaining received signal. This frees the signal from some

interference components and can enhance the achieved capacity. The conventional SIC algorithm computes the $N_R \times 1$ MMSE filter corresponding to each layer's data stream as

$$\boldsymbol{\omega}_k = (\bar{\mathbf{H}}_k \bar{\mathbf{H}}_k{}^H + \frac{\sigma_v^2}{\sigma_s^2}\mathbf{I})^{-1}\mathbf{h}_k. \tag{4.6}$$

where $\bar{\mathbf{H}}_k$ denotes the matrix obtained by taking the columns $k, k+1, \ldots K$ of channel $\mathbf{H}$. Note that that the columns of **H** are assumed to be ordered so that the first columns correspond to the least faded transmit antennas. In this algorithm, the procedure uses nulling and symbol cancellation to successively detect the desired symbol for each data stream $\hat{s}_k, k = 1, \ldots, K$.

$$\hat{s}_k = Q(\boldsymbol{\omega}_k^H \boldsymbol{\varepsilon}_k), \tag{4.7}$$

These detected symbols form a decision vector $\hat{\mathbf{s}} = [\hat{s}_1, \hat{s}_2, ..., \hat{s}_K]^T$.

The successively cancelled received vector in the *k*-th stage is $\boldsymbol{\varepsilon}_k$. The received vector after the cancellation of the previously detected *k-1* symbols is:

$$\begin{cases} \boldsymbol{\varepsilon}_k = \mathbf{r}, & k = 1, \\ \boldsymbol{\varepsilon}_k = \mathbf{r} - \sum_{j=1}^{k-1} \mathbf{h}_j \hat{s}_j, & k \geq 2. \end{cases} \tag{4.8}$$

After subtracting the detected symbols from the received signal vector, the remaining signal vector is processed either by an MMSE or ZF filter for the symbol estimation for the following streams.

The performance of SIC based detection is interior of that of optimal maximum-likelihood solution. The probability of detection error of such detector is generally limited by the remaining interference and the effect of error propagation [Chi97]. Several state-of-the-art solutions [Li12, Li11] are proposed to enhance the performance of SIC based detection and achieve a close to optimal performance while maintaining the low complexity of traditional SIC detectors.

For the present evaluation, in order to clarify the description of TSB of MIMO systems, we assumed linear MMSE detection which results in a good trade-off between performance and complexity.

4.2.2 MMSE performance for isolated MIMO link

By “isolated MIMO" we refer to a MIMO system experiencing only inter-antenna-interference (IAI) and thermal noise, with no interference from other undesired UEs. In order to evaluate the post-processing SNR for an interference free MIMO system, the MMSE criterion [Dai04] is used to design the filter to minimize the inter-antenna interference (IAI) at the detector output. We use the channel model of [Dai04]:

$$\begin{aligned} \mathbf{r} &= \mathbf{H}\mathbf{s} + \mathbf{v} \\ &= \sum_{k=1}^{N_T} \mathbf{h}_k s_k + \mathbf{v} \end{aligned} \tag{4.9}$$

The MMSE filter is given as

$$\mathbf{w}_k = \mathbf{R}^{-1}\mathbf{p}_k \tag{4.10}$$

where $\mathbf{R} = E\{\mathbf{r}\mathbf{r}^H\}$ and $\mathbf{p} = E\{\mathbf{r}s^*\}$. By substituting (4.9) with these functions we obtain

$$\begin{aligned} \mathbf{R} &= \mathbf{H}\mathbf{H}^H + \sigma_v^2 \mathbf{I}_{N_R} \\ &= \mathbf{h}_k \mathbf{h}_k^H + \sum_{j \neq k} \mathbf{h}_j \mathbf{h}_j^H + \Gamma \\ &= \mathbf{h}_k \mathbf{h}_k^H + \mathbf{S} \end{aligned} \tag{4.11}$$

and

$$\mathbf{p}_k = \mathbf{h}_k \tag{4.12}$$

The extracted signal can be expressed as

$$\begin{aligned} \tilde{s}_k &= \mathbf{w}_k^H \mathbf{r} \\ &= \mathbf{w}_k^H \mathbf{h}_k s_k + \sum_{j \neq k} \mathbf{w}_k^H \mathbf{h}_j s_j + \mathbf{w}_k^H \mathbf{v} \end{aligned} \tag{4.13}$$

The mean square error (MSE) of the output of MMSE filter is defined as:

$$\begin{aligned} \varepsilon_{isol,k} &= E\{|\tilde{s}_k - s_k|^2\} \\ &= E\{(s_k - \mathbf{w}_k^H \mathbf{r})(s_k - \mathbf{w}_k^H \mathbf{r})^H\} \\ &= \mathbf{w}_k^H \mathbf{R} \mathbf{w}_k - \mathbf{w}_k^H \mathbf{p}_k - \mathbf{p}_k^H \mathbf{w}_k + 1 \\ &= 1 - \mathbf{w}_k^H \mathbf{p}_k \end{aligned} \tag{4.14}$$

Therefore we may obtain the post-processing SINR of the k-th data stream from [Mad94]:

$$\gamma_{isol,k} = \frac{1}{\varepsilon_{isol,k}} - 1 \tag{4.15}$$

We then use the truncated Shannon bound (section 3) to calculate the throughput of this stream, and hence the total throughput.

4.2.3 MIMO link with interference

A MIMO link in the presence of interference is modelled using:

$$\mathbf{r} = \mathbf{H}\mathbf{s} + \mathbf{H}_{int}\mathbf{s}_{int} + \mathbf{v} \tag{4.16}$$

We suppose an MMSE filter is applied to the received signal $\mathbf{r}$, in this case the MMSE filter is computed as

$$\begin{aligned} \mathbf{w}_{int,k} &= \mathbf{R}_{int}^{-1} \mathbf{p}_{int,k} \\ &= (\mathbf{H}\mathbf{H}^H + \frac{P_{int}}{N_T K_{int}} \mathbf{H}_{int} \mathbf{H}_{int}^H + \sigma_v^2 \mathbf{I})^{-1} \mathbf{h}_k \\ &= (\mathbf{H}\mathbf{H}^H + \mathbf{S})^{-1} \mathbf{h}_k \end{aligned} \tag{4.17}$$

where $\mathbf{R}_{int} = \mathbf{H}\mathbf{H}^H + \mathbf{S}$ and $\mathbf{p}_{int,k} = \mathbf{h}_k$. The MMSE filter output in the presence of interference is

$$\begin{aligned} \varepsilon_{int,k} &= 1 - \mathbf{h}_k^H \mathbf{R}_{int}^{-1} \mathbf{h}_k \\ &= 1 - \mathbf{w}_{int,k}^H \mathbf{h}_k \end{aligned} \tag{4.18}$$

The SINR is obtained as [Mad94]:

$$\gamma_{int,k} = \frac{1}{\varepsilon_{int,k}} - 1 \tag{4.19}$$

Again the throughput can be found using the TSB.

Figure 4-1 shows the average throughput for a (4×4) MIMO link in the presence of interference from N_S = 8 interfering streams, with an interference to noise ratio INR = 10 dB, plotted against SINR. Note that the TSB in this case shows a throughput degradation compared to Shannon corresponding to about 5 dB loss, as well as reaching a maximum throughput of 18 bits/s/Hz, due to the maximum code/modulation capacity of 4.5 bits/s/Hz/stream.

Figure 4-2 shows the cumulative distribution function (CDF) for the same MIMO link in interference, for different interference distributions: for a wide range of INR values, and also for 16 interfering streams instead

of 8. This shows that the throughput CDF is quite insensitive to the distribution of interference, and is mainly determined by SINR. This shows that for use in a system simulator it is sufficient to parameterise a MIMO link by its SINR only: the interference distribution need not be taken into account.

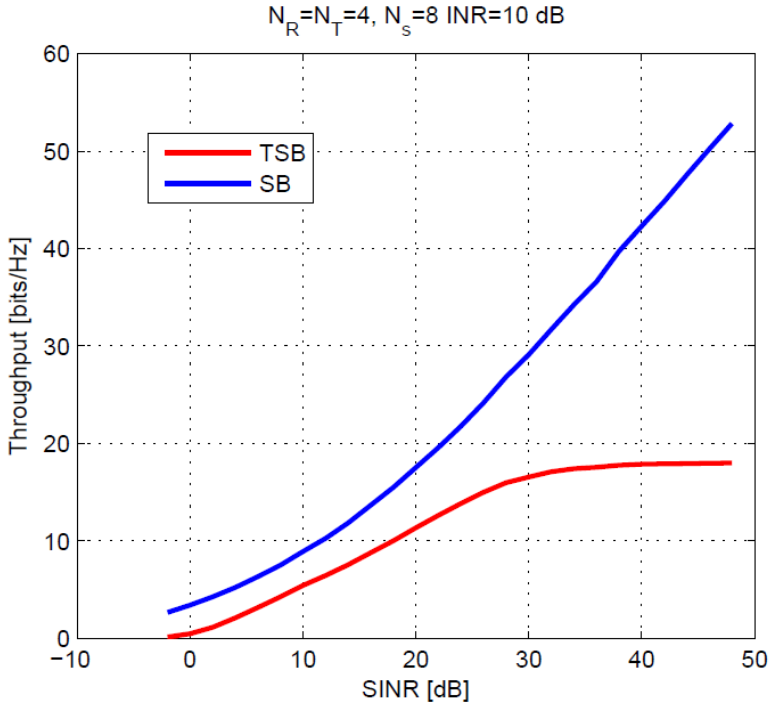

Figure 4-1 Average throughput of MIMO link in interference using Shannon bound (SB) and truncated Shannon bound (TSB)

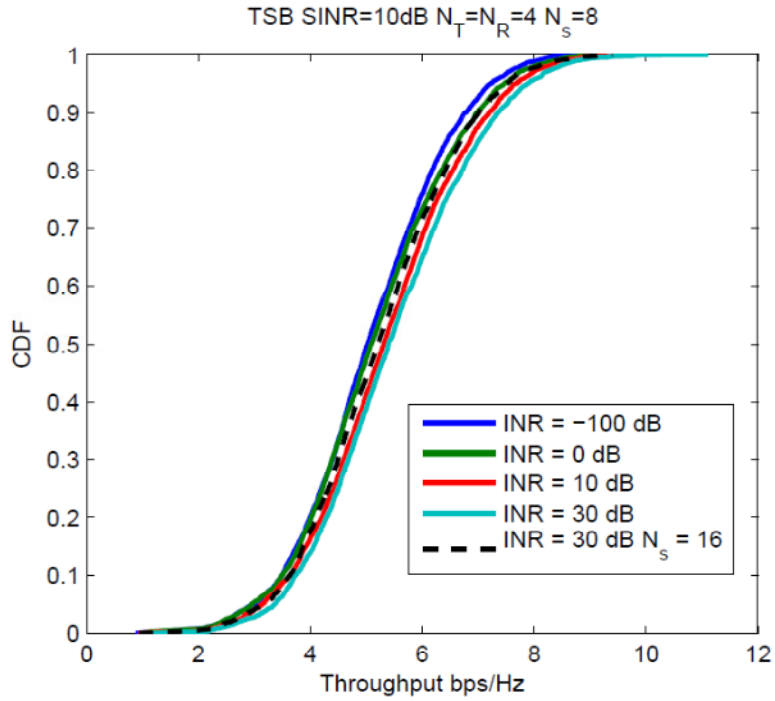

Figure 4-2 Throughput cumulative distribution function for MIMO link in interference at SINR = 10 dB, for various INR, and for 8 and 16 interfering streams

Figure 4-3 shows the CDF of the same link for a wide range of SINR, from -2 to 48 dB. This can be used as a look-up table for link throughput for use in the system-level simulator, using the approach described in section 4.1 above. To use this in a system-level simulator, the following steps are applied:

1. Determine SINR $\overline{s}$ for target link using propagation models in system simulator;
2. Generate uniformly distributed random variable ς between 0 and 1;
3. Use $\overline{s}$ to select appropriate trace from Figure 4-3 and ς to select a value on the CDF axis, and hence look up throughput value. Interpolation may be needed between the values stored in the table.

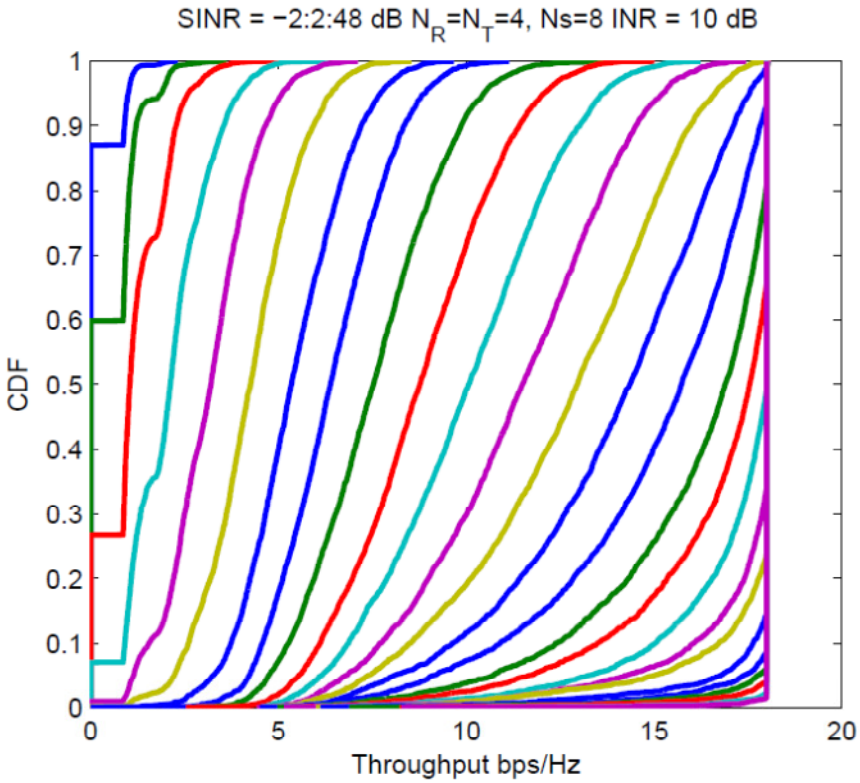

Figure 4-3 Throughput CDF for MIMO link in interference, for a range of SINR

5. Backhaul capacity using Multi-beam Assisted (MBA) MIMO

5.1 State of the art

The MBA-MIMO concept as developed in BuNGee is novel to the BuNGee project. However there have been previous papers on sparsity and the relationship of MIMO with multi-beam antennas formed by the use of a Butler matrix and an antenna array.

The general concept of sparsity relies on the fact that given a set of observations, dimensions or samples, only some of them provide a significant and non-negligible contribution. [Mar09] (and references therein) provides a general and unified overview on the application of sparsity in several concrete areas in signal processing, such as sampling, channel coding, spectral estimation, array processing, component analysis, and channel estimation. Concerning array processing, the three topics that are covered are estimation of direction of arrival, sparse array beamforming and design, and sparse network sensors. The problems that are analyzed in sparse array beamforming are related to how to achieve better resolution for a given maximum number of used array elements from a given higher set of available elements. The selection of elements to be processed is also related with classical problems such as irregular or non-uniform sampling. There are different methods to select such elements, such as techniques based on optimization, while other ones are more heuristic which are based more on the experience. See also [Hol01] for a complete reference on sparsity in array processing. There are also some works in literature related to the application of sparsity in statistics and inference. Some of them deal, for example, with the estimation of a covariance matrix of a high dimensional set of observations. In this situation, the covariance matrix is expected to be sparse and some estimation procedures can be developed taking advantage of such sparsity to obtain a consistent

estimation. See [Kar09] and [Lev08] (and references therein) as two illustrative examples of papers related with this issue.

In terms of the application to MIMO, a series of papers by Grau *et al.* [Gra05a,b,c, Gra06] consider selection diversity using two uniform linear arrays, with and without a Butler matrix. They show that selection diversity based on selecting the strongest signal at the output of each array (either from the strongest antenna, or the strongest beam port at the output of the Butler matrix) gives similar results in terms of diversity gain in the two arrays in rich multipath environments, but the Butler matrix gives significantly improved gain in more sparse environments. A series of papers by Molisch, Sudarshan, *et al.* [Mol03], [Sud04] also consider selection diversity, in this case however, a subset rather than a single antenna/port is selected, and further signal processing is performed on the signals. Maximum Ratio Transmission (equivalent to eigenbeamforming) is applied at the transmitter. Again it is shown that performance is improved in a sparser multipath environment if RF domain pre-processing is used before the selection. In [Mol03] the processing is a Butler matrix; in [Sud04] it is generalized. Rather than selection diversity, Ylitalo [Yli07] appears to assume a form of equal gain combining, showing that direct combining of the outputs of a Butler matrix results in significantly greater gain than for direct combining of the antenna outputs.

Note that none of this previous work considers true MIMO transmission, in the sense that multiple stream transmission is supported. Selection diversity and equal gain combining both allow only one stream to be supported, as does maximum ratio transmission, which explicitly extracts only the strongest eigenvector at the transmitter for data transmission. The papers by Innok *et al.* [Inn09a,b] address only the Shannon capacity of the channel, and it is not clear where the capacity gains they report arise, given that the Butler matrix cannot of itself induce power gain. They also address the practical design of the Butler matrix. Similarly Rose *et al.* [Ros08] is primarily focused on array design.

5.2 MBA-MIMO using joint beam processing

The MBA-MIMO concept as proposed by BuNGee is a true MIMO scheme operating in the beam space rather than antenna aperture space. This concept is developed jointly with the BuNGee high gain multi-beam antenna, and hence is unique. It is therefore capable of yielding further capacity benefits beyond those provided by the previous work [Gra05][Mol03] where the primary benefit is that on relatively sparse channels, resulting in correlation between antennas, selection diversity in the beam space domain is much more efficient. However multiplexing gain is limited because only one stream is transmitted. MBA-MIMO allows more than one data stream to be transmitted simultaneously, and hence provides multiplexing gain. On the other hand it has the advantage over conventional aperture space MIMO in that any sparsity in the channel can be exploited to reduce the complexity of signal processing and potentially also RF/IF hardware. This will also assist with channel estimation.

In order to fulfill the high capacity density demands, BuNGee has designed and developed a novel HBS dual polarized multi-beam antenna, which includes a number of fixed narrow beams providing wireless backhaul to a large number of small HSSs. These multiple narrow beams are created with the use of an antenna array fed by a Butler matrix which essentially implements a fixed beam-former creating a number of narrow beams [Gra05][Gra06]. This can well improve performance as potentially it increases the antenna gain from the HBS. A traditional approach to process beams is to allocate one beam per ABS and each of the N_B beams is processed individually. This is a concept defined as Single-Beam Processing (SBP). However, HSS throughput suffers from Inter-Beam Interference (IBI) from the other beams even though all HBS beams are narrow, as HSSs are not usually located at the boresight of the allocated beam. Hence IBI is typically treated as noise and results in serious capacity loss.

The attained throughput can be further enhanced by integrating MIMO techniques in the beam domain as opposed to the traditional SBP. This integrated approach is defined as MBA-MIMO, as described above. MBA-MIMO is a novel technique applying advanced MIMO processing schemes, which allows the received signals at the N_B ports of the Butler matrix to be jointly processed in the baseband, and hence effectively mitigates IBI and improves the achievable capacity. This technique does not involve interference avoidance. It mitigates interference through joint detection of the multiple data streams (uplink case) or a form of interference pre-cancellation known as pre-coding (downlink case). The present evaluation in this report focuses on the uplink, thus all the MIMO schemes considered refer to joint signal detection. These techniques can be divided into linear and non-linear schemes.

For linear MIMO detection, the signal received by each beam is a superposition of the useful signal and interfering signal components. The contribution of each of these components depends on the state of the wireless channel through which they propagate; this can be described by a matrix of channel coefficients. If this channel matrix is known by the HBS, IBI can be cancelled through post-processing. More specifically the received signal of each beam can be multiplied by a set of weights that are designed so that the contribution of the interfering components is minimized. These weights can be grouped into a matrix which represents the receive filter. The simplest criterion for designing receive filter matrix is Zero-Forcing (ZF), where this matrix is the inverse of **H** and in this way all interference is cancelled. A criterion for designing filter matrix that leads to better results than ZF is the Minimum Mean Square Error (MMSE). These schemes are called linear as the extracted symbols result from a linear combination of the received signals. For further details see [Spe04].

The achieved capacity can be further improved if the interfering signal components are successively cancelled. In this way symbol detection is done successively; the detected symbols are subtracted from the received signal so that they do not interfere with the symbols to be detected later on. The applied filter can either implement ZF or MMSE, with the latter leading to superior performance. Successive interference cancellation (SIC) techniques are non-linear as the extracted symbols no longer result from a linear combination of the received signals. For further details on SIC see [Spe04].

5.2.1 System Model:

We assume that backhaul link for BuNGee in a square cell consists of one HBS equipped with N antennas and K HSSs (here HSS is initially treated as a single antenna terminal to simplify the explanation of MBA-MIMO). We are concerned with the uplink transmission of the Backhaul link but similar ideas can be readily applied in the downlink. The HBS-to-HSS channel is a frequency-selective channel with L taps as described in section 2.1.2. Orthogonal Frequency Division Multiplexing (OFDM) is employed to combat the frequency-selective fading. The number of orthogonal subcarriers is denoted as Q. The total bandwidth is B Hz and hence the subcarrier spacing is $B_c = \frac{B}{Q}$. Let $\mathcal{A}$ be a set of HSSs scheduled for transmission, where $|\mathcal{A}| \leq \mathrm{K} \leq \mathrm{N_B}$ and $|\mathcal{A}|$ is the cardinality of the set $\mathcal{A}$. The concatenated multi-user physical channel matrix is denoted as $\mathbf{H}_\mathrm{q}$, where $\mathbf{H}_\mathrm{q} \in \mathbb{C}^{N\times|\mathcal{A}|}$ and $\mathbb{C}^\mathrm{F}$ represents a complex sapce with F dimensions. A Buter matrix lies between the BS antennas and the RF chains, and has the transfer function $\mathbf{G} = \left[\mathbf{g_1}, \mathbf{g}_2, \cdots, \mathbf{g}_{N_B}\right]^T$ of dimension $N_B \times N$, where $N_B \leq N$. The vector of weights applied to the received signal by the N antennas contributing to the i^{th} beam is $\mathbf{g}_\mathrm{i} \in \mathbb{C}^{N\times 1}$, $i = 1,2,\cdots, N_B$. Incorporating the effects of both the physical multiuser channel and Butler matrix, we obtain a composite channel matrix with dimension $N_B \times |\mathcal{A}|$:

$$\begin{aligned}\tilde{\mathbf{H}}_q &= \mathbf{G}\mathbf{H}_q \\ &= \left[\tilde{\mathbf{h}}_{1,q}, \tilde{\mathbf{h}}_{2,q}, \cdots, \tilde{\mathbf{h}}_{|\mathrm{A}|,q}\right]\end{aligned} \tag{5.1}$$

for the q^{th} subcarrier, where $\tilde{\mathbf{h}}_{j,q} \in \mathbb{C}^{N_B\times 1}$ represents a channel vector for all beams corresponding to the j^{th} scheduled HSS, $j = 1,2,\cdots,|\mathcal{A}|$. The signal vector received at the output of the N_B ports of HBS for the q^{th} subcarrier can be expressed in form of:

$$\tilde{\mathbf{Y}}_q = \mathbf{G}\mathbf{H}_q\mathbf{s}_q + \mathbf{z}_q = \tilde{\mathbf{H}}_q\mathbf{s}_q + \mathbf{z}_q \tag{5.2}$$

where $\tilde{\mathbf{Y}}_q \in \mathbb{C}^{\mathrm{N}\times 1}$ and $s_q \in \mathbb{C}^{|\mathcal{A}|\times 1}$ is the vector of transmit symbols for the q^{th} subcarrier with power:

$$\mathbf{P}_q = \left[p_{1,q}, p_{2,q}, \cdots, p_{|\mathrm{A}|,q}\right] \tag{5.3}$$

Here $\mathbf{z}_q$ represents the additive white Gaussian noise (AWGN) vector for the q^{th} subcarrier with covariance $\boldsymbol{E}\left[\mathbf{z}_q\mathbf{z}_q^{\mathrm{H}}\right] = \sigma_\mathrm{z}^2\mathbf{I}_{N_B}$, where $\sigma_\mathrm{z}^2 = VK_BT_0B_C$. K_B denotes the Boltzman constant and T_0 is the standard noise temperature in kelvin. V represents the noise figure defined as the ratio of the output noise power to the thermal noise power in the input.

In this section we consider an equal power allocation strategy for each subcarrier, resulting in $p_{j,q} = \sigma_s^2 = \frac{P_S}{Q}$, $\forall j \in |\mathcal{A}|$, and $q = 1,2,\cdots,Q$. P_s is the transmit power of one HSS.

5.2.2 Linear Detection:

In the case of linear detection, a beamforming matrix $\mathbf{W}_q = [\mathbf{w}_{1,q}, \mathbf{w}_{2,q}, \cdots, \mathbf{w}_{|\mathcal{A}|,q}]$ of dimension $N_B \times |\mathcal{A}|$ is applied to the received signals $\tilde{\mathbf{Y}}_q$. $\mathbf{w}_{j,q} \in \mathbb{C}^{N_B \times 1}$ represents the beamforming vector corresponding to the j^{th} HSS and the q^{th} subcarrier. The transmitted signal vector from the scheduled HSSs based on the q^{th} subcarrier is extracted at the HBS, expressed as:

$$\mathbf{Y}_q = \mathbf{W}_q^H \tilde{\mathbf{Y}}_q = \mathbf{W}_q^H \tilde{\mathbf{H}}_q \mathbf{s}_q + \mathbf{W}_q^H \mathbf{z}_q \tag{5.4}$$

where the operator $(\cdot)^H$ denotes the transpose conjugate. The filter output for the j^{th} HSS is written as:

$$y_{j,q} = \mathbf{w}_{j,q}^H \tilde{\mathbf{h}}_{j,q} s_{j,q} + \sum_{n=1, n\neq j}^{|\mathrm{A}|} \mathbf{w}_{j,q}^H \tilde{\mathbf{h}}_{n,q} s_{n,q} + \mathbf{w}_{j,q}^H \mathbf{z}_q \tag{5.5}$$

The SINR for the j^{th} HSS and the q^{th} subcarrier is:

$$\gamma_{j,q} = \frac{\left|\mathbf{w}_{j,q}^H \cdot \tilde{\mathbf{h}}_{j,q}\right|^2 \cdot \sigma_s^2}{\underbrace{\sum_{n=1, n\neq j}^{|\mathrm{A}|} \left|\mathbf{w}_{j,q}^H \cdot \tilde{\mathbf{h}}_{n,q}\right|^2 \sigma_s^2}_{\text{IBI}} + \underbrace{\sigma_z^2 \left\|\mathbf{w}_{j,q}^H\right\|^2}_{\text{Noise Enhancement}}} \tag{5.6}$$

The two terms of the denominator have a detrimental effect on the link throughput.

The beamforming matrix can be designed in terms of the Minimum Mean Square Error (MMSE) criterion, in order to achieve an optimal trade-off between noise enhancement and IBI. The beamforming matrix is expressed as:

$$\mathbf{W}_q = \left(\tilde{\mathbf{H}}_q \tilde{\mathbf{H}}_q^H + \frac{\sigma_z^2}{\sigma_s^2} \mathbf{I}_{N_B}\right)^{-1} \tilde{\mathbf{H}}_q \tag{5.7}$$

where $\sigma_s^2 = \frac{P_S}{Q}$ denotes the power of each subcarrier (equal power allocation) and all HSSs have the same total transmit power P_s.

The IBI plus noise term for the j^{th} HSS can be further expressed as:

$$\begin{aligned}
\xi &= \sigma_s^2 \left(\sum_{n=1, n\neq j}^{|\mathrm{A}|} \left|\mathbf{w}_{j,q}^H \cdot \tilde{\mathbf{h}}_{n,q}\right|^2 + \frac{\sigma_z^2}{\sigma_s^2} \left\|\mathbf{w}_{j,q}^H\right\|^2 \right) \\
&= \sigma_s^2 \left(\sum_{n=1, n\neq j}^{|\mathrm{A}|} \mathbf{w}_{j,q}^H \cdot \tilde{\mathbf{h}}_{n,q} \tilde{\mathbf{h}}_{n,q}^H \cdot \mathbf{w}_{j,q} + \frac{\sigma_z^2}{\sigma_s^2} \mathbf{w}_{j,q}^H \mathbf{w}_{j,q} \right) \\
&= \sigma_s^2 \mathbf{w}_{j,q}^H \left[\sum_{n=1, n\neq j}^{|\mathrm{A}|} \tilde{\mathbf{h}}_{n,q} \tilde{\mathbf{h}}_{n,q}^H + \frac{\sigma_z^2}{\sigma_s^2} \right] \mathbf{w}_{j,q} \\
&= \sigma_s^2 \mathbf{w}_{j,q}^H \Lambda \mathbf{w}_{j,q}
\end{aligned} \tag{5.8}$$

Combining equations (5.7) and (5.8), we have:

$$\mathbf{w}_{j,q} = \left(\tilde{\mathbf{h}}_{j,q} \tilde{\mathbf{h}}_{j,q}^H + \Lambda\right)^{-1} \tilde{\mathbf{h}}_{j,q} \tag{5.9}$$

where $\mathbf{\Lambda} = \sum_{n=1, n\neq j}^{|\mathcal{A}|} \tilde{\mathbf{h}}_{n,q} \tilde{\mathbf{h}}_{n,q}^H + \sigma_z^2 / \sigma_s^2$. Hence the IBI plus noise term is equal to:

$$\xi = \sigma_s^2 \mathbf{w}_{j,q}^H \tilde{\mathbf{h}}_{j,q} \left(1 - \mathbf{w}_{j,q}^H \tilde{\mathbf{h}}_{j,q}\right) \tag{5.10}$$

On returning to equation (5.6), the SINR for the j^{th} ABS and the q^{th} subcarrier is:

$$\gamma_{j,q} = \frac{\left|\mathbf{w}_{j,q}^H \cdot \tilde{\mathbf{h}}_{j,q}\right|^2 \sigma_s^2}{\sigma_s^2 \mathbf{w}_{j,q}^H \tilde{\mathbf{h}}_{j,q} \left(1 - \mathbf{w}_{j,q}^H \tilde{\mathbf{h}}_{j,q}\right)} = \frac{\mathbf{w}_{j,q}^H \cdot \tilde{\mathbf{h}}_{j,q}}{\left(1 - \mathbf{w}_{j,q}^H \tilde{\mathbf{h}}_{j,q}\right)} \tag{5.11}$$

This implies that the SINR at the output of the MMSE filter for the j^{th} HSS and the q^{th} subcarrier depends only on $\mathbf{w}_{j,q}$ and $\tilde{\mathbf{h}}_{j,q}$.

MMSE beamforming achieves an optimal trade-off between noise enhancement and IBI reduction. However in some cases where zero forcing is preferred, the beamforming matrix is the Moore-Penrose pseudoinverse of $\tilde{\mathbf{H}}_q$, expressed as $\mathbf{W}_q = (\tilde{\mathbf{H}}_q \tilde{\mathbf{H}}_q^{\mathrm{H}})^{-1} \tilde{\mathbf{H}}_q$. The equivalent SINR can be obtained using equation (5.6).

5.2.3 Successive Interference Cancellation:

The capacity can be further improved if the detection is performed in a successive fashion, i.e., the symbols being detected is subtracted from the remaining received signal. This frees the singal from some interference components and can effectively enhance the achievable capacity. The composite channel of the scheduled users at the q^{th} subcarrier is $\tilde{\mathbf{H}}_q = [\tilde{\mathbf{h}}_{1,q}, \tilde{\mathbf{h}}_{2,q}, \cdots, \tilde{\mathbf{h}}_{|\mathcal{A}|,q}]$ is arranged in an ascending order with regard to their Euclidean norm, such that $\| \tilde{\mathbf{h}}_{1,q} \| \leq \| \tilde{\mathbf{h}}_{2,q} \| \leq \cdots \leq \| \tilde{\mathbf{h}}_{|\mathcal{A}|,q} \|$.

We consider again the MMSE detection for successive interference cancellation. The beamforming vector $\mathbf{w}_{j,q}$ of the j^{th} HSS is the first column of the beamforming matrix,

$$\mathbf{W}_q = \left(\tilde{\mathbf{H}}_{j,q} \tilde{\mathbf{H}}_{j,q}^H + \frac{\sigma_z^2}{\sigma_s^2} \mathbf{I}_{N_B} \right)^{-1} \tilde{\mathbf{H}}_{j,q} \tag{5.12}$$

where $\tilde{\mathbf{H}}_{j,q} = [\tilde{\mathbf{h}}_{j,q}, \tilde{\mathbf{h}}_{j+1,q}, \cdots, \tilde{\mathbf{h}}_{|\mathcal{A}|,q}]$. The SINR for the j^{th} detected HSS and the q^{th} subcarrier is:

$$\gamma_{j,q} = \frac{\left|\mathbf{w}_{j,q}^H \cdot \tilde{\mathbf{h}}_{j,q}\right|^2 \cdot \sigma_s^2}{\sum_{n=j+1}^{|\mathrm{A}|} \left|\mathbf{w}_{j,q}^H \cdot \tilde{\mathbf{h}}_{n,q}\right|^2 \sigma_s^2 + \sigma_z^2 \left\|\mathbf{w}_{j,q}^H\right\|^2} \tag{5.13}$$

Following the same derivation from (5.7) – (5.11), we can also calculate SINR for the case of sucessive interference cancellation using (5.11). However, the beamforming vector $\mathbf{w}_{j,q}$ is re-calculated after cancelling $s_{j-1,q}$.

As each HSS is affected by IBI from HSSs having higher index, the capaciy will be greatly improved as compared with the linear detection.

5.2.4 Numerical Results:

In this section we present the numerical results based on the aforementioned MBA-MIMO detection approaches and on the BuNGee architecture. A ray-tracing simulator which is exclusively developed for the BuNGee project provides data of the pathloss and shadowing. BuNGee is a wireless network with a hierarchical structure, where a high-capacity HBS creates multiple narrow beams by employing a Butler matrix, for the sake of feeding a number of HSSs which in turn serve the users. We are concerned with the

evaluation of the achievable rates in the backhaul network (HBS-HSSs), where SBP and MBA-MIMO techniques are employed. An urban scenario is considered where the HBS is equipped with multiple antennas and is deployed above-roof-top at a height of 25 m. The HBS uses a BM which generates $N_B = 12$ narrow beams feeding $|\mathcal{A}| = 11$ HSSs which are deployed at the street level (below-roof-top) at a height of 5 m. Each HSS employs a single directional antenna which points at the direction of the HBS beam providing the maximum power. The ray-tracing simulator developed provides the average power profile of the composite matrix $\tilde{\mathbf{H}}_q$ describing both effects of the wireless achannel and the Butler matrix.

As described in section 2.1.2, BunGee's backhaul link is a frequency selective channel and hence a 7-tap BuNGee TDL (B-TDL) model is specifically developed. Unlike the most tapped delay line models presented in the literature where tap amplitudes are assumed to be Rayleigh-distributed, magnitudes of all taps in the B-TDL model are all Ricean-distributed instead of Rayleigh. Each tap has a different K-factor and the corresponding B-TDL model parameters are summarized in section 2.2.2. Besides, instead of a zero-phase line-of-sight (LOS) component, the B-TDL employs a uniformly distributed random phase for the LOS component of the tap. We also employ OFDM to combat the frequency-selectivity fading. The number of subcarriers employed in simulation is $Q = 64$ and the cyclic prefix length is equal to D = 4 symbol periods. We consider 1000 randomly chosen channel fading coefficients to calculate SINR of the j^{th} detected HSS and the q^{th} subcarrier. The total bandwidth is $B = 20$ MHz.

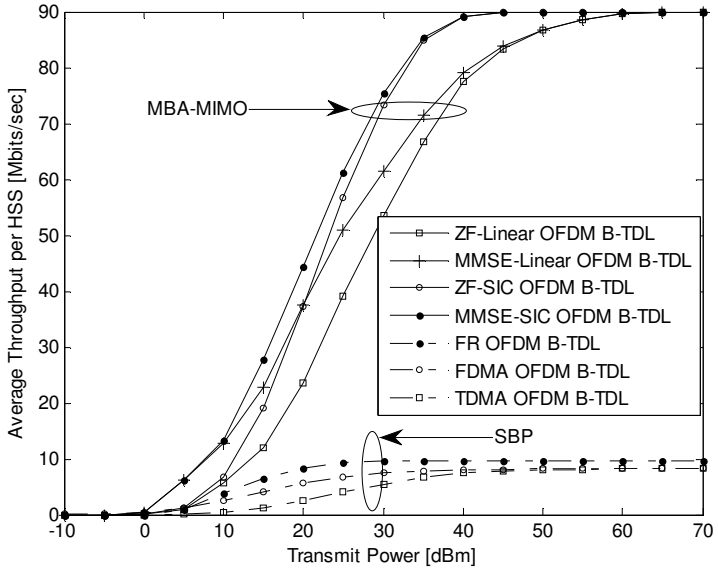

Figure 5-1 Average throughput under TSB against HSS transmit power; B-TDL model; Bandwidth 20 MHz.

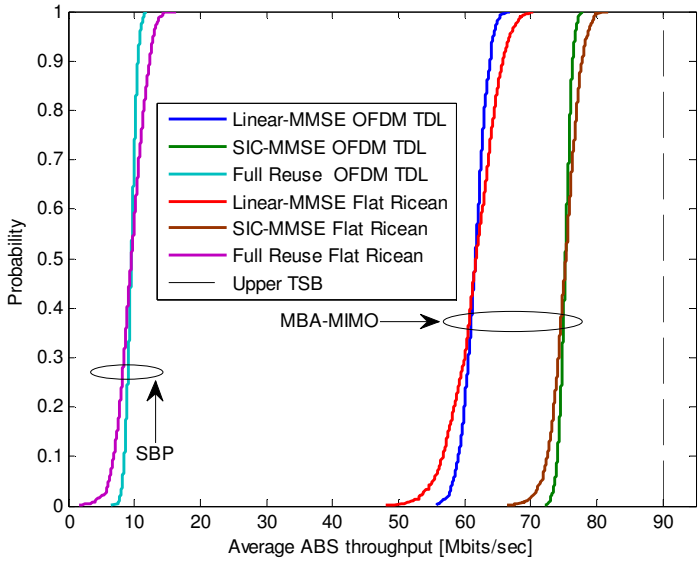

Figure5-2 Average throughput CDF for FR, linear-MMSE and SIC-MMSE under TSB for frequency-selective and flat fading channels; Power = 30 dBm.

Figure 5-1 plots the average truncated throughput of HSSs as a function of the HSS transmit power P_s for the case of SBP and MBA-MIMO detection. SBP is simulated on the basis of an efficient beam allocation algorithm. We give simulation results for the achievable rate in the case of full frequency reuse (FR) where all beams utilize the 20 MHz bandwidth, Frequency Division Multiple Access (FDMA) and of Time Division Multiple Access (TDMA). Amongst these cases, the FR scheme results in superior performance, shown as the dash-dot curve with dot marker. For the case of MBA-MIMO both linear detection and SIC have been considered under ZF and MMSE. It can be seen that detection based on SIC performs the best and MMSE beamforming outperforms ZF as expected. In general MBA-MIMO greatly outperforms SBP when the HSS transmit power exceeds 15 dBm. It should be noted that the achievable rates saturate as a result of the effect of the TSB. The achievable capacity density for the transmit power of 1 W (30 dBm) with SIC is approximately $75 \times 21 = 1.58$ Gbit/s/km^2, as there will be about 21 ABSs deployed per km^2. A typical bandwidth allocation of 40 MHz results in $1.58 \times 2 = 3.16$ Gbit/s/km^2. This shows that MBA-MIMO allows a capacity density well above the required 1 Gbit/s/km^2 which makes it very suitable for future wireless systems.

Figure5-2 plots the Cumulative Distribution Function (CDF) of the average HSS truncated throughput. For SBP we assume that the full reuse scheme is used, while MBA-MIMO is based on either Linear-MMSE or SIC-MMSE. Each HSS transmits the same power of 1 W (30 dBm). The plot also presents a comparison of the achievable rates based on the B-TDL channel model using OFDM and on the flat fading channel. Since the amplitude of each tap in B-TDL is Ricean-distributed, we assume a Ricean fading channel for the flat fading case. It can be seen that SIC-MMSE outperforms the other schemes while the two MBA-MIMO based schemes greatly outperform FR. Furthermore frequency-selective channels offer a diversity advantage which is exploited by OFDM resulting in much steeper CDF curves. This implies that OFDM results in better performance for the users experiencing more severe channel conditions as it exploits the inherent diversity of frequency selectivity.

5.3 Effect of inter-HBS interference

Interference is one of the main difficulties that beyond next generation wireless networks will encounter. Understanding the nature and properties of the interference are crucial in these inherently interference-limited networks. In this section, backhaul capacities are evaluated based on some possible interference models of BuNGee architecture developed by UCL.

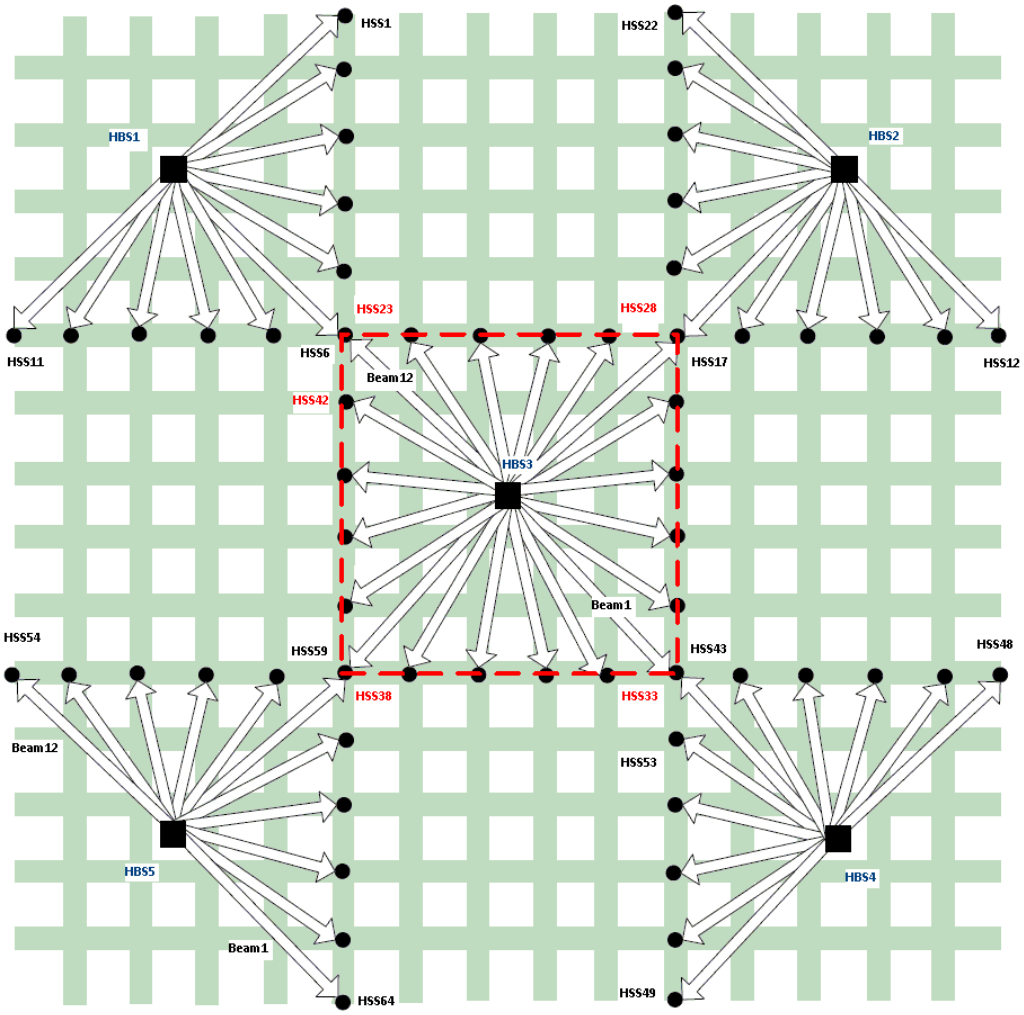

Figure 5-3 Multi-HBS interference secenario with square topology for HSS deployment. [UCL]

A ray-tracing simulator has been developed, which calculates path gain between each beam of HBS and each HSS receive antenna, for multi-HBS interference scenario. (Note that we express the path loss in dB in the form of a negative path gain). In this interference scenario, 5 HBSs are placed as transmit antennas so that they cover a total of 225 building blocks. A total number of 72 beams are utilized in this multi-HBS scenario. Details of this multi-HBS interference scenario are presented in Figure 5-3, where both HBSs and HSSs are numbered in a clockwise direction according to the needs of subsequent work. However, the beams of the HBS antennas are numbered in anti-clockwise direction. This multi-HBS interference scenario becomes very complex due to the large number of blocks and the dense HSS antenna deployment. Therefore, we have extracted results only for two representative base stations, which are HBS5 (Corner case) and HBS3 (Middle case), respectively. Corresponding results for all other HBSs can be evaluated from the symmetric property of the defined scenario. All simulation results are extracted with a $\pm 45^{\circ}$ polarized transmit antenna and $\pm 45^{\circ}$ polarized receive antenna. The corner HSSs (23, 28, 33, and 38) of HBS3 are simulated twice for the respective antenna directions of the two HBSs from which these may be served.

For the corner case, the signals transmitted from HSS54 – HSS64 are the intended signals for HBS5. Signals coming from HSSs of all other HBS (1-4) cells are interference for HBS5. Path loss between each beam of HBS5 and all 60 HSSs have been determined using the ray-tracing simulator. From the results reported in [BunD21], interference from the immediate neighbouring HSS antenna is high at some HBSs. For example, there is significant interference from some HSSs in the cell area of neighbouring HBS1, HBS3 and HBS4. In particular it increases considerably when the HSSs of those cell areas are facing towards HBS5.

For the middle case, signals transmitted from HSS23 – HSS42 are the intended signals for HBS3. Here (unlike the corner HBS scenario) we consider all 20 HSSs around the HBS3 as the in-cell signals which will

be detected by HBS3. All HSSs in the cell coverage of HBSs (1, 2, 4, and 5) serve as the interference. Detailed path gains are summarized in the Appendix of [BunD21].

Without loss of generality, notations denoted in section 5.2 also apply to the multi-cell case. However, we need to add some new notation for the multi-cell interference model. Let P_{int} be the transmit power from each of the interfering HSSs, while we still make the equal power assignment assumption such that the interference power at each subcarrier is $\sigma_{\text{int}}^2 = \frac{P_{\text{int}}}{Q}$. Then we define $\mathbf{M}_{\text{int}} \in \mathbb{C}^{N_B \times N_{\text{int}}}$ and $\mathbf{M} \in \mathbb{C}^{N_B \times |\mathcal{A}|}$ as the path gain matrices for out-of-cell HSSs (interference) and in-cell HSSs, where N_{int} denotes the number of interfering HSSs. The composite channel matrix between the beams of the target HBS and all interfering HSSs for the q^{th} subcarrier is represented as $\widetilde{\mathbf{H}}_{\text{int},q}$. The Interference-to-Noise Ratio (INR) at the $u^{\text{th}}, u = 1, 2, \cdots, N_B$ beam of the in-cell HBS can be expressed as:

$$INR_u = \frac{P_{\text{int}}}{\sigma_z^2} \sum_v \mathbf{M}_{\text{int}}[u, v] \tag{5.14}$$

where $\mathbf{M}_{\text{int}}[u, v]$ denotes the element of the u^{th} row and the v^{th} column of matrix $\mathbf{M}_{\text{int}}$. The average INR at each beam is:

$$\overline{INR} = \frac{1}{N_B} \sum_u INR_u \tag{5.15}$$

and the average SINR at each beam is:

$$\overline{SINR} = \frac{1}{N_B} \sum_u \frac{P_s \cdot \sum_j \mathbf{M}[u, j]}{P_{\text{int}} \cdot \sum_v \mathbf{M}_{\text{int}}[u, v] + \sigma_z^2} \tag{5.16}$$

We are able to determine P_{s} and P_{int} in terms of the given $\overline{INR}$ and $\overline{SINR}$ values. Then we have:

$$P_{\text{int}} = \frac{\overline{INR} \cdot N_B \cdot \sigma_z^2}{\sum_u \sum_v \mathbf{M}_{\text{int}}[u, v]} \tag{5.17}$$

and the transmit power of each HSS in the target cell can be expressed as:

$$P_s = \frac{\overline{SINR} \cdot N_B}{\sum_j \mathbf{M}[u, j]} \Bigg/ \sum_u \frac{1}{\sum_v \mathbf{M}_{\text{int}}[u, v] \cdot \frac{\overline{INR} \cdot N_B \cdot \sigma_z^2}{\sum_u \sum_v \mathbf{M}_{\text{int}}[u, v]} + \sigma_z^2} \tag{5.18}$$

Due to the effects of the multi-cell interference, the filter output for the q^{th} subcarrier and the j^{th} HSS is written as:

$$y_{j,q} = \mathbf{w}_{j,q}^H \tilde{\mathbf{h}}_{j,q} s_{j,q} + \sum_{n \in \text{A}, n \neq j} \mathbf{w}_{j,q}^H \tilde{\mathbf{h}}_{n,q} s_{n,q} + \mathbf{w}_{j,q}^H \tilde{\mathbf{H}}_{\text{int}} s_{\text{int}} + \mathbf{w}_{j,q}^H \mathbf{z}_q \tag{5.19}$$

where s_{int} is a column vector comprising all interfering HSSs signals. Based on the current multi-HBS network deployment, we consider only the case that channel conditions of all interfering HSSs are unknown at the in-cell HBS. We make, however, a reasonable assumption that the interference channels are all independent complex Gaussian channels for the beam domain signal processing at the in-cell HBS. Then in the multi-cell scenario, the equivalent SINR $\rho_{\text{j,q}}$ for the q^{th} subcarrier and the j^{th} HSS after the MMSE filter is:

$$\rho_{j,q} = \frac{\left|\mathbf{w}_{j,q}^H \cdot \tilde{\mathbf{h}}_{j,q}\right|^2 \cdot \sigma_s^2}{\underbrace{\sum_{n=1,n\neq j}^{|\mathrm{A}|} \left|\mathbf{w}_{j,q}^H \cdot \tilde{\mathbf{h}}_{n,q}\right|^2 \sigma_s^2}_{\text{IBI}} + \underbrace{\sigma_{\text{int}}^2 \cdot \sum_{v=1}^{N_{\text{int}}} \mathbf{w}_{j,q}^H \cdot \boldsymbol{E}\left\{\tilde{\mathbf{h}}_{\text{int},v} \cdot \tilde{\mathbf{h}}_{\text{int},v}^H\right\} \mathbf{w}_{j,q}^H}_{\text{Multi-HBS Interference}} + \underbrace{\sigma_z^2 \left\|\mathbf{w}_{j,q}^H\right\|^2}_{\text{Noise Enhancement}}}$$
$$= \frac{\left|\mathbf{w}_{j,q}^H \cdot \tilde{\mathbf{h}}_{j,q}\right|^2}{\sum_{n=1,n\neq j}^{|\mathrm{A}|} \left|\mathbf{w}_{j,q}^H \cdot \tilde{\mathbf{h}}_{n,q}\right|^2 + \frac{\sigma_{\text{int}}^2}{\sigma_s^2} \mathbf{w}_{j,q}^H \cdot \mathrm{Diag}\left(\sqrt{\mathbf{M}_{\text{int}}\mathbf{M}_{\text{int}}^H}\right) \mathbf{w}_{j,q}^H + \frac{\sigma_z^2}{\sigma_s^2} \left\|\mathbf{w}_{j,q}^H\right\|^2} \quad (5.20)$$

Note that σ_{int}^2 and σ_s^2 are the immediate solutions based on equations (5.17) and (5.18). $\tilde{\mathbf{h}}_{\text{int},v}$ is the v^{th} column of the composite channel matrix $\tilde{\mathbf{H}}_{\text{int},q}$. Based on our assumption for the interference channel, $\boldsymbol{E}\{\tilde{\mathbf{h}}_{\text{int},v} \cdot \tilde{\mathbf{h}}_{\text{int},v}^H\}$ produces a diagonal matrix where the elements in the diagonal are the sum of the corresponding complex Gaussian channel variances, which also serve as the path loss. Also, the second term in the denominator of equation (5.20) is the multi-HBS interference which has a further detrimental effect on the link throughput.

The beamforming matrix can be designed in terms of the MMSE or ZF criterion. Here we only show the MMSE beamforming matrix for the q^{th} subcarrier and the j^{th} HSS, expressed as:

$$\mathbf{W}_q = \left(\tilde{\mathbf{H}}_q \tilde{\mathbf{H}}_q^H + \frac{\sigma_{\text{int}}^2}{\sigma_s^2} \mathrm{Diag}\left(\sqrt{\mathbf{M}_{\text{int}}\mathbf{M}_{\text{int}}^H}\right) + \frac{\sigma_z^2}{\sigma_s^2} \mathbf{I}_{N_B}\right)^{-1} \tilde{\mathbf{H}}_q \quad (5.21)$$

The denominator of equation (5.20) can be further expressed as:

$$\xi_{\text{int}} = \sigma_s^2 \left(\sum_{n=1,n\neq j}^{|\mathrm{A}|} \left|\mathbf{w}_{j,q}^H \cdot \tilde{\mathbf{h}}_{n,q}\right|^2 + \frac{\sigma_{\text{int}}^2}{\sigma_s^2} \mathbf{w}_{j,q}^H \cdot \mathrm{Diag}\left(\sqrt{\mathbf{M}_{\text{int}}\mathbf{M}_{\text{int}}^H}\right) \mathbf{w}_{j,q}^H + \frac{\sigma_z^2}{\sigma_s^2} \left\|\mathbf{w}_{j,q}^H\right\|^2 \right)$$
$$= \sigma_s^2 \mathbf{w}_{j,q}^H \left[\underbrace{\sum_{n=1,n\neq j}^{|\mathrm{A}|} \tilde{\mathbf{h}}_{n,q} \tilde{\mathbf{h}}_{n,q}^H + \frac{\sigma_{\text{int}}^2}{\sigma_s^2} \mathrm{Diag}\left(\sqrt{\mathbf{M}_{\text{int}}\mathbf{M}_{\text{int}}^H}\right) + \frac{\sigma_z^2}{\sigma_s^2}}_{\Lambda_{\text{int}}} \right] \mathbf{w}_{j,q} \quad (5.22)$$
$$= \sigma_s^2 \mathbf{w}_{j,q}^H \Lambda_{\text{int}} \mathbf{w}_{j,q}$$

Combining equations (5.21) and (5.22), and performing some algebraic operations, we have:

$$\mathbf{w}_{j,q} = \left(\tilde{\mathbf{h}}_{j,q} \tilde{\mathbf{h}}_{j,q}^H + \Lambda_{\text{int}}\right)^{-1} \tilde{\mathbf{h}}_{j,q} \quad (5.23)$$

The equivalent SINR $\rho_{j,q}$ for the q^{th} subcarrier and the j^{th} HSS is simplified as:

$$\rho_{j,q} = \frac{\mathbf{w}_{j,q}^H \cdot \tilde{\mathbf{h}}_{j,q}}{\left(1 - \mathbf{w}_{j,q}^H \tilde{\mathbf{h}}_{j,q}\right)} \quad (5.24)$$

This is the same as equation (5.11) and also implies that in the case of multi-HBS, the equivalent SINR at the output of the MMSE filter for the q^{th} subcarrier and the j^{th} HSS depends only on the filter vector $\mathbf{w}_{\text{j,q}}$ and $\tilde{\mathbf{h}}_{j,q}$.

We can also calculate SINR in the same way as for the successive interference cancellation, for the multi-HBS case. The equivalent SINR $\rho_{j,q}$ for the q^{th} subcarrier and the j^{th} HSS is:

$$\rho_{j,q} = \frac{\left|\mathbf{w}_{j,q}^H \cdot \tilde{\mathbf{h}}_{j,q}\right|^2}{\sum_{n=j+1}^{|\mathrm{A}|}\left|\mathbf{w}_{j,q}^H \cdot \tilde{\mathbf{h}}_{n,q}\right|^2 + \frac{\sigma_{\mathrm{int}}^2}{\sigma_s^2}\mathbf{w}_{j,q}^H \cdot \mathrm{Diag}\left(\sqrt{\mathbf{M}_{\mathrm{int}}\mathbf{M}_{\mathrm{int}}^H}\right)\mathbf{w}_{j,q}^H + \frac{\sigma_z^2}{\sigma_s^2}\left\|\mathbf{w}_{j,q}^H\right\|^2} \quad (5.25)$$

where the beamforming vector $\mathbf{w}_{j,q}$ of the j^{th} HSS is the first column of the beamforming matrix based on successive interference cancellation:

$$\mathbf{W}_q = \left(\tilde{\mathbf{H}}_{j,q}\tilde{\mathbf{H}}_{j,q}^H + \frac{\sigma_{\mathrm{int}}^2}{\sigma_s^2}\mathrm{Diag}\left(\sqrt{\mathbf{M}_{\mathrm{int}}\mathbf{M}_{\mathrm{int}}^H}\right) + \frac{\sigma_z^2}{\sigma_s^2}\mathbf{I}_{N_B}\right)^{-1}\tilde{\mathbf{H}}_{j,q} \quad (5.26)$$

The definition of $\tilde{\mathbf{H}}_{j,q}$ is shown in section 5.2.

The average throughput C is obtained by averaging over all throughputs of the in-cell HSSs, which is expressed as:

$$C = \frac{1}{|\mathrm{A}|}\sum_{j=1}^{|\mathrm{A}|}\log_2\left(1+\rho_{j,q}\right) \quad (5.27)$$

5.3.1 Numerical Results:

In this section we show the numerical results based on the aforementioned signal processing approaches in the presence of interference, and on the BuNGee architecture. Both corner and middle cases are considered to give the capacity results. The in-cell channel used is the 7-tap B-TDL model which is described in section 2.1.2, and we assume that all interference channels are independent complex Gaussian channels, where the respective path gain is obtained from a ray-tracing simulator developed by UCL.

First, we consider a case where the transmit powers for the in-cell HSSs P_{s} and interfering HSSs P_{int} are the same. Hence we are able to plot figures showing the relationship between the average throughput and power. Note that there are 20 HSSs serving as the useful signals for HBS3, but there are 11 HSSs for HBS5.

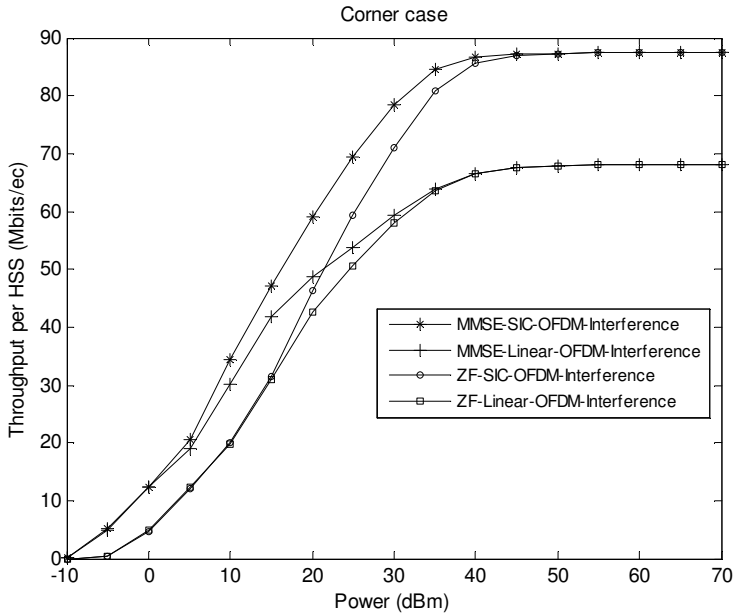

Figure 5-4 Average throughput under TSB against HBS transmit power based on Multi-HBS interference model; B-TDL channel model for the target cell; Bandwidth 20 MHz; OFDM; Corner Case.

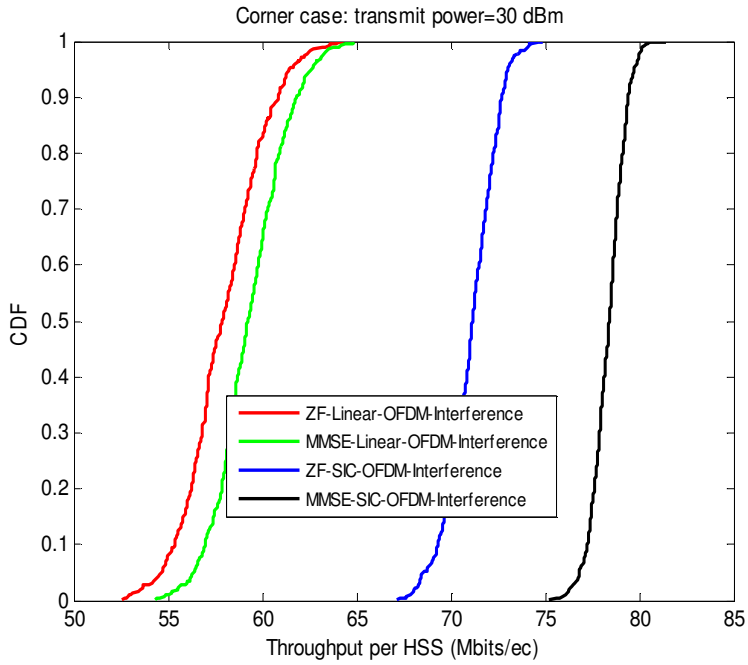

Figure 5-5 Average throughput CDF for Linear and SIC detection under TSB based on Multi-HBS interference model; Bandwidth 20 MHz; OFDM; Corner Case; Power = 30 dBm.

As seen from Figure 5-4, for the corner case, the achievable average throughput for BuNGee's backhaul link in the presence of multi-HBS interference is decreased. Especially for linear detection, the performance is greatly degraded, achieving a maximum average throughput around 68 Mbits/sec (22 Mbits/sec reduction compared to the single HBS case) at high power. For SIC detection, the performance is slightly decreased in comparison to the single HBS case, achieving a maximum average throughput around 87 Mbits/sec at high power.

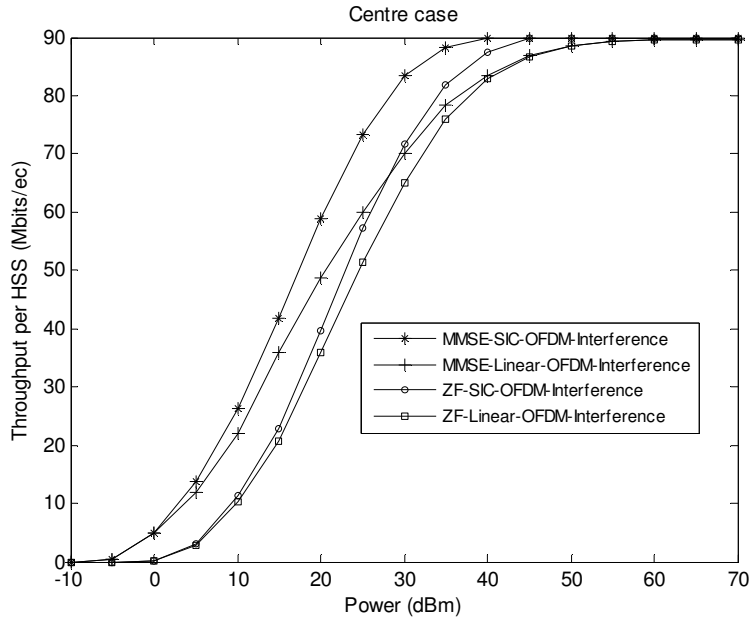

Figure 5-6 Average throughput under TSB against HBS transmit power based on Multi-HBS interference model; B-TDL channel model for the target cell; Bandwidth 20 MHz; OFDM; Middle Case.

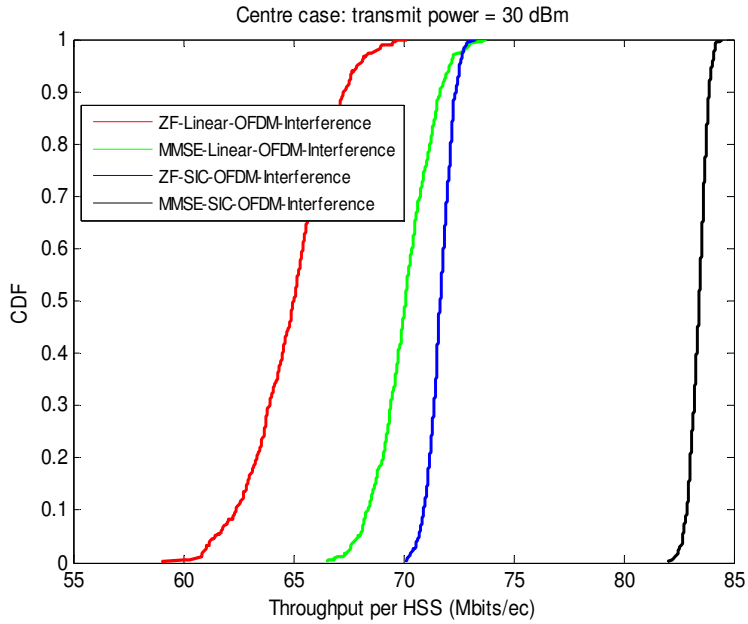

Figure 5-7 Average throughput CDF for Linear and SIC detection under TSB based on Multi-HBS interference model; Bandwidth 20 MHz; OFDM; Middle Case; Power = 30 dBm.

As seen from Figure 5-6, for middle case, the achievable average throughput for BuNGee backhaul link is better than the corner case. The reason is that the interference link of middle case has a reduced level of path gain, in comparison to the corner case (see Table 7-7 - Table 7-16 in [BunD21]). This in fact results in a relatively low interference, increases the equivalent SINR $\rho_{j,q}$ for the q^{th} subcarrier and the j^{th} HSS, and hence improves the average throughput. It can be observed that the maximum achievable average throughputs reach 90 Mbits/sec for both linear and SIC detection; but for corner case, the maximum achievable average throughput based on linear and SIC detection are 87 Mbits/sec and 67 Mbits/sec, respectively.

In the case where the transmit powers P_s and P_{int} are different, it is more reasonable to observe the average throughput in terms of the average SINR and INR.

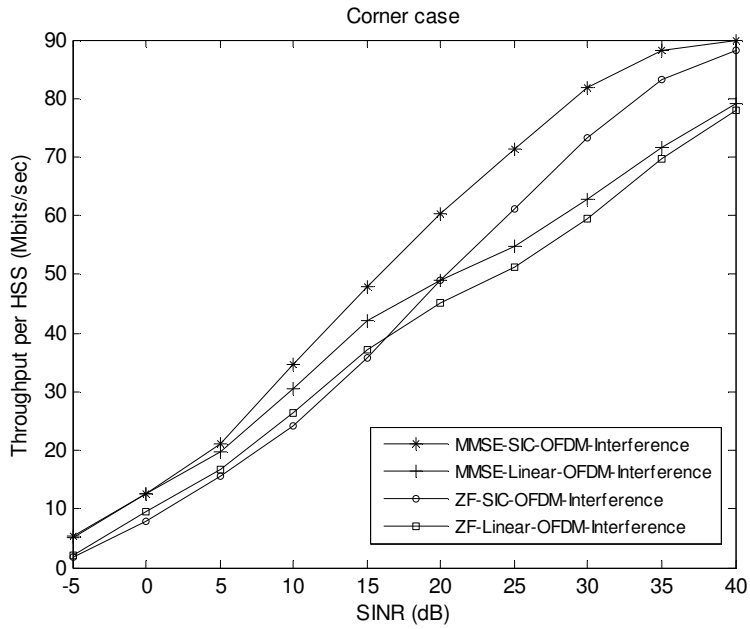

Figure 5-8 Average throughput under TSB against average SINR and fixed average INR=10 dB based on Multi-HBS interference model; B-TDL channel model for the target cell; Bandwidth 20 MHz; OFDM; Corner Case.

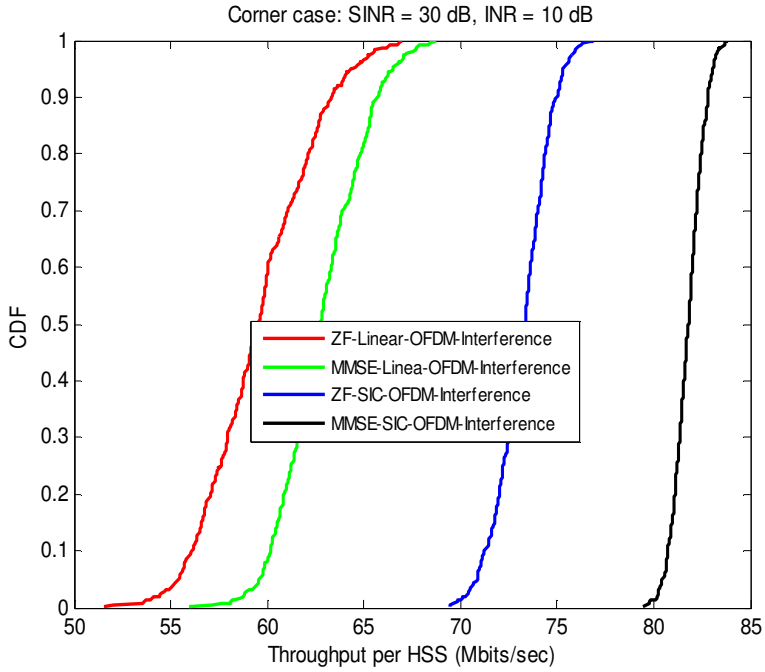

Figure 5-9 Average throughput CDF for Linear and SIC detection under TSB based on Multi-HBS interference model; Bandwidth 20 MHz; OFDM; Corner Case; SINR = 30 dB; INR=10 dB.

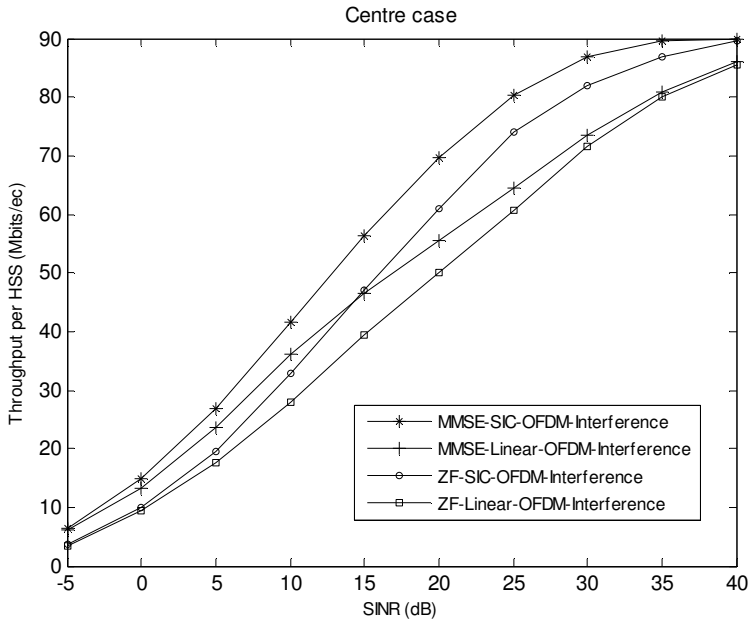

Figure 5-10 Average throughput under TSB against average SINR and fixed average INR=10 dB based on Multi-HBS interference model; B-TDL channel model for the target cell; Bandwidth 20 MHz; OFDM; Middle case.

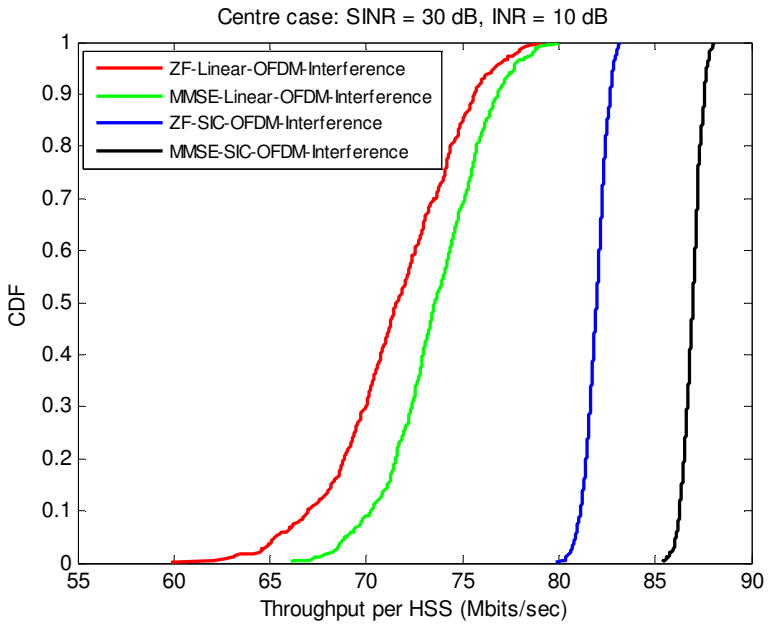

Figure 5-11 Average throughput CDF for Linear and SIC detection under TSB based on Multi-HBS interference model; Bandwidth 20 MHz; OFDM; Middle Case; SINR = 30 dB; INR=10 dB.

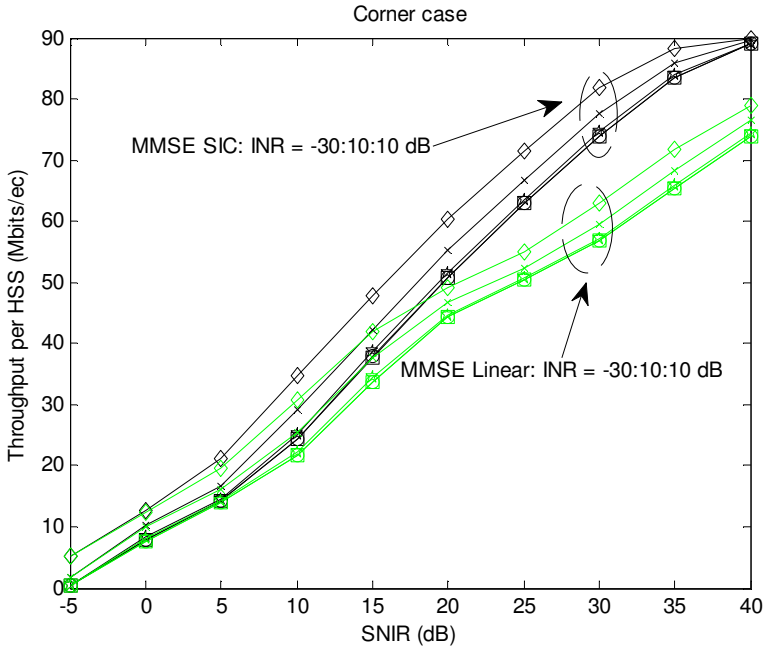

Figure 5-12 Average throughput under TSB against average SINR and different INR values, based on Multi-HBS interference model; B-TDL channel model for the target cell; Bandwidth 20 MHz; OFDM; Corner case.

As seen from Figure 5-12, the average INR has a small influence on the average throughput. We refer to the detailed explanation in [Bur12].

5.4 Dual polarised MBA-MIMO

So far, the concept of MBA-MIMO has been introduced and linear/non-linear MIMO processing techniques based on ZF and MMSE criteria are presented. However the dual-polarized backhaul link in BuNGee has not been taken into. In this section, we extend the results to dual-polarized channels.

In BuNGee, each beam and HSS is associated with a single dual-polarized antenna. Thus, the channels between an HSS and a beam at the HBS can be represented by a 2×2 matrix. Equation (5.1) can be re-written as follows:

$$\tilde{\mathbf{H}}_q = \left[\tilde{\mathbf{h}}^{+}_{1,q}, \tilde{\mathbf{h}}^{-}_{1,q}, \tilde{\mathbf{h}}^{+}_{2,q}, \tilde{\mathbf{h}}^{-}_{2,q}, \cdots, \tilde{\mathbf{h}}^{+}_{|\mathrm{A}|,q}, \tilde{\mathbf{h}}^{-}_{|\mathrm{A}|,q} \right] \tag{5.28}$$

where the channel matrix for the q^{th} subcarrier is $\tilde{\mathbf{H}}_q \in \mathbb{C}^{2N_B \times 2|\mathcal{A}|}$ and $\tilde{\mathbf{h}}^{+}_{i,q} / \tilde{\mathbf{h}}^{-}_{i,q} \in \mathbb{C}^{2\mathrm{N_B} \times 1}$ represents a channel vector for both polarizations of all beams corresponding to $\pm 45^{\circ}$ polarization of the j^{th} scheduled HSS. Omitting the upper index $+/-$ corresponding to the polarization directions and re-ordering the lower index of the channel vectors, the channel matrix $\tilde{\mathbf{H}}_{\mathrm{q}} \in \mathbb{C}^{2\mathrm{N_B} \times 2|\mathcal{A}|}$ remains the same as equation (5.1):

$$\tilde{\mathbf{H}}_q = \left[\tilde{\mathbf{h}}_{1,q}, \tilde{\mathbf{h}}_{2,q}, \cdots, \tilde{\mathbf{h}}_{2|\mathrm{A}|,q} \right]$$

The aforementioned MBA-MIMO processing techniques can then be directly applied for dual-polarized channels.

In ideal propagation conditions in which the two polarizations are orthogonal to each other, as described in Section 2.2, the system throughput is expected to be twice as that without dual-polarized antennas, since the MBA-MIMO system has doubled number of transmitters and receivers. Due to the existence of scattering in the propagation, the two polarizations are not purely orthogonal. In the extreme case where the signal of one polarization is received equally at the two polarization directions, the system will have the same performance as that without adopting polarized antennas. This extreme case often exists when the distance between the transmitter and receiver is large. A typical distance for such a scenario is 2.6 km [Jan04].

In BuNGee, the propagation condition is neither ideal nor extreme. Part of the power of one polarization leaks into the other polarization, resulting in correlated channel coefficients between channels of different polarization pairs. Therefore, the system performance adopting dual-polarized antennas is expected to be better than that without dual-polarized antennas, but less than double.

5.4.1 Numerical Results:

In this part, we evaluate the throughput of the backhaul link with dual-polarized antennas via numerical results obtained in simulation. The same settings of the simulation as those in Section 5.2 are used. Specifically, we consider an OFDM system with bandwidth $B = 20$ MHz and $Q = 64$ sub-carriers. The path loss from different HSSs to the beams at HBS is generated using the same ray-tracing simulator. In the centre cell, 24 beams serve 20 HSSs simultaneously; while in the corner cells, 12 beams are used to serve the 11 HSSs. All the cells in Figure 5-3 use the same frequency band.

The instantaneous channel coefficients are generated according to the procedures presented in Section 2.2. It is important to mention that by assuming that the distance from interfering HSSs to the target HBS is relatively large and to simplify the simulation, signals from cells other than the target cell are assumed to take the extreme propagation condition, i.e., there is no polarizataion discrimination, and hence the interference power is the same in both polarizations. Additionally, the inter-cell interference is treated as noise, i.e., instead of generating random channel coefficients for interference channels, we take the average values according to the path loss.

To provide a fair comparison between the results obtained here using the dual-polarized model and that in Section 5.3, similar simulations are carried out. First, we consider the case that the transmit power of each HSS P_s in the target cell and the power of interfering HSSs P_{int} are the same. Furthermore, the power is equally allocated into the two polarizations. Figure 5-13 and Figure 5-14 show the average throughput over the HSSs for both corner case and centre case. Compared with the performance without dual-polarized antennas, it can be seen that the system throughput increases significantly. At a transmit power at 30 dBm (1W), the average throughput per HSS achieved with MMSE-SIC is 146.3 Mbits/sec and 78.35 Mbits/sec with and without dual-polarization, respectively. Similar results have been obtained for the centre case and in other detection methods.

Again, it can be seen the performance difference between the corner case and the centre case especially for linear detection. With the assumption that all the HSSs have the same transmit power, the averaged signal to noise ratio is related to the ratio between in-cell path loss and inter-cell path loss. For the corner case, since the number of interfering HSSs is larger and inter-cell path loss is stronger, the achievable SNR is smaller.

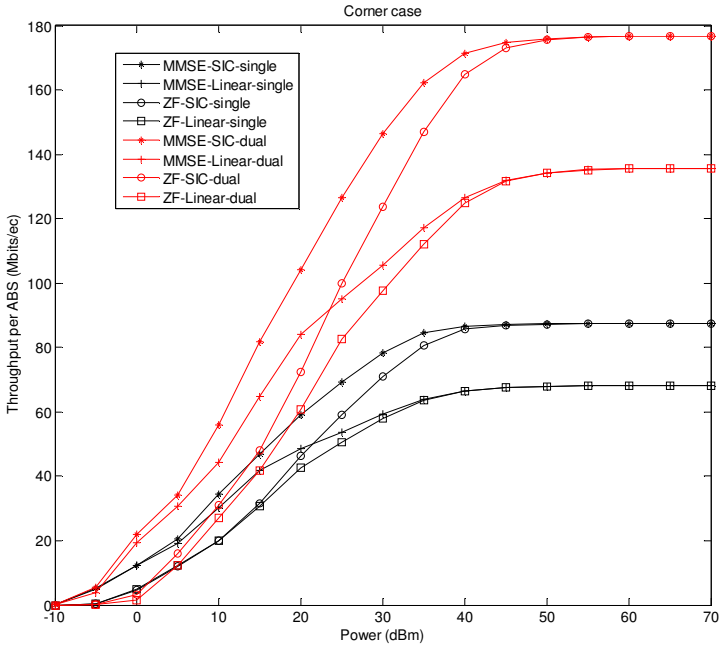

Figure 5-13 Average throughput under TSB against HSS transmit power: Corner case.

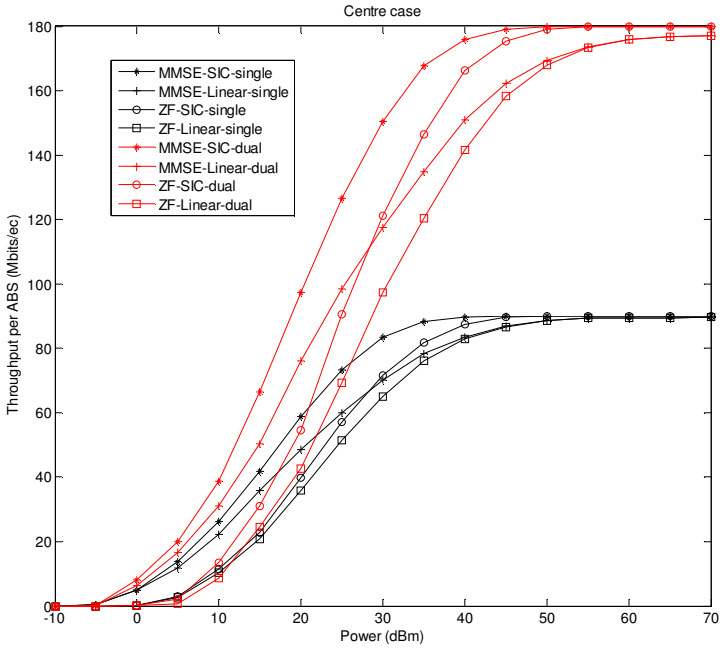

Figure 5-14 Average throughput under TSB against HSS transmit power: Centre case.

In the second simulation settings, the constraint that P_s and P_{int} are the same is relaxed. The results obtained here are presented with respect to the averaged SINR and INR. Figure 5-15 and Figure 5-16 show the average throughput per HSS with respect to the average SINR. The INR is fixed at 10 dB. A considerable throughput increase is achieved by adopting dual-polarized antennas. Figure 5-17 shows the throughput change when INR level varies. The behaviour is similar to that without dual-polarized antennas.

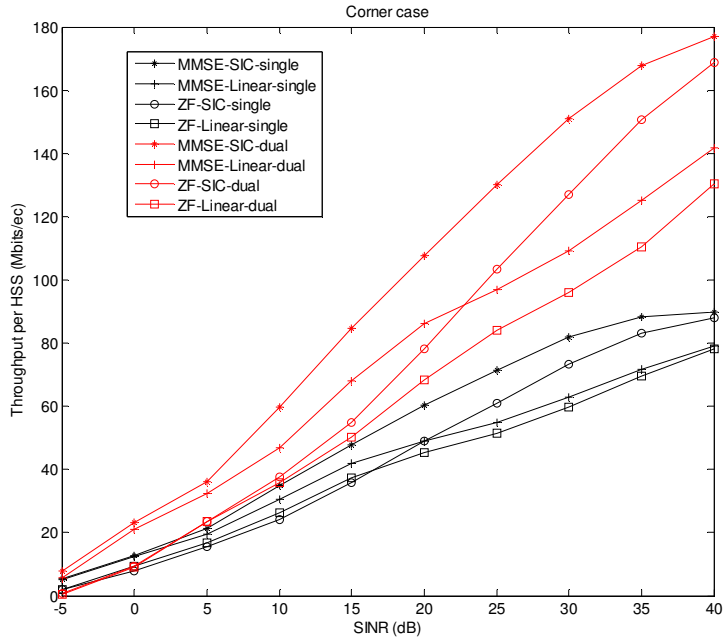

Figure 5-15 Average throughput under TSB against average SNIR and fixed average INR=10 dB based on Multi-HBS interference model: Corner case.

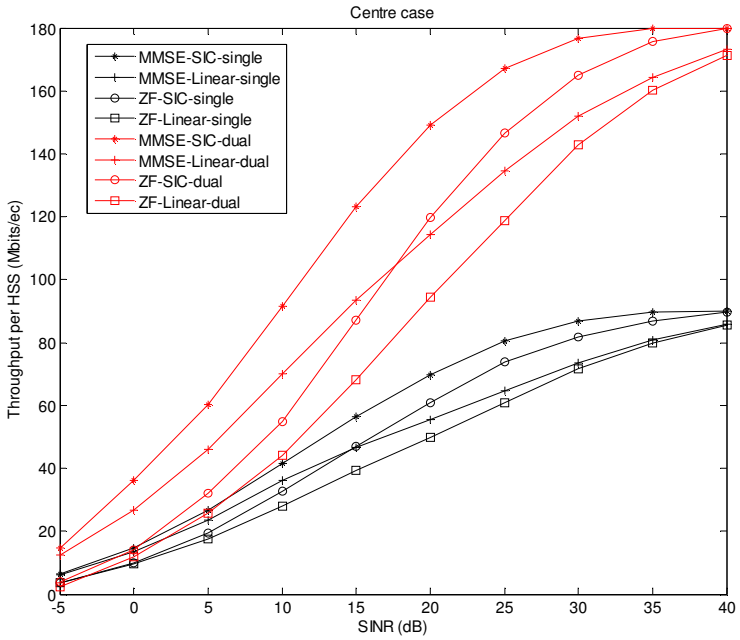

Figure 5-16 Average throughput under TSB against average SNIR and fixed average INR=10 dB based on Multi-HBS interference model: Centre case.

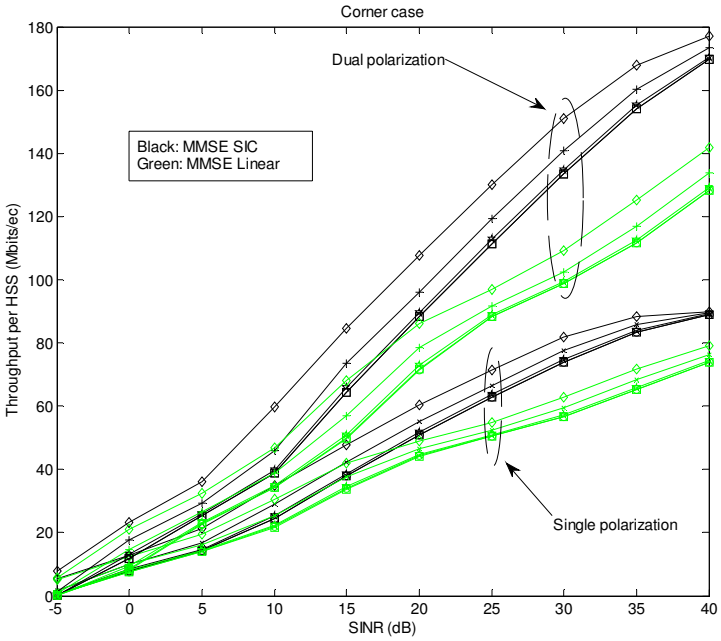

Figure 5-17 Average throughput under TSB against average SNIR, based on Multi-HBS interference model: Corner case, INR = -30:10:10 dB.

5.5 Look-up table for system-level simulation

Typical look-up tables used for system level simulation in T4.1 are presented in Figure 5-18 and Figure 5-19. The linear MMSE detection is used to obtain the CDF. For a range of useful average SINR values, from -5 to 40 dB and for 1 dB step size, we generate 3000 instantaneous channel realizations at each SINR level and measure the throughput of each data stream. These values describe the distribution of the achievable rate with MBA MIMO.

The CDFs in Figure 5-18 are obtained by averaging the throughput of different data streams at each channel instant over the data streams. The result shown in Figure 5-18 is optimistic. At each SINR level, the variance of the distribution is small, verified by the nearly vertical CDF curves. Although this average distribution provides accurate mean value of the achievable data rate, the probability of very small data rate is low due to the small variance. In fact, since the geometry of the backhaul link is fixed and the path losses of different data streams (HSSs) are different, each data stream has its own statistical characteristics, i.e., the mean and standard derivation of the data rate distribution at a given SINR. The results in Figure 5-18 give the correct mean value but an inaccurate distribution, and in particular a greatly reduced variance.

More accurate statistical characteristics can be obtained by combining the distributions of different data streams, instead of taking an average throughput. Specifically, the data rates of different data streams calculated according to instantaneous channel coefficients are put together into the look-up table. The CDF curves are shown in Figure 5-19. The shape of the CDF curves is due to unique throughput distribution for different users, i.e., the mean throughput varies significantly with the users. As a result, the combined distribution has a similar manner to a Gaussian-mixture distribution.

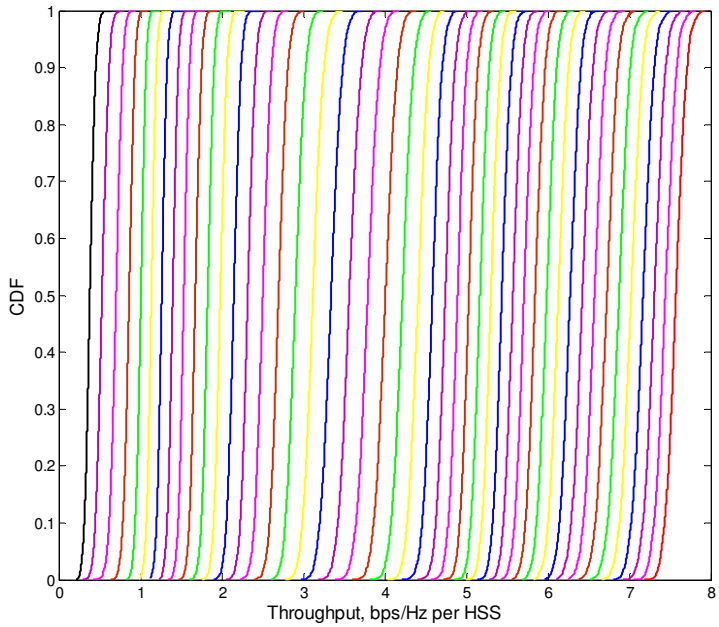

Figure 5-18 Backhaul link CDF for averaged MBA-MIMO data rate distribution.

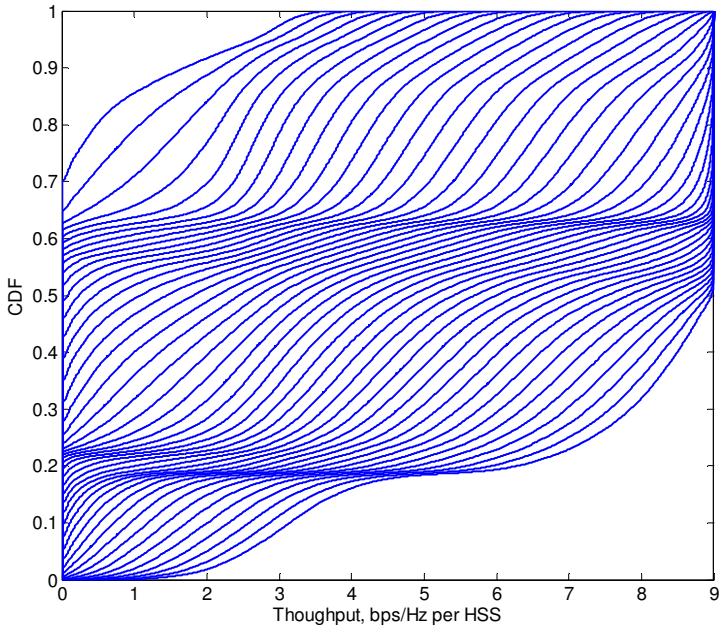

Figure 5-19 Backhaul link CDF for combined MBA-MIMO data rate distribution.

6. Design and evaluation of CSI feedback

Introduction

One of the main novelties of the BuNGee project is the scenario presented, which emerges from the planning of interference-aware all-wireless networks that feature aggressive frequency reuse and where both access and backhaul links are wireless. The novelty of the scenario presented in what follows is that

adaptive spatial processing is considered at both ends of the radio backhaul link, i.e., the links can be adapted dynamically to mitigate incoming interference. This also removes the planning needed when using very directive antennas in the wireless backhaul link. Besides, in order to increase the spectral efficiency of the system, the same frequencies are used for the backhaul and the access networks, which means that cross-segment (or cross-system) interference has to be taken care of.

In what follows (Section 6.1), we present a state-of-the-art section on feedback strategies for MIMO systems.

Next, in Section 6.2, we present a cross-segment (or cross-system) design of the transmit adaptive precoding matrix of the ABS for the communication with the HBS under the following design considerations: first, the backhaul link should be completely transparent to the access network, i.e., the signals sent to the HBS should not cause interference to the MSs, and second, the design should also minimize the effect of interference at the HBS. The interference at the HBS can be due to external sources or to other ABSs in the same cell as the HBS or in neighboring cells transmitting at the same frequency and the same time

In order to satisfy these design criteria, two limited feedback links are proposed to be exploited. The first link transmits the CSI from the MSs to the ABS, while the feedback link from the HBS to the ABS sends information on the second-order statistics of the interference signals present at the HBS. For the design of the feedback links different algorithms are considered, featuring both differential [Sac09] and non-differential quantization [Cha08]. The differential algorithm [Sac09] is based on quantization over the space of Hermitian positive definite matrices using geodesic routes, while the non-differential approach [Cha08] is based on uniform quantization of each coefficient of the matrix to be fed back. The feedback links are assumed delay-free and noise-free, as in [Sac09], [Cha08], [Hua09]. Note that, since there are two independent feedback links that have to be taken into account for the precoder design at the ABS, the optimum transceiver cannot be computed independently at the receivers.

Finally, in Section 6.3, we consider a general multiple-input multiple-output (MIMO) orthogonal frequency division multiplexing based multiuser broadcast system (such as the BuNGee system) with precoding at the transmitter and feedback of channel state information. We present a general framework for the transceiver design, and also for the design of the feedback link based on the quantization of the HSSs' MIMO channel Gram matrices. The proposed design of the feedback link exploits the correlation of the channel response in the frequency domain due to the finite length of the channel time impulse responses to outperform other schemes based on feedback of the per carrier frequency responses. The transceiver design framework is based on a unitary linear transformation applied at the HSSs, which allows the computation of equivalent triangular channel response matrices at the transmitter. We also perform an analytic study of the error propagation due to the channel quantization in the feedback link and the computation of the equivalent triangular channel matrices. Based on the previous concepts, all the usual transceiver design criteria can be applied within this framework, and we derive, as an example, the particular case of a space-frequency precoder for robust mean square error minimization. Finally, the benefits of the proposed strategy are evaluated by means of numerical simulations (with generic channels and also using the BuNGee models) and compared to other existing techniques.

6.1 State-of-the-art

MIMO communication channels are known to provide significant gains in system capacity [Tel99], [Fos98] and resilience to fading [Ala98], [Tar99]. These gains depend strongly on the quantity and quality of the channel state information which is available during the design [Gol03]. Obviously, the best performance is achieved when such CSI is complete and perfect, but this is not a realistic assumption, especially at the transmitter. In scenarios where channel reciprocity does not hold, a feedback link with limited capacity can be used to send the CSI from the receiver to the transmitter, as shown in Figure 6-1. In this sense, proper quantization procedures to be applied to the channel estimates have to be designed.

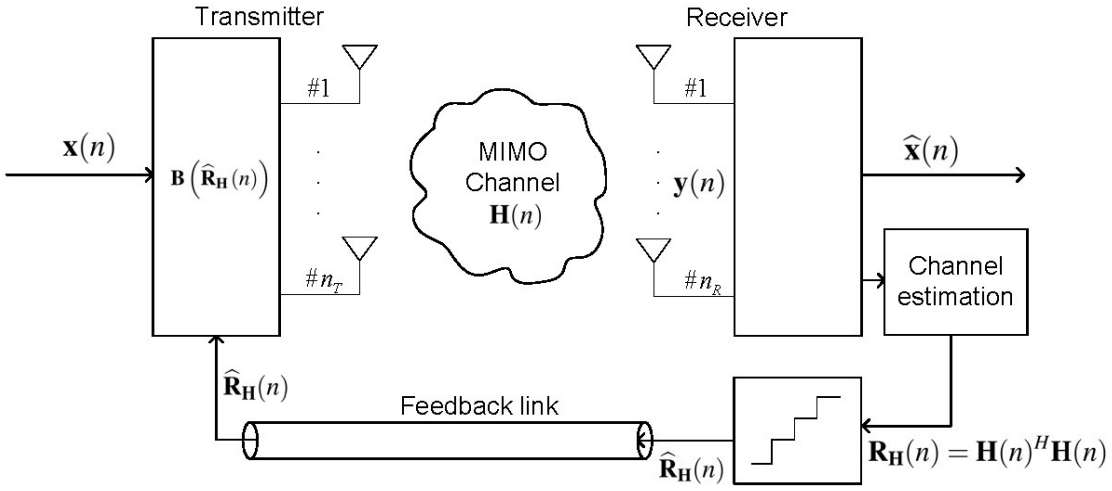

Figure 6-1: A feedback link with limited capacity is used to send CSI from Rx to Tx

Quantization algorithms in the literature can be classified fundamentally according to two different criteria: if they exploit temporal correlation of the parameter (i.e. differential versus non-differential quantization) and according to the objective of the quantization, which depends on the design criterion, for example, if the complete channel response matrix is to be sent through the feedback link or only the Gram of the channel matrix, or even just the subspace spanned by the right singular vectors of the channel matrix. Under the constraint of uniform power allocation among beams, quantization in the Grassmannian manifold, which consists of points that represent the subspaces spanned by transmit beamforming matrices, is optimum for several criteria [Lov03].

In more general cases where the power allocation is not constrained to be uniform, the optimum linear signalling scheme at the transmitter depends on the MIMO channel Gram matrix, i.e., $\mathbf{R}_H = \mathbf{H}^H\mathbf{H}$ (the superscript *H* indicates Hermitian transpose), for any quality measure such as mutual information, mean square error (MSE), SNR, or bit error rate (BER), among others [Pal03], [Pay09a]. Note that in this case, the design is determined by the right singular vectors of the channel matrix **H** (and not only on the subspace spanned by them, as happens in the Grassmannian manifold) in addition to the singular values. Taking this into account, the quantization should be applied over the set of Gram-like matrices, i.e., Hermitian and positive definite matrices (such as $\mathbf{R}_H$), instead of the Grassmannian manifold.

Non-Differential Quantization Techniques. Strategies based on non-differential quantization make use of a codebook, which is a collection of codewords or quantization candidates selected to maximize the distance between them according to a design criterion. Each codeword corresponds to a possible precoding matrix for the system. The codebook is designed off-line and is known to both the transmitter and the receiver. If the statistics of the channel are known beforehand, they can be exploited to improve the design of the codebook. The receiver evaluates all the codewords with the current known channel and sends to the transmitter the index of the codeword that maximizes the system design criterion according to the current channel.

Following this idea, extensive work has been done over the Grassmannian manifold. [Lov03] proposed a quantization technique called Grassmannian beamforming, which is based on codebooks built to maximize the distance between codewords belonging to the Grassmannian manifold [Ede98]. In [Roh06] the authors presented an iterative method for constructing codebooks of also beamforming matrices with uniform power allocation that are optimized to minimize mutual information loss for a given signal-to-noise-ratio (SNR) for general channel distributions.

In [Cha08] the authors proposed a quantization and feedback of the channel Gram matrix featuring a direct quantization of each element of matrix $\mathbf{R}_H$ separately.

While these techniques are conceptually simple, and they usually require the lowest computational complexity, they have a fundamental drawback for the use in real systems. They are designed and optimized under the assumption that the CSI at consecutive time instants is independent, which is usually not true. Measurements show that there is a strong correlation in time of the parameters to be tracked, and some approaches have been developed based on hierarchical codebooks for progressive refinement of the quantization [Hea09] and also on feedback compression to reduce the redundancy of CSI fed back at consecutive time instants [Hua09], [Hua06], [Ino09]. In [Pan07], different interpolation approaches and

cluster-based precoding was performed in the Grassmannian manifold to exploit correlation in the propagation channel of OFDM subcarriers that are close in frequency.

Differential Quantization Techniques. Differential quantization techniques are based on exploiting the correlation in time present in the physical parameters of the propagation channel. Each feedback update sends quantized information on the difference between the last fed back estimate and the current channel. This means that the accuracy of the CSI at the transmitter improves with each feedback update, until it reaches an upper bound determined by the correlation factor of the channel and the feedback rate. Another advantage of differential feedback techniques is that they adapt easily to variable feedback rates, since most require only a minimum of 1 bit per feedback use.

In [Xia09] a CSI feedback scheme is presented which is based on differential pulse code modulation (DPCM) on each element of the matrix and the quantization is related to the MIMO channel matrix **H**.

In [Yan07] the constraint of uniform power allocation was considered and a differential quantization was proposed. The technique involved defining a random geodesic curve over the Grassmannian manifold [Ede98] and indicating through 1 bit of feedback the direction that minimizes the distance to the optimum beamforming matrix, which is also a point in the manifold.

The technique in [Sac09] is applied to the channel Gram matrix as a whole, exploiting the intrinsic differential geometry of the set of positive definite Hermitian matrices and using geodesic curves. One of the benefits of this technique is that the feedback overhead is independent of the number of antennas.

The technique from [Roh07] performs a parameterization of the channel singular vectors prior to the quantization to obtain statistically independent parameters, but suffers from propagation of the quantization error when reversing the transformation at the transmitter. The parameters are quantized component-wise following either non-differential or DPCM-based quantization, and quantization of power allocation information is also considered, element-wise.

6.2 Differential feedback of MIMO channel Gram matrices based on geodesic curves

In this final deliverable for WP2 in the BuNGee project, we consider a scenario in order to analyze and evaluate the impact of having limited feedback information for the CSI. We consider a wireless network with one ABS, one HBS, K MSs and backhauling and access links as depicted in Figure 6-2, where the antennas drawn at the HBS in such figure represent the available fixed beams. The ABS has n_A transmit antennas, while the HBS has n_H beams and the i th MS has n_{M_i} receive antennas, with $\sum_{i=1}^{K} n_{M_i} < n_A$ (in the BuNGee project, n_H refers to the number of available beams at the HBS, where the signals received through them are allowed to be processed jointly). The channel matrix from the ABS to the HBS at time instant t is denoted by $\mathbf{H}_{AH}(t) \in C^{n_H \times n_A}$, and the channel matrices of the links between ABS and the MSs are represented by $\mathbf{H}_{AM_i}(t) \in C^{n_{M_i} \times n_A}$. $\mathbf{B} \in C^{n_A \times n_S}$ is the precoding matrix of the backhaul link, to be used at the ABS to transmit n_S streams to the HBS. $\mathbf{x} \in C^{n_S}$ represents the n_S streams of signals to be transmitted from the ABS to the HBS with $E[\mathbf{x}\mathbf{x}^H] = \mathbf{I}$. The additive white Gaussian noise (AWGN) at the HBS is $\mathbf{w} \in C^{n_H}$, with $E[\mathbf{w}\mathbf{w}^H] = \sigma_w^2 \mathbf{I}$. The received signal at the HBS is, therefore (we drop the dependency with respect to the time index t for the sake of clarity in the notation):

$$\mathbf{y} = \mathbf{H}_{AH}\mathbf{B}\mathbf{x} + \mathbf{y}_{int} + \mathbf{w} \in C^{n_H} \tag{6.1}$$

where $\mathbf{y}_{int}$ is the interference received at the HBS with covariance $\mathbf{R}_{int}$ and can be caused by external sources or by other ABSs in the same cell as the HBS or in neighboring cells transmitting at the same

frequency and the same time. Therefore, the interference plus noise at the HBS, $\mathbf{y}_{int} + \mathbf{w}$ has a covariance matrix which is expressed as:

$$\mathbf{R}_n = \sigma_w^2 \mathbf{I} + \mathbf{R}_{int} \tag{6.2}$$

and it is assumed that it can be estimated at the HBS.

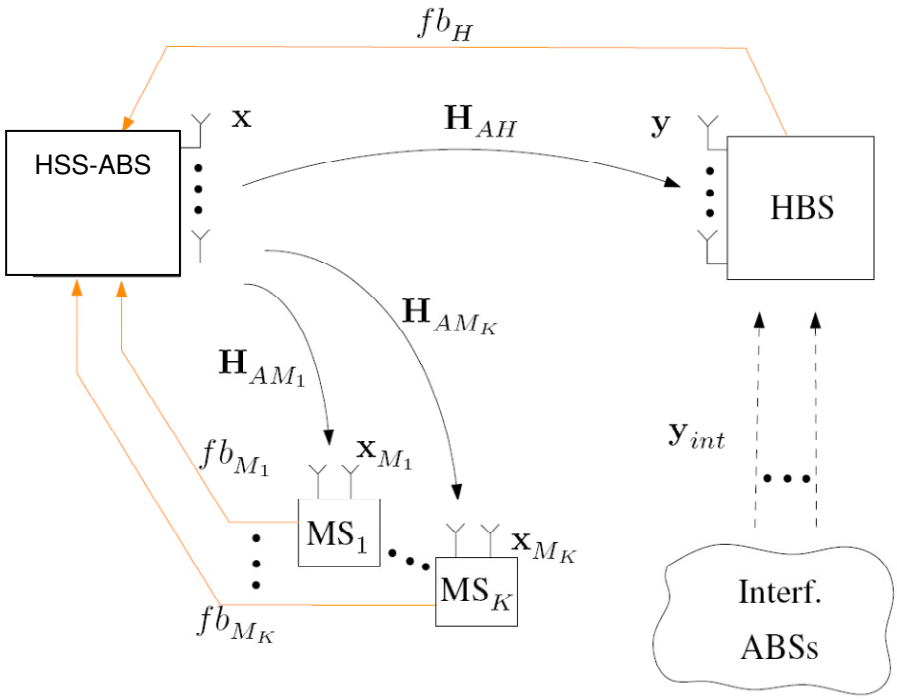

Figure 6-2: System model of the wireless backhaul link.

6.2.1 Channel model

The scenario described in Figure 6-2 contains two different types of propagation channels:

- Channel from the ABS to the HBS: This channel is static, or very slow varying, since both ABS and HBS have no mobility. Therefore the channel response matrix $\mathbf{H}_{AH}$ can be assumed to be known at both ends.
- Channels from the ABS to the MSs: The MSs have a given mobility, which translates into a Doppler-shift. These channels $\mathbf{H}_{AM_i}$ are considered to be time varying, and the MSs are assumed to be able to estimate them with the help of pilot symbols.

6.2.2 Feedback links

The scenario presented in this section considers the following feedback links, which are depicted in Figure 6-2:

- Link from HBS to ABS (fb_H): The HBS estimates the interference plus noise correlation matrix $\mathbf{R}_n$ and sends it to the ABS through the limited feedback link fb_H. The ABS then uses this knowledge to minimize the effect of $\mathbf{R}_n$ on the performance of the backhaul link by a proper design of the transmit matrix $\mathbf{B}$.
- Links from the MSs to the ABS (fb_{M_i}): The i th MS estimates the propagation channel $\mathbf{H}_{AM_i}$ and sends its Gram matrix $\mathbf{H}_{AM_i}^H\mathbf{H}_{AM_i}$ through fb_{M_i} to the ABS. This CSI is used at the ABS to reduce the interference caused by the backhaul link over the MSs by a proper design of the precoding matrix $\mathbf{B}$.

6.2.3 Quantization and feedback algorithm for positive definite Hermitian matrices

In [Sac09] a feedback algorithm for single user point-to-point MIMO systems based on the differential quantization of the channel Gram matrix $\mathbf{H}^H\mathbf{H}$ is presented. It has been proved that, for single user MIMO, the channel Gram matrix contains the sufficient information to design a transmitter that maximizes criteria such as signal to noise ratio (SNR), mutual information, or minimizes bit error rate (BER) or mean square error (MSE) [Pay09a].

However, this algorithm can be applied to the general case of quantization and feedback of any positive definite Hermitian matrix, not just the channel Gram matrices. Here, we will apply the same strategy designed for the channel Gram matrix to the feedback of $\mathbf{R}_n$ (feedback link fb_H), which is positive definite and Hermitian by construction (see (6.2)), and also to the feedback of $\mathbf{H}_{AM_i}^H\mathbf{H}_{AM_i}$ [1] (feedback links fb_{M_i}). This section summarizes this quantization algorithm for positive definite and Hermitian matrices.

Preliminaries on some differential geometry definitions

The objective of the quantization is a Hermitian and positive definite matrix $\mathbf{R}$ of dimensions $m \times m$. As shown in [Tal07] the set of Hermitian positive definite matrices $S = \{\mathbf{R} \in C^{m\times m} : \mathbf{R}^H = \mathbf{R}, \mathbf{R} \succ 0\}$ is a convex cone[2], i.e., $\forall \mathbf{R}_1, \mathbf{R}_2 \in S, \forall s \geq 0, \mathbf{R}_1 + s\mathbf{R}_2 \in S$. This set is described properly by the following definitions [Tal07], [Pen04]:

- *Scalar product and norm:* The scalar product between two Hermitian matrices $\mathbf{A}$ and $\mathbf{B}$ at any point $\mathbf{R}$ in the set S is defined as:

$$< \mathbf{A}, \mathbf{B} >_{\mathbf{R}} = \mathrm{Tr}(\mathbf{R}^{-1}\mathbf{A}\mathbf{R}^{-1}\mathbf{B}) \tag{6.3}$$

- *Geodesic curve:* The geodesic curve $\Gamma(l)$ is the path that connects two points $\mathbf{R}_1$ and $\mathbf{R}_2$ in S with

[1] Although the matrix $\mathbf{H}_{AM_i}^H\mathbf{H}_{AM_i}$ is not strictly positive definite, it is possible to work straightforwardly with extended Gram matrices defined as $\mathbf{H}_{AM_i}^H\mathbf{H}_{AM_i} + \varepsilon\mathbf{I}$, for any $\varepsilon > 0$, which are positive definite by construction. This is done by adding $\varepsilon\mathbf{I}$ before the quantization is carried out at the MSs, and subtracting $\varepsilon\mathbf{I}$ from the received feedback at the ABS.

[2] Actually, reference [Tal07] is devoted to the case of real matrices, although the results and conclusions can be extended directly to the complex case.

minimum distance and with all of its points belonging to S:

$$\Gamma(l) = \mathbf{R}_1^{1/2} \exp(l\mathbf{C})\mathbf{R}_1^{1/2} \in S, \ \forall l \in R, \tag{6.4}$$

where $\mathbf{C} = \mathbf{C}^H = \log(\mathbf{R}_1^{-1/2}\mathbf{R}_2\mathbf{R}_1^{-1/2})$, $\Gamma(0) = \mathbf{R}_1$, and $\Gamma(1) = \mathbf{R}_2$. The *direction* of the curve at $l = 0$ is the derivative at $l = 0$, and is given by $\dot{\Gamma}(0) = \mathbf{R}_1^{1/2}\mathbf{C}\mathbf{R}_1^{1/2}$.

- *Geodesic distance:* The distance between any two points in S is given by the length of the geodesic curve that connects them. It is expressed as:

$$\text{dist}_g(\mathbf{R}_1, \mathbf{R}_2) = (\sum_i |\log \lambda_i|^2)^{1/2} = \|\mathbf{C}\|_F, \tag{6.5}$$

where $\{\lambda_i\}$ are the eigenvalues of $\mathbf{R}_1^{-1/2}\mathbf{R}_2\mathbf{R}_1^{-1/2}$.

In order to understand the generation of curves in the quantization algorithm explained next, we define the *orthogonality between two geodesic curves*. Consider two curves $\Gamma_1(l) = \mathbf{R}^{1/2} \exp(l\mathbf{C}_1)\mathbf{R}^{1/2}$ and $\Gamma_2(l) = \mathbf{R}^{1/2} \exp(l\mathbf{C}_2)\mathbf{R}^{1/2}$ that pass through a common point $\mathbf{R}$ at $l = 0$. We say that they are orthogonal if their directions at $l = 0$ are orthogonal, i.e. $<\dot{\Gamma}_1(0), \dot{\Gamma}_2(0)>_{\mathbf{R}} = 0$, which, from the equation of the derivative and (6.3), can be written as:

$$\text{Tr}(\mathbf{R}^{-1}\mathbf{R}^{1/2}\mathbf{C}_1\mathbf{R}^{1/2}\mathbf{R}^{-1}\mathbf{R}^{1/2}\mathbf{C}_2\mathbf{R}^{1/2}) = 0 \Longleftrightarrow \text{Tr}\left(\mathbf{C}_1\mathbf{C}_2\right) = 0. \tag{6.6}$$

Algorithm description

This quantization algorithm is differential and, as such, the result at any instant n depends on the result of the previous quantization $(\text{instant } n-1)$. The differential nature of the procedure allows exploiting the temporal correlation of the matrix to be quantized and to adapt to dynamic scenarios like the one considered. The mobility of the MSs is taken into account in the algorithm through the quantization step Δ, which can be optimized according to the mobility of the scenario. The objective of the quantization is to minimize the geodesic distance between the actual matrix $\mathbf{R}$ and its fed back estimate $\hat{\mathbf{R}}$, i.e., its quantized version. The five steps of the feedback algorithm are described in Table 6-1:

Table 6-1: Matrix geodesic quantization and feedback algorithm.

Initialization: the algorithm starts from the cone vertex: $\hat{\mathbf{R}}(0) = \mathbf{I}$.

1) The receiver and the transmitter generate a common set of Q random Hermitian matrices $\{\tilde{\mathbf{C}}_i\}_{i=1}^{Q}$ that satisfy the following constraint: $\text{Tr}\left(\tilde{\mathbf{C}}_m\tilde{\mathbf{C}}_j\right) = \delta_{mj}$, as in (6.6). Then, each matrix $\tilde{\mathbf{C}}_i$ is re-scaled individually by Δ, the quantization step: $\mathbf{C}_i = \Delta\tilde{\mathbf{C}}_i$.

2) The receiver and the transmitter use $\{\mathbf{C}_i\}_{i=1}^{Q}$ to generate a set of Q geodesic curves $\{\Gamma_i(l)\}_{i=1}^{Q}$ having all of them the same initial point $\hat{\mathbf{R}}(n-1)$ and with

orthogonal directions: $\Gamma_i(l) = \hat{\mathbf{R}}^{1/2}(n-1)\exp(l\mathbf{C}_i)\hat{\mathbf{R}}^{1/2}(n-1)$. The maximum number of orthogonal routes is given by the dimension of the set of Hermitian matrices, i.e., $Q \le m^2$.

3) Each of these geodesic curves is used to generate two candidates for the feedback in the next iteration $\hat{\mathbf{R}}(n)$, all of them equidistant to $\hat{\mathbf{R}}(n-1)$:

$$\hat{\mathbf{R}}^{(2i-1)}(n) = \Gamma_i(-1), \quad 1 \le i \le Q,$$
$$\hat{\mathbf{R}}^{(2i)}(n) = \Gamma_i(1), \quad 1 \le i \le Q.$$

4) Each candidate is evaluated, and the one with the smallest geodesic distance to the actual $\mathbf{R}$ is selected. Its index i_{FB} is sent to the transmitter through the feedback link.

5) The selected matrix will be used for the transmitter design and as the starting point in the next iteration:

$$i_{FB} = \text{argmin}_i \, \text{dist}_g\left(\hat{\mathbf{R}}^{(i)}(n), \mathbf{R}(n)\right), \quad 1 \le i \le 2Q,$$
$$\hat{\mathbf{R}}(n) = \hat{\mathbf{R}}^{(i_{FB})}(n)$$

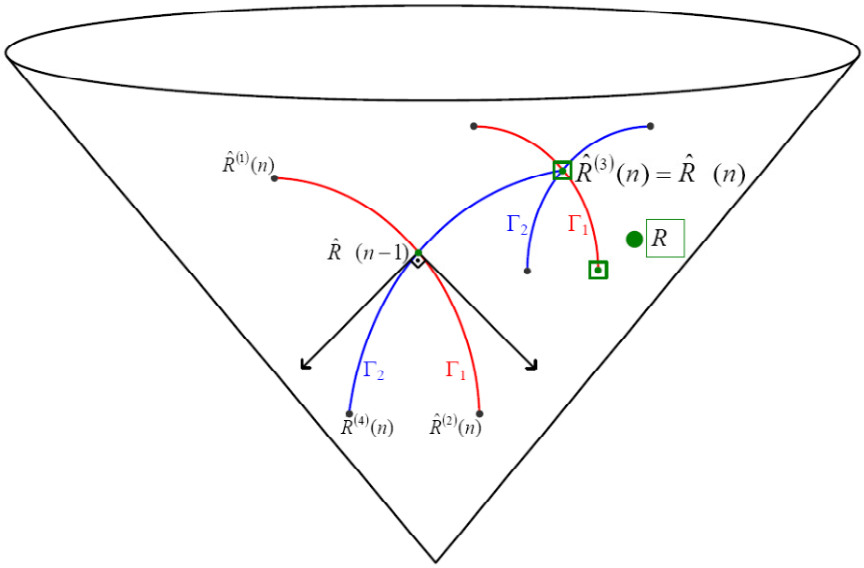

Figure 6-3: Differential quantization using 2 bits in the space of positive definite matrices.

Figure 6-3 shows the differential quantization process using 2 bits. Starting from $\hat{\mathbf{R}}(n-1)$, the algorithm generates 2 orthogonal geodesic routes $\Gamma_1(l)$ and $\Gamma_2(l)$. The four quantization candidates are: $\hat{\mathbf{R}}^{(1)}(n) = \Gamma_1(-1)$, $\hat{\mathbf{R}}^{(2)}(n) = \Gamma_1(1)$, $\hat{\mathbf{R}}^{(3)}(n) = \Gamma_2(-1)$, and $\hat{\mathbf{R}}^{(4)}(n) = \Gamma_2(1)$. At the receiver, each candidate is compared to the actual $\mathbf{R}$ and the one with smallest geodesic distance to $\mathbf{R}$ (in this example candidate 3) is selected. That is, its index $i_{FB} = 3$ is sent to the transmitter through the feedback link and

$\hat{\mathbf{R}}(n) = \hat{\mathbf{R}}^{(3)}(n)$. The quantization at next time instant starts from this point, generates 2 orthogonal routes and 4 quantization candidates, selects the candidate with the smallest geodesic distance to $\mathbf{R}$, and so on.

6.2.4 Precoding matrix design

The optimization of the precoding matrix $\mathbf{B}$ in the backhaul link can be done according to several quality criteria, such as maximization of the mutual information, signal to interference plus noise ratio (SINR), or minimization of the BER. Given the constraint of zero-interference to the MSs and taking into account interfering signals at the HBS, the design of $\mathbf{B}$ according to a general design criterion $f\left(\mathbf{B}, \mathbf{H}_{AH}, \mathbf{R}_n\right)$, can be formulated as the following maximization problem:

$$\max_{\mathbf{B}} \quad f\left(\mathbf{B}, \mathbf{H}_{AH}, \mathbf{R}_n\right) \tag{6.7}$$

$$\text{s.t.} \quad \mathrm{Tr}\left(\mathbf{B}\mathbf{B}^H\right) \le P_T, \tag{6.8}$$

$$\mathbf{H}_{AM_i}\mathbf{B} = 0, \ \forall i \ (i = 1...K), \tag{6.9}$$

where the effect of $\mathbf{R}_n$ is considered in the cost function in (6.7), the constraint on the total power available for the transmission is expressed in (6.8), and (6.9) represents the zero-interference constraints to the MSs links. This last constraint can also be written as:

$$\hat{\mathbf{H}}_{AM}\mathbf{B} = 0, \tag{6.10}$$

where $\hat{\mathbf{H}}_{AM}$ is defined as:

$$\hat{\mathbf{H}}_{AM} = \left[\mathbf{H}_{AM_1}^T \ldots \mathbf{H}_{AM_K}^T\right]^T. \tag{6.11}$$

From (6.10), $\mathbf{B}$ is forced to have the following structure:

$$\mathbf{B} = \mathbf{V}_0\tilde{\mathbf{B}}, \tag{6.12}$$

where $\tilde{\mathbf{B}} \in C^{(n_A - \sum_{i=1}^{K} n_{M_i}) \times n_S}$ and the orthonormal columns of $\mathbf{V}_0 \in C^{n_A \times (n_A - \sum_{i=1}^{K} n_{M_i})}$ span the right-nullspace of $\hat{\mathbf{H}}_{AM}$ (as in [Spe04]). Since the nullspace of $\hat{\mathbf{H}}_{AM}$ is equal to the nullspace of $\hat{\mathbf{H}}_{AM}^H\hat{\mathbf{H}}_{AM}$, and $\hat{\mathbf{H}}_{AM}^H\hat{\mathbf{H}}_{AM}$ can be written as (see (6.11)):

$$\tilde{\mathbf{H}}_{AM}^H\tilde{\mathbf{H}}_{AM} = \sum_{i=1}^{K}\mathbf{H}_{AM_i}^H\mathbf{H}_{AM_i}, \tag{6.13}$$

then, the matrix $\mathbf{V}_0$ can be computed containing as columns the singular vectors associated to the null eigenvalues of $\sum_{i=1}^{K}\mathbf{H}_{AM_i}^H\mathbf{H}_{AM_i}$. Note that from each MS, only the channel Gram matrix $\mathbf{H}_{AM_i}^H\mathbf{H}_{AM_i}$ is needed, and also that the zero forcing applied to each additional MS reduces the degrees of freedom available at the ABS for the communication with the HBS, reducing the performance of the backhaul link.

The total power in (6.8) can be written as a function of $\tilde{\mathbf{B}}$: Since $\mathbf{V}_0^H\mathbf{V}_0 = \mathbf{I}$, then $\mathrm{Tr}\left(\mathbf{B}\mathbf{B}^H\right) = \mathrm{Tr}\left(\tilde{\mathbf{B}}\tilde{\mathbf{B}}^H\right)$. Taking this into account, the optimization problem can be rewritten as:

$$\max_{\bar{\mathbf{B}}} \quad f\left(\mathbf{V}_0\bar{\mathbf{B}}, \mathbf{H}_{AH}, \mathbf{R}_n\right) \tag{6.14}$$

$$\text{s.t.} \quad \mathrm{Tr}\left(\bar{\mathbf{B}}\bar{\mathbf{B}}^H\right) \le P_T. \tag{6.15}$$

This optimization problem can be easily solved now for the different design criteria, such as maximization of the mutual information, SINR, minimization of the BER, etc. We now comment two examples of design criterion f, however the same procedure can be applied to other criteria following the same steps as in [Pal03].

Example 1: Maximization of the mutual information

In this case the cost function is defined as

$$\begin{aligned} f &= \log_2\left|\mathbf{I}+\mathbf{B}^H\mathbf{H}_{AH}^H\mathbf{R}_n^{-1}\mathbf{H}_{AH}\mathbf{B}\right| \\ &= \log_2\left|\mathbf{I}+\bar{\mathbf{B}}^H\mathbf{V}_0^H\mathbf{H}_{AH}^H\mathbf{R}_n^{-1}\mathbf{H}_{AH}\mathbf{V}_0\bar{\mathbf{B}}\right| \\ &= \log_2\left|\mathbf{I}+\bar{\mathbf{B}}^H\overline{\mathbf{R}}_H\bar{\mathbf{B}}\right|, \end{aligned} \tag{6.16}$$

where $\overline{\mathbf{R}}_H = \mathbf{V}_0^H\mathbf{H}_{AH}^H\mathbf{R}_n^{-1}\mathbf{H}_{AH}\mathbf{V}_0$.

The solution to the maximization problem (6.14) for this cost function is known to be [Cov06]:

$$\bar{\mathbf{B}} = \mathbf{V}\mathbf{P}^{1/2}, \ \mathbf{P} = \mathrm{diag}(p_1,\cdots,p_{n_S}), \tag{6.17}$$

where $\mathbf{V}$ consists of n_S columns that are the n_S eigenvectors of $\overline{\mathbf{R}}_H$ associated to its n_S maximum eigenvalues $\{\lambda_i\}_{i=1}^{n_S}$. The power $\mathbf{P}$ is allocated according to the waterfilling solution ($p_i = \max\{0, \mu - 1/\lambda_i\}$ where μ is a constant such that $\sum_{i=1}^{n_S} p_i = P_T$).

Example 2: Maximization of the SINR with single beamforming

In this case the beamforming matrix $\bar{\mathbf{B}}$ has only 1 column (therefore the notation $\tilde{\mathbf{b}}$ will be used), and the cost function is defined as:

$$f = \left\|\tilde{\mathbf{b}}^H\mathbf{V}_0^H\mathbf{H}_{AH}^H\mathbf{R}_n^{-1}\mathbf{H}_{AH}\mathbf{V}_0\tilde{\mathbf{b}}\right\|^2 = \left\|\tilde{\mathbf{b}}^H\overline{\mathbf{R}}_H\tilde{\mathbf{b}}\right\|^2, \tag{6.18}$$

and the solution to (6.14) using this criterion as cost function is:

$$\tilde{\mathbf{b}} = \sqrt{P_T}\mathbf{u}_{\max}(\overline{\mathbf{R}}_H), \tag{6.19}$$

where $\mathbf{u}_{\max}(\cdot)$ stands for the unit-norm eigenvector of maximum associated eigenvalue.

Preliminary simulation results considering this scenario are presented in the following section.

6.2.5 Numerical results

In this section, simulations of system performance are presented, for the scenario described in the previous subsections. There are several factors that are considered and have a direct effect on the performance of the communication in the backhaul link of the proposed scenario. First, the performance loss in the link between ABS and HBS when the constraint of zero interference at the MSs is enforced will be presented. Then we will analyze the gain obtained when using different feedback techniques to send information of the second order statistics of the interference from the HBS to the ABS, as a function of the transmission rate of the feedback link. Finally, the degradation in performance will be simulated for different values of the interfering power and different number of ABSs interfering to the HBS at the same time and the same frequency.

For all the simulations a normalized noise power is considered $(\sigma_w^2 = 1)$, and the correlation in time of the propagation channel $\mathbf{H}_{AM}$ is modeled using a first-order autoregressive time variation model described by the following expression:

$$\mathbf{H}(n) = \rho\mathbf{H}(n-1) + \sqrt{1-\rho^2}\,\mathbf{N}(n), \tag{6.20}$$

where $\mathbf{N}(n)$ and the initial value, $\mathbf{H}(n=0)$, are assumed to be independent and composed of i.i.d. zero-mean complex Gaussian entries with unit variance. The time correlation factor ρ models the variability of the channel and depends on the Doppler frequency f_D caused by the movement of the MSs through the expression $\rho = J_0(2\pi f_D \tau)$, where J_0 is the zeroth-order Bessel function of the first kind, τ corresponds to the time difference between consecutive feedback instants and $f_r = \frac{1}{\tau}$ is the feedback rate. In the simulations we consider this simple channel model as a way to obtain preliminary results on the impact of having feedback for the CSI in the design of an adaptive precoder for the radio backhauling link.

It is important to note that the CSI sent from the MSs to the ABS through the feedback link is quantized and may contain errors, but this does not affect the average performance of the backhaul link ABS-HBS. Imperfect CSI received through the links fb_{M_i} degrades the performance of the communication between the ABS and the MSs but it does not degrade the performance of the backhaul link. Only the rank of the transmitted $\mathbf{H}_{AM_i}^H \mathbf{H}_{AM_i}$ reduces the average performance of the backhaul link. For this reason, the accuracy of the feedback links fb_{M_i} is not relevant for the simulations and will not be commented explicitly.

First, we consider a scenario where $n_A = 10$, $n_H = 8$ and there are up to 3 MSs with $n_M = 2$. There are also other interfering ABSs transmitting at the same time and the same frequency, each one with a transmission power 10 dB higher than the AWGN. Also, in order to provide some initial simple simulations, it has been considered that each interfering ABS has two antennas. Figure 6-4 shows the achievable rate of the ABS-HBS link as a function of the transmit power and averaged over 1000 realizations of the propagation channel, for the cases where the precoding matrix is constrained to put nulls in the directions of the MSs.

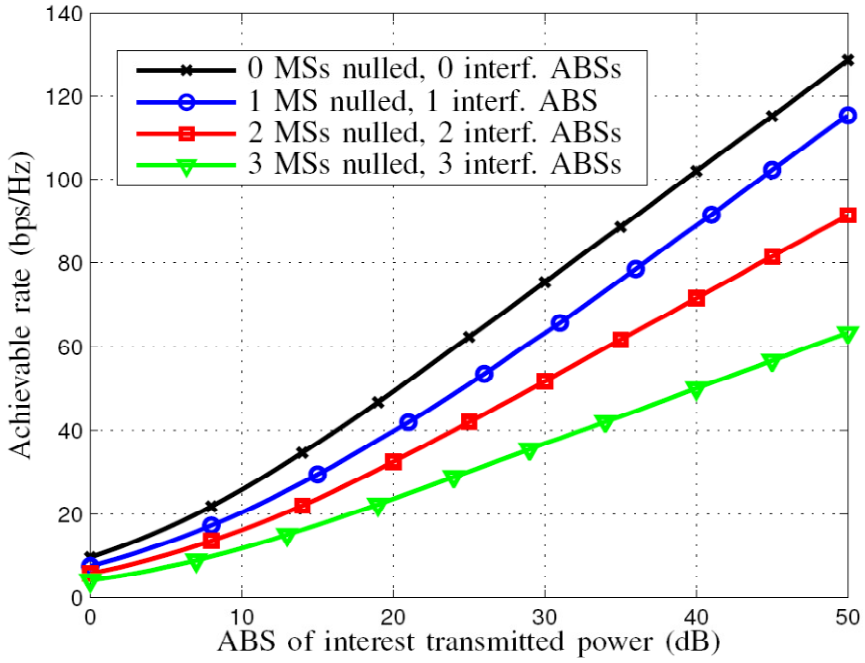

Figure 6-4: Effect of interference nulling at the MSs.

As expected, the simulation shows that the highest rate is achieved when there are 0 MSs. The slope of the curve is reduced when the number of degrees of freedom of the system decreases. It is interesting to observe that, with this setup, in the presence of 1 MS with 2 antennas, the ABS can perform interference nulling at the MS without losing degrees of freedom in the link with the HBS (the curves have the same slope for 0 and 1 MSs). There is some performance loss due to the fact that system resources are used in the interference nulling, but it is a constant loss that does not scale with the transmitted power. The presence of a second MS with 2 antennas does reduce the number of degrees of freedom, and a third MS decreases it further, as shown by the slope of the curves. The maximum degrees of freedom of the ABS-HBS link with interference nulling at all K MSs is $\min\left(n_A - \sum_{i=1}^{K} n_{M_i}, n_H\right)$.

The covariance matrix of the interference plus noise (6.2) can be estimated at the HBS and sent to the ABS of interest through fb_H. Figure 6-5 shows the gains that can be achieved by the use of such feedback link averaged over 3000 channel realizations, as a function of the number of feedback bits and after 30 feedback intervals for a system with $n_A = 6$, $n_H = 5$ 1 MS with $n_M = 2$, and 1 interfering ABS with 2 antennas. The simulation shows that the differential algorithm outperforms the one based on non-differential quantization [Hua09], which features a uniform quantization of the real and imaginary parts of the elements of $\mathbf{R}_n$ (i.e. there are 25 scalar parameters to quantize since $\mathbf{R}_n$ has dimensions 5×5), because it is capable of exploiting the correlation in time present in the propagation channel. In Figure 6-5, for the scheme presented in [Hua09], the x-axis represents the number of feedback bits for each of the 25 parameters to be quantized.

Also note that having a very inaccurate CSI is worse than having no CSI at all, as shown in the curve corresponding to the non-differential scheme.

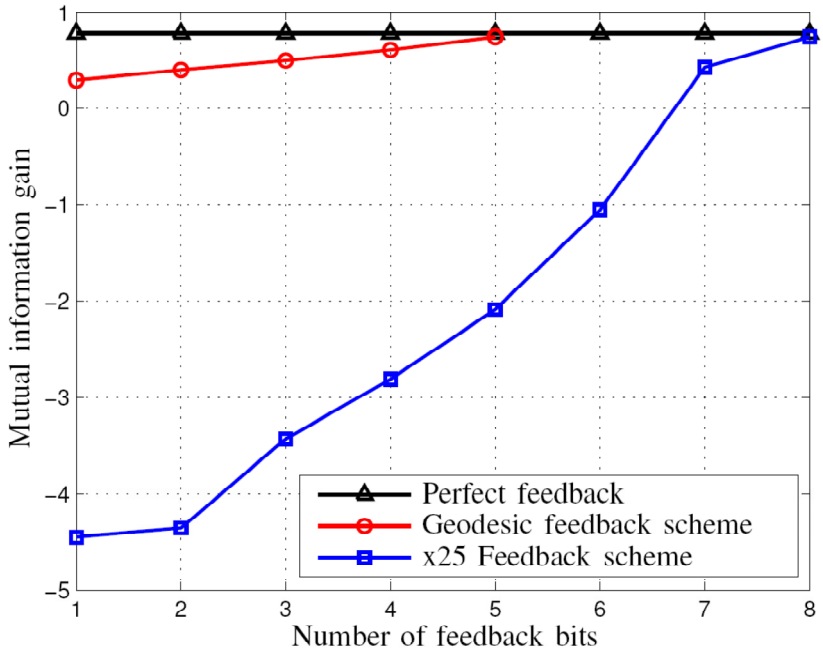

Figure 6-5: Mutual information gain as a function of the number of bits of feedback.

The performance in terms of SINR and BER using a BPSK modulation is evaluated as a function of the interfering power in the simulations corresponding to Figure 6-6 and Figure 6-7 respectively. For these simulations the following setup was used: $n_A = 8$, $n_H = 6$, $n_M = 2$, and the ABS transmits at a power 10dB higher than the AWGN, assuming a normalized channel such that the mean channel coefficients are equal to one (0 dB), for each transmit receive antenna pair. Of course, if the path-loss is to be incorporated in the simulation results, such path-loss should be added to the transmitted power. To simplify the system setup in these preliminary simulations, it has been considered that the number of ABSs interfering over the HBS equals the number of MSs to which nulls have to be synthesized from the ABS of interest. The number of antennas at each interfering ABS is 2. The curves show how the performance of the backhaul link is degraded by increasing the power of the interfering ABSs, and part of this loss can be compensated by using a feedback link with limited capacity to convey the second order statistics of the interfering signal from the HBS to the ABS. The feedback strategy considered is the one described in Section 6.2.3, and the results are plotted after 30 feedback intervals and averaged over 6000 channel realizations. These simulations also show that the performance loss due to having to null additional MSs is higher than the loss due to an increase in power of the interfering ABSs.

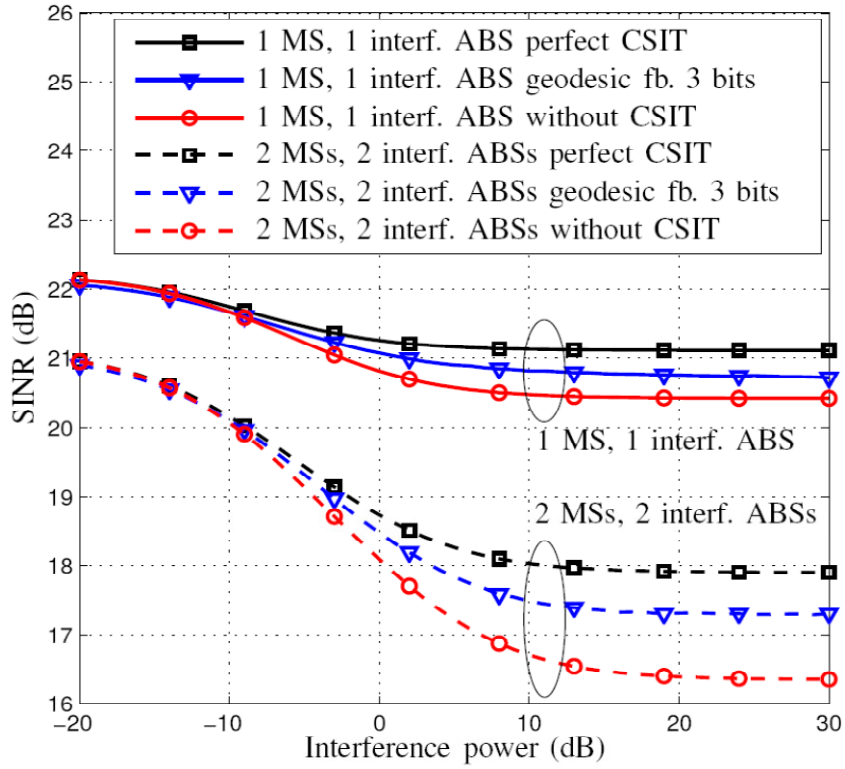

***Figure 6-6*: SINR as a function of the interference power.**

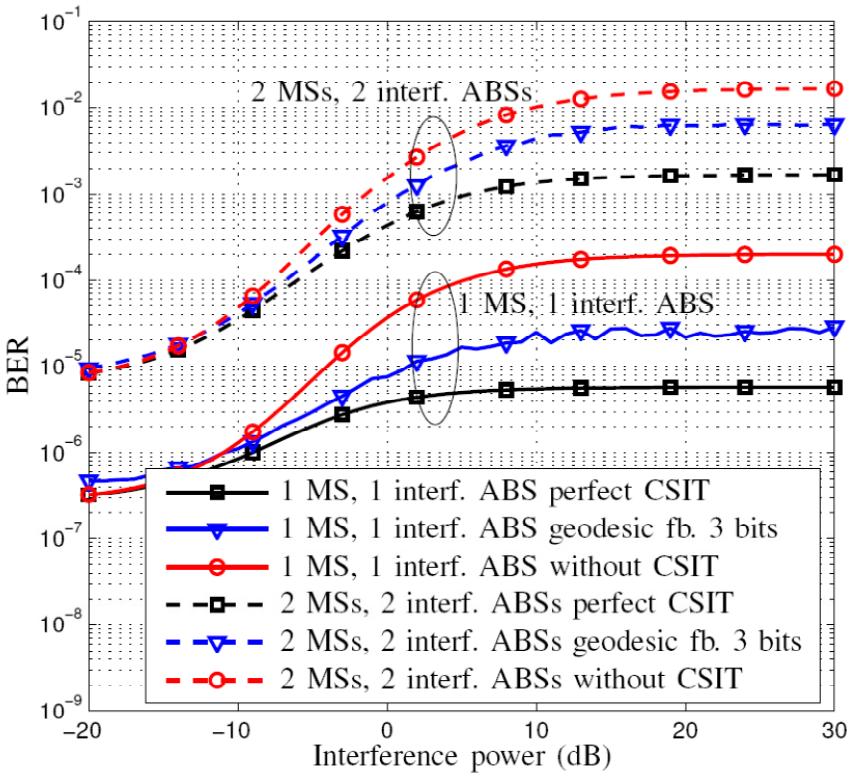

***Figure 6-7*: BER as a function of the interference power.**

6.2.6 Conclusion

In this study for WP2 in the BuNGee project, we have presented a novel scenario for the backhaul link in an all-wireless network. The communication between a static ABS of interest and a static HBS is considered, in the presence of external interference at the HBS that come from other ABSs different from the ABS of interest (these interfering ABS transmitting at the same time and frequency can be located at the same cell or at neighboring cells). The scenario features two types of limited feedback links, one from the HBS to the ABS of interest which is used to transmit information on the second order statistics of the interference plus noise at the HBS and another feedback link from each MS to the ABS which sends information of the Grammian of their current channel propagation matrix.

It is a design decision that the link between ABS and HBS does not interfere with the access network and also that the effect of the interference at the HBS is taken into account for the design of the precoding matrix at the ABS. The solution presented here is the optimum precoding matrix given these considerations.

Simulations show the performance of the proposed solution, and the gain achieved by using both a differential and a non-differential quantization algorithm in the feedback links. The differential algorithm achieves better performance because it exploits the geometry of the domain space and also the correlation in time of the propagation channel.

6.3 Transceiver design framework for the BuNGee system based on channel Gram matrix feedback

This section presents a framework for the transceiver design in multiuser MIMO-OFDM BC systems which, instead of the feedback of the MIMO channel response matrix for each user, considers the feedback of the channel Gram matrices. It is important to highlight here that, as it can be seen from the block diagram in Figure 6-8, this general framework admits, as a particular case, the BuNGee system architecture.

This idea is based on the previous works [Pay09a], [Sac10a], where it was proved that, for point-to-point single-user MIMO systems, the minimum amount of channel state information (CSI) required at the transmitter in order to perform the optimum linear precoding corresponds to such channel Gram matrix. This conclusion is extended here for the multiuser scenario and also to robust designs through a unique decomposition of the channel Gram matrix of each user (HSS in the BuNGee architecture), which results in a triangular equivalent propagation channel response matrix.

Additionally, a feedback based on the temporal channel impulse response is proposed, as opposed to the usual quantization and feedback based on the frequency response per carrier. This enables to exploit the frequency correlation of the CSI in order to further improve the efficiency of the quantization and feedback. The propagation of the CSI quantization error through the computation of the equivalent channel is also studied analytically and this result is later used, as an example, in the design of a robust precoding scheme.

The proposed framework is valid for any design criterion and we considered, as an illustrative example, the robust minimization of the sum of the mean square errors (MSE) of all the symbol streams for all the users, with fixed decoders. This design maps information symbols to antennas and carriers in order to exploit both spatial and frequency diversity, and requires estimates of the multiuser channel responses at the transmitter. It is a robust design in the sense that it takes into account the errors in the quantization for the feedback transmission to optimize the performance.

Note that there is a wide range of designs based on MSE in the literature, such as: [Wan10], [Sun09] which also consider fixed decoders, or [Ten04], [Shi07] and [Vuc09], which present iterative designs. Note that the algorithm presented in this section could be applied in iterative designs such as the ones in [Ten04], [Shi07] and [Vuc09], at the step where the transmitter is computed at each iteration. Other works such as [Cai10], [Cha07] assume single-antenna receivers, in which case the decoder design is not an issue.

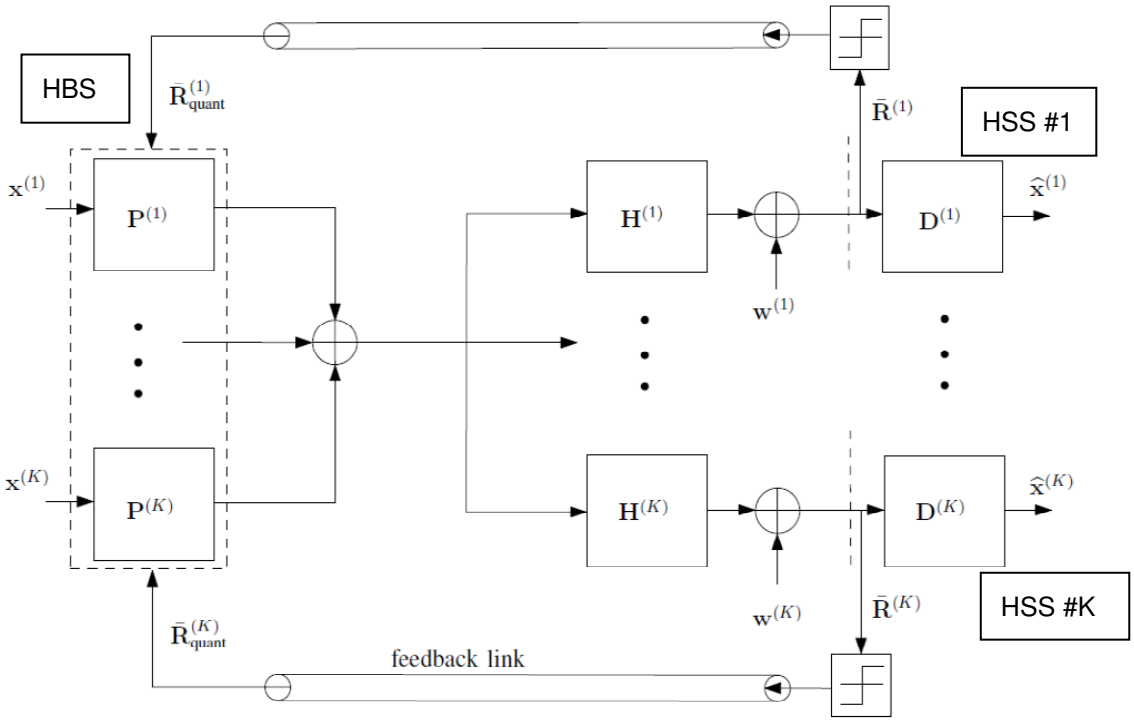

***Figure 6-8*: Block diagram of the BuNGee architecture where an HBS is depicted as a transmitter and a set of HSSs are depicted as receivers.**

We consider a general multiuser MIMO-OFDM BC system (which, as pointed out before, whenever needed can be particularized to the specific BuNGee architecture) with F carriers and K users (in the BuNGee architecture the users would correspond to the HSSs), denoted by the indices $f = 0,...,F-1$ and $k = 1,...,K$, respectively. The transmitter features n_T antennas (for the BuNGee architecture the transmission antennas would correspond to the HBS beams) and the k th receiver has $n_R^{(k)}$ antennas. The propagation channel of user k is characterized by its temporal impulse response, which consists of a maximum of L taps[3] and is denoted by $\bar{\mathbf{H}}_l^{(k)} \in C^{n_R^{(k)} \times n_T}$, $l = 0,...,L-1$ (the horizontal overline is used to denote that the variable is defined in the time domain). Accordingly, the frequency channel response at carrier f and user k is given by:

$$\mathbf{H}_f^{(k)} = \sum_{l=0}^{L-1} \bar{\mathbf{H}}_l^{(k)} e^{-j\frac{2\pi}{F}fl} \in C^{n_R^{(k)} \times n_T}. \tag{6.21}$$

Classically, parallel linear precoding per carrier at the transmitter is considered, which is denoted by a precoding matrix $\mathbf{P}_f^{(k)} \in C^{n_T \times n_{S_f}^{(k)}}$, for user k and carrier f, where $n_{S_f}^{(k)}$ is the number of streams transmitted to the k th receiver through the f th carrier. The corresponding linear processing at the k th receiver for carrier f is represented by the decoding matrix $\mathbf{D}_f^{(k)} \in C^{n_{S_f}^{(k)} \times n_R^{(k)}}$. Following this model, the estimated symbols $\hat{\mathbf{x}}_f^{(k)} \in C^{n_{S_f}^{(k)}}$ corresponding to the f th carrier at the k th receiver are given by:

[3]For the case where the channel impulse responses of the different users have different number of taps, L is defined as the maximum among the number of taps for all users.

$$\hat{\mathbf{x}}_f^{(k)} = \mathbf{D}_f^{(k)}\mathbf{H}_f^{(k)}\sum_{i=1}^{K}\mathbf{P}_f^{(i)}\mathbf{x}_f^{(i)} + \mathbf{D}_f^{(k)}\mathbf{w}_f^{(k)} \in C^{n_{S_f}^{(k)}}, \quad \forall f,k, \tag{6.22}$$

where $\mathbf{x}_f^{(k)} \in C^{n_{S_f}^{(k)}}$ is the vector containing the streams of symbols transmitted to user k through carrier f and $\mathbf{w}_f^{(k)} \in C^{n_R^{(k)}}$ is the additive white Gaussian noise (AWGN) at receiver k.

Using a notation with block diagonal matrices to group the symbols transmitted through all carriers corresponding to each receiver, the estimated symbols at the k th receiver are given by:

$$\hat{\mathbf{x}}^{(k)} = \mathbf{D}^{(k)}\mathbf{H}^{(k)}\sum_{i=1}^{K}\mathbf{P}^{(i)}\mathbf{x}^{(i)} + \mathbf{D}^{(k)}\mathbf{w}^{(k)} \in C^{\sum_{f=0}^{F-1} n_{S_f}^{(k)}}, \quad \forall k, \tag{6.23}$$

where $\mathbf{D}^{(k)} = \text{blockdiag}\left(\mathbf{D}_0^{(k)},...,\mathbf{D}_{F-1}^{(k)}\right) \in C^{\sum_{f=0}^{F-1} n_{S_f}^{(k)} \times F n_R^{(k)}}$, $\hat{\mathbf{x}}^{(k)} = \left[\hat{\mathbf{x}}_0^{(k)T},...,\hat{\mathbf{x}}_{F-1}^{(k)\,T}\right]^T \in C^{\sum_{f=0}^{F-1} n_{S_f}^{(k)}}$, $\mathbf{x}^{(k)} = \left[\mathbf{x}_0^{(k)\,T},...,\mathbf{x}_{F-1}^{(k)\,T}\right]^T \in C^{\sum_{f=0}^{F-1} n_{S_f}^{(k)}}$, $\mathbf{H}^{(k)} = \text{blockdiag}\left(\mathbf{H}_0^{(k)},...,\mathbf{H}_{F-1}^{(k)}\right) \in C^{F n_R^{(k)} \times F n_T}$, $\mathbf{w}^{(k)} = \left[\mathbf{w}_0^{(k)T},...,\mathbf{w}_{F-1}^{(k)T}\right]^T \in C^{F n_R^{(k)}}$, and $\mathbf{P}^{(k)} = \text{blockdiag}\left(\mathbf{P}_0^{(k)},...,\mathbf{P}_{F-1}^{(k)}\right) \in C^{F n_T \times \sum_{f=0}^{F-1} n_{S_f}^{(k)}}$ (see Figure 6-8 for a complete diagram of the BC system).

Note that in expressions (6.22) and (6.23) each symbol is constrained to be transmitted over one single carrier as shown by the fact that the precoding and decoding matrices, $\mathbf{P}^{(k)}$ and $\mathbf{D}^{(k)}$, are block-diagonal. It is possible to achieve higher diversity by not forcing a block-diagonal structure at the precoding $\mathbf{P}^{(k)}$ and decoding $\mathbf{D}^{(k)}$ stages. According to this, in this work a space-frequency precoder is designed as a mean to extract both spatial and frequency diversity and, consequently, the precoding and decoding matrices are not constrained to be block-diagonal. Since the symbols are now spread among the carriers, it does not make sense to use the notation $n_{S_f}^{(k)}$ corresponding to the number of symbols per carrier. Instead we consider a total number of streams $n_S^{(k)}$ transmitted to receiver k through all carriers, a global precoder $\mathbf{P}^{(k)} \in C^{F n_T \times n_S^{(k)}}$ for receiver k, and a global decoder $\mathbf{D}^{(k)} \in C^{n_S^{(k)} \times F n_R^{(k)}}$ for receiver k. Note that equation (6.23) is still correct in this setup (with $\mathbf{P}^{(k)}$ and $\mathbf{D}^{(k)}$ no longer being forced to be block diagonal), by simply substituting $\sum_{f=0}^{F-1} n_{S_f}^{(k)}$ by $n_S^{(k)}$. Observe that for some particular cases the precoder and decoder matrices do turn out block-diagonal as a result of the optimization and without being imposed from the beginning.

For the sake of compactness in the notation, it is convenient to further group the symbols estimated at all receivers in a single vector $\hat{\mathbf{x}}$, which can be expressed as:

$$\hat{\mathbf{x}} = \mathbf{DHPx} + \mathbf{Dw} \in C^{\sum_{k=1}^{K} n_S^{(k)}}, \tag{6.24}$$

where

$\mathbf{x} = \left[\mathbf{x}^{(1)^T},...,\mathbf{x}^{(K)^T}\right]^T \in C^{\sum_{k=1}^{K} n_S^{(k)}}$, $\hat{\mathbf{x}} = \left[\hat{\mathbf{x}}^{(1)^T},...,\hat{\mathbf{x}}^{(K)^T}\right]^T \in C^{\sum_{k=1}^{K} n_S^{(k)}}$,

$\mathbf{H} = \left[\mathbf{H}^{(1)^T},...,\mathbf{H}^{(K)^T}\right]^T \in C^{F\sum_{k=1}^{K} n_R^{(k)} \times F n_T}$, $\mathbf{P} = \left[\mathbf{P}^{(1)},...,\mathbf{P}^{(K)}\right] \in C^{F n_T \times \sum_{k=1}^{K} n_S^{(k)}}$,

$\mathbf{w} = \left[\mathbf{w}^{(1)^T},...,\mathbf{w}^{(K)^T}\right]^T \in C^{F\sum_{k=1}^{K} n_R^{(k)}}$, and

$\mathbf{D} = \text{blockdiag}\left(\mathbf{D}^{(1)},...,\mathbf{D}^{(K)}\right) \in C^{\sum_{k=1}^{K} n_S^{(k)} \times F\sum_{k=1}^{K} n_R^{(k)}}$.

Here we have defined $\mathbf{R}_x^{(k)} = E\left\{\mathbf{x}^{(k)}\mathbf{x}^{(k)\,H}\right\}$ and $\mathbf{R}_w^{(k)} = E\left\{\mathbf{w}^{(k)}\mathbf{w}^{(k)^H}\right\}$; therefore, $\mathbf{R}_x = E\left\{\mathbf{xx}^H\right\} = \text{blockdiag}\left(\mathbf{R}_x^{(1)},...,\mathbf{R}_x^{(K)}\right)$ and $\mathbf{R}_w = E\left\{\mathbf{ww}^H\right\} = \text{blockdiag}\left(\mathbf{R}_w^{(1)},...,\mathbf{R}_w^{(K)}\right)$.

6.3.1 Feedback and equivalent channels

As will be seen in Section 6.2.4, in general, in order to optimally design the precoding matrix $\mathbf{P}$ at the transmitter under a generic optimization criterion, the CSI needed from each user corresponds to the channel propagation matrices for all F carriers. That is, knowledge of $\mathbf{H}_f^{(k)} \in C^{n_R^{(k)} \times n_T}$, $\forall f,k$ (or, equivalently, $\mathbf{H}^{(k)}$ as defined in (6.23)) is used to build the optimum precoder. In [Pay09a], [Pal03], however, the authors proved that, for the single user point-to-point MIMO scenario, the optimum linear precoding design can be calculated with just the channel Gram matrix (which is defined as $\mathbf{R}_f^{(k)} = \mathbf{H}_f^{(k)\,H}\mathbf{H}_f^{(k)}$), for all the usual criteria. This fact was applied in [Sac10a], [Cha08], [Sac09] to design more efficient feedback algorithms that exploit the differential geometry of the set of all possible channel Gram matrices, which are Hermitian and positive semidefinite by construction, and that perform better than the feedback of the channel matrix $\mathbf{H}_f^{(k)}$. The motivation for using Gram matrix feedback is that it contains less information than the channel matrix feedback, but this information is sufficient for the precoder designs. Since less information has to be quantized and sent through the feedback link, the feedback can be performed more efficiently and the system performance is better, as shown in the related works [Sac10a], [Pal03] among others. In some specific multiuser systems, such as in the BC with block diagonalization (BD) [Spe04], the transmitter design also depends only on the channel Gram matrix of each user and, therefore, the efficient techniques for quantization and feedback presented in [Sac10a], [Cha08], [Sac09] could also be applied, as shown in [Sac10b]. Note, however, that in the general multiuser scenario (i.e., without constraining a BD transmission and/or for a general quality criterion), as well as in robust precoder designs, complete knowledge of each $\mathbf{H}_f^{(k)}$ has been assumed so far by the research community. As a contribution of the BuNGee project, in Section 6.2.3, we present a linear transformation technique that still enables the use of channel Gram matrix feedback even in the general multiuser scenario by adding a unitary pre-transformation at the decoder to identify uniquely an equivalent triangular MIMO channel for each receiver. That is, knowledge of $\mathbf{R}_f^{(k)} \equiv \mathbf{H}_f^{(k)\,H}\mathbf{H}_f^{(k)} \in C^{n_T \times n_T}$ of each carrier and user is sufficient to design the optimum precoder.

In this work we also analyze the possibility of performing feedback of the temporal CSI instead of the frequency CSI in a per carrier basis, as is usually done in OFDM systems. Following from (6.21), the F Gram matrices $\mathbf{R}_f^{(k)}$ of size $n_T \times n_T$ for each user can also be computed as:

$$\mathbf{R}_f^{(k)} \equiv \mathbf{H}_f^{(k)\,H}\mathbf{H}_f^{(k)} = \sum_{n=0}^{L-1}\sum_{m=0}^{L-1} \bar{\mathbf{H}}_n^{(k)\,H}\bar{\mathbf{H}}_m^{(k)} e^{-j\frac{2\pi}{F}f(m-n)} \in C^{n_T \times n_T}, \quad f = 0,\ldots,F-1. \tag{6.25}$$

Using this, the necessary CSI corresponding to the k th user at the transmitter can be computed with knowledge of the L matrices $\bar{\mathbf{H}}_l^{(k)} \in C^{n_R^{(k)} \times n_T}$ or, alternatively, using one temporal Gram matrix $\bar{\mathbf{R}}^{(k)} \in C^{Ln_T \times Ln_T}$ defined as (note that the sub-blocks of the following matrix are used directly within the sum in (6.25)):

$$\bar{\mathbf{R}}^{(k)} \equiv \begin{bmatrix} \bar{\mathbf{H}}_0^{(k)\,H} \\ \bar{\mathbf{H}}_1^{(k)\,H} \\ \vdots \\ \bar{\mathbf{H}}_{L-1}^{(k)\,H} \end{bmatrix} \begin{bmatrix} \bar{\mathbf{H}}_0^{(k)} & \bar{\mathbf{H}}_1^{(k)} & \cdots & \bar{\mathbf{H}}_{L-1}^{(k)} \end{bmatrix}$$

$$= \begin{bmatrix} \bar{\mathbf{H}}_0^{(k)\,H}\bar{\mathbf{H}}_0^{(k)} & \bar{\mathbf{H}}_0^{(k)\,H}\bar{\mathbf{H}}_1^{(k)} & \cdots & \bar{\mathbf{H}}_0^{(k)\,H}\bar{\mathbf{H}}_{L-1}^{(k)} \\ \bar{\mathbf{H}}_1^{(k)\,H}\bar{\mathbf{H}}_0^{(k)} & \bar{\mathbf{H}}_1^{(k)\,H}\bar{\mathbf{H}}_1^{(k)} & \cdots & \vdots \\ \vdots & \vdots & \ddots & \vdots \\ \bar{\mathbf{H}}_{L-1}^{(k)\,H}\bar{\mathbf{H}}_0^{(k)} & \bar{\mathbf{H}}_{L-1}^{(k)\,H}\bar{\mathbf{H}}_1^{(k)} & \cdots & \bar{\mathbf{H}}_{L-1}^{(k)\,H}\bar{\mathbf{H}}_{L-1}^{(k)} \end{bmatrix} \in C^{Ln_T \times Ln_T}.$$

Observe that matrices $\mathbf{R}_f^{(k)}$ and $\bar{\mathbf{R}}^{(k)}$ are positive semidefinite and Hermitian by construction. Since, as will be seen in the following subsections, the precoder design depends on the propagation channel of each user through $\mathbf{R}_f^{(k)}$, the most straightforward approach would be to quantize and feed back $\mathbf{R}_f^{(k)}$ individually for each carrier and user. However, this is suboptimal because: a) it does not exploit the correlation in frequency of the propagation channel, and b) in systems with many carriers the feedback overhead would be too large. Therefore, in order to improve the performance of the CSI quantization, the scheme proposed in this section considers the possibility of feeding back the temporal channel Gram matrix $\bar{\mathbf{R}}^{(k)}$ of each user. This allows to exploit the correlation in frequency of the channel and also the fact that the size of the matrix to be quantized grows with the number of channel impulse response taps L instead of the number of carriers F. This can help to greatly improve the performance of the CSI quantization in some situations, as will be shown in Section 6.2.5.

From the knowledge of the temporal channel Gram matrix $\bar{\mathbf{R}}^{(k)}$ (and therefore, the individual Gram matrices $\mathbf{R}_f^{(k)}$ associated to each carrier), it is possible to compute (as is described in the next section), for each user and carrier, a unique equivalent channel response triangular matrix which can be used to apply any type of multiuser design on top of it (without the restrictions of BD, which spends degrees of freedom to completely avoid inter-user interference), for any quality criterion in the same way as if knowledge of the actual channel response matrix $\mathbf{H}_f^{(k)}$ was available.

Equivalent channel transformation

Following the feedback model presented in the previous section, knowledge of an estimation of the channel Gram matrix of each user is assumed at the transmitter. Note that there are multiple possible channel matrices $\mathbf{H}^{(k)}$ that generate the same Gram matrix $\mathbf{R}^{(k)} = \mathbf{H}^{(k)H}\mathbf{H}^{(k)}$ (for example $\mathbf{H}^{(k)}$ and $\mathbf{U}\mathbf{H}^{(k)}$, with $\mathbf{U}$ being a unitary matrix, generate the same Gram matrix). Since the transmitter has knowledge only of the Gram matrix, it cannot know which of the multiple channel matrices that generate that Gram matrix is the actual channel matrix. However, there is only one of the possible matrices that can generate the Gram matrix that is upper triangular and with real positive elements in the diagonal, and this matrix can be computed at the transmitter, as will be shown in this subsection. On the other hand, note also that, by applying a properly calculated unitary linear transformation $\mathbf{Q}^{(k)H}$, with $\mathbf{Q}^{(k)} \in C^{Fn_R^{(k)} \times Fn_R^{(k)}}$ at each receiver k, it is possible to generate an equivalent channel response matrix $\mathbf{T}^{(k)} \in C^{Fn_R^{(k)} \times Fn_T}$ from the transmitter to the output of such unitary transformation at each receiver (as shown in Figure 6-9), which is upper triangular and with real elements in the diagonal.

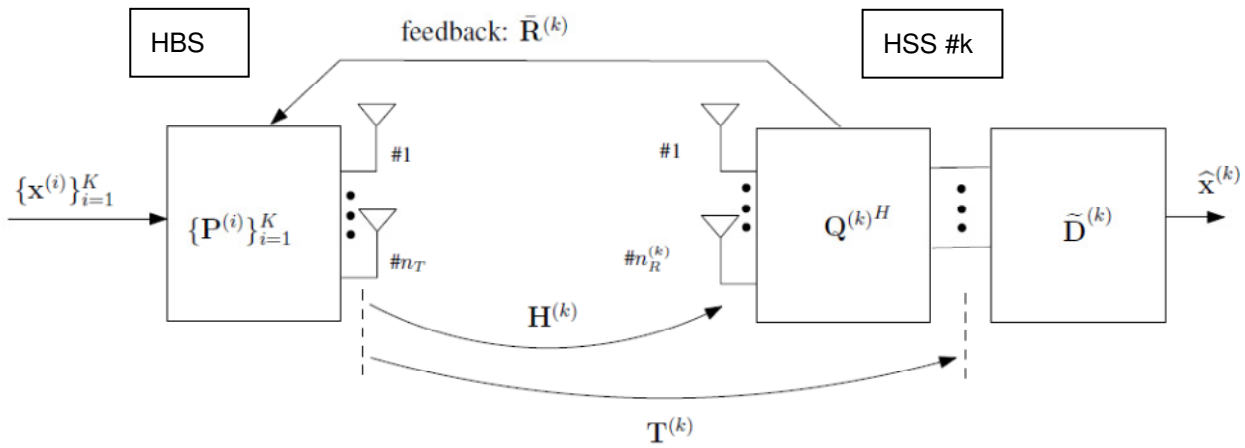

Figure 6-9*: *Equivalent channel model of the BuNGee architecture.

Since there is only one possible upper triangular matrix with real elements in the diagonal associated to the Gram matrix, and the unitary transformation does not change the Gram matrix, the equivalent channel matrix computed at the transmitter and the equivalent channel generated by the application of such unitary transformation $\mathbf{Q}^{(k)}$ at the receiver are the same. This scheme is depicted in Figure 6-9 (note that in Figure 6-9, $\bar{\mathbf{D}}^{(k)}$ is defined as $\bar{\mathbf{D}}^{(k)} = \mathbf{D}^{(k)}\mathbf{Q}^{(k)} \in C^{n_S^{(k)} \times F n_R^{(k)}}$, so that $\mathbf{D}^{(k)} = \bar{\mathbf{D}}^{(k)}\mathbf{Q}^{(k)^H}$).

Finally, it is important to note that this matrix $\mathbf{Q}^{(k)}$ does not introduce a penalty in the performance of the system since it is a unitary linear transformation that could be reversed at the receiver by a proper processing after such unitary transformation, and it allows any arbitrary multiuser transmission design to be applied on top of the basis of these new equivalent channel matrices $\left\{\mathbf{T}^{(k)}\right\}_{k=1}^{K}$, where now the transmitter is required to know only the channel Gram matrices $\mathbf{R}_f^{(k)}$ or $\bar{\mathbf{R}}^{(k)}$.

According to the previous definitions, the equivalent triangular channel, $\mathbf{T}^{(k)}$, is such that satisfies:

$$\mathbf{H}^{(k)} = \mathbf{Q}^{(k)}\mathbf{T}^{(k)}, \quad \forall k = 1,...,K. \tag{6.26}$$

The computation of the equivalent channel response matrix $\mathbf{T}^{(k)}$ at the transmitter is given as a function of the matrix $\mathbf{R}^{(k)}$. At the receiver, matrices $\mathbf{Q}^{(k)}$ and $\mathbf{T}^{(k)}$ are computed from $\mathbf{H}^{(k)}$.

Observe that, since $\mathbf{H}^{(k)}$ is a block diagonal matrix (we recall that $\mathbf{H}^{(k)} = \text{blockdiag}\left(\mathbf{H}_0^{(k)},...,\mathbf{H}_{F-1}^{(k)}\right)$), the resulting $\mathbf{Q}^{(k)}$ and $\mathbf{T}^{(k)}$ are also block diagonal. In fact, the computation can be performed in parallel for each block of $\mathbf{H}^{(k)}$, which corresponds to the channel response matrix for each carrier, $\mathbf{H}_f^{(k)}$ $\forall f = 0,...,F-1$. This greatly reduces the required computational complexity, and, for this reason, the transformation will be presented next for each individual matrix $\mathbf{H}_f^{(k)}, \mathbf{R}_f^{(k)}$.

The channel response matrix for the f th carrier and the k th receiver $\mathbf{H}_f^{(k)}$ can be written as:

$$\mathbf{H}_f^{(k)} = \mathbf{Q}_f^{(k)}\mathbf{T}_f^{(k)}, \quad \forall f = 0,...,F-1, \tag{6.27}$$

where $\mathbf{Q}_f^{(k)} \in C^{n_R^{(k)} \times n_R^{(k)}}$ is unitary and $\mathbf{T}_f^{(k)} \in C^{n_R^{(k)} \times n_T}$ is upper triangular [Hor85] (consequently, the channel Gram matrix $\mathbf{R}_f^{(k)}$ can also be written as $\mathbf{R}_f^{(k)} = \mathbf{H}_f^{(k)^H}\mathbf{H}_f^{(k)} = \mathbf{T}_f^{(k)^H}\mathbf{T}_f^{(k)}$). The decomposition that allows to calculate $\mathbf{T}_f^{(k)}$ from $\mathbf{R}_f^{(k)}$ is unique if we force $\mathbf{T}_f^{(k)}$ to be upper triangular and with the elements $t_{i,i}$ on the main diagonal being positive and real, as will be shown next.

Calculation of $\mathbf{T}_f^{(k)}$ at the transmitter

Matrix $\mathbf{R}_f^{(k)}$ is obtained at the transmitter from the $\bar{\mathbf{R}}^{(k)}$ received through the feedback link using (6.25). Using $\mathbf{R}_f^{(k)}$, the transmitter can uniquely compute $\mathbf{T}_f^{(k)}$ as described next. Observe that there is only one possible $\mathbf{T}_f^{(k)} \in C^{n_R^{(k)} \times n_T}$ satisfying that the elements $t_{i,i}$ are real and positive and $t_{i,j} = 0, \forall i > j$.

From $\mathbf{R}_f^{(k)} = \mathbf{T}_f^{(k)^H}\mathbf{T}_f^{(k)}$, matrix $\mathbf{T}_f^{(k)}$ is computed as ($j \geq i$):[4]

[4]Note that the presented decomposition is not exactly the Cholesky factorization because the resulting matrix $\mathbf{T}_f^{(k)} \in C^{n_R^{(k)} \times n_T}$ is not forced to be square (the equivalent channel propagation matrix $\mathbf{T}_f^{(k)}$ must have the same dimensions as the actual channel propagation matrix $\mathbf{H}_f^{(k)}$).

$$\mathrm{t}_{i,j}=\begin{cases}\sqrt{r_{1,1}}, & i=j=1,\\ \frac{r_{1,j}}{t_{1,1}}, & i=1,\forall\, j>1,\\ \frac{r_{i,j}-\sum_{k=1}^{i-1} t_{k,i}^{*} t_{k,j}}{t_{i,i}}, & \forall\, i,j;1<i<j,\\ \sqrt{r_{i,i}-\sum_{k=1}^{i-1}|t_{k,i}|^{2}}, & \forall\, i,j;i=j>1,\end{cases}$$

where $\mathrm{r}_{i,j}$ and $t_{i,j}$ are the elements i,j of $\mathbf{R}_f^{(k)}$ and $\mathbf{T}_f^{(k)}$, respectively, and where, for the sake of clarity in the notation, we have dropped the dependence of $r_{i,j}$ and $t_{i,j}$ on f.

Calculation of $\mathbf{T}_f^{(k)}$ and $\mathbf{Q}_f^{(k)}$ at the receiver

The receiver knows $\mathbf{H}_f^{(k)}$ and can obtain $\mathbf{T}_f^{(k)}=\mathbf{Q}_f^{(k)\,H}\mathbf{H}_f^{(k)}$, as is described in the following algorithm based on the QR decomposition. From (6.27) we have that matrices $\mathbf{T}_f^{(k)}$ and $\mathbf{Q}_f^{(k)}$ can be computed as[5]:

$$\mathbf{q}_i=\begin{cases}\frac{\mathbf{h}_1}{\|\mathbf{h}_1\|} & i=1,\\ \frac{\left(\mathbf{I}-\sum_{k=1}^{i-1}\mathbf{q}_k\mathbf{q}_k^{H}\right)\mathbf{h}_i}{\left\|\left(\mathbf{I}-\sum_{k=1}^{i-1}\mathbf{q}_k\mathbf{q}_k^{H}\right)\mathbf{h}_i\right\|}, & \forall i;1<i\le n_T,\end{cases} \tag{6.28}$$

$$t_{i,j}=\begin{cases}\mathbf{q}_i^{H}\mathbf{h}_j, & \forall\, i<j,\\ \|\mathbf{h}_1\|, & i=j=1,\\ \left\|\left(\mathbf{I}-\sum_{k=1}^{i-1}\mathbf{q}_k\mathbf{q}_k^{H}\right)\mathbf{h}_i\right\|, & \forall\, i,j;i=j>1,\end{cases} \tag{6.29}$$

where $\mathbf{q}_i$ and $\mathbf{h}_i$ correspond to the ith column of matrices $\mathbf{Q}_f^{(k)}$ and $\mathbf{H}_f^{(k)}$, respectively, and, again, the dependence on f is omitted for clarity in the notation.

In the case where $n_R^{(k)}>n_T$, the last $n_R^{(k)}-n_T$ columns of $\mathbf{Q}_f^{(k)}$ are chosen such that $\mathbf{Q}_f^{(k)\,H}\mathbf{Q}_f^{(k)}=\mathbf{I}$, i.e., they just have to be orthogonal with each other and with the previous columns and have a norm equal to 1 and they can be calculated following the Gram-Schmidt procedure. In this case, we assume that the rank of the matrix $\mathbf{R}_f^{(k)}$ is given by n_T. It is important to note that the equivalent channel $\mathbf{T}_f^{(k)}$ is a tall matrix with the last $n_R^{(k)}-n_T$ rows equal to zero. This means that, at the receiver, after the application of the transformation represented by $\mathbf{Q}_f^{(k)\,H}$, the last $n_R^{(k)}-n_T$ outputs contain only noise, which is uncorrelated with the data. Observe that, in the case of spatially white noise, i.e., if $\mathbf{R}_{w_f}^{(k)}=\sigma_{w_f}^2\mathbf{I}$, the last $n_R^{(k)}-n_T$ outputs contain no useful information. Consequently, for the computation of the estimates of the transmitted symbols at the receiver, the last $n_R^{(k)}-n_T$ columns of $\mathbf{Q}_f^{(k)}$ could be ignored, reducing the complexity of

[5]Note that, since at the receiver there is knowledge of $\mathbf{H}_f^{(k)}$, it would also be possible to calculate $\mathbf{R}_f^{(k)}=\mathbf{H}_f^{(k)\,H}\mathbf{H}_f^{(k)}$ and compute $\mathbf{T}_f^{(k)}$ locally as explained in the previous subsection describing the decomposition to be calculated at the transmitter.

computing $\mathbf{Q}_f^{(k)}$. In the case where $n_R^{(k)} \leq n_T$ we assume that the rank of the matrix $\mathbf{R}_f^{(k)}$ is given by $n_R^{(k)}$ and the transformation is performed as already described in this subsection.

6.3.2 Error analysis

In general, robust transceiver designs require the characterization of the CSI error in order to minimize its effect. In the presented framework, this characterization has been performed in terms of the second-order statistics of the resulting error at the equivalent triangular channel matrix, as will be shown in this section. This will exploited in the robust design presented in Section 6.3.3 as an illustrative example of application.

The error in the equivalent triangular channel is the result of the propagation of the initial error generated in the CSI quantization. In general, only the second-order statistics of the initial quantization error are known. This section presents the analytic study of the linear relation, for small errors, between the initial quantization error and the final error in the equivalent triangular channel matrix. From this derivation it will be possible to compute the second order statistics of the error in the equivalent triangular channel, which is often required in statistical robust designs.

Error model

There are three different sources of inaccuracies in the CSI sent through the feedback link from the receiver to the transmitter: estimation errors at the receiver, quantization errors which are inherent to the feedback process, and errors due to noise in the feedback link. In practical situations, where the part of the transmission dedicated to feedback is greatly constrained, the quantization error is the dominant factor of the error. Consequently, in this section we will consider only the errors resulting from the quantization process. The CSI at the transmitter $\overline{\mathbf{R}}_{\text{quant}}^{(k)} \equiv \text{quantiz}\left(\overline{\mathbf{R}}^{(k)}\right)$ is then modeled with the error matrix $\overline{\mathbf{R}}_{\text{err}}^{(k)}$:

$$\overline{\mathbf{R}}^{(k)} = \overline{\mathbf{R}}_{\text{quant}}^{(k)} + \overline{\mathbf{R}}_{\text{err}}^{(k)} \in C^{Ln_T \times Ln_T}. \tag{6.30}$$

Note that, although the rank of matrix $\overline{\mathbf{R}}^{(k)} \in C^{Ln_T \times Ln_T}$ before the quantization is $\min\left(n_R^{(k)}, Ln_T\right)$, depending on the quantization strategy that is applied and if $n_R^{(k)} < Ln_T$ it is possible that after the quantization the rank of the resulting matrix is increased up to Ln_T. Consequently, if $n_R^{(k)} < Ln_T$, then matrix $\overline{\mathbf{R}}_{\text{quant}}^{(k)}$ should be projected on the space of the matrices with a rank equal to $n_R^{(k)}$ at the transmitter in order to maintain the rank.[6] The error after the projection, is then propagated at the transmitter through the Fourier transformation used to compute the channel Gram matrix associated to carrier f and user k based on the Fourier transform and through the computation of the equivalent triangular channel $\mathbf{T}_f^{(k)}$. The final error in the resulting knowledge of $\mathbf{T}_f^{(k)}$ is denoted in the following by $\mathbf{T}_{\text{err}_f}^{(k)}$:

$$\mathbf{T}_f^{(k)} = \mathbf{T}_{\text{quant}_f}^{(k)} + \mathbf{T}_{\text{err}_f}^{(k)}, \tag{6.31}$$

where $\mathbf{T}_{\text{quant}_f}^{(k)}$ is the estimated value of the actual equivalent triangular channel $\mathbf{T}_f^{(k)}$ calculated using the quantized and projected channel Gram matrix sent through the feedback link. The expression of $\mathbf{T}_{\text{err}_f}^{(k)}$ as a result of the error propagation is derived in the following subsection.

Following this notation, (6.24) can be rewritten reflecting the errors in the CSI at the transmitter and incorporating the notation corresponding to the equivalent channels as:

[6] In the case where $n_R^{(k)} \geq Ln_T$ the quantization process maintains the rank of the matrix, but in the case that $n_R^{(k)} < Ln_T$ the projection presented here is required in order to keep the same rank.

$$\hat{\mathbf{x}} = \bar{\mathbf{D}}\mathbf{T}_{\text{quant}}\mathbf{P}\mathbf{x} + \bar{\mathbf{D}}\mathbf{T}_{\text{err}}\mathbf{P}\mathbf{x} + \bar{\mathbf{D}}\mathbf{Q}^H\mathbf{w} \in C^{\sum_{k=1}^{K} n_S^{(k)}}, \tag{6.32}$$

where $\mathbf{T}_{\text{quant}}^{(k)} = \text{blockdiag}\left(\mathbf{T}_{\text{quant }0}^{(k)},...,\mathbf{T}_{\text{quant }F-1}^{(k)}\right) \in C^{Fn_R^{(k)} \times Fn_T}$, $\mathbf{T}_{\text{err}}^{(k)} = \text{blockdiag}\left(\mathbf{T}_{\text{err }0}^{(k)},...,\mathbf{T}_{\text{err }F-1}^{(k)}\right) \in C^{Fn_R^{(k)} \times Fn_T}$,

$\bar{\mathbf{D}} = \text{blockdiag}\left(\bar{\mathbf{D}}^{(1)},...,\bar{\mathbf{D}}^{(K)}\right) \in C^{\sum_{k=1}^{K} n_S^{(k)} \times F\sum_{k=1}^{K} n_R^{(k)}}$,

$\mathbf{Q} = \text{blockdiag}\left(\mathbf{Q}^{(1)},...,\mathbf{Q}^{(K)}\right) \in C^{F\sum_{k=1}^{K} n_R^{(k)} \times F\sum_{k=1}^{K} n_R^{(k)}}$, $\mathbf{T}_{\text{quant}} = \left[\mathbf{T}_{\text{quant}}^{(1)^T},...,\mathbf{T}_{\text{quant}}^{(K)^T}\right]^T \in C^{F\sum_{k=1}^{K} n_R^{(k)} \times Fn_T}$, and

$\mathbf{T}_{\text{err}} = \left[\mathbf{T}_{\text{err}}^{(1)^T},...,\mathbf{T}_{\text{err}}^{(K)^T}\right]^T \in C^{F\sum_{k=1}^{K} n_R^{(k)} \times Fn_T}$.

Error propagation

As shown in the previous subsection, the CSI inaccuracies are defined in the matrix $\bar{\mathbf{R}}^{(k)}$, which is quantized and then sent through the feedback link. At the transmitter, the received matrix $\bar{\mathbf{R}}_{\text{quant}}^{(k)}$ is projected, if needed, to guarantee that its rank is $\min(n_R^{(k)}, Ln_T)$ and an estimation of the channel Gram matrix $\mathbf{R}_{\text{quant}_f}^{(k)}$ is computed using the projected matrix $\bar{\mathbf{R}}_{\text{quant,p}}^{(k)}$, following (6.25). In a third step, the estimated equivalent channel $\mathbf{T}_{\text{quant}}^{(k)}$ is computed from $\mathbf{R}_{\text{quant}_f}^{(k)}$.

First, the propagation of the error through the semidefinite projection is presented. Next, the transformation of the resulting error through the computation of $\mathbf{R}_f^{(k)}$ at the transmitter is studied. Finally, the result is further propagated through the equivalent channel computation, in order to obtain an expression of $\mathbf{T}_{\text{err}}^{(k)}$. This result will then be used for the design of the robust precoder in Section 6.3.3.

Propagation through the semidefinite projection

As it has been pointed out above, the first step where the quantization error propagates through is the positive semidefinite projection. Note that if $n_R^{(k)} \geq Ln_T$ this step is not necessary, since $\bar{\mathbf{R}}_{\text{quant}}^{(k)}$ already maintains the same rank as $\bar{\mathbf{R}}^{(k)}$, so, in the following of this subsection we will assume that $n_R^{(k)} < Ln_T$. The positive semidefinite projection operator, P, is defined as:

$$P(\mathbf{X}, N) = \sum_{i=1}^{N} \lambda_i(\mathbf{X})\mathbf{u}_i(\mathbf{X})\mathbf{u}_i(\mathbf{X})^H, \tag{6.33}$$

where $\mathbf{X}$ represents any Hermitian matrix, $\lambda_i(\mathbf{X})$ is the i-th eigenvalue of $\mathbf{X}$ (sorted in decreasing order), and $\mathbf{u}_i(\mathbf{X})$ is its associated unitary eigenvector.

Consequently, this first step can be formally written as $\bar{\mathbf{R}}_{\text{quant,p}}^{(k)} = P(\bar{\mathbf{R}}_{\text{quant}}^{(k)}, n_R^{(k)})$ and, from (6.30), we have that $\bar{\mathbf{R}}_{\text{quant,p}}^{(k)} = P(\bar{\mathbf{R}}^{(k)} - \bar{\mathbf{R}}_{\text{err}}^{(k)}, n_R^{(k)})$. This can also be written as:

$$\bar{\mathbf{R}}_{\text{quant,p}}^{(k)} = P(\bar{\mathbf{R}}^{(k)} - \bar{\mathbf{R}}_{\text{err}}^{(k)}, n_R^{(k)}) = P(\bar{\mathbf{R}}^{(k)}, n_R^{(k)}) - \bar{\mathbf{R}}_{\text{err,p}}^{(k)} = \bar{\mathbf{R}}^{(k)} - \bar{\mathbf{R}}_{\text{err,p}}^{(k)}, \tag{6.34}$$

where the error after the projection is defined as $\bar{\mathbf{R}}_{\text{err,p}}^{(k)} P(\bar{\mathbf{R}}^{(k)}, n_R^{(k)}) - P(\bar{\mathbf{R}}^{(k)} - \bar{\mathbf{R}}_{\text{err}}^{(k)}, n_R^{(k)}) = \bar{\mathbf{R}}^{(k)} - P(\bar{\mathbf{R}}^{(k)} - \bar{\mathbf{R}}_{\text{err}}^{(k)}, n_R^{(k)})$. Now, it remains to linearly relate the

real and imaginary parts of the elements in $\overline{\mathbf{R}}_{\text{err,p}}^{(k)}$ with those in $\overline{\mathbf{R}}_{\text{err}}^{(k)}$, which can be done using a first order approximation and the results in [Mag02] as:

$$\overline{\text{vec}}\left(\overline{\mathbf{R}}_{\text{err,p}}^{(k)}\right)\left(\mathrm{D}_{\overline{\mathbf{r}}^{(k)}}P(\overline{\mathbf{R}}^{(k)},n_R^{(k)})\right)\overline{\text{vec}}\left(\overline{\mathbf{R}}_{\text{err}}^{(k)}\right), \tag{6.35}$$

where we have used the operator $\overline{\text{vec}}(\cdot)=[\text{vech}(\Re\text{e}(\cdot))^T\ \text{veci}(\Im\text{m}(\cdot))^T]^T$ [7] and $\overline{\mathbf{r}}^{(k)}=\overline{\text{vec}}\left(\overline{\mathbf{R}}^{(k)}\right)$. Finally, with a modicum of algebra and using the results in [Pay09b], the expression of the Jacobian matrix $\mathrm{D}_{\overline{\mathbf{r}}^{(k)}}P(\overline{\mathbf{R}}^{(k)},n_R^{(k)})$ can be computed as:

$$\begin{aligned}\mathrm{D}_{\overline{\mathbf{r}}^{(k)}}P(\overline{\mathbf{R}}^{(k)},n_R^{(k)}) &= \sum_{i=1}^{n_R^{(k)}}\text{vec}(\mathbf{u}_i(\overline{\mathbf{R}}^{(k)})\mathbf{u}_i(\overline{\mathbf{R}}^{(k)})^H)\left(\mathrm{D}_{\overline{\mathbf{r}}^{(k)}}\lambda_i(\overline{\mathbf{R}}^{(k)})\right)\\ &+\sum_{i=1}^{n_R^{(k)}}\lambda_i(\overline{\mathbf{R}}^{(k)})(\mathbf{u}_i(\overline{\mathbf{R}}^{(k)})^*\otimes\mathbf{I}_{n_T})(\mathrm{D}_{\overline{\mathbf{r}}^{(k)}}\mathbf{u}_i(\overline{\mathbf{R}}^{(k)}))+\sum_{i=1}^{n_R^{(k)}}\lambda_i(\overline{\mathbf{R}}^{(k)})(\mathbf{I}_{n_T}\otimes\mathbf{u}_i(\overline{\mathbf{R}}^{(k)}))(\mathrm{D}_{\overline{\mathbf{r}}^{(k)}}\mathbf{u}_i(\overline{\mathbf{R}}^{(k)}))^*,\end{aligned} \tag{6.36}$$

where the explicit expressions for $\mathrm{D}_{\overline{\mathbf{r}}^{(k)}}\lambda_i(\overline{\mathbf{R}}^{(k)})$ and $\mathrm{D}_{\overline{\mathbf{r}}^{(k)}}\mathbf{u}_i(\overline{\mathbf{R}}^{(k)})$ can be straightforwardly found from the results in [Mag02] and are not reproduced here for the sake of space.

Propagation through the Fourier transformation

Equation (6.25) describes the computation of $\mathbf{R}_f^{(k)}$ from $\overline{\mathbf{R}}^{(k)}$, which corresponds to the Fourier transformation of the projected time domain Gram matrix. The error propagation through the computation of $\mathbf{R}_f^{(k)}$ is studied next. From (6.25) and (6.34) it follows that:

$$\mathbf{R}_f^{(k)}={\mathbf{F}_f}^H\overline{\mathbf{R}}^{(k)}\mathbf{F}_f={\mathbf{F}_f}^H\left(\overline{\mathbf{R}}_{\text{quant,p}}^{(k)}+\overline{\mathbf{R}}_{\text{err,p}}^{(k)}\right)\mathbf{F}_f, \tag{6.37}$$

where $\mathbf{F}_f$ is the extended Fourier matrix defined as

$$\mathbf{F}_f=\left[e^{-j\frac{2\pi}{F}(f-0)},e^{-j\frac{2\pi}{F}(f-1)},\ldots,e^{-j\frac{2\pi}{F}(f-(L-1))}\right]^T\otimes\mathbf{I}_{n_T}\in C^{Ln_T\times n_T}.$$

Following from (6.37), the error in the computation of $\mathbf{R}_f^{(k)}$ at the transmitter is given by

$$\mathbf{R}_{\text{err}_f}^{(k)}\equiv{\mathbf{F}_f}^H\overline{\mathbf{R}}_{\text{err,p}}^{(k)}\mathbf{F}_f, \tag{6.38}$$

where we have that $\mathbf{R}_f^{(k)}=\mathbf{R}_{\text{quant}_f}^{(k)}+\mathbf{R}_{\text{err}_f}^{(k)}$ and $\mathbf{R}_{\text{quant}_f}^{(k)}$ is the estimated Gram matrix associated to receiver k and carrier f, i.e., $\mathbf{R}_{\text{quant}_f}^{(k)}={\mathbf{F}_f}^H\overline{\mathbf{R}}_{\text{quant,p}}^{(k)}\mathbf{F}_f$. Following the structure used in the previous subsection, the propagation of the error through the Fourier transformation, (6.38), can be expressed as: $\overline{\text{vec}}\left(\mathbf{R}_{\text{err}_f}^{(k)}\right)=\tilde{\mathbf{F}}_f\overline{\text{vec}}\left(\overline{\mathbf{R}}_{\text{err,p}}^{(k)}\right)$, where

$$\tilde{\mathbf{F}}=\begin{bmatrix}\mathbf{D}_{n_T}^{+}\left(\mathbf{F}_{fr}^T\otimes\mathbf{F}_{fr}^T+\mathbf{F}_{fi}^T\otimes\mathbf{F}_{fi}^T\right)\mathbf{D}_{Ln_T} & \mathbf{D}_{n_T}^{+}\left(\mathbf{F}_{fr}^T\otimes\mathbf{F}_{fi}^T-\mathbf{F}_{fi}^T\otimes\mathbf{F}_{fr}^T\right)\mathbf{D}_{Ln_T}\\ \mathbf{C}_{n_T}^{+}\left(\mathbf{F}_{fi}^T\otimes\mathbf{F}_{fr}^T-\mathbf{F}_{fr}^T\otimes\mathbf{F}_{fi}^T\right)\mathbf{C}_{Ln_T} & \mathbf{C}_{n_T}^{+}\left(\mathbf{F}_{fr}^T\otimes\mathbf{F}_{fr}^T+\mathbf{F}_{fi}^T\otimes\mathbf{F}_{fi}^T\right)\mathbf{C}_{Ln_T}\end{bmatrix}, \tag{6.39}$$

[7] The operators $\text{vec}(\cdot)$, $\text{vech}(\cdot)$ and $\text{veci}(\cdot)$ act upon matrices and transform them into vectors. First, $\text{vec}(\cdot)$ represents the vector obtained by stacking the columns from left to right. Next $\text{vech}(\cdot)$ transforms its matrix argument into a vector, by stacking only the elements of each column that lie on or below the main diagonal. Similarly, $\text{veci}(\cdot)$ represents the result of stacking only the elements of each column that lie strictly below the main diagonal.

and the following notation was used: $\mathbf{F}_{fr} = \Re\mathrm{e}(\mathbf{F}_f)$ and $\mathbf{F}_{fi} = \Im\mathrm{m}(\mathbf{F}_f)$. Also, $(\cdot)^+$ stands for the pseudo-inverse operation and $\mathbf{D}_n$ corresponds to the duplication matrix, whose definition is given in [Mag02]. Similarly, the antiduplication matrix $\mathbf{C}_n$ is defined as the unique matrix such that, for all $\mathbf{X} \in R^{n\times n}$, $\mathrm{vec}(\mathbf{X}-\mathbf{X}^T) = \mathbf{C}_n \mathrm{veci}(\mathbf{X}-\mathbf{X}^T)$.

Propagation through the equivalent channel computation

After the computation of $\mathbf{R}_{\mathrm{quant}_f}^{(k)}$, the error $\mathbf{R}_{\mathrm{err}_f}^{(k)}$ is propagated through the matrix factorization at the transmitter. The objective now is to obtain the expression of the error in the equivalent triangular channel response matrix $\mathbf{T}_{\mathrm{err}_f}^{(k)}$ as a function of $\mathbf{R}_{\mathrm{err}_f}^{(k)}$. A first order approximation of the error propagation is considered, which is valid for small errors. From (6.37) we have that

$$\mathbf{R}_f^{(k)} = \mathbf{T}_f^{(k)\,H}\mathbf{T}_f^{(k)}, \tag{6.40}$$

$$\mathbf{R}_{\mathrm{quant}_f}^{(k)} + \mathbf{R}_{\mathrm{err}_f}^{(k)} = \left(\mathbf{T}_{\mathrm{quant}_f}^{(k)} + \mathbf{T}_{\mathrm{err}_f}^{(k)}\right)^H \left(\mathbf{T}_{\mathrm{quant}_f}^{(k)} + \mathbf{T}_{\mathrm{err}_f}^{(k)}\right). \tag{6.41}$$

After some manipulations described in appendix 8, the error in the equivalent channel response matrix $\mathbf{T}_{\mathrm{err}_f}^{(k)}$ can be expressed as a function of $\mathbf{R}_{\mathrm{err}_f}^{(k)}$ as: $\overline{\mathrm{vec}}\left(\mathbf{T}_{\mathrm{err}_f}^{(k)\,T}\right) \approx \left(\mathrm{D}_{\mathbf{r}_f^{(k)}}\mathbf{t}_f^{(k)}\right)\overline{\mathrm{vec}}\left(\mathbf{R}_{\mathrm{err}_f}^{(k)}\right)$, where $\mathrm{D}_{\mathbf{r}_f^{(k)}}\mathbf{t}_f^{(k)}$ is the Jacobian matrix of $\mathbf{t}_f^{(k)}$ and its expression is derived in [Sac12].

Summary

Mathematically, the complete error propagation process can be expressed from (6.35), (6.38) and (6.40) as:

$$\overline{\mathrm{vec}}\left(\mathbf{T}_{\mathrm{err}_f}^{(k)\,T}\right) \approx \mathbf{X}_f^{(k)}\overline{\mathbf{r}}_{err}^{(k)}, \tag{6.42}$$

where $\overline{\mathbf{r}}_{err}^{(k)} = \overline{\mathrm{vec}}\left(\overline{\mathbf{R}}_{\mathrm{err}}^{(k)}\right) \in R^{L^2 n_T^2 \times 1}$ and $\mathbf{X}_f^{(k)}$ is the linear transformation that results from the error propagation through all the steps: $\mathbf{X}_f^{(k)} = \begin{cases} \left(\mathrm{D}_{\mathbf{r}_f^{(k)}}\mathbf{t}_f^{(k)}\right)\mathbf{F}_f\left(\mathrm{D}_{\overline{\mathbf{r}}^{(k)}}P(\overline{\mathbf{R}}^{(k)}, n_R^{(k)})\right), & \text{if } n_R^{(k)} < Ln_T \\ \left(\mathrm{D}_{\mathbf{r}_f^{(k)}}\mathbf{t}_f^{(k)}\right)\mathbf{F}_f, & \text{if } n_R^{(k)} \geq Ln_T \end{cases}$

Finally, in [Sac12] a notation that relates the subindices of the error in the triangular matrix $\mathbf{T}_{\mathrm{err}_f}^{(k)}$ with the corresponding row index of matrix $\mathbf{X}_f^{(k)}$ is presented. This notation will be used in the following section.

6.3.3 Application to robust precoder design

In this section we present an example of robust design of the precoder matrix taking into account the error in the available CSI due to the quantization for the feedback transmission. As explained before, with the help of the transformation described in Section 6.3.1, the transmitter is able to compute an equivalent propagation channel using the channel Gram matrices sent through the feedback links. This will allow applying a robust MSE precoding strategy, which takes into account explicitly the statistics of the inaccuracies in the CSI at the transmitter defined by $\overline{\mathbf{R}}_{\mathrm{err}}^{(k)}$ in (6.30). The advantage of the robust design is that it is less sensitive to such errors.

Optimization of the MSE

It is important to emphasize that the equivalent channel transformation from Section 6.3.1 can be used to apply any arbitrary design criterion and system architecture (also for joint precoder and decoder design) on top of it. In this section, and for illustrative purposes, the specific design criterion of minimization of the MSE with fixed decoders is considered as an example of application and because it is analytically tractable. First, the expression of the MSE is presented and then the robust precoder design is derived.

In order to adjust the dynamic range of $\hat{\mathbf{x}}$ before computing the MSE, the factor β is included, as in [Joh02], [Cho02], which could be understood as a gain control at the receivers. The MSE is then given by:

$$\begin{aligned}\mathrm{MSE}(\mathbf{P},\beta) &= \sum_{k=1}^{K} E_{\mathbf{T}_{\mathrm{err}}^{(k)},\mathbf{x}^{(k)},\mathbf{w}^{(k)}}\left\{\left\|\mathbf{x}^{(k)}-\beta^{-1}\hat{\mathbf{x}}^{(k)}\right\|_2^2\right\} = E_{\mathbf{T}_{\mathrm{err}},\mathbf{x},\mathbf{w}}\left\{\left\|\mathbf{x}-\beta^{-1}\hat{\mathbf{x}}\right\|_2^2\right\} \\ &= \frac{1}{\beta^2}\mathrm{tr}\left(\mathbf{D}\mathbf{T}_{\mathrm{quant}}\mathbf{P}\mathbf{R}_x\mathbf{P}^H\mathbf{T}_{\mathrm{quant}}^H\mathbf{D}^H-\beta\mathbf{D}\mathbf{T}_{\mathrm{quant}}\mathbf{P}\mathbf{R}_x-\beta\mathbf{R}_x\mathbf{P}^H\mathbf{T}_{\mathrm{quant}}^H\mathbf{D}^H+\beta^2\mathbf{R}_x\right) \\ &\quad+\frac{1}{\beta^2}\mathrm{tr}\left(\mathbf{P}\mathbf{R}_x\mathbf{P}^H\Delta\right)+\frac{1}{\beta^2}\mathrm{tr}\left(\mathbf{D}\mathbf{Q}^H\mathbf{R}_w\mathbf{Q}\mathbf{D}^H\right),\end{aligned} \tag{6.43}$$

with $\Delta = E_{\mathbf{T}_{\mathrm{err}}}\left\{\mathbf{T}_{\mathrm{err}}^H\mathbf{D}^H\mathbf{D}\mathbf{T}_{\mathrm{err}}\right\} = \sum_{k=1}^{K} E_{\mathbf{T}_{\mathrm{err}}^{(k)}}\left\{\mathbf{T}_{\mathrm{err}}^{(k)H}\mathbf{D}^{(k)H}\mathbf{D}^{(k)}\mathbf{T}_{\mathrm{err}}^{(k)}\right\}$. Note that matrix Δ depends on the second-order statistics of the error in the equivalent channel matrix $\mathbf{T}_{\mathrm{err}}$. Such statistics can be computed assuming that the second-order statistics of the original quantization error $\bar{\mathbf{R}}_{\mathrm{err}}^{(k)}$ are known and using the analytic study of the error propagation presented in Section 6.3.2.

Robust precoder design

The robust system design can be expressed as the following optimization problem based on the MSE criterion (6.43) and including a constraint on the maximum power P_t available at the transmitter:

$$\left[\mathbf{P}_{rob},\beta_{rob}\right] = \arg\min_{\{\mathbf{P},\beta\}} \quad \mathrm{MSE}(\mathbf{P},\beta) \tag{6.44}$$

$$\text{s.t.:} \quad E\left\{\left\|\mathbf{P}\mathbf{x}\right\|_2^2\right\} = P_t. \tag{6.45}$$

Note that the MSE is not jointly convex in $\mathbf{P}$ and β. However, two necessary conditions arise from the fact that the optimum solution must fulfill that the optimum $\mathbf{P}$ minimizes the MSE for the optimum β subject to the power constraint and at the same time, the optimum value of β must minimize the MSE for $\mathbf{P}$ equal to its optimum value:

$$\mathbf{P}_{rob} = \arg\min_{\mathbf{P}} \quad \mathrm{MSE}(\mathbf{P},\beta_{rob}) \tag{6.46}$$

$$\text{s.t.:} \quad E\left\{\left\|\mathbf{P}\mathbf{x}\right\|_2^2\right\} = P_t. \tag{6.47}$$

and

$$\beta_{rob} = \arg\min_{\beta} \quad \mathrm{MSE}(\mathbf{P}_{rob},\beta). \tag{6.48}$$

The problem (6.46)-(6.47) is convex and therefore the optimum solution must satisfy the expression obtained by constructing the Lagrangian function $L(\mathbf{P};\lambda)$ with Lagrange multiplier $\lambda \in R^+$ and setting its derivatives equal to zero [Boy04]:

$$L(\mathbf{P};\lambda) = E\left\{\left\|\mathbf{x}-\beta_{rob}^{-1}\hat{\mathbf{x}}\right\|_2^2\right\}+\lambda\left(\mathrm{tr}(\mathbf{P}\mathbf{R}_x\mathbf{P}^H)-P_t\right). \tag{6.49}$$

$$\nabla_{\mathbf{P}^H} L = \frac{1}{\beta_{rob}^2}\mathbf{T}_{\text{quant}}^H \mathbf{D}^H \mathbf{D}\mathbf{T}_{\text{quant}}\mathbf{P}\mathbf{R}_x - \frac{1}{\beta_{rob}}\mathbf{T}_{\text{quant}}^H \mathbf{D}^H \mathbf{R}_x + \frac{1}{\beta_{rob}^2}\Delta\mathbf{P}\mathbf{R}_x + \lambda\mathbf{P}\mathbf{R}_x = 0.$$

Similarly, the condition (6.48) is convex in β and deriving the MSE with respect to β results in:

$$\frac{\partial \text{MSE}(\mathbf{P}_{rob},\beta)}{\partial\beta} = -\frac{2}{\beta^3}\text{tr}\left(\mathbf{D}\mathbf{T}_{\text{quant}}\mathbf{P}_{rob}\mathbf{R}_x\mathbf{P}_{rob}^H\mathbf{T}_{\text{quant}}^H\mathbf{D}^H\right) - \frac{2}{\beta^3}\text{tr}\left(\mathbf{P}_{rob}\mathbf{R}_x\mathbf{P}_{rob}^H\Delta\right)$$
$$-\frac{2}{\beta^3}\text{tr}\left(\mathbf{D}\mathbf{Q}^H\mathbf{R}_w\mathbf{Q}\mathbf{D}^H\right) + \frac{1}{\beta^2}\text{tr}\left(\mathbf{D}\mathbf{T}_{\text{quant}}\mathbf{P}_{rob}\mathbf{R}_x\right) + \frac{1}{\beta^2}\text{tr}\left(\mathbf{R}_x\mathbf{P}_{rob}^H\mathbf{T}_{\text{quant}}^H\mathbf{D}^H\right) = 0$$

which implies that:

$$-\text{tr}\left(\mathbf{D}\mathbf{T}_{\text{quant}}\mathbf{P}_{rob}\mathbf{R}_x\mathbf{P}_{rob}^H\mathbf{T}_{\text{quant}}^H\mathbf{D}^H\right) - \text{tr}\left(\mathbf{P}_{rob}\mathbf{R}_x\mathbf{P}_{rob}^H\Delta\right) - \text{tr}\left(\mathbf{D}\mathbf{Q}^H\mathbf{R}_w\mathbf{Q}\mathbf{D}^H\right) + \beta\,\text{tr}\left(\mathbf{D}\mathbf{T}_{\text{quant}}\mathbf{P}_{rob}\mathbf{R}_x\right) = 0.$$

We now introduce the following change of variables $\xi = \lambda\beta^2$ and $\mathbf{P} = \beta\mathbf{P}$. Then (6.49) results in:

$$\xi\beta^2\text{tr}\left(\mathbf{P}_{rob}\mathbf{R}_x\mathbf{P}_{rob}^H\right) - \text{tr}\left(\mathbf{D}\mathbf{Q}^H\mathbf{R}_w\mathbf{Q}\mathbf{D}^H\right) = 0 \Rightarrow \xi_{rob} = \frac{\text{tr}\left(\mathbf{D}\mathbf{Q}^H\mathbf{R}_w\mathbf{Q}\mathbf{D}^H\right)}{P_t}.$$

From (6.49), it follows that:

$$\mathbf{P}_{rob} = \beta_{rob}\left(\mathbf{T}_{\text{quant}}^H\mathbf{D}^H\mathbf{D}\mathbf{T}_{\text{quant}} + \Delta + \xi_{rob}\mathbf{I}\right)^{-1}\mathbf{T}_{\text{quant}}^H\mathbf{D}^H, \tag{6.50}$$

and from the power constraint $\text{tr}\left(\mathbf{P}\mathbf{R}_x\mathbf{P}^H\right) = P_t$ and (6.50), it follows directly that:

$$\beta_{rob} = \sqrt{\frac{P_t}{\text{tr}\left[\left(\mathbf{T}_{\text{quant}}^H\mathbf{D}^H\mathbf{D}\mathbf{T}_{\text{quant}} + \Delta + \xi_{rob}\mathbf{I}\right)^{-2}\mathbf{T}_{\text{quant}}^H\mathbf{D}^H\mathbf{R}_x\mathbf{D}\mathbf{T}_{\text{quant}}\right]}}. \tag{6.51}$$

Since there is only one solution (up to a phase change) that satisfies the two necessary conditions, (6.46)-(6.47) and (6.48), this solution will be the optimum one.

Note that, for the computation of 6.49), an additional parameter associated to the noise power of each user, $\xi^{(k)} = \text{tr}\left(\mathbf{D}^{(k)}\mathbf{Q}^{(k)H}\mathbf{R}_w^{(k)}\mathbf{Q}^{(k)}\mathbf{D}^{(k)H}\right)$, has to be fed back to the transmitter. However, this scalar parameter varies very slowly over time and does not imply a relevant increase in the feedback load. From (6.49), it follows that $\xi_{rob} = \frac{\sum_{k=1}^{K}\xi^{(k)}}{P_t}$. Observe that, in the case that there is no knowledge of the CSI error at the transmitter, a naive design would assume $\Delta = 0$, and in this case (6.50)-(6.51) results in a non-robust design which coincides with the optimum non-robust design derived in [Joh02].

Particular case: independent processing per carrier

In the particular case where the decoder matrix of each user $\mathbf{D}^{(k)}$ is constrained to be block diagonal, which is the case for example when joint-processing of the signals from different carriers is not possible at the receiver, the optimum solution given by (6.49)-(6.51) is also block diagonal. This means that if the decoder is not capable of processing the signals of different carriers jointly, the optimum precoder does not spread the information symbols across carriers. Consequently, in this particular case, the solution from (6.49)-(6.51) is also valid for the MIMO-OFDM scheme as described in (6.22).

6.3.4 Numerical results

This section numerically evaluates the performance of the proposed example of use of our design framework detailed in the previous section. For the simulations, we consider a scenario featuring a transmitter with

$n_T = 4$ antennas and $K = 2$ receivers with $n_R^{(k)} = 2, k = 1,2,$ antennas each. The lth tap of the channel impulse response is generated as $\bar{\mathbf{H}}_l^{(k)} = \sigma_l \mathbf{N}_l^{(k)}$, where σ_l characterizes the power delay profile and $\mathbf{N}_l^{(k)}$ is composed of i.i.d. zero-mean circularly symmetric complex Gaussian entries with unit variance. For the simulations, we considered an exponential decaying power delay profile given by $\sigma_l^2 = ae^{\frac{-l}{\tau}}$, (where $a = (\sum_{n=0}^{L-1} e^{\frac{-n}{\tau}})^{-1}$) with a normalized delay spread of $\tau = 3$. The simulations are averaged over a sufficiently large number of realizations. Since the joint optimal design of $\mathbf{P}$ and $\mathbf{D}$ is still an open problem, a decoder matrix $\mathbf{D}$ has to be fixed for the simulations. A simple choice is to set $\mathbf{D}^{(k)} = \mathbf{I}$, as in [Sun09]. Note that this implies that the number of streams is chosen as $n_S^{(k)} = Fn_R^{(k)}$.

Evaluation of the robust precoder

In this subsection the performance of the proposed robust algorithm, implemented within the presented feedback framework, is numerically compared with that of the non-robust algorithm from [Joh02]. To show the applicability of the presented framework, both the naive (i.e., non-robust) and the robust versions of BD [Spe04] are also implemented and compared, in a setup with $L = 16$ taps and $F = 128$ carriers.

Using this setup, Figure 6-10 shows the MSE versus the transmit power P_t for different values of the variance of each element of the error matrix $\bar{\mathbf{R}}_{\text{err}}^{(k)}$, represented by $\sigma_e^{\ 2}$. These simulations show that the improvement in terms of MSE of the robust design with respect to the non-robust solution is higher as the error in the quantization and feedback increases. The same conclusion applies to the case when a SER cost function is used, as shown in Figure 6-11 for a scenario featuring a QPSK constellation.

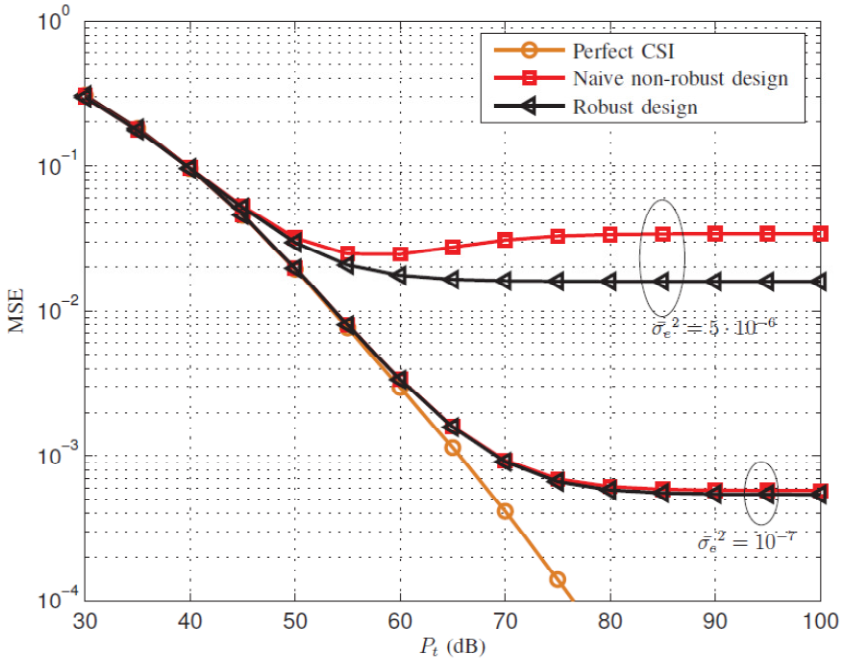

***Figure 6-10**: MSE versus the total transmission power allocated among all the 128 carriers in a 4x{2,2} system with $\bar{\mathbf{R}}_{\text{err}}^{(k)}$ generated using i.i.d. elements following a Gaussian distribution with zero mean and variance $\sigma_e^{\ 2}$.*

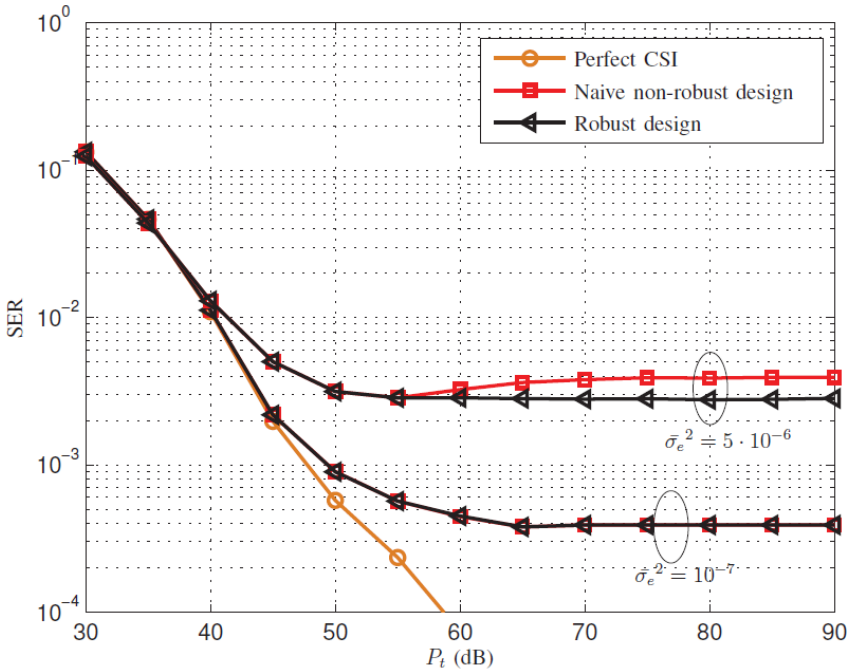

***Figure 6-11*: SER versus the total transmission power allocated among all the 128 carriers in a 4x{2,2} system with QPSK constellation and with 512 symbols transmitted simultaneously. $\bar{\mathbf{R}}_{\text{err}}^{(k)}$ consists of i.i.d. elements following a Gaussian distribution with zero mean and variance σ_e^2.**

The framework allows also other design implementations and, as an example, a design based on BD [Spe04] is now considered. Using this, the robust and non-robust BD designs are applied, and the results in the considered scenario are shown in Figure 6-12. Note that this is shown as an example of the applicability of the framework, but, if the designs based on BD were to be compared to the non-BD designs, the performance in terms of MSE would be worse for the BD schemes since they spend degrees of freedom to force interference nulling among users.

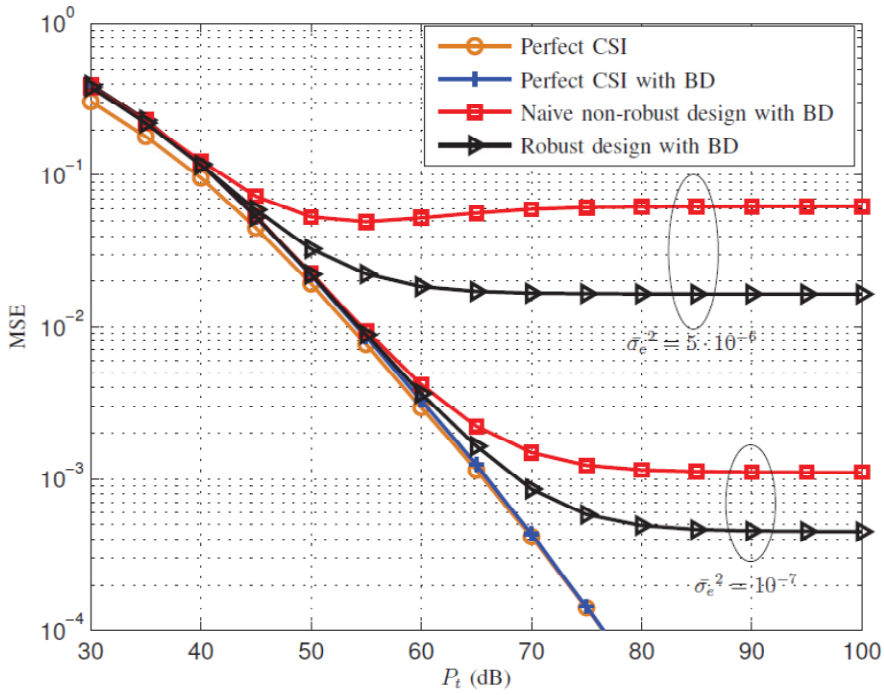

***Figure 6-12*: MSE versus the total transmission power allocated among all the 128 carriers in a 4x{2,2} system with $\bar{\mathbf{R}}_{\text{err}}^{(k)}$ generated using i.i.d. elements following a Gaussian distribution with zero mean and variance σ_e^2, and an implementation of a BD design.**

The performance as a function of the amount of error in the CSI is considered next. Figure 6-13 shows the achievable MSE versus the SNR in the estimation of $\bar{\mathbf{R}}^{(k)}$, defined as $\text{SNR}_e = \frac{1}{\sigma_e^2}$, for a fixed value of the transmit power $P_t = 60$ dB. The curves show that the robust designs outperform the other precoding techniques when the estimation of $\bar{\mathbf{R}}^{(k)}$ is not very good, i.e., when the SNR_e is low and consequently the error is high, while at high SNR_e the error in the CSI is very small and the curves corresponding to the non-robust techniques converge to the curves corresponding to the robust designs as it is to be expected. The designs based on BD show a small performance loss due to the fact that some degrees of freedom are used to guarantee an interference-free transmission.

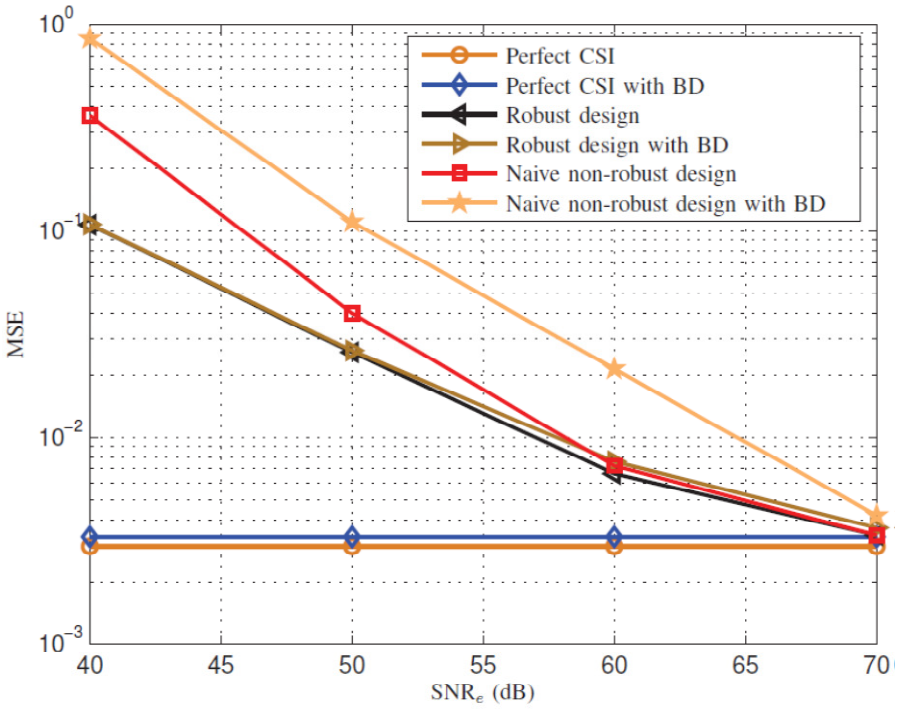

***Figure 6-13*: MSE versus SNR_e in a 4x{2,2} system with a total transmission power allocated among all the 128 carriers of $P_t = 60$ dB above the noise level.**

Comparison of feedback strategies

A numerical analysis of the performance of the feedback scheme based on the quantization and feedback of one temporal channel Gram matrix $\bar{\mathbf{R}}^{(k)}$ per user, instead of the usual feedback per carrier per user and the traditional feedback of the complete channel propagation matrix is presented in this subsection. This performance comparison is numerically characterized by constraining the same number of quantization bits for the different approaches in order to obtain a fair evaluation. There are multiple quantization and feedback algorithms that can be used to quantize either $\bar{\mathbf{R}}^{(k)} \in C^{Ln_T \times Ln_T}$ or the F matrices $\mathbf{R}_f^{(k)} \in C^{n_T \times n_T}$. Since the focus of this work is on the objective of the quantization and not on the algorithm itself, the algorithm from [Cha08] will be taken as a reference for the comparison of due to its simplicity. The performance of a system

using both the quantization of $\bar{\mathbf{R}}^{(k)}$ and the quantization of the F matrices $\mathbf{R}_f^{(k)}$ and featuring the same number of feedback bits for both cases will be shown next.

First, a comparison of the feedback based on the channel Gram matrix versus the feedback of the complete channel response matrix is presented. A scenario with $L=16$ taps and $F=16$ carriers is considered, and the results are shown in Figure 6-14. It can be seen that the feedback of the Gram matrix provides a lower MSE than the technique based on direct quantization of the channel response matrix, for the cases of $B=1536$ and $B=2560$ total feedback bits.

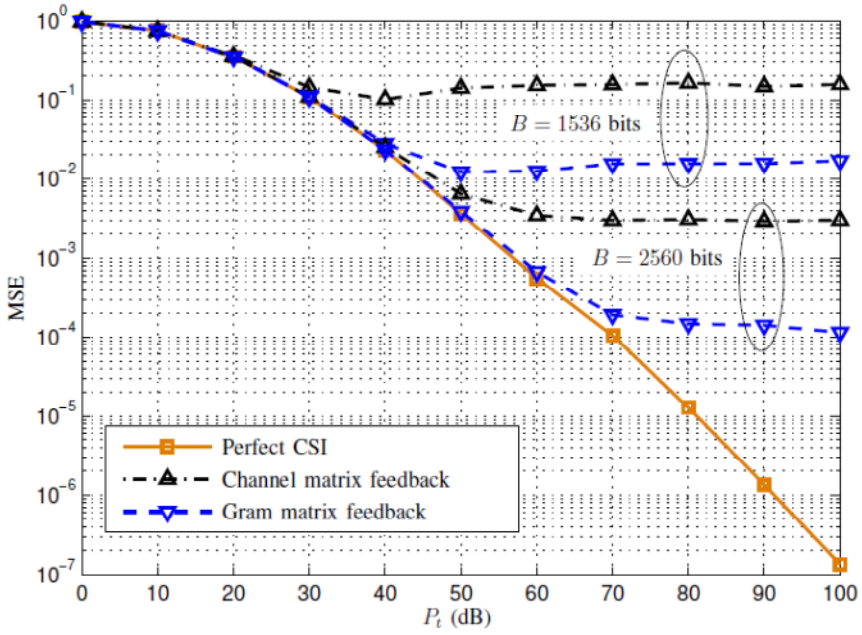

***Figure 6-14*: Feedback based on the channel Gram matrix versus feedback based on the complete channel response matrix, for different values of the feedback overhead in number of bits.**

Next, Figure 6-15 shows a comparison of the performance using feedback of the time domain CSI versus feedback of the frequency domain CSI in a scenario with $L=8$ taps and $F=128$ carriers, for different values of the feedback load. First, we considered $B=12288$ bits of feedback. This means that each of the 1024 real and scalar parameters that have to be fed back in the time domain CSI feedback is quantized using 12 bits, while each of the 2048 parameters corresponding to the frequency domain CSI feedback case is quantized using 6 bits. The figure also shows the results of simulations featuring 14336 bits per feedback update (which corresponds to 14 bits for the quantization of each element in the scheme based on time domain CSI and 7 bits for each element in the scheme based on frequency domain CSI). These curves show that, for this specific setup, the quantization and feedback of matrix $\bar{\mathbf{R}}^{(k)}$ (which is based on the time domain CSI) provides a lower SER than the quantization and feedback of $\mathbf{R}_f^{(k)}$ (which is based on frequency domain CSI) when using the same feedback algorithm. This is due to the fact that, in the case of time domain CSI feedback, the number of parameters to be quantized is half the number of parameters to be quantized using the same number of bits in the case of frequency domain CSI feedback. In a scenario such as the one evaluated in Figure 6-16, with $F=64$ carriers instead of the 128 carriers considered in Figure 6-15, the number of elements to be quantized is higher in the time domain CSI feedback than in the frequency domain CSI feedback and the later shows better performance.

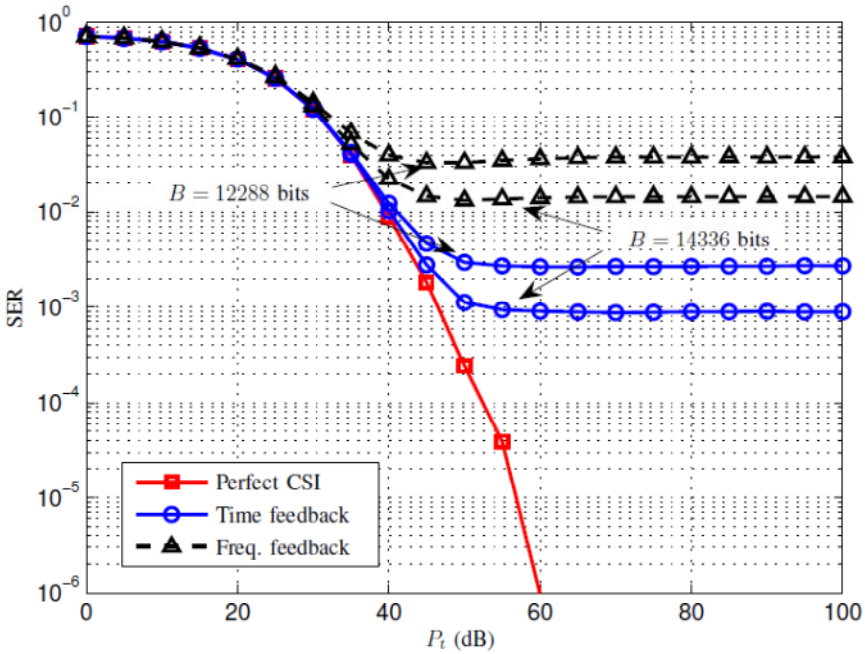

***Figure 6-15*: Feedback of the frequency domain CSI versus feedback of the time domain CSI. Scenario with $L = 8$ taps, $F = 128$ carriers, and different values of the feedback overhead in number of bits. The transmit power P_t is spread over all 128 carriers and all 4 antennas, and 512 QPSK symbols are transmitted simultaneously.**

From this we conclude that the choice of the most adequate feedback scheme (feedback of the time domain CSI or feedback of the frequency domain CSI) depends on the number of taps of the temporal channel response and the number of carriers, and this should be taken into consideration at the system design stage. Note that the trend in wireless communication systems is to increase the number of carriers (WiMAX for example supports up to 1728 usable carriers [Iee05]), in which case the feedback of the time domain CSI provides better performance.

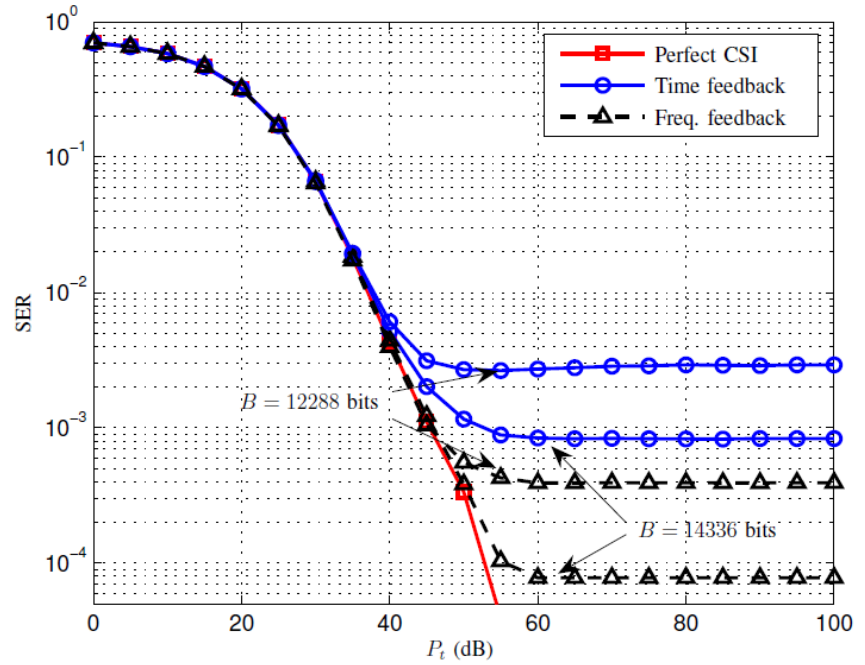

***Figure 6-16*: Feedback of the frequency domain CSI versus feedback of the time domain CSI. Scenario with $L = 8$ taps, $F = 64$ carriers, and different values of the feedback overhead in number of bits. The transmit power P_t is spread over all 64 carriers and all 4 antennas, and 256 QPSK symbols transmitted simultaneously.**

Simulations using the BuNGee channel model

The following simulations consider the grid scenario described in Figure 3-10 from [Bun11] with one HBS transmitting through 24 dual-polarized beams to 20 HSSs. Due to the symmetry of the scenario only one quarter of the grid is numerically simulated, as shown in Figure 6-17, and the results are averaged over the links from the HBS to the HSSs and over 2000 channel realizations.

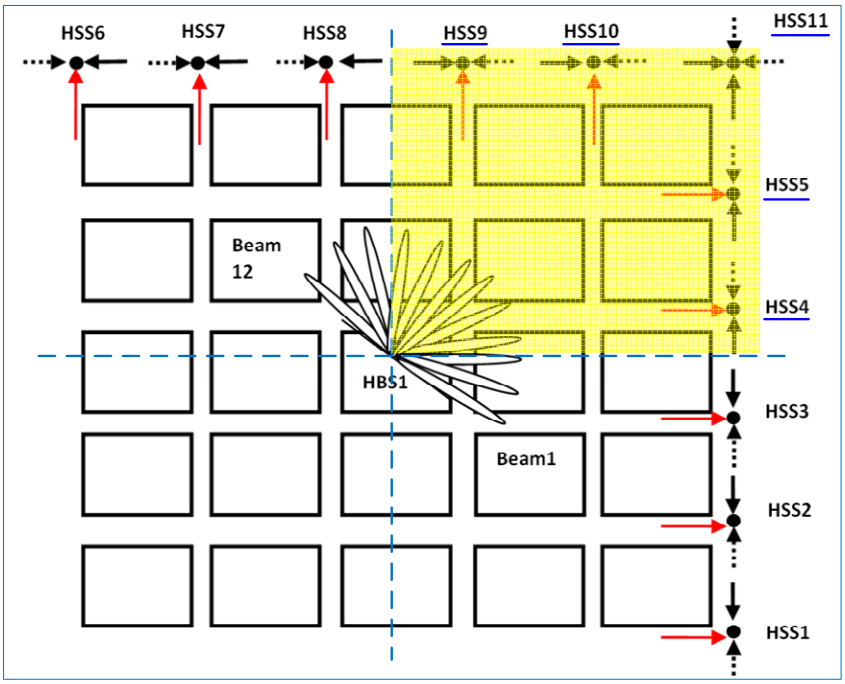

***Figure 6-17*: Scenario considered for the simulations. Due to the symmetry, only the upper right quarter, containing HSS4, HSS5, HSS9, HSS10 and HSS11 was used in the numerical computations.**

The channels were generated according to the power delay profile data from Table 3-12 and normalized path loss coefficients obtained from Tables 3-5 and 3-6 from [Bun11].

The simulated scenario features 128 carriers and a cross-carrier transceiver design based on block diagonalization with beamforming for SINR maximization described in this document and in [Spe04]. The performance was obtained for the case of perfect CSI at the transmitter and also for imperfect CSI (at the receiver side, perfect CSI was always assumed). In the case of imperfect CSI at the transmitter, the CSI error is modeled as Gaussian with zero mean and a given error variance. Note that the errors in the CSI available at the transmitter are due to the quantization errors inherent to the feedback process, the channel estimation at the receiver and and noise and delay during the feedback transmission.

Figure 6-18 shows the SINR obtained, averaged over the HSSs and over 2000 channel realizations for different values of the CSI error. Observe that in the case of perfect CSI the SINR is an increasing linear function of the transmit power Pt, while in the case of imperfect CSI there is an upper bound to the performance due to the effect of self-interference. The self-interference is produced because the block-

diagonalization design is done using imperfect CSI at the transmitter, which results in a precoder that does not completely avoid interference to the other receivers.

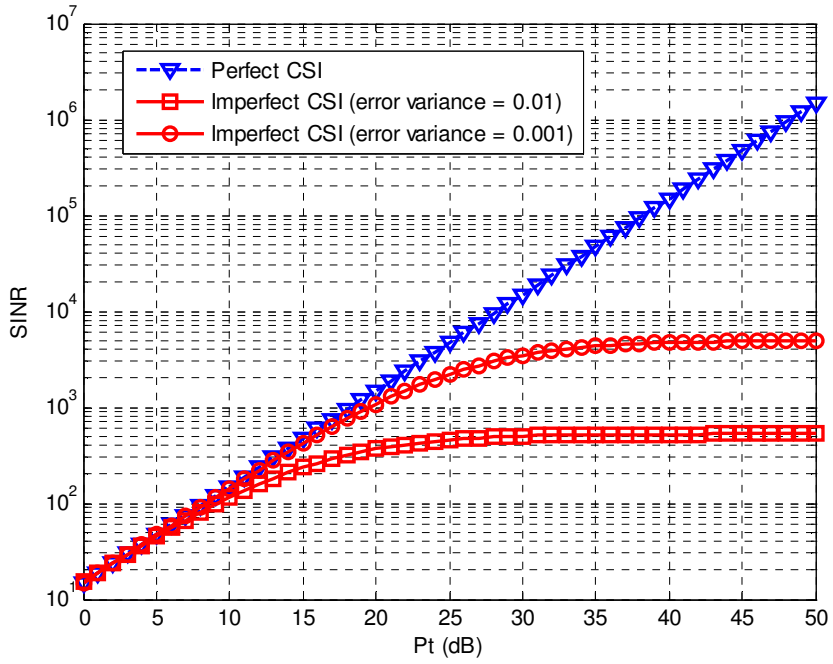

***Figure 6-18*: SINR versus Pt for different values of CSI accuracy**

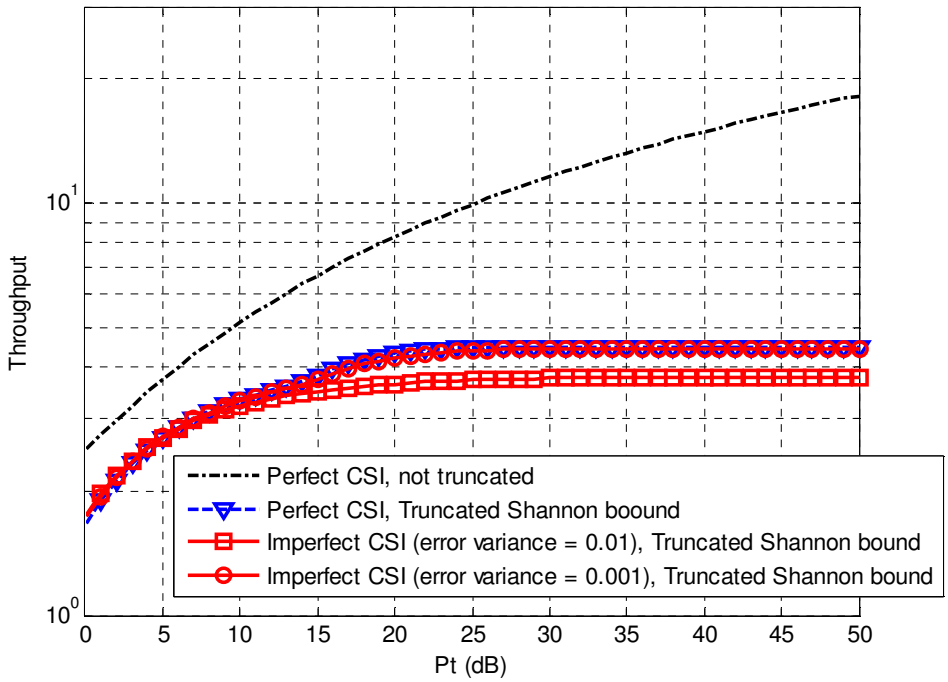

***Figure 6-19*: Throughput versus Pt for different values of CSI accuracy**

6.3.5 Conclusions

In Section 6.3 a framework for the design of multiuser MIMO-OFDM BC systems with CSI feedback was presented. The proposed framework is based on the computation of an equivalent triangular channel response matrix, and enables the use of efficient CSI feedback techniques based on the quantization of the Gram matrix of the temporal response of the channels. This scheme is valid for and can be applied to any given design quality criterion. An analytical study of the propagation of CSI quantization error through the channel Gram matrix computation and the posterior equivalent channel response matrix computation is also presented. As an illustrative example of the potential of this framework for transceiver designs, the case of MSE minimization has been considered and a closed form expression for a robust space-frequency linear precoding design has been derived. Numerical simulations reveal the advantages of the proposed feedback scheme and also of the MSE minimization precoding technique compared to other feedback techniques and to the non-robust counterpart precoding techniques.

7. Precoder selection for MIMO access link

This section describes part of the work on the performance of the access links, between the ABS and the mobile station (MS). In BuNGee either the WiMAX (IEEE 802.16e/m) [IEE05] or the 3GPP LTE [3GP06] or LTE-Advanced standards are likely to be used in these links. Both these standards employ linear precoding for MIMO transmission in closed loop MIMO systems, where CSI is available at the transmitter of the link. Linear precoding [Sam01] involves firstly demultiplexing of the transmitted data into one or more streams (or layers in LTE terminology), together with the use of a precoding matrix to map these streams onto the transmit antennas. Choice of precoding matrix can implement conventional spatial multiplexing, transmit antenna selection or a combination of these, as well as a range of other transmission formats.

Most previous work on adaptive linear precoding and on detection of spatial multiplexing has assumed that linear receivers, such as ZF or MMSE [Ver98][Hea05], or ordered successive interference cancellation (OSIC) [Wol98], are used. However these do not allow the full receive end diversity to be achieved. Maximum Likelihood (ML) detection [Zhu02] or iterative interference cancellation [Bur04] can achieve full receive end diversity, but on their own do not provide transmit end diversity. This can of course be provided by transmit diversity techniques such as space time block codes (STBC) [Tar99], but these can restrict capacity. Adaptive schemes can, however, provide full transmit end diversity, and schemes exist which provide the optimum trade-off between diversity and multiplexing gain. Work has been done on adaptive MIMO schemes to achieve transmitter end spatial diversity [Hea05], and on OFDM to achieve frequency diversity [Czy96].

In this contribution we assume that a specific set of available precoding matrices is defined in the standard, as is the case for both WiMAX and LTE/LTE-Advanced. This provides an alternative solution to the problem of transmitting the CSI to that proposed in previous section above, since instead of quantising the estimated channel at the receiver and transmitting it back to the transmitter for precoder selection, the selection is performed at the receiver from among the set of available precoder matrices (the codebook), and only the index of the selected precoder matrix need be transmitted back to the transmitter. This restricts the range of precoders that can be used, since they must be defined *a priori*, but it is more compatible with the standards currently under consideration for the BuNGee access links.

The objective of this contribution is to propose criteria for the selection of the precoder matrix for a specific channel. It is important to note in particular that the selection criterion is dependent on the detector to be used, and hence we consider a number of potential detectors, for both coded and uncoded systems. In particular for uncoded systems we compare the maximum likelihood (ML) detector with linear (ZF/MMSE) detectors. For coded systems we introduce a new criterion based on mutual information.

Because the focus is on selection criteria the precoder codebook we use is relatively simple and arbitrarily selected, with no attempt at optimisation. In particular for two transmit antennas we use the set defined by the LTE standard [3GP07]. We assume that channel information is accurately estimated and the feedback loop is fast and accurate, and hence the transmitter knows exactly the stream mapping according to the selection criterion.

We also assume throughout that OFDM is used but here assume a flat fading channel, so that the same precoder is used for all subcarriers. For a frequency selective channel precoder selection would be performed per sub-band, where a sub-band comprises a set of subcarriers subject to a very similar channel.

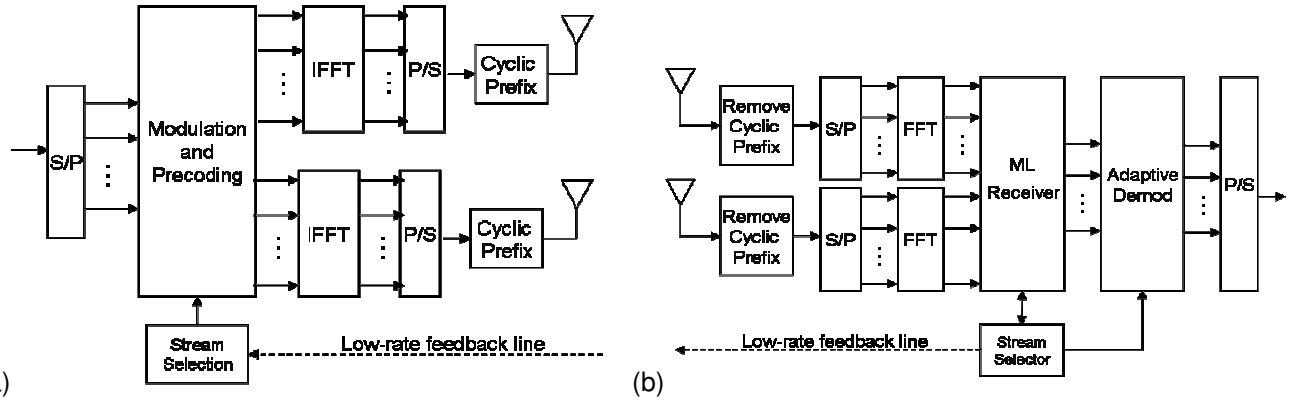

Figure 7-1 Uncoded system block diagram: (a) transmitter; (b) receiver

7.1 System model

7.1.1 Uncoded system

The uncoded MIMO-OFDM system under consideration is illustrated in Figure 7-1. We assume N_t transmit and N_r receive antennas, and that *M* bits are transmitted per sub-carrier per OFDM symbol. According to the stream mapping information from the feedback loop, the *M* bits assigned to the *i*th subcarrier of the *k*th OFDM symbol are assigned to $R_{i,k}$ $(1 \le R_{i,k} \le N_t)$ streams (or layers). Here we assume that the same number of bits are assigned to each stream on a given subcarrier, i.e. $M/R_{i,k}$ per stream. Note that this number must be an integer for all permitted values of $R_{i,k}$. These bits are then modulated onto symbols taken from a constellation of size $2^{M/R_{i,k}}$. The data symbols on the *i*th subcarrier in a given OFDM symbol period can be represented by the vector $\mathbf{s}_{i,k} = \left[s_{i,k,1} \cdots s_{i,k,R_{i,k}} \right]^T$. The modulated symbols are then mapped onto the N_t transmit antennas using the precoding matrix $\mathbf{F}_{i,k}$.

Here we assume a quasi-static Rayleigh fading channel, which means the channel is constant within one frame and changes in the next frame such that the channels in successive frames are uncorrelated. The channel is also subject to frequency selective fading, so that the MIMO channel matrix $\mathbf{H}_{i,k}$ is in principle different for each subcarrier. Hence the number of streams, $R_{i,k}$, the precoding matrix $\mathbf{F}_{i,k}$ and the modulation schemes used at the transmitter vary from subcarrier to subcarrier. For demonstration purposes we assume that perfect channel estimation is available at the receiver, and that the CSI is fed back to the transmitter over a low rate channel without errors or delay.

The received modulated vector symbol for the *k*th OFDM symbol and the *i*th subcarrier is then:

$$\mathbf{y}_{i,k} = \sqrt{P_s}\mathbf{H}_{i,k}\mathbf{F}_{i,k}\mathbf{s}_{i,k} + \mathbf{n}_{i,k} \ , \tag{7.1}$$

where P_s is the total transmit power per sub-carrier from all antennas, and $\mathbf{n}_{i,k}$ is the white Gaussian noise vector distributed as $\mathcal{CN}(0, N_0)$. The precoding matrix $\mathbf{F}_{i,k}$ determines how the streams are mapped to the antennas. Note that all precoding matrices in the set from which $\mathbf{F}_{i,k}$ is chosen are unitary, i.e. $\left\|\mathbf{F}_{i,k}\right\|^2 = 1$,

and hence do not affect transmit power, and that the modulated data symbols $s_{i,k,1} \cdots s_{i,k,R_{i,k}}$ also have unit mean power.

A number of alternative detection techniques can be used at the receiver. Linear detectors such as zero forcing (ZF), minimum mean square error (MMSE) are commonly used. However the maximum likelihood (ML) detector has better performance than the linear detectors, although it is more complex. In particular with linear detectors the receive end spatial diversity order is restricted to $N_r - N_t$, while for ML detection the full diversity order N_r is available. Here we will compare the ML detector with results given in [Hea05] for the MMSE detector.

The ML detector is vector symbol based: the estimate of $\mathbf{s}_{i,k}$ can be obtained as:

$$\hat{\mathbf{s}}_{i,k} = \arg\max_{n} P(\mathbf{y}_{i,k} | \mathbf{s}_n) , \tag{7.2}$$

where $\mathbf{s}_n$ $(n = 1 \ldots 2^M)$ is the *n*th member of the set of permitted transmit symbol vectors. (7.2) can be rewritten as:

$$\hat{\mathbf{s}}_{i,k} = \arg\min_{n} \left\| \sqrt{P_s} \mathbf{H}_{i,k} \mathbf{F}_{i,k} \mathbf{s}_n - \mathbf{y}_{i,k} \right\|^2 . \tag{7.3}$$

When $R = 1$, the ML receiver can be simplified to a maximum ratio combining (MRC) receiver. Let $\mathbf{\Phi}_{i,k} = \mathbf{H}_{i,k} \mathbf{F}_{i,k}$: then the MRC receiver can be represented as a linear detector $\mathbf{G}_{i,k} = \left(\left\| \varphi_n \right\|^2 \right)^{-1} \mathbf{\Phi}^*_{i,k}$. The estimated received symbol is written as follows:

$$\hat{\mathbf{s}}_{i,k} = \mathbf{G}\mathbf{y}_{i,k} = \sqrt{P_s} \mathbf{G}_{i,k} \mathbf{H}_{i,k} \mathbf{F}_{i,k} \mathbf{s}_{i,k} + \mathbf{G}\mathbf{n}_{i,k} , \tag{7.4}$$

where φ_n is the *n*th column of $\mathbf{\Phi}_{i,k}$ and * denotes conjugate transpose.

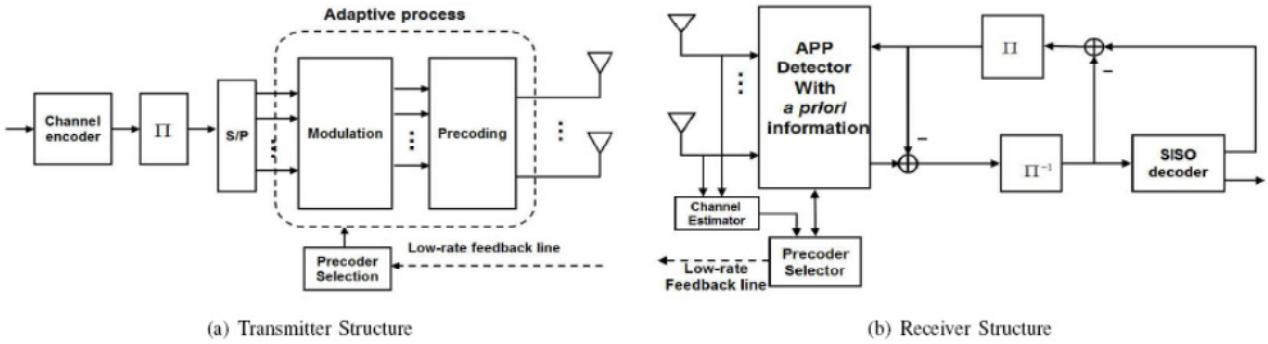

Figure 7-2 Coded system with iterative detection

7.1.2 Coded system with iterative detection

Figure 7-2 shows the coded system under consideration. The data is convolutionally encoded in each frame separately. Then the coded bits are interleaved by a well designed block interleaver that guarantees neighbouring code bits are distributed in different layers of the MIMO system. In each symbol period, M bits are transmitted. Depending on the precoder selected, the M bits are mapping to R constellation symbols and then mapped to the N_t antennas using the precoder matrix **F**. Note that M is constant while R $(1 \le R \le N_t)$ is variable according to the selected precoder matrix, being equal to the number of columns in the precoder matrix. Hence the modulation varies according to the precoder: the modulation order is given by $2^{M/R}$. The received signal at the receiver can be expressed as:

$$\mathbf{y} = \sqrt{P_s} \mathbf{H}\mathbf{F}\mathbf{s} + \mathbf{n} \tag{7.5}$$

where P_s is the total transmit power per sub-carrier from all antennas, and **n** is the white Gaussian noise vector distributed as $C\mathrm{N}(0, \sigma_n^2)$. Note that the sum of vector norms of all the columns in a precoding matrix

in the set is unity, and hence the choice of matrix does not affect transmit power, and that the modulated data symbols $s_1 \ldots s_R$ also have unit mean power. A Rayleigh flat fading quasi-stationary channel is assumed here, in which **H** remains constant within one frame period and changes from frame to frame. Also for simplicity and without loss of generality we set $P_s = 1$.

At the receiver, an *a posteriori* probability (APP) detector and a soft in, soft out (SfISfO) decoder are used. Soft information is exchanged iteratively between them. The extrinsic output of the detector, in the form of log likelihood ratio (LLR), can be written as:

$$L(b_l) = \log\left(\frac{\sum_{\mathbf{s},b_l=1} \exp\left(-\frac{\left|\mathbf{r}-\mathbf{HFs}\right|^2}{2\sigma_n^2} + \sum_{i=1,i\neq l}^{M} b_i L_p(b_i)\right)}{\sum_{\mathbf{s}',b_l=0} \exp\left(-\frac{\left|\mathbf{r}-\mathbf{HFs}'\right|^2}{2\sigma_n^2} + \sum_{i=1,i\neq l}^{M} b_i L_p(b_i)\right)}\right) \tag{7.6}$$

where b_l denotes the l^{th} bit of the data corresponding to the vector symbol **s**. The summation in the numerator is over all vector symbols such that the l^{th} bit is '1'; in the denominator such that it is '0'. This detector can be simplified with negligible performance loss using the Max-Log-MAP approximation (which is used in this work) giving:

$$\begin{aligned} L(b_l) \;&= \max_{\mathbf{s},b_l=1}\left(-\frac{\left|\mathbf{r}-\mathbf{HFs}\right|^2}{2\sigma_n^2} + \sum_{i=1,i\neq l}^{M} b_i L_p(b_i)\right) \\ &\quad - \max_{\mathbf{s}',b_l=0}\left(-\frac{\left|\mathbf{r}-\mathbf{HFs}'\right|^2}{2\sigma_n^2} + \sum_{i=1,i\neq l}^{M} b_i L_p(b_i)\right), \end{aligned} \tag{7.7}$$

This extrinsic information is then fed to the SfISfO decoder for the convolutional code (via a deinterleaver corresponding to the interleaver at the transmitter), which returns extrinsic information to the APP detector.

7.2 Precoder selection criteria

A number of papers have proposed precoder selection criteria. For example [Gor00] mainly considers selection for maximum system capacity while in [Hea01a][Hea01b] maximum post-processing SNR and vector symbol error rate (VSER) were considered. It is clear that the selection criterion must take into account the detector used, since different detectors may respond differently to the precoding matrix. In particular coded and uncoded systems will employ different criteria. Here we propose a criterion based on bit error rate (BER) performance for the uncoded case, and a criterion based on mutual information for the coded case.

7.2.1 Selection criterion for uncoded transmission, with ML detector

For the purpose of the BER criterion we develop an approximate BER prediction method based on the vector symbols nearest neighbour union bound (NNUB). As stated in [Gol05], the error probability of vector symbols $\mathbf{y}_{i,k}$ can be computed from the well known formula as

$$P_{VSE} = \sum_{\mathbf{s}_{i,k}\in S} P(\hat{\mathbf{s}}_{i,k} \neq \mathbf{s}_{i,k} \,|\, \mathbf{s}_{i,k}) P(\mathbf{s}_{i,k}). \tag{7.8}$$

In the ML receiver $P(\hat{\mathbf{s}}_{i,k} \neq \mathbf{s}_{i,k} \,|\, \mathbf{s}_{i,k})$ is approximated by the NNUB as

$$P(\hat{\mathbf{s}}_{i,k} \neq \mathbf{s}_{i,k} \,|\, \mathbf{s}_{i,k}) \approx Q\left(\sqrt{\frac{\min_n \left\|\sqrt{P_s}\mathbf{H}_{i,k}\mathbf{F}_{i,k}\mathbf{s}_n - \mathbf{y}_{i,k}\right\|^2}{4\sigma^2}}\right), \tag{7.9}$$

where σ is the received noise standard deviation. Normally, the probabilities of transmitting all $\mathbf{s}_{i,k}$ are equal. Substituting (6) in (5), the P_{VSE} can be rewritten as

$$P_{VSE} \approx \frac{1}{M}\sum_{\mathbf{s}_{i,k}} Q\left(\sqrt{\frac{\min\limits_{n}\left\|\sqrt{P_s}\mathbf{H}_{i,k}\mathbf{F}_{i,k}\mathbf{s}_n - \mathbf{y}_{i,k}\right\|^2}{4\sigma^2}}\right). \tag{7.10}$$

Given (7.10), the BER can be written:

$$P_{BER} = N_e P_{VSE}, \tag{7.11}$$

where N_e is the average number of error bits if a transmitted vector were detected as nearest neighbour. In the ML receiver, the nearest neighbour symbol is approximately equally likely to be any other symbol except the transmitted one itself. So $N_e \approx \frac{1}{2^M - 1}\sum_{n=1}^{2^M} n \cdot {}^{n}C_{2^M}$, where ${}^{n}C_{2^M}$ is the number of combinations of 2^M from n.

Let $D_{\min}(\mathbf{s}_{i,k})$ denote $\min\limits_{n}\left\|\sqrt{P_s}\mathbf{H}_{i,k}\mathbf{F}_{i,k}\mathbf{s}_n - \mathbf{y}_{i,k}\right\|$ for $\mathbf{S}_{i,k}$, together with (7.10), (7.11) can be simplified as

$$P_{BER} \approx N_e Q\left(\sqrt{\frac{\min\limits_{\mathbf{s}_{i,k}} D^2_{\min}(\mathbf{s}_{i,k})}{4\sigma^2}}\right) \tag{7.12}$$

When $R=1$, the simplified ML receiver is a linear MRC receiver. According to [Hea01a], the post-processing SNR is

$$\begin{aligned} SNR_{MRC} &= \frac{P_s\left|\mathbf{g}_n^*\varphi_n\right|^2}{N_0\left\|\mathbf{g}_n^*\right\|^2 + P_s\sum_{j\neq n}\left|\mathbf{g}_n^*\varphi_j\right|^2} \\ &= \frac{P_s}{N_0}\left\|\mathbf{h}_n\right\|^2 \end{aligned} \tag{7.13}$$

where $\mathbf{g}_n^*$ is the *n*th row of $\mathbf{G}_{i,k}$. The BER in this case is

$$P_{BER}(R=1) \approx N_e Q\left(\sqrt{\frac{P_s d^2_{\min}}{4\sigma^2}}\right) = N_e Q\left(\sqrt{\frac{SNR_{MRC} d^2_{\min}}{2}}\right) \tag{7.14}$$

where $d_{\min}$ is the minimum Euclidean distance of neighbouring symbols in the transmit constellation diagram.

To sum up, for a given M and $\mathbf{H}$ the system performance is determined by R and $\mathbf{F}$. The selection criterion is to choose the best combination of R and $\mathbf{F}$ to achieved the minimum $P_{BER}(R,\mathbf{F})$. Note that since the data throughput per symbol period is kept constant, the constellation used depends on the number of streams, *R*.

7.2.2 Mutual information criterion for coded transmission with soft decision detection

For coded transmission with soft decision detection the important criterion is the BER after the soft decision decoder. Decisions are not made at symbol level, but at codeword level. Hence the simple BER criterion described above, being based on errors occurring at a symbol level, is not appropriate. The approach we use here treats the whole transmission path from the binary input to the modulator to the bit-level soft output of the detector as a virtual binary-input, continuous output channel, and evaluates the mutual information between the input and the output of this channel. According to Shannon's theorem, provided the information rate of the system is less than the mutual information of this virtual channel, the decoded BER will be low, tending to zero with increasing code length. Conversely if the capacity of the channel is less than the information rate, the decoded BER will be high. Hence, for given system information rate, a precoder that

maximises the mutual information also minimises the decoded BER. The mutual information criterion therefore chooses the precoder that maximises the mutual information of the virtual channel.

We can quantify this argument with reference to the EXIT chart analysis of ten Brink [Bri01]. We assume that the soft output of a SfISfO decoder is given by the LLR of the k^{th} data bit d_k given the received codeword **y**:

$$L(d_k) = \log\left(\frac{P(\mathbf{y}|d_k = +1)}{P(\mathbf{y}|d_k = -1)}\right) \tag{7.15}$$

and further that the LLR can be modelled as a Gaussian random variable:

$$L(d_k) = \mu d_k + w \tag{7.16}$$

where w is a zero mean Gaussian variable with standard deviation σ, and $\mu = \sigma^2/2$. The mutual information between d and $L(d_k)$ is given by:

$$\begin{aligned} I(L(d);d) &= 1 - \int_{-\infty}^{+\infty} p(L(d)\,|\,d = \pm 1)\log_2(1+\exp(-d\cdot L(d)))dL \\ &= 1 - \mathbf{E}\left[\log_2(1+\exp(-d\cdot L(d)))\right] \end{aligned} \tag{7.17}$$

(7.17) defines a monotonically increasing relationship between $I(L(d);d)$ and σ^2. An ML decision rule for the decoded data will return $\hat{d}_k = +1$ if $L > 0$, -1 otherwise, and hence the decoded BER may be estimated as:

$$P_b = Q\left(\frac{\mu}{\sigma}\right) = Q\left(\frac{\sigma^2/2}{\sigma}\right) = Q\left(\frac{\sigma}{2}\right) \tag{7.18}$$

which of course decreases monotonically with increasing σ. Hence P_b also decreases monotonically with increasing $I(L(d);d)$.

Ten Brink also describes the Extrinsic Information Transfer (EXIT) chart of a decoder, which relates the output mutual information of the decoder to the input, assuming the Gaussian model applies to both input and output. For well-behaved decoders this transfer function is monotonically increasing, hence implying that decoded BER decreases monotonically with increasing mutual information at the decoder input, $I(L(b);b)$, where $L(b)$ is given by (7.7), again showing that the mutual information criterion for precoder selection minimises decoded BER. Note that for a non-iterative decoder the feedback between the decoder and the APP detector in Figure 7-2 is omitted, and the feedback terms in (7.7) are zero. Then the mutual information criterion can be expressed as:

$$\hat{\mathbf{F}} = \arg\max_{\mathbf{F}}\left(I\left(L(b);b\right)\right) \tag{7.19}$$

7.2.3 Mutual information criterion for coded system with iterative decoding

However in the iterative decoder of Figure 7-2 the final mutual information, and hence the final decoded BER, is not simply determined by the output mutual information of the APP detector. The complete operation of the iterative decoder can, however, be described by the EXIT chart of [Bri01], incorporating the transfer function of the APP detector and of the SfISfO decoder. The final converged mutual information is then determined by the intersection of these two characteristics, as shown in Figure 7-3. We can therefore select the precoder for a particular channel according to this intersection point. Since the EXIT function of the decoder is fixed when the channel coding is defined, it can be pre-calculated and has negligible effect on complexity. Moreover the EXIT function of the iterative ML detector can be approximated by a straight line. The intersection points can be calculated at low complexity using analytical geometry if the EXIT functions are known. The straight line can be set by two points defined by the instantaneous channel: $I(L_p(b);b) = 0$ and $I(L_p(b);b) = 1$, where $L_p(b)$ is the fed back *a priori* information in (7.7), corresponding to the ordinate of Figure 7-3. The two corresponding values of output mutual information of the decoder, the intersections of the detector EXIT characteristic with the axes on the left and the right of the plot, can be obtained analytically from (7.7) and (7.17), given **F** and **H**. The mutual information criterion in this case becomes the precoder matrix **F** which maximises the mutual information at this intersection point.

Figure 7-3 EXIT chart for iterative decoder

7.3 Numerical results

7.3.1 Uncoded system

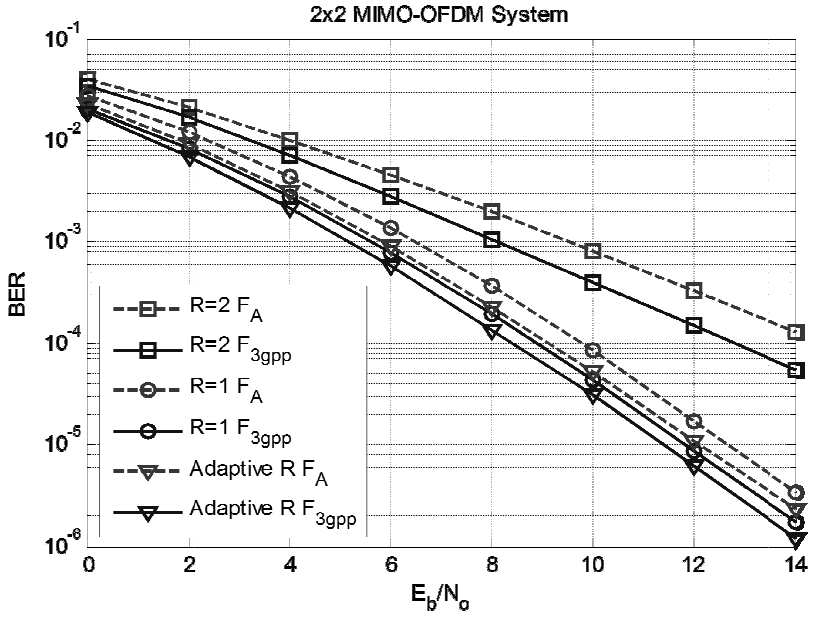

Figure 7-4 Probability of bit errors for different stream selection scheme and different precoder code sets in 2x2 MIMO-OFDM system.

In Figure 7-4, the results of different precoding codebooks in a 2x2 MIMO-OFDM system are shown. In order to better evaluate the adaptive scheme performance, two different precoder code sets were tested. One is simple antenna selection, in which:

$$\mathbf{F}_A = \left\{ \begin{bmatrix} 1 \\ 0 \end{bmatrix}, \begin{bmatrix} 0 \\ 1 \end{bmatrix}, \sqrt{\frac{1}{2}} \begin{bmatrix} 1 & 0 \\ 0 & 1 \end{bmatrix} \right\}. \tag{7.20}$$

The other is the set defined in the 3GPP LTE standard [3GP06], which provides a larger set.

$$\mathbf{F}_{3gpp} = \left\{ \begin{array}{c} \begin{bmatrix} 1 \\ 0 \end{bmatrix}, \begin{bmatrix} 0 \\ 1 \end{bmatrix}, \sqrt{\frac{1}{2}} \begin{bmatrix} 1 & 0 \\ 0 & 1 \end{bmatrix}, \\ \sqrt{\frac{1}{2}} \begin{bmatrix} 1 \\ 1 \end{bmatrix}, \sqrt{\frac{1}{2}} \begin{bmatrix} 1 \\ -1 \end{bmatrix}, \frac{1}{2} \begin{bmatrix} 1 & 1 \\ 1 & -1 \end{bmatrix}, \\ \sqrt{\frac{1}{2}} \begin{bmatrix} 1 \\ j \end{bmatrix}, \sqrt{\frac{1}{2}} \begin{bmatrix} 1 \\ -j \end{bmatrix}, \frac{1}{2} \begin{bmatrix} 1 & 1 \\ j & -j \end{bmatrix} \end{array} \right\}. \tag{7.21}$$

In each case we also consider the restriction of the codebook to a fixed number of layers (streams). QPSK is used when two streams are selected while 16QAM is used for the single stream case. The result with R = 2 and codebook $\mathbf{F}_A$ corresponds to conventional spatial multiplexing MIMO-OFDM. We observe that this achieves only second order diversity, as a result of ML detection at the receive end. However, both the two fully adaptive cases and the one stream case (i.e. R = 1) can fully exploit the transmit end diversity as well, giving fourth order diversity altogether. The adaptive case is about 0.5 dB better than the one stream case and around 3 dB better than the conventional case at $P_{BER} = 10^{-3}$. Also, a noticeable improvement occurs when the precoder code set is extended from $\mathbf{F}_A$ to $\mathbf{F}_{3gpp}$.

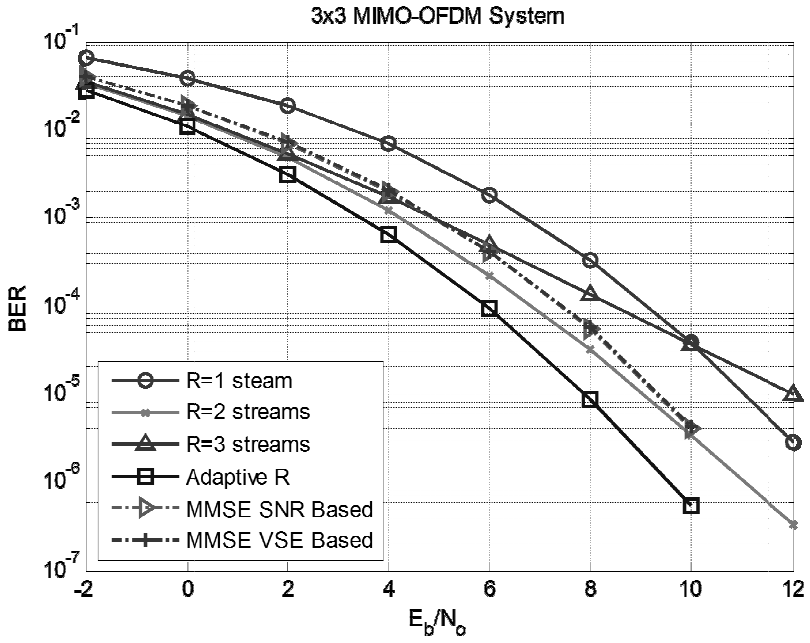

Figure 7-5 Probability of bit errors for different precoder selection criteria, detection algorithms and different precoder code sets in 3x3 MIMO-OFDM system

Figure 7-5 shows the performance for the 3x3 MIMO-OFDM system. QPSK is used when three streams are selected while 8PSK and 64QAM are used for the two stream and single stream cases respectively. For simplicity we use the precoder codebook of corresponding to spatial multiplexing over all three antennas, single antenna selection, and spatial multiplexing over the optimum pair of antennas.

$$\left\{ \begin{array}{c} \sqrt{\frac{1}{3}}\begin{bmatrix} 1 & 0 & 0 \\ 0 & 1 & 0 \\ 0 & 0 & 1 \end{bmatrix}, \begin{bmatrix} 1 \\ 0 \\ 0 \end{bmatrix}, \begin{bmatrix} 0 \\ 1 \\ 0 \end{bmatrix}, \begin{bmatrix} 0 \\ 0 \\ 1 \end{bmatrix}, \\ \sqrt{\frac{1}{2}}\begin{bmatrix} 1 & 0 \\ 0 & 1 \\ 0 & 0 \end{bmatrix}, \sqrt{\frac{1}{2}}\begin{bmatrix} 1 & 0 \\ 0 & 0 \\ 0 & 1 \end{bmatrix}, \sqrt{\frac{1}{2}}\begin{bmatrix} 0 & 0 \\ 1 & 0 \\ 0 & 1 \end{bmatrix}, \end{array} \right\} \quad (7.22)$$

Again the adaptive stream mapping scenario achieved the best performance among all those schemes, achieving approximately the same diversity order as antenna selection, but with about 3 dB performance improvement. Also it is around 4 dB better than the conventional 3x3 spatial multiplexing (R=3) case at a BER of 10^{-5}. The MMSE results use the approach of [Hea05] based on the best SNR and VSE criteria for precoder selection. The ML receiver in our adaptive scheme with the BER criterion provides 1.5 dB extra gain over these linear receiver results.

7.3.2 Coded system with iterative decoding

Figure 7-6 and Figure 7-7 show numerical results for the BER of the coded system with iterative decoding and precoder selection based on the mutual information criterion with convergence estimation. We use a memory 2 rate ½ convolutional code for channel coding, with generator polynomials (7, 5) in octal notation. Figure 7-3 (in which the detector EXIT chart is shown for one channel instance only) shows that the EXIT function of the ML detector output is well matched with the estimated curve. Also the final intersection point is predicted.

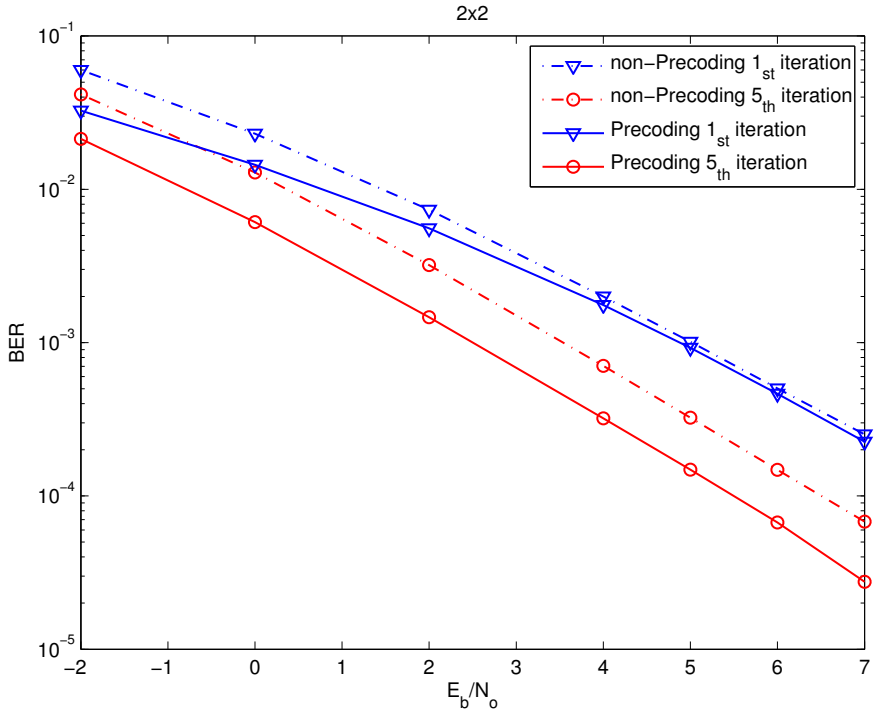

Figure 7-6 Probability of bit errors for coded MIMO systems with two transmit and two receive antennas

The proposed mutual information criterion is tested in 2x2 and 3x3 MIMO systems. It is assumed that the channel is perfectly estimated at the receiver, where the selection criterion is applied, and that the precoder index is transmitted back to the transmitter without delay. For both schemes $2N_t$ bits were transmitted per MIMO symbol. The “non-precoded" results shown in both figures assume simple spatial multiplexing, which is in fact equivalent to an identity matrix precoder. This system is approximately equivalent to “Turbo-BLAST" [Sel02]. Figure 7-6 shows results for a 2×2 precoded MIMO system, using the 3GPP precoder set from (7.21).

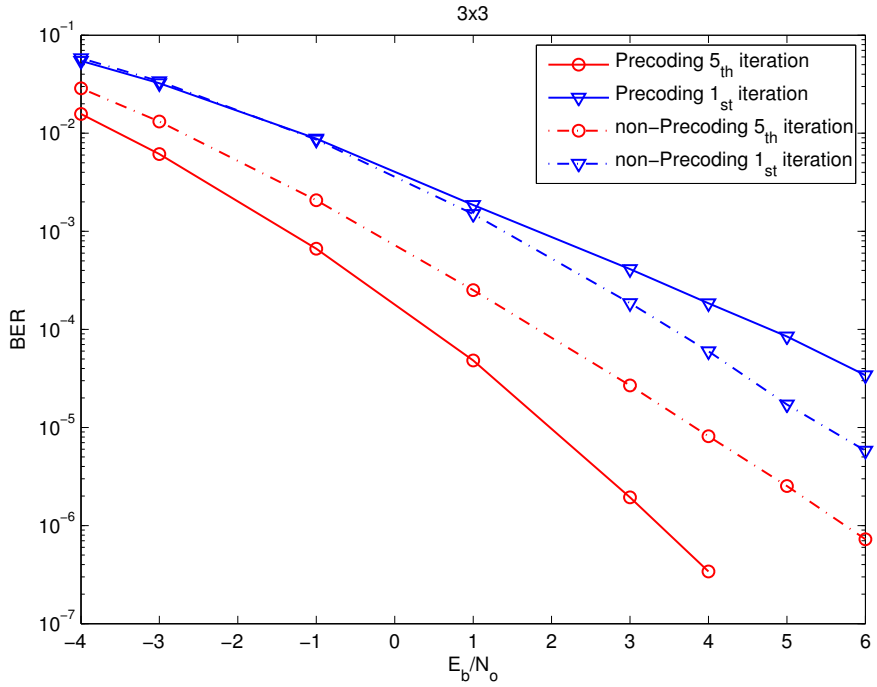

Figure 7-7 Probability of bit errors for coded MIMO systems with three transmit and three receive antennas

In Figure 7-7, the proposed scheme is tested with 3 transmit and 3 received antennas with 6 bits per MIMO symbol. 16QAM, 8QM-AM and QPSK modulation with Gray coded mapping are used respectively for R = 1, 2 and 3 data streams (the number of columns in **F**). An artificial precoding codebook is used here, without significant loss of generality. Precoders for 3 streams are:

$$\left\{ \begin{bmatrix} 1 & 0 & 0 \\ 0 & 1 & 0 \\ 0 & 0 & 1 \end{bmatrix}, \begin{bmatrix} 1 & 1 & 1 \\ 1 & \exp(2\pi j/3) & \exp(4\pi j/3) \\ 1 & \exp(4\pi j/3) & \exp(8\pi j/3) \end{bmatrix}, \begin{bmatrix} 1 & 1 & 1 \\ \exp(\pi j/3) & \exp(3\pi j/3) & \exp(5\pi j/3) \\ \exp(2\pi j/3) & \exp(6\pi j/3) & \exp(10\pi j/3) \end{bmatrix} \right\} \quad (7.23)$$

while the precoders for 1 and 2 streams are given by the combinations of 1 and 2 columns of these matrices.

It is interesting to note that at the first iteration the precoded system gives poorer performance than non-precoded, especially at high E_b/N_0. This is because the selection criterion optimises the converged performance, rather than that at the first iteration. At the 5th iteration, when the system is converged, the precoded system outperforms the non-precoded by nearly 4dB at BER = 10^{-5}. The diversity order, defined by the slope of the curve, approaches 9, which is full diversity in this system.

8. Capacity of access network with network-enabled MIMO

8.1 Introduction

BuNGee aims at implementing next generation wireless networks which will provide access to high-speed data applications, which requires spectrally efficient communications in both downlink and uplink cellular systems. Networked MIMO, also termed CoMP, has been highlighted in 4th Generation and beyond cellular network standards such as 3GPP LTE-Advanced. Since the available spectrum is limited, system capacity can be improved by introducing a higher frequency reuse and by use of small cells. In such a network configuration, a higher spectral efficiency is obtained, however, inter-cell interference (ICI) will become dominant at the cell edges and the system is said to be interference limited. This will apply particularly in BuNGee's aggressive frequency reuse scenario, with full frequency reuse.

The application of interference mitigation techniques is necessary in these systems to prevent a restricted data rate of the users located at the cell edge and improve the system fairness. An alternative promising solution to deal with ICI is multi-cell cooperation which leads to the concept of network MIMO. In Network MIMO, a number of ABSs cooperatively serve the MSs by forming a virtual multiple antenna array. High capacity HBS to ABS backhaul links are required for inter-base signalling as well as user data routing. [Pap08]. Multi-cell cooperation transmission techniques have been theoretically investigated and their capacity analysis is summarised in [Jin07] [Boc07] for a simplistic Wyner model, and for a more realistic model. In the following text, we discuss several challenges for implementing network MIMO and some state-of-the-art solutions are listed as the candidates which could potentially be used in the BuNGee architecture to further improve the system spectral efficiency.

8.2 Challenges and Solutions

8.2.1 Interference limited cellular network

In conventional cellular systems, each BS transmits signals for the intended users within its geometrical cell coverage. Depending on the channel conditions, interference caused by neighbouring cell transmissions can significantly degrade the received signal quality, so that the users located at the edge of cells suffer from low SINR and throughput is severely limited by the inter-cell interference.

In order to circumvent this problem, conventional frequency-reuse is introduced to partition the cluster of cells, so that lower co-channel interference is obtained for a frequency re-use factor less than 1. Other techniques are also considered to mitigate the interference between cells such as user scheduling schemes and power control at the transmitter side. In all these techniques, the inter-cell interference is treated as noise at the receiver and the per cell throughput is purely dependent on the signal processing and error control coding techniques used for point-to-point communications links between the BSs and users [Ges10]. The inter-cell links introduce pure interference, and the throughput per user is upper bounded by the isolated cell capacity when perfect inter-cell interference cancellation is assumed.

8.2.2 Networked MIMO

Instead of the conventional passive treatment of interference in the approaches discussed above, the concept of network MIMO is introduced to *exploit* inter-cell interference by jointly processing the user data received by several cooperating ABSs to form a large scale virtual MIMO system for both downlink and uplink. Multi-cell coordination is required across multiple ABSs to form a virtual MIMO system. The coordinated ABSs exploit the HBS to ABS backhaul wireless links to share the user data and global channel state information (CSI). All received signals are considered to carry useful messages for the joint precoder/decoder, and in this way the interference is exploited. With this networked configuration, there are no signals which cause pure interference, and additionally the statistically independent interfering links provide extra spatial diversity for precoding/decoding.

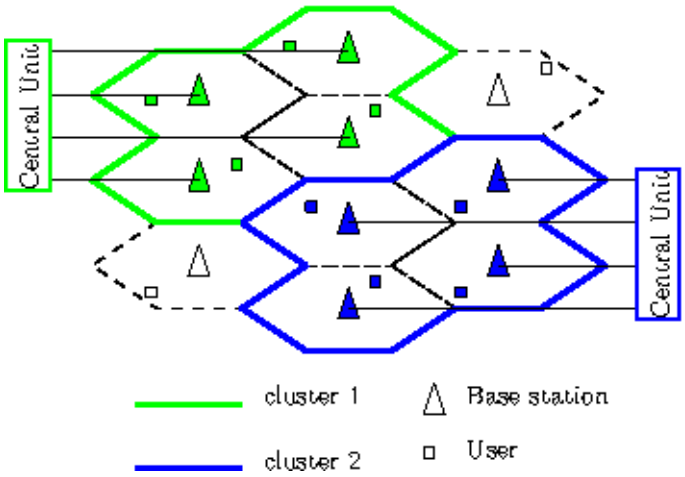

Figure 8-1 Base stations cooperating to perform JMD, each cluster has 4 BSs and 4 users

With network MIMO, the ABS no longer decodes the desired signal independently, but joint coding and decoding (JCC) is assumed, utilising global (CSI) as well as user data information which is exchanged among multiple coordinated ABSs [Ges10]. Both array and diversity gains are obtained resulting in a substantial increase in system sum-user capacity [Kha08]. Despite the optimality of JCC, it needs to exchange all the quantized information between the cooperative ABSs via the wireless backbone network and results in about heavy backhaul traffic. To reduce the backhaul, clusters are introduced to the network applying JCC, where a group of ABSs form a cluster and JCC is performed in a central unit, as shown in Figure 8-1. Since the receive antennas (ABSs) are separated from each other and located in the centre of each cell, the signals are joint processed at a central point, in BuNGee this can be the hub base station (HBS). This is also equivalent to the distributed antenna system (DAS) [Kha08]. In this way a virtual MIMO system is therefore formed [Ges10]. In this structure, the information is exchanged within the cluster which reduces the backhaul and the detection complexity in each JCC. Even with the benefits mentioned above, the restrictions of JCC are listed below:

1. By assuming unlimited backhaul capacity, the performance of JCC is optimal for an isolated cluster. However the performance degrades in a large network with many clusters, especially at the boundaries of the clusters.
2. The central processing units are required to support a large number of users in the cluster with many cells which introduces substantial complexity even taking into account that the central units usually have high computational power.
3. It requires transmission of quantized channel state and user data information over the HBS to ABS link which causes an extra information sharing overhead. Sophisticated network design to accommodate this overhead is required for efficient transmission in a MIMO network. [Ges10]
4. As regards implementation, the organization of cells and clusters is a complex task which requires additional scheduling and signalling information to be transferred via the backhaul.

The above problems can be partially addressed by reducing the number of cells in each cluster and by introducing advanced interference mitigating techniques among the adjacent clusters at the cost of additional backhaul traffic between the clusters. In the extreme case, each cluster has a single cell and therefore a distributed iterative decoding (DID) is reported as an alternative of JCC. With the DID configuration, iterative signal processing is performed at the network level. The ABS communicates with each user at its corresponding cell and iteratively refines the estimate of the transmitted symbol with the help of the information provided by other cooperating cells. Each BS detects the desired user/stream only; the other interfering signal is treated as noise. The output of the decoder is used to reconstruct the transmitted symbol and the estimates are spread to the cooperating ABSs. Each ABS has an interface to exchange the estimation results to its neighbours, and the reconstructed interfering signals are cancelled from the received signal and the power of the interference reduces as more iterations are performed. As for JCC, the complexity of computing extrinsic information is exponential in both the number of transmit antennas and the number of cells. With DID, for each cell, the complexity of the search required to compute the ML solution is restricted to the number of data streams inside the cell, this results in a significant reduction in complexity. Although with the advantages, the restrictions of DID are listed below:

1. The DID scheme does not benefit from array gain and diversity gain since the energy received from the cooperating BSs is cancelled without utilization: the performance is bounded by that of an isolated single-user single-cell system.
2. The iterative interference cancellation is performed at the network level, which requires additional backhaul traffic between interfering BSs. A number of iterations is required to achieve an acceptable performance and may result in detection delay that must be minimised.
3. In order to perform the interference cancellation in either a serial or parallel manner, the estimated symbols have to be shared among the ABSs. An effective quantization algorithm is required to reduce the backhaul traffic and improve the system efficiency.

8.3 System model and traditional methods

In the symmetric networked-MIMO scenario, let us consider a group of user K equipments (UE) which are served by a number of M cooperating ABS which are connected to an HBS via the backhaul network. Each UE is served by a local ABS and several other ABSs from cooperating cells. Let us assume the backhaul links always have sufficient bandwidth to exchange information between the ABSs and HBS. With this configuration a distributed antenna system is formed, in which the ABSs forward the received signals to HBS and the HBS performs the joint multiuser detection.

Let us assume the UEs are perfectly synchronized and a $k \times 1$ symbol vector

$$\mathbf{s} = \left[s_1, s_2, \ldots, s_K \right]^T \tag{8.1}$$

is transmitted by all K UEs simultaneously. At base station m, the received symbols r_m are given by

$$r_m = \mathbf{g}_m \mathbf{s} + n \tag{8.2}$$

The entries of a $1 \times K$ row vector $\underline{\mathbf{g}}_m$ are the element-wise products of $\underline{\mathbf{h}}_m$ and ρ_m where $\mathbf{h}_m = [h_{m,1}, \ldots, h_{m,k}, \ldots, h_{m,K}]$, and $\rho_m = [\rho_{m,1}, \ldots, \rho_{m,k}, \ldots, \rho_{m,K}]$.

The entry $h_{m,k}$ is the complex channel realization from the k-th user to the m-th BS with independent identically distributions (i.i.d). The coefficients $\rho_{m,k}$ define the effect of the path loss of the link between ABS m and UE We further separate r_m into four terms

$$\begin{aligned} r_m &= g_{m,d} s_d + \sum_{n \in \mathbb{C}_m} g_{m,n} s_n + \sum_{n \in \hat{\mathbb{C}}_m} g_{m,o} s_o + n_m, \\ &= \rho_{m,d} h_{m,d} s_d + \rho_{m,n} \sum_{n \in \mathbb{C}_m} h_{m,n} s_n + \rho_{m,o} \sum_{n \in \hat{\mathbb{C}}_m} h_{m,o} s_o + n_m \end{aligned} \tag{8.3}$$

where the first term denotes the signal collected from the local cell (indexed by *d*), the second and the third terms denote the interference from the adjacent cells and the interference from far away cells (indexed by *n* and *o*, respectively). The coefficients $\rho_{m,n}$ and $\rho_{m,o}$ characterize the channel gains with adjacent and far away interferers, separately. The set of indices of interference from adjacent cells at ABS m is denoted as $\mathbb{C}_m$ and the weakly received interference is denoted as $\hat{\mathbb{C}}_m$ For example, for a system with $K = M = 4$ and 2 strong interferers, we assume that the weak interference $\rho_{m,n}$ is zero and $\rho_{m,o}$ = 1, the coupling matrix is formed as

$$\mathbf{P} = \begin{bmatrix} 1 & \rho_{m,n} & \rho_{m,n} & 0 \\ 0 & 1 & \rho_{m,n} & \rho_{m,n} \\ \rho_{m,n} & 0 & 1 & \rho_{m,n} \\ \rho_{m,n} & \rho_{m,n} & 0 & 1 \end{bmatrix} \tag{8.4}$$

Hence:

$$\mathbf{r} = (\mathbf{P} \circ \mathbf{H})\mathbf{s} + \mathbf{n} \tag{8.5}$$

where $\circ$ is the Hadamard (element-wise) product and

$$\mathbf{r} = [r_1, \ldots, r_m, \ldots, r_M]^T \tag{8.6}$$

and

$$\mathbf{P} = [\rho_1^T, \ldots, \rho_m^T, \ldots, \rho_M^T]^T \tag{8.7}$$

$$\mathbf{H} = [\mathbf{h}_1^T, \ldots, \mathbf{h}_m^T, \ldots, \mathbf{h}_M^T]^T \tag{8.8}$$

The power loss coefficients $\rho_{m,d}$, $\rho_{m,n}$, $\rho_{m,o}$ introduced here are used to characterize long term attenuation corresponding to a cellular scenario. The i.i.d. elements in $\mathbf{H}$ are introduced to model the short term fading.

With this system model, effort should be made in exploiting the available physical resources such as space and time. The model can be seen as a virtual MIMO system and the coordinated transmission of all cooperating ABSs is required to minimize the inter-cell interference. In the downlink, examples of such coordinated transmission including joint prefiltering of the transmit signals by a ZF or MMSE matrix which results in interference free reception at the user's end. Alternatively a precoding matrix can be obtained by using a pseudo-inverse with dirty paper coding (DPC) which is conceptually similar to successive interference cancellation (SIC) in the MIMO uplink scenario.

8.3.1 ZF/MMSE Precoded MIMO Network

For a spatial multiplexing MIMO network with global channel gain $\mathbf{H} \in \mathbb{C}^{M \times K}$ with $M \geq K$, the CSI can be exploited at the transmitter to mitigate inter-cell interference. We will focus on the linear-precoding method for designing the precoding matrix. The precoding can be represented by a weight matrix $\mathbf{A} \in \mathbb{C}^{K \times K}$ and the precoded symbol vector $\mathbf{s} \in \mathbb{C}^{K \times 1}$ can be expressed as

$$\mathbf{s} = \mathbf{A}\mathbf{x} \tag{8.9}$$

where $\mathbf{x}$ is the original user message for transmission. In the case where MMSE precoding is employed, by assuming the channel is full rank and CSI is perfectly known at the transmitter, the MMSE weight matrix is obtained as

$$\begin{aligned} \Omega_{\text{MMSE}} &= \beta \arg_{\Omega_{\text{MMSE}}} \min E\{\beta^{-1}(\mathbf{H}\mathbf{s} + \mathbf{v}) - \mathbf{x}\|^2\} \\ &= \beta \boldsymbol{H}^{\dagger} \end{aligned} \tag{8.10}$$

where β is used to meet the total power constraint which is given as [Joh05]

$$\beta = \sqrt{\frac{K}{Tr(\boldsymbol{H}^{\dagger}\boldsymbol{H}^{\dagger H})}} \tag{8.11}$$

and $\boldsymbol{H}^{\dagger} = \boldsymbol{H}^{H}(\boldsymbol{H}^{H}\boldsymbol{H} + \frac{\sigma_v^2}{\sigma_s^2}\boldsymbol{I})^{-1}$. Alternatively to MMSE precoding, ZF can also be used for precoding the user message. In a similar way to the MMSE solution, the ZF precoding matrix is obtained as

$$\begin{aligned} \Omega_{ZF} &= \beta \arg_{\Omega_{ZF}} \min E\{\beta^{-1}\mathbf{H}\mathbf{s} - \mathbf{x}\|^2\} \\ &= \beta \boldsymbol{H}^{-1} \end{aligned} \tag{8.12}$$

The equation is the same as the MMSE except $\boldsymbol{H}^{\dagger}$ is replaced with $\boldsymbol{H}^{-1}$.

Figure 8-2 shows the BER performance of the ZF and MMSE precoder at the transmitter side and MMSE decoding on the receiver side. We assume 4 independent data streams are jointly processed by 4 ABSs and each of them has a single receive antenna. The channel is uncorrelated with i.i.d elements. We also assume that CSI is perfectly known at both sides. Note that the precoding scheme at the transmitter side outperforms the receiver side detection; this because the receiver suffers from noise enhancement.

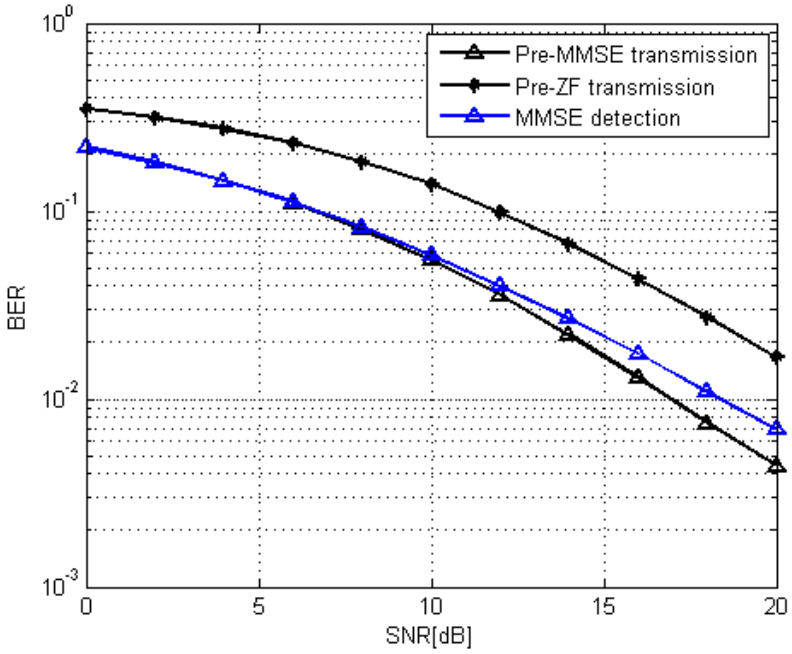

Figure 8-2 Performance comparison: ZF and MMSE precoding.

8.3.2 Dirty paper coding

Besides the channel inversion approach introduced in the previous subsection, interference cancellation at the ABS is also developed to improve the throughput for the downlink broadcast channel, by subtracting the potential interference before transmission. DPC can be applied when CSI is perfectly known to the transmitter, and an interference free transmission can be realized. The k-th user's signal is given by $s_k \in$ and

$$\begin{bmatrix} r_1 \\ \vdots \\ r_K \end{bmatrix} = \begin{bmatrix} \boldsymbol{h}_1 \\ \vdots \\ \boldsymbol{h}_K \end{bmatrix} \begin{bmatrix} x_1 \\ \vdots \\ x_K \end{bmatrix} + \begin{bmatrix} n_1 \\ \vdots \\ n_K \end{bmatrix} \tag{8.13}$$

where $\boldsymbol{h}_k \in$ $^{1\times M}$ is the channel gain between cooperative ABSs and user k. The channel matrix can also be LQ-decomposed as follows

$$\begin{aligned} \boldsymbol{H} &= \begin{bmatrix} l_{1,1} & 0 & \cdots & 0 & 0 \\ l_{2,1} & l_{2,2} & 0 & 0 & 0 \\ \vdots & \vdots & \ddots & 0 & \vdots \\ l_{M-1,1} & l_{M-1,2} & \cdots & l_{M-1,M-1} & 0 \\ l_{M_r,1} & l_{M,2} & \cdots & l_{M,M-1} & l_{M,M} \end{bmatrix} \begin{bmatrix} \boldsymbol{q}_1 \\ \vdots \\ \boldsymbol{q}_M \end{bmatrix} \\ &= \boldsymbol{LQ} \end{aligned} \tag{8.14}$$

where $\boldsymbol{q}_k \in$ $^{1\times M}$ are orthogonal row vectors. The precoded message vector $\boldsymbol{s} = \left[s_1, \cdots, s_K\right]^T$ is then multiplied by $\boldsymbol{Q}^H$ and the effect of $\boldsymbol{Q}$ is removed through the channel. This forms a lower-triangular matrix, and the received signal at the user side is given by

$$\begin{bmatrix} r_1 \\ \vdots \\ r_K \end{bmatrix} = \begin{bmatrix} \boldsymbol{h}_1 \\ \vdots \\ \boldsymbol{h}_K \end{bmatrix} \boldsymbol{Q}^H \boldsymbol{S} + \begin{bmatrix} n_1 \\ \vdots \\ n_K \end{bmatrix} = \begin{bmatrix} l_{1,1} & 0 & \cdots & 0 & 0 \\ l_{2,1} & l_{2,2} & 0 & 0 & 0 \\ \vdots & \vdots & \ddots & 0 & \vdots \\ l_{K-1,1} & l_{K-1,2} & \cdots & l_{K-1,K-1} & 0 \\ l_{K,1} & l_{K,2} & \cdots & l_{K,K-1} & l_{K,K} \end{bmatrix} \begin{bmatrix} s_1 \\ \vdots \\ s_K \end{bmatrix} + \begin{bmatrix} n_1 \\ \vdots \\ n_K \end{bmatrix} \tag{8.15}$$

From the above equation, we can obtain the received signal of the first user which is given by

$$r_1 = l_{1,1} s_1 + n_1 \tag{8.16}$$

For the first user, we give the estimate of symbol as $s_1 = x_1$ and the received signals for the following user can be obtained by solving the following simple equations:

$$s_k = x_k - \sum_{j=1}^{K} \frac{l_{k,j}}{l_{k,k}} x_j \tag{8.17}$$

we can see from above equation that the precoded signals s_1 to s_{k-1} are composed of the known user signal x_1 and x_{k-1} . When decoding the k-th user, the previously detected x_1 to x_{k-1} are interference components. By successively stripping off the detected signals, the precoded signal for the k-th user is computed. DPC on the transmitter side is similar to the successive interference cancellation on the receiver side, a higher precoding diversity can be provided as shown in Figure 8-3, with four users with independent CSI which are perfectly known at the ABS side. Four user signals are jointly precoded before transmission. We also assume there are four cooperative ABSs and QPSK modulated symbols are used.

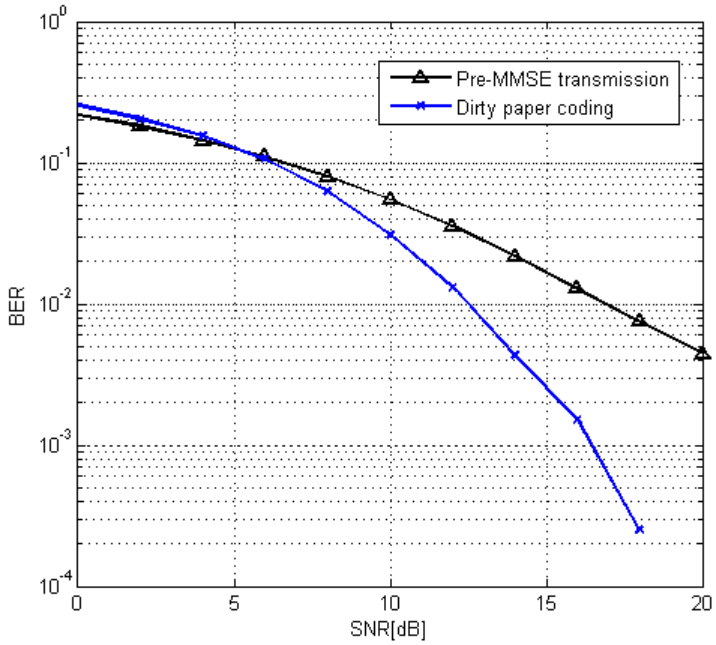

Figure 8-3 BER performance against SNR for a precoded system

8.4 State of the Art

The strategies to deal with the ICI in the system uplink including the JCC and DID [Kha08]. In terms of JCC, the ABSs for each cell make the received signals available to all cooperating ABSs. With this set up, the receivers not only use the desired signal energy but also the energy from the interferers leading to much improved received SNR. As for the downlink, precoding techniques such as linear zero-forcing and DPC can be applied within the cooperation cluster to form a multiple-antenna broadcast channel with distributed

antennas as discussed in previous section. The multiple interfering transmitters in multiple ABSs share the user's message and joint signal processing is performed. However, all these above mentioned conventional approaches have many restrictions such as full CSI requirement, high signal processing complexity for precoding and decoding for large clusters which support many users. Lower backhaul traffic (or message backhaul efficiency) and delay should also be considered in the design of cooperating systems.

In order to circumvent these problems, several state-of-the-art techniques are discussed in the following section, specifically, dynamic clustering approach, sparse precoding techniques, DID with reduced message passing for efficiently transmitting reliability information. All these techniques can be potentially implemented in the networked MIMO enabled BuNGee scenario.

8.4.1 Static and Dynamic clustering approach

The sharing of the data symbols and channel information imposes very large demands on the backhaul link: the traffic burden increases rapidly as the number of coordinating ABSs increases. In the conventional architecture, static clusters [Ven07] are used to alleviate the traffic of cooperating ABSs and the user data is only shared inside the cluster. Static cluster planning only show its effectiveness in the symmetric model. For a more realistic asymmetric model, the inter-cluster interference may be strong at cell edges and reduce per-cell throughput. Therefore there is growing interest in finding more efficient clustering methods in network MIMO systems. An optimized dynamic greedy ABS clustering approach is developed in [Pap08] and the dynamic clustering approach outperforms the static clustering approach in terms of sum-rate per cell.

8.4.2 Sparse precoding in cooperating MIMO systems

In another work [Ker12], the authors proposed a precoding technique for Network MIMO downlink applications. Joint precoding across all coordinated ABSs is considered in a sparse link environment. The users' data symbols are jointly optimized and shared among the ABSs before transmission. A sparse precoder is investigated to achieve a very efficient symbol sharing algorithm. Let us assume the ABS and users have only one antenna so that the transmission can be mathematically described as

$$\begin{bmatrix} r_1 \\ \vdots \\ r_K \end{bmatrix} = \boldsymbol{H}\boldsymbol{x} + \boldsymbol{n} = \begin{bmatrix} \boldsymbol{h}_1^H \boldsymbol{x} \\ \vdots \\ \boldsymbol{h}_K^H \boldsymbol{x} \end{bmatrix} + \begin{bmatrix} n_1 \\ \vdots \\ n_K \end{bmatrix} \tag{8.18}$$

where the transmitted signal $\boldsymbol{x} \in \mathbb{C}^{K\times 1}$ is obtained from the vector of transmit K user's symbol vector as

$$\boldsymbol{x} = \boldsymbol{T}\boldsymbol{s} = \begin{bmatrix} \boldsymbol{t}_1 & \cdots & \boldsymbol{t}_K \end{bmatrix} \begin{bmatrix} s_1 \\ \vdots \\ s_K \end{bmatrix} \tag{8.19}$$

where $\boldsymbol{t}_k \in \mathbb{C}^{K\times 1}$ is the beamforming vector for transmitting s_k. In [Ker12], a threshold is applied to the channel matrix, so that many of the coefficients corresponding to the interference links (off-diagonal elements in G) can be quantized as zeros, leading to a sparse presentation of the channel. The sparsity of the channel gives the advantage of low backhaul requirement. In additional, a routing matrix $\boldsymbol{D} \in \{0,1\}^{K\times K}$ is proposed and the (*k,m*)-th element is 1 if the corresponding link is strong and 0 otherwise. An effective precoder is given in the form of an element-wise product of $\boldsymbol{D} \circ \boldsymbol{H}$. The beamforming vector $\boldsymbol{t}_k$ for each user's signal is obtained by

$$\mathbf{t}_k = \arg\min_{\mathbf{t}_k} \| \mathbf{H}(\mathbf{D} \circ \mathbf{t}_k) - \mathbf{e}_k \|^2 \tag{8.20}$$

An efficient message routing pattern is then derived, and this sparse precoding technique requires only a fraction of the message routing overhead with low complexity and limited performance losses.

8.4.3 Distributed Iterative Detection and Decoding with Reduced Message Passing

The setup for performing the uplink distributed detection with the information exchange between base stations is shown in Figure 8-4. Each ABS is equipped with a communication interface for exchanging information with the cooperating ABSs. The information is in the form of a bit sequence with hard decisions or quantized soft estimates. Via these interfaces, each cooperating ABS is connected to the HBS and is ready to receive and transmit information. The distributed iterative detection and decoding with reduced message passing (DIDRMP) limits the computational power required of an HBS.

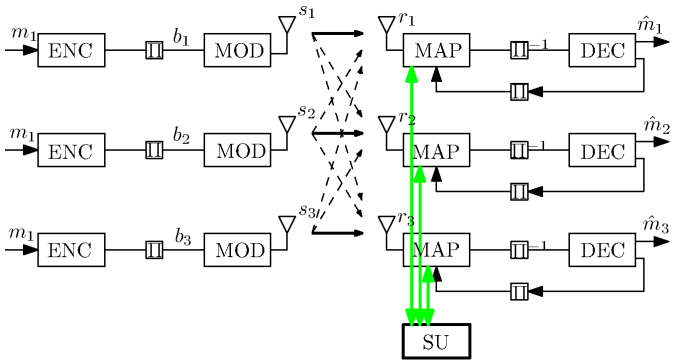

Figure 8-4 An example configuration showing a cooperating 3-cell network.

In Figure 8-4 the dashed lines between the transmitter and receiver denote the other-cell interference while the solid lines denote the desired signal. In each BS, a block of received signals $\mathrm{r_m}$ is used by the MAP demapper to compute the a posteriori probability in the form of log-likelihood-ratios (LLRs), which are given by $\Lambda_1[b_{j,k}[i]] = \log \frac{P[b_{j,k}[i]=+1 \mid r_k]}{P[b_{j,k}[i]=-1 \mid r_k]}$. The detector and decoder are serially concatenated to form a 'turbo' structure, the extrinsic information is exchanged by the two components. We denote the intrinsic information provided by the decoder a $\Lambda_2[b_{j,k}[i]] = \log \frac{P[b_{j,k}[i]=+1 \mid \text{decoding}]}{P[b_{j,k}[i]=-1 \mid \text{decoding}]}$ and the post-decoding bit LLRs are obtained. From [Wan99] the bit-wise probability is computed by

$$P[b_{j,k}[i]=\bar{b}_j] = \frac{1}{2}[1+\bar{b}_j \tanh(\frac{1}{2}\Lambda_2[b_{j,k}[i]))] \tag{8.21}$$

where $\bar{b}_j \in \{+1,-1\}$. The symbol probability $P[s_k[i]=c_q]$ is obtained from the corresponding bit-wise probability, assuming the bits are statistically independent as described by [Wan99]

$$P[s_k[i]] = \prod_{j=1}^{J} P[b_{j,k}[i]=\bar{b}_j] \tag{8.22}$$

where $P[s_k[i]] \triangleq P[s_k[i]=c_q]$ and c_q is an element chosen from the constellation A . From the above equations we can conclude that $\sum_{|\mathrm{A}|} P[s_k[i]] = 1.$

In each ABS, a list of tentative decisions of $s_k[i]$ is obtained by sorting the probabilities $\mathrm{L}_k \triangleq \{c_1, c_2, \ldots, c_\tau\}_k, \quad 1 \le \tau \le |\mathrm{A}|$, obtained by (1.22) in decreasing order, where $|\bullet|$ denotes cardinality, and $Pr[c_1] \ge Pr[c_2] \ge \ldots, Pr[c_\tau]$ where $Pr[c_q] \triangleq P[s_k[i]=c_q \mid r_m]$. For the sake of simplicity, we remove any symbol with $P[s_k[i]] \le p_{\mathrm{th}}$ from the list. The threshold p_{th} may be fixed or varied as a function of SINR. By listing all the combinations of the elements across *K* users, a length Γ tentative decision list is formed. Each entry of the list denotes a possible transmitted symbol vector $\mathbf{s}'_l$ where $l = 1, \ldots, \Gamma$. The number of column vectors in the list is obtained by

$$\Gamma = \prod_{k=1}^{K} | \mathbb{L}_k |, 1 \le \Gamma \le | \mathrm{A} |^K \tag{8.23}$$

In order to obtain an improved performance, the maximum likelihood (ML) rule can be used to select the best candidate among the Γ column symbol vectors. The cost function of the ML criterion is given by

$$\mathbf{s}'_{\mathrm{ML}} = \arg\min_{l=1,\ldots,\Gamma} \| \mathbf{r}[i] - \mathbf{G}\mathbf{s}_{l'}[i] \|^2, \tag{8.24}$$

where $\mathbf{r}[i] = [r_1[i], \ldots, r_m[i], \ldots, r_M[i]]^T$ and $\mathbf{G} = [\mathbf{g}_1^T, \ldots, \mathbf{g}_m^T, \ldots, \mathbf{g}_M^T]^T$, are received signals and the user channels for all cooperating cells.

In the above expression, the knowledge of $\mathbf{g}_m$ and the received signal $\mathrm{r}_m[\mathrm{i}]$ for each cell need to be passed to the HBS, which lead to high backhaul traffic. However, we may distribute the norm operation to each cell.

In a complex space C^K, the common Euclidean norm is $\| \mathbf{d}[i] \| \le \sqrt{| d_{1,m}[i] |^2 + \ldots + | d_{K,m}[i] |^2}$ where $\mathbf{d}[i] = \mathbf{r}[i] - \mathbf{G}\mathbf{s}_{l'}[i]$.

For each BS, we separately calculate minimum partial weights by

$$l_m^{\min} = \arg\min_l | r_m[i] - \mathbf{g}_m \mathbf{s}'_l[i] \ |^2 \tag{8.25}$$

The index $l_m^{\min}$ is obtained by the SU via backhaul and an enhanced detection is obtained. In each iteration, the received signal is subtracted by $\tilde{r}_k[i] = r_k[i] - \mathbf{h}_k \tilde{\mathbf{u}}_k^{\mathrm{ML}}[i]$, where the symbol cancellation vector consists of

$$\tilde{\mathbf{u}}^{\mathrm{ML}}[i] = \left[\tilde{s}_1^{\mathrm{ML}}[i], \ldots, \tilde{s}_{k-1}^{\mathrm{ML}}[i], 0, \tilde{s}_{k+1}^{\mathrm{ML}}[i], \ldots, \tilde{s}_K^{\mathrm{ML}}[i] \ \right] \tag{8.26}$$

With this multiple candidate structure, an enhanced ICI suppression is obtained. The indices of the symbols on the tentative decision list L are propagated among the neighbouring ABSs, requiring reduced backhaul traffic compared with that of the soft signal cancellation algorithm. Additionally, as more cancellation iterations are performed, the size of the list reduces as the recovered bits become more reliable. This further decreases the backhaul traffic with the following iterations which is not the case with the approach that adopts a soft interference cancellation strategy.

In the simulations, we assume $\rho_{m,o}$ is zero, $\rho_{m,d} = 1$ and the strongly received interference terms have $\rho_{m,n} = 0.5$. All ABSs are assumed to have the same SNR and the interfering ABSs are also assumed to have the same signal-to-interference ratio (SIR). In order to evaluate the performance of the distributed turbo system, we select a rate half convolutional code with encoding polynomial $[7,5]_{\mathrm{oct}}$. The coded bits are modulated as QPSK symbols before transmission. The decoding is performed by a max-log-MAP decoder and the block length is set to 1024. The number of detector and decoder iterations (inner iterations) is set to 10. The loop of interference cancellation performed by the network stops at the fifth iteration, if not otherwise stated. In the soft interference cancellation applications [May06], [Wan99] a uniform quantizer is applied in order to quantize the soft estimates. (We use 3 bits per dimension which requires 6 bits per symbol, since QPSK modulation is used.) In terms of hard cancellation, the number of bits used for quantizing the estimated symbol is equal to the modulation level $J = \log_2(| \mathrm{A} |)$, where $| \mathrm{A} |$ is number of constellation symbols.

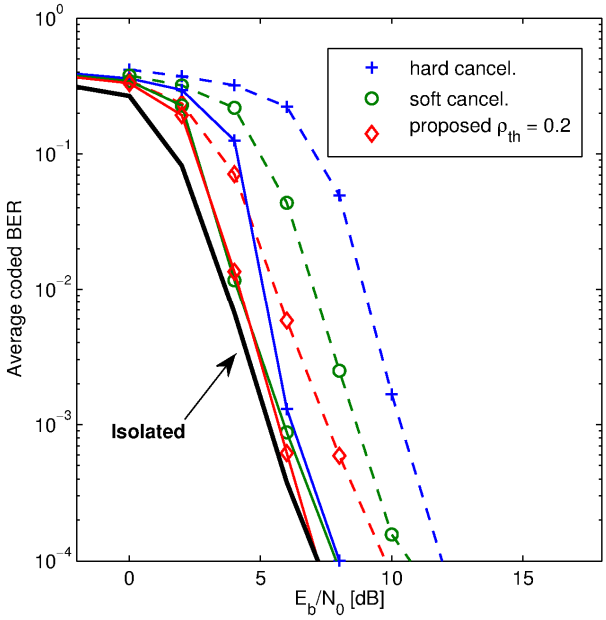

Figure 8-5 The coded BER performance of distributed iterative detection.

In Figure 8-5 the solid lines denote a cooperating 4-cell network with $\zeta = 2$ strong interferers per cell. The dashed lines denote a cooperating network with 9 cells with $\zeta = 3$ strong interferers per cell. We observe that the DIDRMP architecture outperforms the soft interference cancellation scheme; the improvement is more pronounced with a larger number of strong interferers ζ . With $\zeta = 3$ interferers, the proposed scheme achieves about 3 dB gain as compared with the system using hard cancellation at the target $\mathrm{BER} = 10^{-3}$. For the conventional soft and hard interference cancellation techniques, in order to keep the backhaul traffic low, only the energy received in the ABS located in the local cell is used for recovering the transmitted signal. The diversity order is restricted inside the cell. On the other hand with the DIDRMP scheme, the received signals from the cooperating cells are also used, therefore an enhanced performance is achieved. In the extreme case, we assume the threshold $\rho_{\mathrm{th}} = 0$, and the size of the decision list Γ equals $|\mathrm{A}|^K$. This is an ML solution and full receive diversity order can be achieved, however, extremely high backhaul is required for symbol detection in such a network.

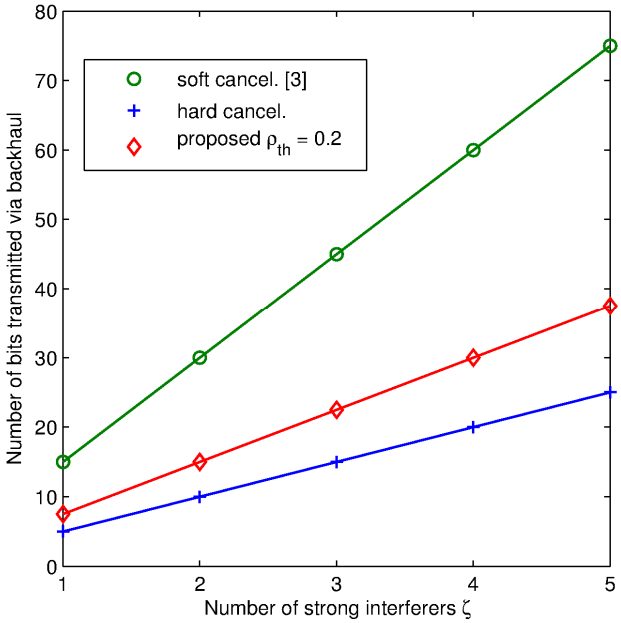

Figure 8-6 Number of bits exchanged per symbol detection in a 9-cell network.

Figure 8-6 illustrates the backhaul traffic as a function of the number of strong interferers ζ. The backhaul traffic is illustrated in terms of number of bits required to be transmitted via the network in order to recover a constellation symbol. As the QPSK constellation is used, 2 bits are required to convey the information about one constellation symbol to perform hard interference cancellation. As for the soft interference cancellation, we use 3 bits per dimension which requires 6 bits to be transmitted via the backhaul per symbol detection [Kha08]. The plots indicate that an increase in the number of strong interferers for each cell leads to an increase in the backhaul traffic. The backhaul traffic of the proposed architecture is directly related to Γ. We have discussed joint multiuser multicell detection through base station cooperation in an uplink, high frequency reuse scenario. Distributed iterative detection has been introduced as an interference mitigation technique. We have compared the soft and hard information exchange and cancellation schemes and introduce a novel multiple candidate exchange strategy based on interference cancellation. DIDRMP algorithm significantly reduces the backhaul data compared with the soft information exchange while it obtains a better bit error performance.

8.5 Networked MIMO and TSB estimation

In this section, we illustrate the method with reference to MMSE detection of spatially multiplexed systems. We consider the post-processing SNR and TSB of the isolated MIMO system, the MIMO system in the presence of interference and the networked MIMO system in the following subsections.

8.5.1 Isolated MIMO

We use the term "isolated MIMO" to describe a MIMO system experiencing only inter-antenna-interference (IAI) and thermal noise, the interfering signal transmitted by other undesired UEs being assumed to be zero. In order to evaluate the post-processing SNR for an interference free MIMO system, the MMSE criterion [Dai04] is used to design the filter to minimize the IAI at the detector output. The MMSE filter is given as

$$\omega_k = \mathbf{R}^{-1}\mathbf{p}_k \tag{8.27}$$

where $\mathbf{R} = E\{\mathbf{r}\mathbf{r}^H\}$ and $\mathbf{p} = E\{\mathbf{r}s^*\}$. By substituting above equation with these functions we obtain

$$\begin{aligned}\mathbf{R} &= \mathbf{H}\mathbf{H}^H + \sigma_n^2\mathbf{I}_M \\ &= \mathbf{h}_k\mathbf{h}_k^H + \sum_{j\neq k}\mathbf{h}_j\mathbf{h}_j^H + \Gamma \\ &= \mathbf{h}_k\mathbf{h}_k^H + \Sigma\end{aligned} \tag{8.28}$$

The extracted signal can be expressed as

$$\tilde{s}_k = \omega_k^H\mathbf{r} = \omega_k^H\mathbf{h}_k s_k + \sum_{j\neq k}\omega^H{}_k\mathbf{h}_j s_j + \omega_k^H\boldsymbol{n} \tag{8.29}$$

The mean square error (MSE) of the output of MMSE filter is defined as

$$\begin{aligned}\mathrm{MMSE} &= \mathrm{E}\{|\,\tilde{s}_k - s_k\,|^2\} \\ &= \mathrm{E}\{(s_k - \omega_k^H\mathbf{r})(s_k - \omega_k^H\mathbf{r})^H\} \\ &= \omega_k^H\mathbf{R}\omega_k - \omega_k^H\mathbf{p}_k - \mathbf{p}_k^H\omega_k + 1 \\ &= 1 - \omega_k^H\mathbf{p}_k\end{aligned} \tag{8.30}$$

Therefore, we may obtain the post-processing SINR of the k-th data stream using

$$\gamma_k = \frac{1}{\mathrm{MMSE}} - 1 \tag{8.31}$$

In terms of capacity, if the channel matrix is unknown at the transmitter, the Shannon capacity is given by

$$C_k = \log_2\,[1+\gamma_k]$$

and the corresponding BuNGee specified TSB can be obtained according to

$$C_{\mathrm{TSB}}(\gamma) = \begin{cases}0, & \gamma < \gamma_0 \\ W\alpha\log_2(1+\gamma/\gamma_{\mathrm{sh}}) & \gamma_0 \le \gamma < \gamma_{\max} \\ C_{\max} & \gamma_{\max} < \gamma\end{cases} \tag{8.32}$$

where γ is the post-processing SNR. The quantity γ_0 is the lower limit on SNR, the throughput is zero when γ is lower than this threshold. The maximum achievable throughput of the system is denoted as $C_{\max}$. The scaling factor γ_{sh} is introduced to down-shift the Shannon bound to approximate the actual throughput in a real system.

8.5.2 Networked MIMO and inter-cluster interference

This subsection considers a system in the presence of interference. We suppose an MMSE filter is applied to the received signal ***r***; in this case the MMSE filter is computed as

$$\begin{aligned}\omega_{\mathrm{int},k} &= \mathbf{R}_{\mathrm{int}}^{-1}\mathbf{p}_{\mathrm{int},k} \\ &= (\mathbf{H}\mathbf{H}^H + \frac{P_{\mathrm{int}}}{N_T K_{\mathrm{int}}}\mathbf{H}_{\mathrm{int}}\mathbf{H}_{\mathrm{int}}^H + \sigma_n^2\mathbf{I})^{-1}\mathbf{h}_k \\ &= (\mathbf{H}\mathbf{H}^H + \boldsymbol{\Sigma})^{-1}\mathbf{h}_k\end{aligned} \tag{8.33}$$

where $\mathbf{R}_{\mathrm{int}} = \mathbf{H}\mathbf{H}^H + \boldsymbol{\Sigma}$ and $\mathbf{p}_{\mathrm{int},k} = \mathbf{h}_k$. The MMSE filter output in presence of interference is

$$\mathrm{MMSE}_{\mathrm{int},k} = 1 - \mathbf{h}_k^H\mathbf{R}_{\mathrm{int}}^{-1}\mathbf{h}_k = 1 - \boldsymbol{\omega}_{\mathrm{int},k}^H\mathbf{h}_k \tag{8.34}$$

The SINR is obtained as [Mad94]

$$\gamma_{\mathrm{int},k} = \frac{1}{\mathrm{MMSE}_{\mathrm{int},k}} - 1 \tag{8.35}$$

If the channel matrix is unknown at the transmitter, the Shannon capacity is given by

$$C_{\text{int},k} = \log_2[1+\gamma_{\text{int},k}] \tag{8.36}$$

the corresponding TSB can be obtained according to [Bur12] (see also section 4.2).

In terms of network MIMO, we adopt a direct forward structure where several ABSs are connected to the HBS via backhaul links. Each ABS forwards its received signal to the HBS and joint multiple user detection is performed. Since the ABSs are physically separate from each other, the fading at the receive antennas is independent. The ABSs make the received signals available to the connected HBS. With this set up, the receivers not only use the desired signal energy but also the energy from the interferers leading to much improved received SINR. Both array and diversity gains are obtained resulting in substantial increase in system capacity [Kha08]

With the previously mentioned conventional isolated MIMO systems, the spatial distance between the transmit antennas or receiver antennas are much smaller than the distance between the UE and ABS: in this scenario we may model each radio link as having the same path loss. We consider only the shadowing effect here: Rayleigh fading is modelled by the channel matrix $\mathbf{H}$. However, in the network-enabled MIMO system, the distance between UEs/ABSs are comparable to the distance between any UE and ABS pairs, therefore, the introduction of the path gain parameters $\rho_{m,d}, \rho_{m,n}, \rho_{m,o}$ are essential. They can be modeled with three terms:

$$\rho_m = \mathrm{G}_{Tx} + \mathrm{G}_{Rx} + \mathrm{PL}(d) \tag{8.37}$$

where $\mathrm{G}_{Tx}, \mathrm{G}_{Rx}$ denotes the transmit and receive antenna gains, respectively, and $\mathrm{PL}(d)$ is the path loss as a function of spatial distance d.

8.5.3 Throughput CDFs for System Level Simulations

Let us assume that the number of UEs equals the number of their serving ABSs, and each of UEs and ABSs have a single antenna. The HBS-ABS links always have sufficient capacity for the backhaul traffic. We define each UE's pre-processing SNR as the ratio of the total signal power received at all local ABS from this UE, to the noise power per ABS antenna, which is defined as follows

$$SINR_k = \mathrm{E}\left\{ \frac{\| \boldsymbol{h}_k \|^2}{No + \sum_{j \neq k} \| \boldsymbol{h}_j \|^2} \right\} \tag{8.38}$$

where No is the noise power and j indexing interfering signals from other cells. In terms of TSB, we use the following parameters: $\alpha = 0.65$, $\gamma_0 = 1.8$ dB, $\gamma_{\max} = 21$ dB, $\gamma_{sh} = 1$, $C_{\max} = 4.5$ bps/Hz. In order to obtain sum-rate throughput for system level capacity evaluation, the post-processing SINR is calculated to estimate the link TSB throughput. In a spatial multiplexing system, K data streams can be transmitted simultaneously, the sum-rate should be obtained by evaluating the throughput of each UE.

Network MIMO in the presence of interference

In this section we illustrate the uplink TSB performance and that of a cooperative multi-user system in the presence of other-cell interference. Let us assume that all terminals are equipped with uniform linear antenna arrays and Rayleigh fading is used to model the MIMO channel. Linear MMSE detection described is adopted for the receiver filter design. The number of active UEs is equal to the number of serving ABSs *M*. There may be one or more interfering data streams K_{int}.

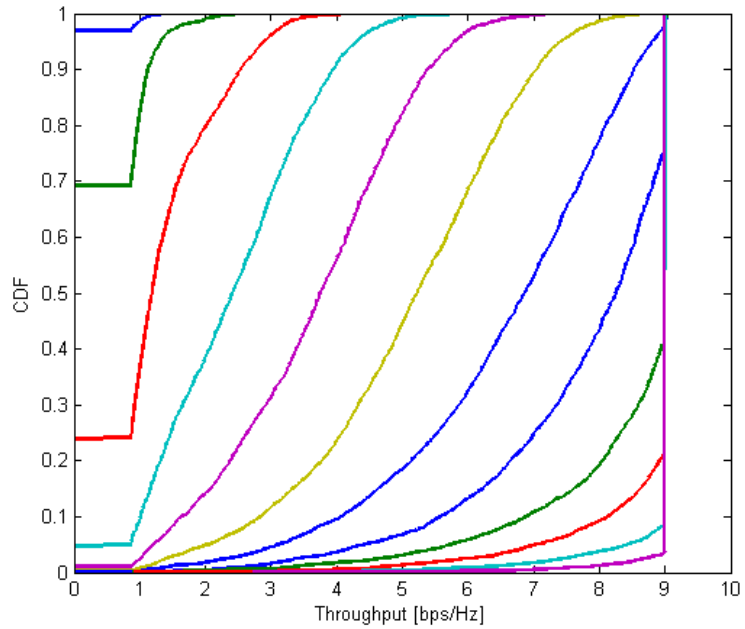

Figure 8-7 Sum-rate CDF for a Network MIMO system with 2 UEs which are served by 2 cooperative ABSs. SINR = -4:4:40 dB and INR = 10dB.

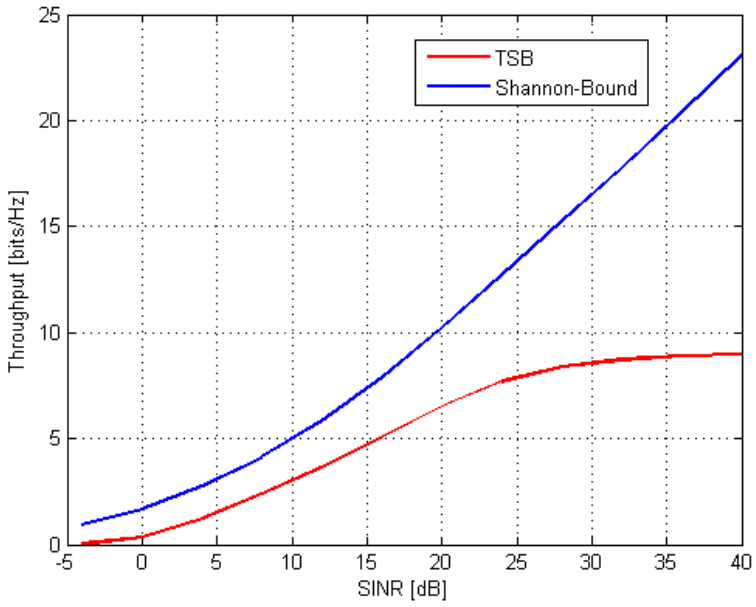

Figure 8-8 SINR vs. TSB and SB capacity for Network MIMO with 2 UEs which are served by 2 cooperative ABSs

Figure 8-7 compares the Shannon bound and truncated Shannon bound with the same MMSE post-processing SINR. The TSB introduces a maximum throughput C_{max} which restricts the throughput of each data stream. Therefore, TSB constrains the overall network throughput to 4.5 x 2 = 9 bps/Hz. The parameter α = 0.65 reduces the throughput compared to the Shannon bound in the low SINR region.

8.6 BuNGee-specific Network-enabled MIMO

In the network MIMO scenario, let us consider a group of K user equipments which are served by M cooperating ABS which are connected to a HBS via the backhaul network. Each user is served by a local ABS and several other ABSs from cooperating cells. Let us assume that the ABS-HBS backhaul links always have sufficient bandwidth to exchange information between the ABSs and HBS, that the ABSs forward the received signal to HBS, and the HBS performs joint multiuser detection.

Let us assume the UEs are perfectly synchronized and a $k \times 1$ symbol vector is formed

$$\mathbf{s} = \left[s_1, s_2, \ldots, s_K \right]^T \tag{8.39}$$

is transmitted by all K UEs simultaneously. At base station m, the received symbols r_m are given by

$$r_m = \underline{\mathbf{g}}_m \mathbf{s} + n \tag{8.40}$$

The entries of a $1 \times K$ row vector $\underline{\mathbf{g}}_m$ are the element-wise products of $\underline{\mathbf{h}}_m$ and $\underline{\rho}_m$ where $\underline{\mathbf{h}}_m = [h_{m,1}, \ldots, h_{m,k}, \ldots, h_{m,K}]$, and $\underline{\rho}_m = [\rho_{m,1}, \ldots, \rho_{m,k}, \ldots, \rho_{m,K}]$. The entry elements are the complex channel realization from the k-th user to the m-th ABS. The coefficients $\rho_{k,m}$ reflect the power gain with respect to the link between ABS m and UE k . The global complex channel realization is obtained by

$$\boldsymbol{H} = [\underline{\mathbf{h}}_1^{\,T}, \ldots, \underline{\mathbf{h}}_M^{\,T}] = \begin{bmatrix} h_{1,1} & \cdots & h_{1,K} \\ \vdots & \ddots & \vdots \\ h_{M,1} & \cdots & h_{M,K} \end{bmatrix} \tag{8.41}$$

where each element has an independent identically distribution (i.i.d). The channel power gain matrix is provided as

$$\boldsymbol{\rho} = \begin{bmatrix} \rho_{1,1} & \cdots & \rho_{1,K} \\ \vdots & \ddots & \vdots \\ \rho_{M,1} & \cdots & \rho_{M,K} \end{bmatrix} \tag{8.42}$$

where each element $\rho_{k,m}$ denotes the long-term power gain between user *k* and ABS *m*. The power loss matrix is calculated by taking into account both the receiver and transmitter antenna gains and the path loss values obtained from the WINNER II B1 and WINNER II B4 channel models. It can be defined as:

$$\rho_{m,k} = G_k + G_m - PL_{m,k} \tag{8.43}$$

where $\rho_{m,k}$ is the power loss between the entity *k* and *m*. G_k and G_m are the antenna gains of *k* and *m* respectively. $PL_{k,m}$ is the path loss between *k* and *m* that is obtained from the appropriate WINNER II channel models. Therefore, we have an effective channel gain matrix given as the element-wise product $\boldsymbol{H} \circ \boldsymbol{\rho}$ and we have:

$$\boldsymbol{G} = \boldsymbol{H} \circ \boldsymbol{\rho} = \begin{bmatrix} g_{1,1} & \cdots & g_{1,K} \\ \vdots & \ddots & \vdots \\ g_{M,1} & \cdots & g_{M,K} \end{bmatrix} \tag{8.44}$$

For user *k*, the signal collected by all M ABSs is given as

$$\begin{bmatrix} \tilde{r}_1 \\ \vdots \\ \tilde{r}_M \end{bmatrix} = \begin{bmatrix} g_{1,k} \\ \vdots \\ g_{M,k} \end{bmatrix} s_k \tag{8.45}$$

$$\tilde{\boldsymbol{r}}_k = \boldsymbol{g}_k s_k$$

where $\boldsymbol{g}_k$ is the column vector denoting the channel between user *k* and all *M* ABS. The *K* users' signals are combined at *M* ABSs with thermal noise, described as

$$\boldsymbol{r} = \sum_{K} \tilde{\boldsymbol{r}}_k + \boldsymbol{n} \tag{8.46}$$

where each element of the noise vector $\boldsymbol{n}$ is $n_m \sim \mathcal{CN}(\sigma_n^2, 0)$.

8.6.1 Power control in Network MIMO

Let us introduce the power control factor p_k for user *k*. For user *k*, the signal collected by all *M* ABSs is rewritten as

$$\tilde{\boldsymbol{r}}_k = \boldsymbol{g}_k p_k s_k \tag{8.47}$$

where s_k is the message signal with unity power. By introducing power control, the *K* users' signals are received with equal power *P* at all *M* cooperating ABSs,

$$P = \|\boldsymbol{g}_k\|^2 p_k, \quad \forall k \tag{8.48}$$

therefore, the transmitted power for each user can be obtained by

$$p_k = P/\|\boldsymbol{g}_k\|^2, \quad \forall k \tag{8.49}$$

This defines the SNR as

$$SNR = \frac{P}{\sigma_n^2} \tag{8.50}$$

The SINR for each user is given as

$$SINR = \frac{P}{P(K-1) + \sigma_n^2} \tag{8.51}$$

And the interference to noise ratio (INR) for each user is given as

$$INR = \frac{(K-1)P}{\sigma_n^2} \tag{8.52}$$

By using the power control mechanism described above, the pre-processing SNR, SINR and INR is the same for all jointly served users. The total power transmitted by all users is obtained as

$$P_{TOTAL} = \sum_{K} p_k \tag{8.53}$$

8.6.2 Joint MMSE Multiuser Signal Detection

Each ABS forwards its received signal to the connected HBS to perform joint multiuser detection. Linear detection methods recover the desired data stream from the co-channel data streams by applying a linear transformation followed by a decision of the transmitted symbol. The interference signals from the other transmit antennas are suppressed or nulled before detecting the data streams from the desired transmit antenna. In the linear multiuser detection algorithm, each symbol is estimated by a linear combination of the received signals and the filter matrix $\Omega \in \mathbb{C}^{M \times K}$.

The linear transformation is often expressed as a filter matrix and can be obtained by solving the following optimisation problem under the MMSE criterion,

$$\begin{aligned} \Omega_{\mathrm{MMSE}} &= \arg\min_{\Omega_{\mathrm{MMSE}}} \{\mathbf{s} - \Omega_{\mathrm{MMSE}}^H \mathbf{r}\} \\ &= (\mathbf{G}^H \mathbf{G} + \frac{\sigma_n^2}{\sigma_s^2} \mathbf{I})^{-1} \mathbf{G}^H \end{aligned} \tag{8.54}$$

The estimate of the transmitted vector **s** is obtained by processing the received vector **r** with the filter matrix Ω_{MMSE}, which is given by

$$\begin{aligned}\tilde{\mathbf{s}} &= \Omega_{\mathrm{MMSE}}^{H}\mathbf{r} \\ &= (\mathbf{G}^{H}\mathbf{G} + \frac{\sigma_n^2}{\sigma_s^2}\mathbf{I})^{-1}\mathbf{G}^{H}\mathbf{r} \\ &= \mathbf{s} + (\mathbf{G}^{H}\mathbf{G} + \frac{\sigma_n^2}{\sigma_s^2}\mathbf{I})^{-1}\mathbf{G}^{H}\boldsymbol{n} \\ &= \mathbf{s} + \boldsymbol{n}_{\mathrm{MMSE}}\end{aligned} \tag{8.55}$$

where $\boldsymbol{n}_{\mathrm{MMSE}}$ is the MMSE effective noise. The mean square error (MSE) of the estimates of the signal transmitted from user *k* is defined as

$$\begin{aligned}\mathrm{MMSE} &= \mathrm{E}\{|\tilde{s}_k - s_k|^2\} \\ &= \mathrm{E}\{(s_k - \boldsymbol{\omega}_k^{H}\mathbf{r})(s_k - \boldsymbol{\omega}_k^{H}\mathbf{r})^{H}\} \\ &= \boldsymbol{\omega}_k^{H}\mathbf{R}\boldsymbol{\omega}_k - \boldsymbol{\omega}_k^{H}\mathbf{p}_k - \mathbf{p}_k^{H}\boldsymbol{\omega}_k + 1 \\ &= 1 - \boldsymbol{\omega}_k^{H}\mathbf{p}_k\end{aligned} \tag{8.56}$$

Therefore, we may obtain the post-processing SINR of the k-th data stream with $\gamma_k = \frac{1}{\mathrm{MMSE}} - 1$ and the corresponding BuNGee-specific TSB can be obtained according to

$$C_{\mathrm{TSB}}(\gamma) = \begin{cases} 0, & \gamma < \gamma_0 \\ W\alpha\log_2(1+\gamma/\gamma_{\mathrm{sh}}) & \gamma_0 \le \gamma < \gamma_{\max} \\ C_{\max} & \gamma_{\max} < \gamma \end{cases} \tag{8.57}$$

where γ is the post-processing SNR. The quantity γ_0 is the lower limit on SNR: the throughput is zero when γ is lower than this threshold. The maximum achievable throughput of the system is denoted as $C_{\max}$. The scaling factor γ_{sh} is introduced to down-shift the Shannon bound to approximate the actual throughput in a real system.

8.6.3 Frequency Planning

By separating the available bandwidth into several channels, for a cellular system, a frequency planning strategy can be applied to reduce the interference from adjacent cells. The channel between the *k*-th user and the *M* ABSs is given as

$$\boldsymbol{g}_k = \begin{bmatrix} g_{k,1} \\ \vdots \\ g_{k,M} \end{bmatrix} \tag{8.58}$$

The strongest link to user *k* can be obtained using

$$m^k{}_{\max} = \arg\max |g_{k,m}|^2 \tag{8.59}$$

Each user *k* is then assign to the ABS with the strongest link $m^k{}_{\max}$. The operating frequency for each ABS is assigned according to the frequency planning strategy, a Manhattan-grid environment is applied in this scenario, and the square topology is applied as in Figure 8-9. ABSs located at the top and bottom of the cell are designed to serve North to South streets, and ABSs on the left and right serve the East to West streets. The two ABS beams pointing in opposite directions use two different channels to prevent from interference.

For user *k*, the SINR at the receiver side is given as

$$SINR = \frac{p_k \mid g_{k,m_{\max}} \mid^2}{p_k \sum_{j \neq k,\, j \subset FP} \mid g_{k,m_{\max}} \mid^2 + \sigma_n^2} \tag{8.60}$$

where *j* denotes interfering users operating in the same frequency band as the desired user *k*. The users assigned to the same frequency band suffer from the interference from one another.

8.7 Simulation

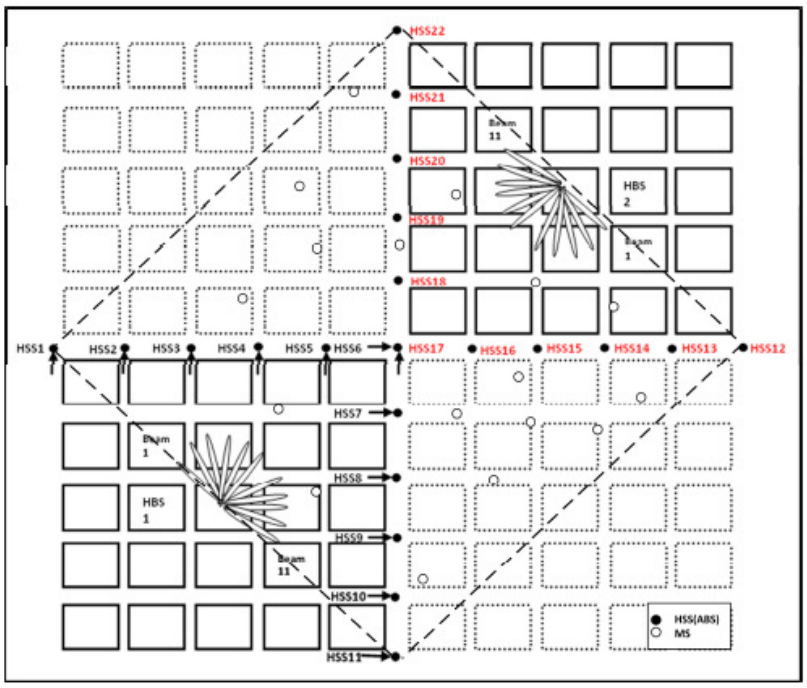

Figure 8-9 Service area and locations of ABSs.

This simulation is carried to compare the systems using network-enabled MIMO and the frequency planning strategy used in BuNGee, where 22 users which are served by 22 ABSs in the service area. The service area is detailed as the dashed square obtained by connecting ASS1, ASS12, ASS11 and ASS22 in Figure 8-9. The 22 users are randomly distributed within the square. The simulation takes into account the indoor users as well as the users on the streets. The throughput of users are compared by measuring the BuNGee defined TSB uplink throughput for each user in terms of different transmit power values. TDD duplexing is used in the simulation to compare the averaged user throughput of networked-MIMO and frequency planned cellular system. A 50%-50% split is assumed for the downlink and uplink. We have 20MHz bandwidth for the access link in total. By using network MIMO, all 22 co-channel users share the same 20MHz bandwidth, which significantly increases the system spectral efficiency. On the other hand, four 5 MHz channels are utilized in the access link in the frequency planning scheme, and there are 4 frequency bands provided to group the 22 users into 4 channels. The interference within each channel is generally lower compared with 100% frequency reuse schemes.

In the simulation of network MIMO, the users are evenly located across the service area and share the same 20 MHz bandwidth; the random location of users also tests the fairness of the throughput distribution among users. The received signal is forwarded to the HBS to perform MMSE joint multiuser detection. In this simulation, we assume the ABS to HBS links have unlimited bandwidth; for more realistic analysis, this assumption can be replaced by introducing quantization noise to the received signal at each ABSs. We select frequency planning as the baseline scheme for comparison with the network-enable MIMO scheme, the frequency planning is designated in terms of streets. The ABSs located along the horizontal line (connecting ABS1 to ABS12) serve North to South streets while the ABSs located along the vertical line

(ABS11 to ABS22) serve East to West streets. All the odd indexed ABSs for horizontal streets share frequency f1, while the even indexed ABSs for horizontal streets share frequency f2. Similarly all odd indexed ABSs for vertical streets share frequency f3, and even indexed ABSs for vertical streets share frequency f4. Each frequency band has 5 MHz bandwidth. This reduces interference at the ABS receivers.

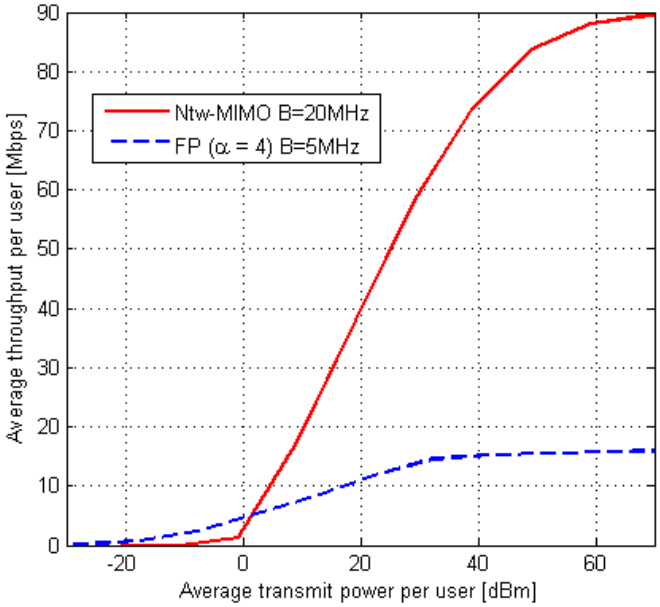

Figure 8-10 Throughput comparison

Figure 8-10 compares the average throughput per user with Network MIMO and frequency planning. The average throughput of network MIMO benefits from two effects, firstly the bandwidth, where every user shares 20MHz instead of 5MHz, and secondly spectrum efficiency which is compared in Figure 8-11. All the CDF curves in Figure 8-11 are obtained by assuming each user has an average transmit power of 32dBm. The CDFs are obtained by using 3000 channel samples across all 22 users in the service area. The users are randomly distributed and MMSE joint detection is used at the HBS. The throughput CDFs are calculated using the TSB with the post-processing SINR given by MMSE detection. Network MIMO has the ability to exploit the space resource to improve the spectrum efficiency compared with the frequency planned system by about 1 bps/Hz when each MS has a averaged transmit power equal to 32dBm.

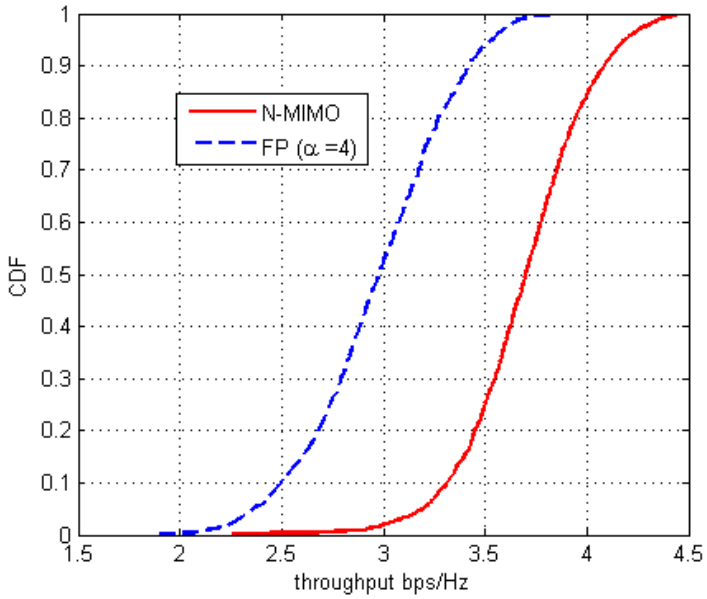

Figure 8-11 Spectrum efficiency vs. CDFs

In system simulator, there is a much larger number of users operating in the service area (eg. 1500 users according to Deliverable 4.1.2.) In this scenario, we may divide the 1500 users into z={1500/22} groups and orthogonal multiple access techniques can be used to separate these groups.

9. Backhaul link optimization for the communication between two ABSs with arbitrary inputs

9.1 Introduction

In the architecture considered in the BuNGee project, optimizing the rates that can be achieved in the HBS-ABS link (backhaul link) is of paramount importance. Although the primary use of the backhaul link is to forward information from the HBS to the MSs (or vice versa), the amount of control information and CSI that is to be exchanged between ABSs cannot be neglected as it may constitute an important amount of the total data (e.g., in collaborative MIMO the CSI of the link between ABSs and MSs needs to be exchanged among the ABSs very frequently due to the time varying nature of the ABS-MS links). It must be highlighted that the result of optimizing the rates at which ABSs can interchange information may have two different practical outcomes: either, given a fixed fraction of the total time that is assigned to control/CSI data, the amount of control/CSI data is maximized or, for a fixed desired amount of control/CSI data to be exchanged, the fraction of time devoted to this type of transmission is minimized (and, thus, the time used for user data transmission/reception is maximized).

The main particularity of the communication between two ABSs is that there is no direct link between them and, thus, the communication has to be performed via the HBS (that is why, for this particular mode of communication, it is said that the HBS acts as a relay). Consequently, in this section we focus our attention on the communication scenario between two ABSs, where each ABS has a message to be delivered to the other ABS and where the connection between ABSs is established through the HBS (see Figure 9-1 where the studied communication scenario is depicted: each ABS has a message to be delivered to the other ABS. In the first transmission phase, both ABSs communicate their messages to the HBS. In the second phase, the HBS transmits a unique signal (which is a function of the two messages) so that each ABS can decode its own corresponding message). The capacity region of this two-way relay channel is open; however, there has been a considerable recent interest in developing novel achievability techniques and tight outer bounds for this model due to its practical relevance. Several achievability schemes have been proposed in the literature based on the type of coding used and the operation at the HBS. The classical amplify-and-forward and decode-and-forward (DF) schemes have been extended to this scenario in [Ran05]. The more advanced compress-and-forward (CF) scheme is considered in [Gun08] and [Sch08] while structured codes, rather than random coding, have been proposed in [Nar07], [Bai08]. Recently, the capacity of the Gaussian two-way relay channel has been computed to within 1/2 bit in [Nam10].

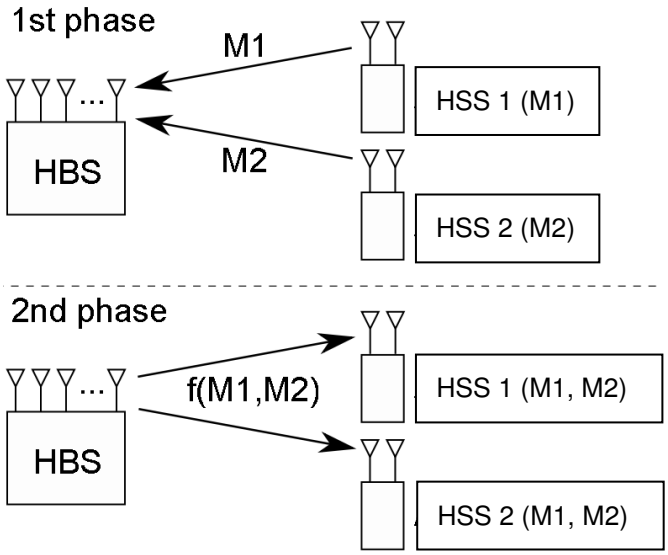

Figure 9-1: Illustration of the two-way relay channel model in which an HBS acts as a relay terminal helping two separate ABS exchange messages simultaneously.

While no single scheme dominates the others in all channel conditions, schemes based on CF relaying or structured codes are more complicated when it comes to practical applications as they require the use of joint source-channel coding for the broadcasting of the HBS's received signal, which, at the time being, is not a practical assumption for the BuNGee architecture. Hence, our focus here is on the DF strategy, in which both messages of the ABSs are decoded at the HBS, before being forwarded to their respective recipients. Hence, as depicted in Figure 9-1, the transmission can be divided into two phases, the first one is a multiple access channel from the ABSs to the HBS, and the second stage is a special broadcast channel, in which each receiver has access to the message that is to be decoded by the other receiver.

In this section, we explicitly focus on the second stage of the transmission, i.e., the broadcast phase. It can be seen, using the result of [Tun06], that, in the case of Gaussian channels, the HBS can transmit simultaneously to both ABSs at the capacity of each channel, as if each ABS is the sole receiver in the system. In a way, the transmissions to the ABSs do not interfere with each other. This is due to the fact that the interfering message is already known at the receiver, and each ABS receives at a rate as if she is the sole receiver. This can be achieved by transmitting a modulo sum of the coded bits from the HBS rather than superimposing the signals or time-sharing between the messages. This can be considered as an analog network coding strategy.

In this section we focus on the achievable rate region over the above described two-way relay channel, i.e., the set of information rate pairs at which the two ABSs can exchange information simultaneously. We study the problem of optimal power allocation to identify the region of achievable rate pairs for the case where the channel between the HBS and ABSs can be modeled as a set of parallel channels. Observe that this model is motivated by the following reasoning. In the BuNGee architecture, both the HBS and ABS are employing multiple antennas and, thus, a MIMO channel is created between them, which, assuming that the HBS performs spatial multiplexing and the ABSs are equipped with SIC receivers, can be modeled as a set of parallel spatial channels.

In the studied case of independent parallel channels, the mutual information to each ABS is maximized by a Gaussian input; however, the optimal power allocation among the subchannels is not a direct extension of the classical waterfilling solution which achieves the highest mutual information for a given power constraint [Cov06]. Here our focus is on practical applications that can be implemented in the BuNGee architecture, and hence, we allow arbitrary input constellations at the HBS input rather than simply focusing on the case of Gaussian input distributions. Our goal is to find the optimal power allocation strategy that achieves a specific point on the boundary of the achievable rate region with DF relaying over independent parallel Gaussian channels with arbitrary input constellations.

9.2 System model and problem statement

As pointed out in the introduction, the MIMO channel between the HBS and the two ABSs is modeled as n parallel broadcast channels (see Figure 9-2). The input-output relationship of the i th channel from the HBS to the k th ABSs, $k = 1, 2$, is

$$Y_{k,i} = h_{k,i} X_i + W_{k,i}, \tag{9.1}$$

where X_i is the HBS transmitted signal at the i th channel, $W_{k,i}$ is a zero-mean unit variance complex Gaussian random variable independent of the noise at the other ABS or at the other channels, and $h_{k,i}$ is the complex channel coefficient.

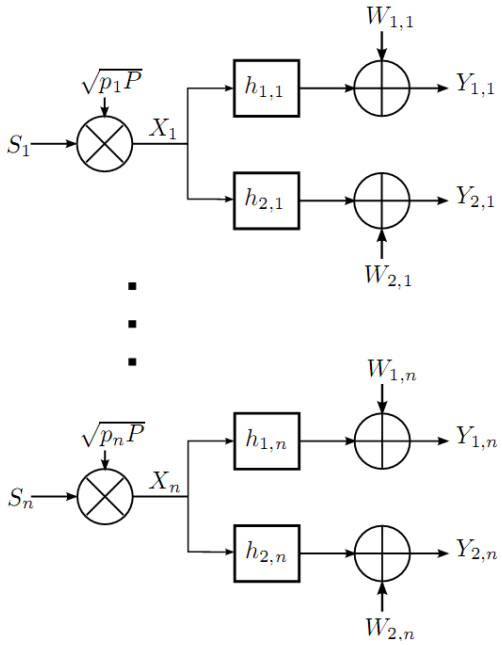

Figure 9-2: Bidirectional broadcast channel with n parallel channels

We assume that the two ABSs perfectly know their own channel coefficient, while the HBS knows the magnitudes of the channel coefficients to both receivers, which is a reasonable assumption since, in the BuNGee architecture, the link between the HBS and the ABSs is static.

The transmission power at the HBS is constrained by

$$\sum_{i=1}^{n} E[|X_i|^2] \le P. \tag{9.2}$$

Then, the transmitted signal X_i can be expressed as a scaled version of a unit-power zero-mean arbitrarily distributed input signal S_i according to

$$X_i = \sqrt{p_i P} S_i, \tag{9.3}$$

where p_i allocates the power among the channels satisfying

$$\sum_{i=1}^{n} p_i \le 1. \tag{9.4}$$

Now, defining the normalized mutual information $I_i(\rho)$ as

$$I_i(\rho) = I(S_i; \sqrt{\rho} S_i + W), \tag{9.5}$$

the mutual information between the i th input signal, S_i, and the i th output of ABS k is simply given by

$$I(S_i; Y_{k,i}) = I_i(|h_{k,i}|^2 \; p_i P). \tag{9.6}$$

Now the goal is to maximize a weighted average of the information flow to each ABS:

$$\sum_{k=1}^{2} \sum_{i=1}^{n} \alpha_k I(S_i; Y_{k,i}) = \sum_{k=1}^{2} \sum_{i=1}^{n} \alpha_k I_i(|h_{k,i}|^2 \; p_i P), \tag{9.7}$$

where $\alpha_1, \alpha_2 \geq 0$ and $\alpha_1 + \alpha_2 = 1$.

With this formulation, we can characterize the whole rate region by considering all possible weight pairs. For a fixed weight pair (α_1, α_2), the optimal power allocation problem can be expressed as follows

$$\max_{\{p_i\}} \quad \sum_{k=1}^{2} \sum_{i=1}^{n} \alpha_k I_i(p_i \gamma_{k,i}) \tag{9.8}$$

$$s.t. \quad p_1, \ldots, p_n \geq 0 \tag{9.9}$$

$$\sum_{i=1}^{n} p_i = 1, \tag{9.10}$$

where we defined the received signal-to-noise ratio of ABS k on channel i as $\gamma_{k,i}$, i.e., $\gamma_{k,i} P |h_{k,i}|^2$ and where we have written the inequality constraint in (9.4) as an equality in (9.10) as the optimal $\{p_i\}$ will make use of all available power.

9.3 Optimal power allocation

9.3.1 Preliminaries

In order to study and solve the optimization problem in (9.8-10), we will make use of the results that stem from the relation between the minimum mean-square error (MMSE) and the mutual information, [Guo05], [Pay09b]. Consequently, we will now briefly review them.

Consider the generic scalar Gaussian channel $Y = \sqrt{\rho} S_i + W$. Given an observation of the channel output y, the MMSE estimation of S_i is given by the conditional mean

$$\hat{S}_i(\rho, y) = E[S_i \mid y = \sqrt{\rho} S_i + W], \tag{9.11}$$

where we have explicitly indicated the dependence of $\hat{S}_i$ on the channel coefficient ρ and the channel output y. For the sake of notation, this dependence will be dropped in the following.

We now define the following two quantities

$$\Phi_i(\rho, y) = E[|S_i - \hat{S}_i|^2 | \, y], \tag{9.12}$$

$$\overline{\Phi}_i(\rho, y) = E[(S_i - \hat{S}_i)^2 \mid y]. \tag{9.13}$$

It is straightforward to check that the corresponding mean-square error of the estimation in (9.11) is given by

$$MMSE_i(\rho) = E[\Phi_i(\rho, y)], \tag{9.14}$$

where the expectation is with respect to the statistics of the channel output y. Note that $MMSE_i(\rho) \in [0,1]$ due to the unit power assumption on S_i.

Now we can recall the result, which will be instrumental in solving the optimal power allocation problem for non-Gaussian channel input distributions.

Lemma 1. For any input distribution of S_i we have

$$\dot{I}_i(\rho) = E[\Phi_i(\rho, y)] = MMSE_i(\rho), \tag{9.15}$$

$$\ddot{I}_i(\rho) = -E[(\Phi_i(\rho, y))^2 + |\overline{\Phi}_i(\rho, y)|^2], \tag{9.16}$$

where we have used $\dot{f}(\rho) = df(\rho)/d\rho$.

Proof. Equation (9.15) is derived in [Guo05] and (9.16), in [Pay09b].

Corollary 2. For the particular case of low power ($\rho = 0$), the derivatives of the mutual information in Lemma 1 read as

$$\dot{I}_i(0) = \dot{I}(0) = 1, \tag{9.17}$$

$$\ddot{I}_i(0) = -(E[|S_i|^2])^2 - |E[S_i^2]|^2 \tag{9.18}$$

$$= -1 - |E[S_i^2]|^2 . \tag{9.19}$$

Proof. The proof follows from Lemma 1 and by noting that $\hat{S}_i(0, y) = E[S_i] = 0$, $\forall y$. In (9.17) and (9.19) we have used the unit power assumption for S_i, $E[|S_i|^2] = 1$. It must be highlighted that the first derivative in (9.17) is a constant value and that the value of the second derivative in (9.18), which can be easily computed, depends only on the distribution of the input S_i.

Proper complex constellations (i.e., those that are quadrature symmetric, such as QPSK, 8-PSK or 16-QAM) fulfill $E[S_i^2] = 0$, as given in [Nee93], which, from Corollary 2 implies that $\ddot{I}_i^{\text{proper}}(0) = -1$. Alternatively, for real valued constellations (for example BPSK and m-PAM) we have that $E[S_i^2] = E[|S_i|^2] = 1$ and, thus, $\ddot{I}_i^{\text{real}}(0) = -2$. Observe that both cases agree with the results given in [Ver02]. Since $E[|S_i|^2] \geq |E[S_i^2]|$, for general (not necessarily proper) complex input distributions we will thus have

$$-2 \leq \ddot{I}_i(0) \leq -1. \tag{9.20}$$

9.3.2 Problem solution

We are now ready to solve the problem stated in (9.8-10). First, we equivalently put it into the standard minimization form

$$\min_{\{p_i\}} \quad -\sum_{k=1}^{2}\sum_{i=1}^{n} \alpha_k I_i(p_i\gamma_{k,i}) \tag{9.21}$$

$$s.t. \quad -p_i \le 0, \quad i \in [1,n] \tag{9.22}$$

$$\sum_{i=1}^{n} p_i - 1 = 0. \tag{9.23}$$

From (9.16), it can be easily seen that the mutual information is a concave function, $\ddot{I}_i(\rho) < 0$, $\forall \rho$, which, together with the fact that the constraints in (9.22) and (9.23) are linear, implies that (9.21-23) is a convex optimization problem [Boy04].

Introducing the Lagrange multipliers λ_i for the inequality constraints on each power p_i in (9.22) and η for the equality constraint on the sum power in (9.23), the Karush-Kuhn-Tucker conditions give us necessary and sufficient conditions for the optimal power allocation, which is denoted by $\{p_i\}$, as

$$-p_i \le 0, i \in [1,n], \tag{9.24}$$

$$\sum_{i=1}^{n} p_i - 1 = 0, \tag{9.25}$$

$$\lambda_i \ge 0, i \in [1,n], \tag{9.26}$$

$$-\lambda_i p_i = 0, i \in [1,n], \tag{9.27}$$

$$\sum_{k=1}^{2} \alpha_k \gamma_{k,i} MMSE_i(p_i \gamma_{k,i}) + \lambda_i - \eta = 0, i \in [1,n]. \tag{9.28}$$

Here, λ_i's act as slack variables and, thus, can be eliminated. The remaining following conditions can be rewritten as

$$p_i \left[\eta - \sum_{k=1}^{2} \alpha_k \gamma_{k,i} MMSE_i(p_i \gamma_{k,i}) \right] = 0, i \in [1,n], \tag{9.29}$$

$$\sum_{i=1}^{n} p_i - 1 = 0, \tag{9.30}$$

$$-p_i \le 0, i \in [1,n], \tag{9.31}$$

$$\sum_{k=1}^{2} \alpha_k \gamma_{k,i} MMSE_i(p_i \gamma_{k,i}) - \eta \le 0, i \in [1,n]. \tag{9.32}$$

Unfortunately, the optimal power allocation policy for this problem cannot be expressed in a simpler closed-form using a threshold value as in the case of waterfilling or mercury/waterfilling [Loz06]. This is true even in the case of Gaussian inputs. Hence, we are not able to provide an intuitive graphical interpretation for the optimal power allocation in the general case and, rather, provide numerical results. Nonetheless, in the special cases of low and high power regimes, the MMSE function can be approximated using a series expansion and closed form solutions for the optimal power allocation exist as shown in the following two sections.

9.4 Low power regime

Using a first order Taylor expansion and applying Corollary 2, the low power behavior of the MMSE function is given by

$$MMSE_i(\rho) = \dot{I}_i(0) + \ddot{I}_i(0)\rho + O(\rho^2) \tag{9.33}$$

$$= 1 + \ddot{I}_i(0)\rho + O(\rho^2), \tag{9.34}$$

similarly as it was done in [Pay09b], [Loz06], [Guo08]. We recall that, $\ddot{I}_i(0)$ is a constant value that depends only on the input distribution used in the i th channel (see (9.19)).

With the approximation in (9.34), the optimal power allocation $\{p_i\}$ that solves (9.21-23) can be put into the simpler form

$$\begin{aligned} p_i &= 0, \quad \text{if } \gamma_i^w \le \eta, \\ \gamma_i^w + \ddot{I}_i(0)\, p_i\, (\alpha_1\gamma_{1,i}^2 + \alpha_2\gamma_{2,i}^2) &= \eta, \quad \text{if } \gamma_i^w > \eta, \end{aligned} \tag{9.35}$$

where γ_i^w denotes the weighted channel quality defined as

$$\gamma_i^w \alpha_1\gamma_{1,i} + \alpha_2\gamma_{2,i} = P(\alpha_1 |h_{1,i}|^2 + \alpha_2 |h_{2,i}|^2). \tag{9.36}$$

In the case of a single receiver, as studied in [Loz06], the optimal policy in the asymptotic low power regime is to allocate all the power to the channel with the highest coefficient. If there are multiple channels with the strongest channel coefficient, then the power is allocated equally among them in the case of Gaussian inputs (waterfilling), or inversely proportional to the second derivative of the mutual information at zero power in the case of constrained input constellations.

A similar argument applies to the two-way relay channel model studied here as well. However, in our case we compare the weighted averages of the channel strengths of the two ABSs as in (9.36) to determine the channel (or channels) to which positive power is allocated. All the power is allocated to the channel with the highest value for $\alpha_1 |h_{1,i}|^2 + \alpha_2 |h_{2,i}|^2$. If multiple channels have the same maximum value, indexed by $i \in M$, then the power is divided as

$$\begin{aligned} p_i &= \frac{\theta}{\ddot{I}_i(0)}, \quad i \in M, \\ p_i &= 0, \quad i \notin M, \end{aligned} \tag{9.37}$$

with $\theta = (\sum_{i\in M} (\ddot{I}_i(0))^{-1})^{-1}$ being the normalization factor such that $\sum_{i=1}^{n} p_i = 1$.

Note that the channels to which non-zero power is allocated depend on the objective function, i.e., α_1 and α_2. Hence, different channels can be chosen for different operating points on the boundary of the rate region. Once the channels for which the power is to be allocated are chosen, the power allocation is the same as in the case of a single receiver, and depends only on the constellation used in those channels.

9.5 High power regime

In the limit of high power, $MMSE_i(\rho)$, in the case of Gaussian inputs, expands as [Loz06]

$$MMSE_i^G(\rho) = \frac{1}{\rho} + O(1/\rho^2).$$

Plugging this expansion in the KKT conditions in (9.29-32), we can see that the optimal power allocation behaves as

$$p_i^G \doteq \frac{1}{n} + O(1/P),$$

which is the same behavior as in the case of a single receiver: for Gaussian inputs, in the high power regime, power is allocated uniformly among the channels.

In the case of discrete m -ary constellations, the high power behavior of $MMSE_i(\rho)$ depends on the minimum distance, d_i, between any two points of the constellation used in i th channel. Then $MMSE_i(\rho)$ decays exponentially as [Loz06]

$$MMSE_i(\rho) = K_i(\rho)\exp\left(-\frac{d_i^2}{4}\rho\right), \tag{9.38}$$

with $O(1/\sqrt{\rho}) \le K_i(\rho) \le C_i$, where C_i is a constant value.

It can be shown that, in the high power regime, power is allocated to all the channels, i.e., $p_i \doteq 0$, $\forall i$, which further implies that the condition in (9.32) is fulfilled with equality. With this result and plugging (9.38) into (9.32) we obtain

$$\sum_{k=1}^{2} \alpha_k \gamma_{k,i} K_i(p_i \gamma_{k,i}) \exp\left(-\frac{d_i^2}{4} p_i \gamma_{k,i}\right) = \eta, \quad \forall i. \tag{9.39}$$

It is now easy to see that, as $P \to \infty$ and with $\alpha_1, \alpha_2 > 0$, the term with the smallest $\gamma_{k,i}$ dominates the sum in (9.39) obtaining, thus, the new condition, $\forall i$,

$$\alpha_{k_{\min}^{(i)}} \gamma_{k_{\min}^{(i)},i} K_i(p_i \gamma_{k_{\min}^{(i)},i}) \exp\left(-\frac{d_i^2}{4} p_i \gamma_{k_{\min}^{(i)},i}\right) = \eta, \tag{9.40}$$

where we have used $k_{\min}^{(i)} = \operatorname{argmin}_k \{\gamma_{k,i}\}$. Observe that, if either $\alpha_1 = 0$ or $\alpha_2 = 0$, one of the terms in the summation in (9.39) disappears obtaining a similar expression as in (9.40).

We now apply the similar operations as in [Loz06] to the expression in (9.40) and we obtain the optimal power allocation in the high power regime with discrete constellations:

$$p_i \doteq \frac{\theta}{d_i^2 \min_k |h_{k,i}|^2} + O\left(\frac{\log P}{P}\right), \tag{9.41}$$

with $\theta = (\sum_{i=1}^{n} (d_i^2 \min_k |h_{k,i}|^2)^{-1})^{-1}$.

Observe that the expression in (9.41) has been obtained assuming that both α_1 and α_2 are different from 0. Interestingly, under this assumption, the expression for the optimal power allocation in the high power regime in (9.41) is independent of the actual values of α_1 and α_2.

However, for the case where one of the α_k is equal to zero, the expression in (9.41) is no longer valid and is replaced by

$$p_i \doteq \frac{\theta}{d_i^2 |h_{\bar{k},i}|^2} + O\left(\frac{\log P}{P}\right), \tag{9.42}$$

where $\bar{k}$ is such that $\alpha_{\bar{k}} > 0$. Note that (9.42) agrees with [Loz06].

9.6 Simulations

Firstly, we consider the case with $n = 3$ parallel channels with the following channel coefficients

$$|h_{1,1}|^2 = 2, |h_{1,2}|^2 = 1.2, |h_{1,3}|^2 = 0.2, \quad (9.43)$$

$$|h_{2,1}|^2 = 0.8, |h_{2,2}|^2 = 3, |h_{2,3}|^2 = 1.2, \quad (9.44)$$

and we assume that the input to each channel is from a QPSK constellation. Observe that, in the simulations section, we have assigned numerical values to the channel coefficients that are greater than one. It is important to recall that, in practical scenarios, the channel coefficients are always lower than one because they represent the path-loss. However, for the sake of simplicity, in this section we have skipped this restriction as the path-loss can always be incorporated in the transmitted power constraint or in the noise power. For this scenario, we study the evolution of $\{p_i\}_{i=1}^{i=3}$ as a function of the available power, P, and for different choices of α_k. The corresponding $\{p_i\}_{i=1}^{i=3}$ are plotted in Figure 9-3, Figure 9-4, and Figure 9-5 together with the limiting distribution obtained when $P \to \infty$, given by (9.41). In Figure 9-3 and Figure 9-4, it can be seen that the limiting distribution for the power allocation does not depend on the specific values of α_k as long as both of them are nonzero. Precisely, in Figure 9-3, we have that $\alpha_1 = \alpha_2 = 0.5$. This implies that $\gamma_1^w = 1.4P$, $\gamma_2^w = 2.1P$, and $\gamma_3^w = 0.7P$, which means that, in the low power regime, all the power is allocated to channel 2. The limiting distribution as $P \to \infty$ is given by $p_1 \approx 0.18$, $p_2 \approx 0.12$, and $p_3 \approx 0.7$. In Figure 9-4 we have $\alpha_1 = 0.1$ and $\alpha_2 = 0.9$. This implies that $\gamma_1^w = 0.9P$, $\gamma_2^w = 2.8P$, and $\gamma_3^w = 1.1P$, which means that, in the low power regime, all power is allocated to channel 2. Observe that the limiting power allocation is the same as in Figure 9-3.

It can also be observed that, whenever we have that $\alpha_k = 0$, the limiting distribution changes as it is now given by (9.42). See, for example, Figure 9-5, where we have $\alpha_1 = 1$ and $\alpha_2 = 0$. This further implies that $\gamma_1^w = 2P$, $\gamma_2^w = 1.2P$, and $\gamma_3^w = 0.2P$, which means that, in the low power regime, all the power is allocated to channel 1. Observe that the limiting power allocation ($p_1 \approx 0.08$, $p_2 \approx 0.12$, and $p_3 \approx 0.8$) is different than in Figure 9-3 and Figure 9-4 as we now have $\alpha_2 = 0$.

Finally, also from Figure 9-3, Figure 9-4, and Figure 9-5, it is also clear that, as $P \to 0$ all the power is allocated to the channel with highest $\gamma_i^w = P(\alpha_1 |h_{1,i}|^2 + \alpha_2 |h_{2,i}|^2)$, which, for this particular case, corresponds to channel 2 in Figure 9-3 and Figure 9-4 and to channel 1 in Figure 9-5

Secondly, we consider the following two configurations:

$$|h_{1,1}|^2 = 4, |h_{1,2}|^2 = 0.1, |h_{1,3}|^2 = 0.1, \quad (9.45)$$

$$|h_{2,1}|^2 = 2.1, |h_{2,2}|^2 = 1.9, |h_{2,3}|^2 = 0.1, \quad (9.46)$$

which will be referred to as *balanced* configuration because the best channel for the two ABSs is the same (channel 1), and

$$|h_{1,1}|^2 = 0.1, |h_{1,2}|^2 = 0.1, |h_{1,3}|^2 = 4, \quad (9.47)$$

$$|h_{2,1}|^2 = 2.1, |h_{2,2}|^2 = 1.9, |h_{2,3}|^2 = 0.1, \quad (9.48)$$

which will be referred to as *unbalanced* configuration because the best channels for the two ABSs are different (channel 3 for ABS 1 and channel 1 for ABS 2). Observe that the only difference between the two channels is that, in the unbalanced case, the values of $|h_{1,1}|^2$ and $|h_{1,3}|^2$ are swapped.

For the unbalanced configuration, we plot, in Figure 9-6, the achievable rate regions for the case of Gaussian and QPSK inputs and for different P values. It can be observed that, as P increases, the Gaussian rate region is always larger and grows faster than the QPSK region. Moreover, it can be observed that as $P \to \infty$ the QPSK region saturates as the mutual information with an input with 3 QPSK constellations is upper bounded by $\log 2^6 \approx 4.16$ nat. At low power, both regions coincide providing yet another evidence of the excellent performance of QPSK in the low power regime.

In Figure 9-7, we compare the achievable rate regions for the balanced and unbalanced configurations. It can be seen that the unbalanced region is always included inside the balanced region. Moreover, it must be highlighted that the borders of both regions coincide near the axes because this situation corresponds to the case where the information flow to only one of the ABSs is maximized, thus, the achievable rate is a function of the channel coefficients of that ABSs, independently of the order of these channels (since the input is QPSK for all the channels).

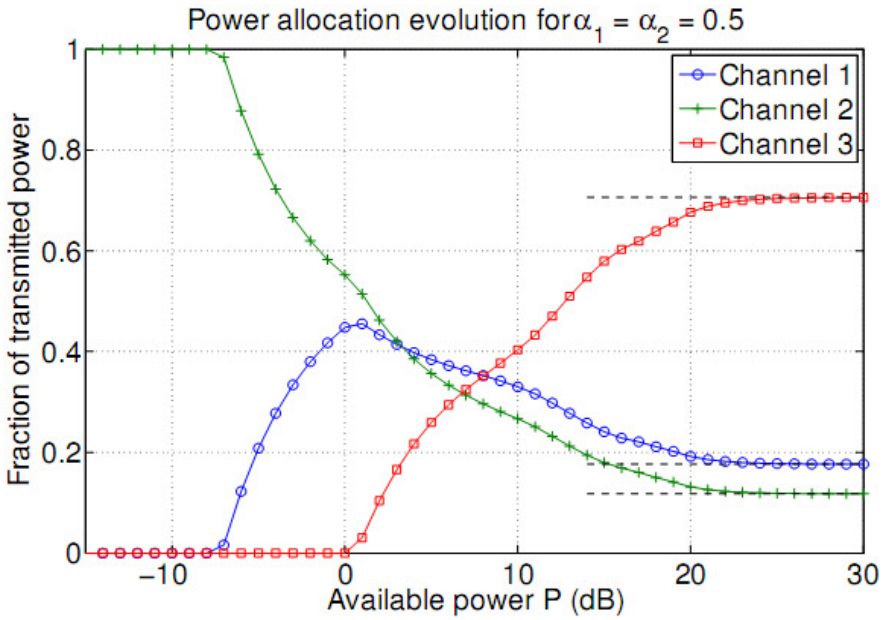

***Figure 9-3**: Power allocation evolution as a function of the total available power – Configuration 1.*

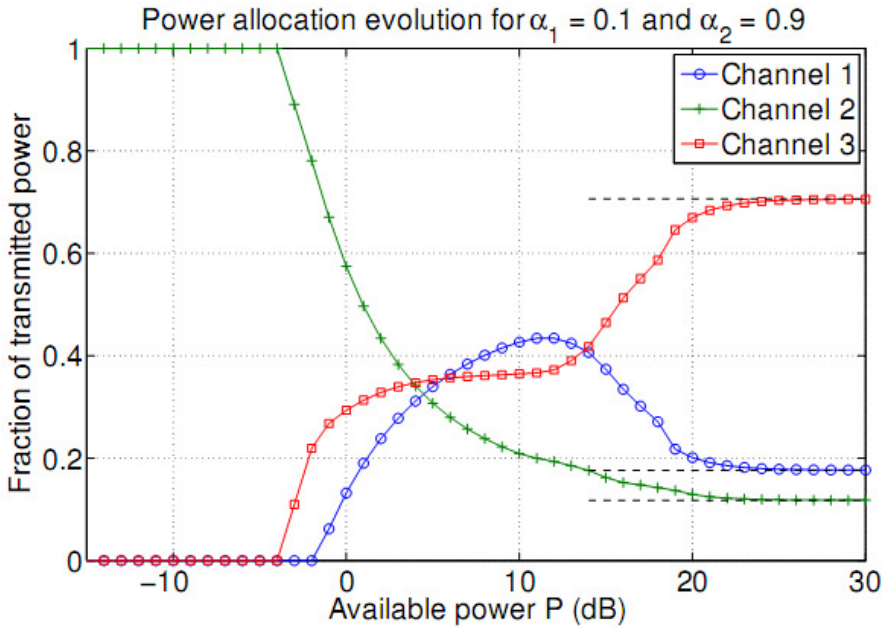

Figure 9-4*: *Power allocation evolution as a function of the total available power – Configuration 2.

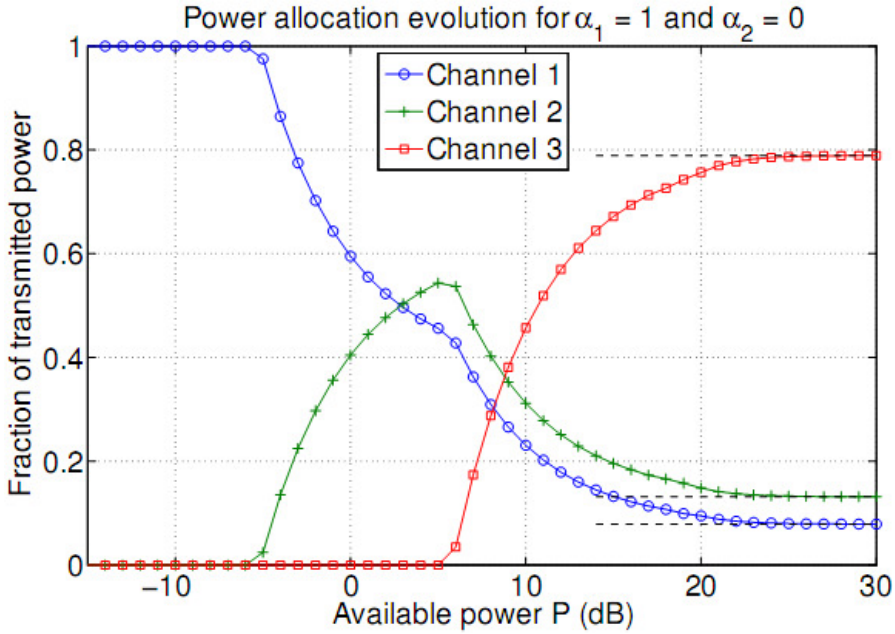

Figure 9-5: Power allocation evolution as a function of the total available power – Configuration 3.

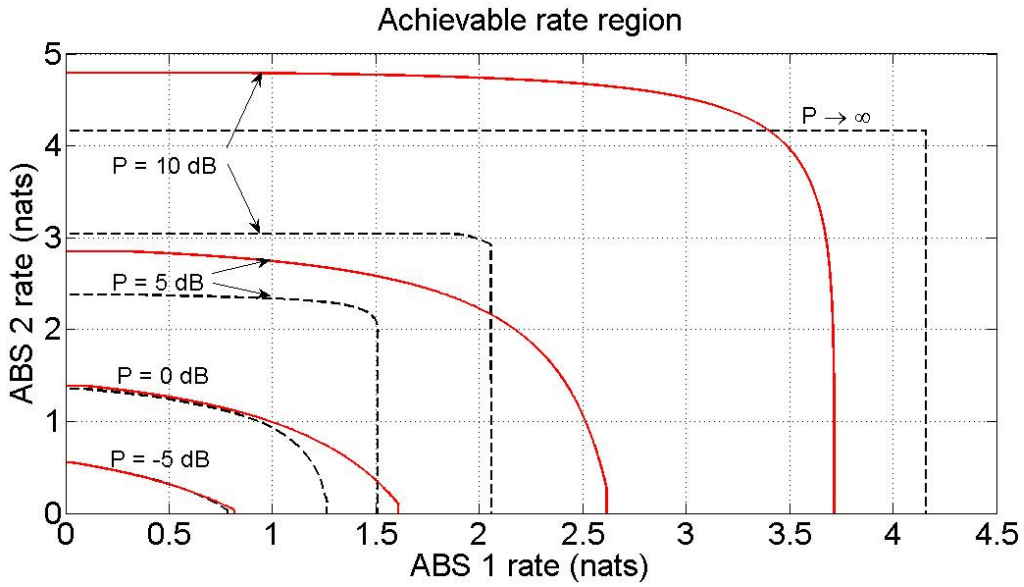

Figure 9-6: Achievable rate region for different input distributions.

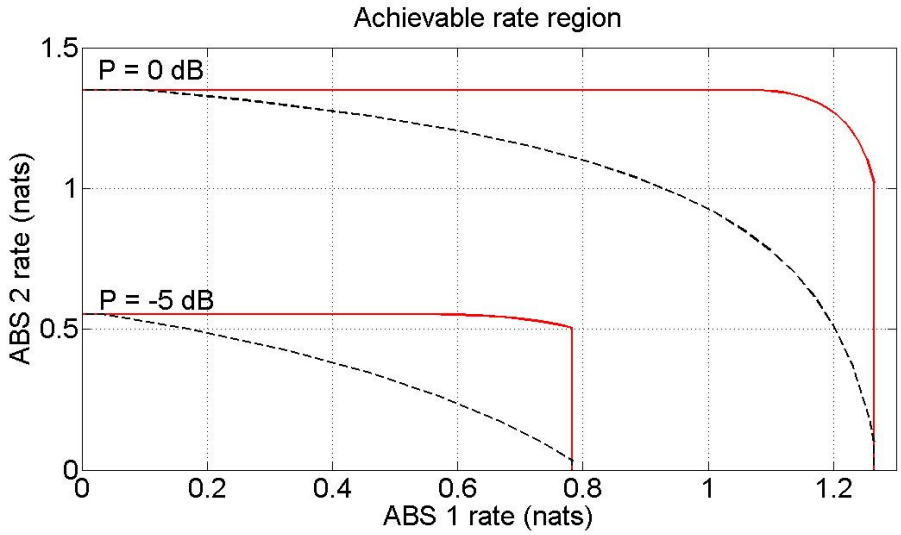

***Figure 9-7*: Comparison of the achievable rate region in the balanced (red, solid) and unbalanced (black, dashed) cases.**

9.7 Conclusion

We have studied the optimal power allocation policy at the HBS to achieve the boundary points of the rate region to the two ABSs by considering arbitrary input constellations, which is a constraint that will always be encountered in practice. We have identified the necessary and sufficient conditions for the optimal power allocation policy and provided numerical solutions. Unfortunately, the well-known waterfilling or mercury/waterfilling interpretations do not apply in this setup due to the weighting in the objective function. As solutions which require low computational complexity, we have also considered the low and the high power regimes. In the low power regime, all the power is allocated to the channels with the highest weighted channel quality, whereas in the high power regime, the power is allocated uniformly in the case of Gaussian inputs, and according to the minimum distances and the minimum of the channel qualities in the case of discrete constellations.

Finally, it is important to highlight that, in this section, we have performed an optimization (through the power allocation) of the rates achieved in the HBS-ABS link. Consequently, the results obtained in this section will clearly help in improving the system level throughput achievable by the BuNGee architecture.

10. Physical layer network coding for improved joint access/backhaul performance

As has been mentioned above, one of the main problems resulting from the use of network MIMO to increase the capacity of the access segment of the BuNGee network is that it also increases several-fold the load on the backhaul segment. In this section we consider a number of novel approaches which may be used to reduce this load, which have in common the use of *physical layer network coding* (PLNC) [Zha06].

One of the issues of in-band backhauling is that the duplex constraint on the ABSs prevents the same spectrum resource being used in both the access and backhaul segment in the same location. It may be possible to re-use it elsewhere in the backhaul, but this requires careful frequency planning. [Zha06] introduced the concept of the *two-way relay*, in which two nodes which wish to exchange information with the aid of a relay node can use the same channel at the same time, reducing the number of time slots required for the full transfer from four (which would be required by conventional forwarding schemes) to two. In a two-tier hierarchical network architecture like BuNGee, the ABS can take the role of the relay, with the HBS and the user equipment (UE) taking the roles of the two source/destination nodes. However the dense deployment of ABSs in the BuNGee networks results in high co-channel interference (CCI) between adjacent ABSs which limits system performance. In the literature the issue of CCI has been identified for two-way relaying systems [Mar08, Yil11, Kno06], however its effects have not been investigated for the hierarchical system architecture of interest in BuNGee. In section 10.1 we consider two different approaches to allow the sharing of resources not only between access and backhaul, but also between adjacent ABSs, and show that this can give rise to benefits similar to those provided by network MIMO.

Section 10.2 introduces an alternative approach based on direct sequence code division multiple access (DS-CDMA) in which the user terminals employ different orthogonal signature sequences, and the ABSs perform decode and forward two-way relaying. This also allows them to collaborate to serve a given user, providing a network MIMO-like benefit.

Section 10.210.3 considers the up- and down-link separately, and introduces a novel approach applying network coding at the ABSs, which provides most of the benefits of network MIMO with no increase in the backhaul load.

Section 10.4 considers a form of compress and forward for fading two-way relay channels, in which soft detection of the network coded data is performed at the ABS and forwarded to the destinations. A method is described by which compensation for the effects of fading can be provided at the destinations.

In this section, for simplicity, we consider the simplest possible network in which these effects may be observed: a network containing the HBS, and two ABSs jointly serving two UEs. We refer to this as a *minimal hierarchical network*, using the terminology of [Bur10], which describes a generic network involving one or more layers of relay nodes (or *relay base stations*) between hub and user terminals as a *hierarchical wireless network* (HWN).

10.1 Strategies for interfering two-way relay channels

10.1.1 System model

We consider a hierarchical system consisting of two single-antenna MSs (nodes 1 and 2), two half-duplex single-antenna ABSs (nodes 5 and 6), and an HBS with two directional antennas which are assumed not to interfere (designated as nodes 3 and 4) as shown in Figure 10-1. The MS and ABS antennas are assumed to be omni-directional. The HBS and the MS nodes want to exchange messages via the ABS nodes; node 1 with node 3 and node 2 with node 4. Nodes 1 and 2 receive/cause interference from/to nodes 6 and 5 respectively. The wireless links between the HBS antennas and the ABSs are defined as the *backhaul network*, while the links between the ABSs and the MSs are defined as the *access*

network. The wireless channels between any pair of nodes are assumed to experience flat fading. The channel coefficient between nodes k and n is

$$h_{k,n} = \Gamma_{k,n}\sqrt{\overline{\gamma}_{k,n}} \tag{10.1}$$

where $\Gamma_{k,n}$ denotes the normalized fading coefficient and $\overline{\gamma}_{k,n}$ denotes the average signal-to-noise ratio (SNR) of the link. Transmission is corrupted by unit variance zero-mean circularly symmetric additive white Gaussian noise (AWGN).

The MS and HBS nodes are assumed to be transmitting unit variance symbols grouped in vector $x = \left[x_1, x_2, x_3, x_4\right]^T$. The ABS nodes receive the signal vector $y_R = \left[y_5, y_6\right]^T$. It should be noted that the elements of vectors x and y_R can be transmitted and received in different time slots depending on the employed cooperative protocol.

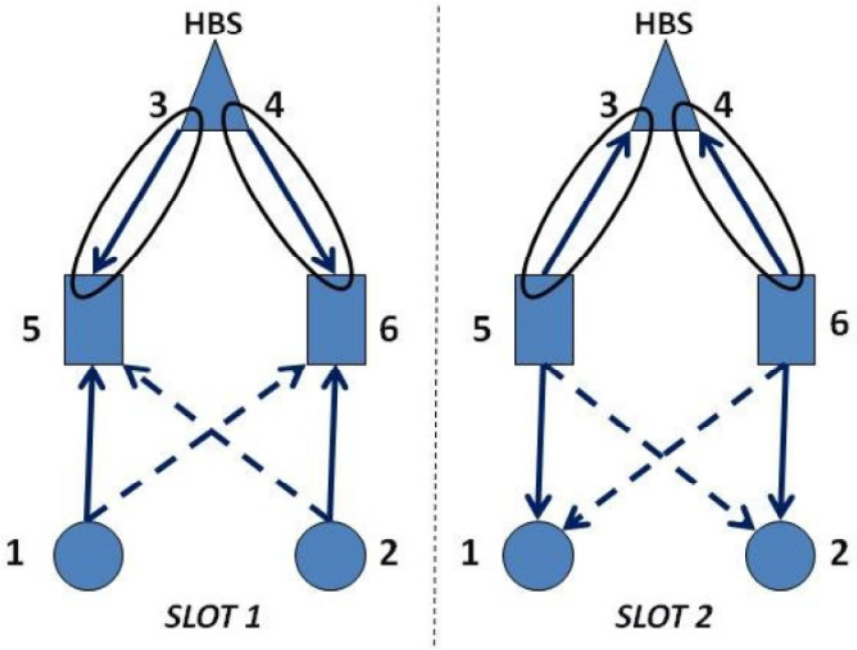

Figure 10-1 : The considered system under a 2-slot protocol: an HBS with two directional antennas (nodes 3, 4), two MSs (nodes 1, 2), and two ABSs (nodes 5, 6).

10.1.2 DF with Network Coding

In this section we present a cooperative strategy and some communication protocols based on DF. The ABSs decode the wanted signals treating the received interference as noise. The decoded symbols are combined with the use of the bitwise XOR operation and forwarded to the destination nodes. Communication can take place in two, three or four time slots. As the number of time slots grows the impact of CCI on the attained performance becomes less significant. However increasing the number of slots incurs a pre-log penalty that limits the achievable capacity.

2-slot DF-XOR

In the first time slot the HBS transmits the symbol vector $x_B = \left[x_3, x_4\right]^T$ and the MSs transmit the symbol vector $x_U = \left[x_1, x_2\right]^T$. Node 5 decodes x_1, x_3 treating x_2 as interference and node 6 decodes x_2, x_4 treating x_1 as interference. In the second time slot nodes 5 and 6 transmit $x_5 = x_1 \oplus x_3$ and $x_6 = x_2 \oplus x_4$ respectively. Nodes 1 and 3 decode x_5 and retrieve the symbol x_3 and x_1 respectively. Similarly, nodes 2 and 4 decode x_6 and retrieve x_4 and x_2 respectively.

We define some rate expressions for the multiple access (MAC) phase of the first time slot in the following, which will be used as rate constraints later. $C_{15}=\frac{1}{2}C\left(\frac{\left|h_{5,1}\right|^2}{\left|h_{5,2}\right|^2+1}\right)$, $C_{35}=\frac{1}{2}C\left(\frac{\left|h_{5,3}\right|^2}{\left|h_{5,2}\right|^2+1}\right)$, $C_{M5}=\frac{1}{2}C\left(\frac{\left|h_{5,1}\right|^2+\left|h_{5,3}\right|^2}{\left|h_{5,2}\right|^2+1}\right)$, $C_{26}=\frac{1}{2}C\left(\frac{\left|h_{6,2}\right|^2}{\left|h_{6,1}\right|^2+1}\right)$, $C_{46}=\frac{1}{2}C\left(\frac{\left|h_{6,4}\right|^2}{\left|h_{6,1}\right|^2+1}\right)$ and $C_{M6}=\frac{1}{2}C\left(\frac{\left|h_{6,2}\right|^2+\left|h_{6,4}\right|^2}{\left|h_{6,1}\right|^2+1}\right)$. The rate expressions for the broadcast (BC) phase of the second time slot are defined as: $C_{53}=\frac{1}{2}C\left(\left|h_{3,5}\right|^2\right)$, $C_{51}=\frac{1}{2}C\left(\frac{\left|h_{1,5}\right|^2}{\left|h_{1,6}\right|^2+1}\right)$, $C_{62}=\frac{1}{2}C\left(\frac{\left|h_{2,6}\right|^2}{\left|h_{2,5}\right|^2+1}\right)$ and $C_{64}=\frac{1}{2}C\left(\left|h_{4,6}\right|^2\right)$.

3-slot DF-XOR

According to this protocol, in the first time slot nodes 1 and 3 transmit symbols x_1 and x_3 respectively and ABS 5 decodes them in the absence of any CCI. In the second time slot nodes 2 and 4 transmit symbols x_2 and x_4 respectively and ABS 6 decodes them also in the absence of any CCI. In the third time slot nodes 5 and 6 transmit $x_5=x_1\oplus x_3$ and $x_6=x_2\oplus x_4$ respectively. Furthermore, nodes 1 and 3 decode x_5 and retrieve the symbol x_3 and x_1 respectively. Similarly, nodes 2 and 4 decode x_6 and retrieve x_4 and x_2 respectively. It should be noted that nodes 1 and 2 experience CCI while attempting to decode x_3 and x_4.

The rate expressions for the MAC phase of the 3-slot protocol are the following: $C_{15}=\frac{1}{3}C\left(\left|h_{5,1}\right|^2\right)$, $C_{35}=\frac{1}{3}C\left(\left|h_{5,3}\right|^2\right)$, $C_{M5}=\frac{1}{3}C\left(\left|h_{5,1}\right|^2+\left|h_{5,3}\right|^2\right)$, $C_{26}=\frac{1}{3}C\left(\left|h_{6,2}\right|^2\right)$, $C_{46}=\frac{1}{3}C\left(\left|h_{6,4}\right|^2\right)$ and $C_{M6}=\frac{1}{3}C\left(\left|h_{6,2}\right|^2+\left|h_{6,4}\right|^2\right)$. The rate expressions for the BC phase are defined as: $C_{53}=\frac{1}{3}C\left(\left|h_{3,5}\right|^2\right)$, $C_{51}=\frac{1}{3}C\left(\frac{\left|h_{1,5}\right|^2}{\left|h_{1,6}\right|^2+1}\right)$, $C_{62}=\frac{1}{3}C\left(\frac{\left|h_{2,6}\right|^2}{\left|h_{2,5}\right|^2+1}\right)$ and $C_{64}=\frac{1}{3}C\left(\left|h_{4,6}\right|^2\right)$.

4-slot DF-XOR

The 4-slot protocol frees the system from any CCI and serves as a performance benchmark. In the first time slot nodes 1 and 3 transmit symbols x_1 and x_3 respectively and ABS 5 decodes them. In the second time slot node 5 transmits $x_5=x_1\oplus x_3$ and nodes 1 and 3 decode x_5 and retrieve the symbols x_3 and x_1 respectively. Similarly, in the third time slot nodes 2 and 4 transmit symbols x_2 and x_4 respectively and ABS 6 decodes them. In the fourth time slot node 6 transmits $x_6=x_2\oplus x_4$ and nodes 2 and 4 decode x_6 and retrieve the symbols x_2 and x_4 respectively

The rate expressions for the MAC phase of the 4-slot protocol are the following: $C_{15}=\frac{1}{4}C\left(\left|h_{5,1}\right|^2\right)$, $C_{35}=\frac{1}{4}C\left(\left|h_{5,3}\right|^2\right)$, $C_{M5}=\frac{1}{4}C\left(\left|h_{5,1}\right|^2+\left|h_{5,3}\right|^2\right)$, $C_{26}=\frac{1}{4}C\left(\left|h_{6,2}\right|^2\right)$, $C_{46}=\frac{1}{4}C\left(\left|h_{6,4}\right|^2\right)$ and $C_{M6}=\frac{1}{4}C\left(\left|h_{6,2}\right|^2+\left|h_{6,4}\right|^2\right)$. The rate expressions for the BC phase are defined as: $C_{53}=\frac{1}{4}C\left(\left|h_{3,5}\right|^2\right)$, $C_{51}=\frac{1}{4}C\left(\left|h_{1,5}\right|^2\right)$, $C_{62}=\frac{1}{4}C\left(\left|h_{2,6}\right|^2\right)$ and $C_{64}=\frac{1}{4}C\left(\left|h_{4,6}\right|^2\right)$.

Let $r=\left[R_1,R_3,R_2,R_4\right]^T$ be the vector containing the transmit rates of HBS and MS nodes. Let $b_1=\left[C_{15},C_{35},C_{M5},C_{26},C_{46},C_{M6}\right]^T$, $b_2=\left[C_{53},C_{51},C_{64},C_{62}\right]^T$ be the vectors containing the rate constraints of the MAC and BC phases respectively. The maximum sum-rate can be expressed as

$$\begin{aligned} R_{DF} \quad &= \quad \max \sum_{k=1}^{4} R_k \\ &\text{s.t.} \quad Ar \le b_1 \\ &\qquad Ir \le b_2 \end{aligned} \tag{10.2}$$

where I is the identity matrix and

$$A=\begin{bmatrix} 1 & 0 & 0 & 0 \\ 0 & 1 & 0 & 0 \\ 1 & 1 & 0 & 0 \\ 0 & 0 & 1 & 0 \\ 0 & 0 & 0 & 1 \\ 0 & 0 & 1 & 1 \\ & & & \end{bmatrix}. \tag{10.3}$$

10.1.3 AF with Network MIMO

In the present section it is proposed that AF relaying can be applied combined with Network MIMO in order to mitigate the effects of CCI. The proposed strategy can utilise two or three time slots.

2-slot AF

In the first slot MS and HBS nodes transmit their symbols, grouped in vector x, and the ABSs receive the following signal vector

$$y_R=H_R x+n_R \tag{10.4}$$

where n_R is a vector of AWGN coefficients, $\mathrm{E}\left[n_R n_R^H\right]=I$, and

$$H_R=\begin{bmatrix} h_{5,1} & h_{5,2} & h_{5,3} & 0 \\ h_{6,1} & h_{6,2} & 0 & h_{6,4} \end{bmatrix}. \tag{10.5}$$

Note that the zero elements in H_R reflect the fact that the HBS antennas (nodes 3 and 4) are assumed not to interfere. In the second time slot both ABSs transmit an amplified version of their received signal and the amplification factors take the following values for ABS nodes 5 and 6

$$\alpha_5 = \left[\left|h_{5,1}\right|^2 + \left|h_{5,2}\right|^2 + \left|h_{5,3}\right|^2 + 1 \right]^{-1/2}$$
$$\alpha_6 = \left[\left|h_{6,1}\right|^2 + \left|h_{6,2}\right|^2 + \left|h_{6,4}\right|^2 + 1 \right]^{-1/2}. \quad (10.6)$$

The MSs and the HBS antennas receive the signal vectors $y_U = \left[y_1, y_2\right]^T$ and $y_B = \left[\tilde{y}_1, \tilde{y}_2\right]^T$ respectively, which can be expressed as

$$y_U = H_U H_R x + H_U n_R + n_U = H_U x + n_U$$
$$y_B = H_B H_R x + H_B n_R + n_B = H_B x + n_B \quad (10.7)$$

where $H_U = H_U H_R$, $H_B = H_B H_R$, $n_U = H_U n_R + n_U$, $n_B = H_B n_R + n_B$ and

$$H_U = \begin{bmatrix} \alpha_5 h_{1,5} & \alpha_6 h_{1,6} \\ \alpha_5 h_{2,5} & \alpha_6 h_{2,6} \end{bmatrix} \quad (10.8)$$

$$H_B = \begin{bmatrix} \alpha_5 h_{3,5} & 0 \\ 0 & \alpha_6 h_{4,6} \end{bmatrix}.$$

The noise covariances are

$$R_{\tilde{n}_U} = \mathrm{diag}\left\{ \sum_{n=1}^{2} \left|H_U\left[1,n\right]\right|^2 + 1, \sum_{n=1}^{2} \left|H_U\left[2,n\right]\right|^2 + 1 \right\}$$
$$R_{\tilde{n}_B} = \mathrm{diag}\left\{ \left|H_B\left[1,1\right]\right|^2 + 1, \left|H_B\left[2,2\right]\right|^2 + 1 \right\}. \quad (10.9)$$

As MS nodes are remote they can only process signals individually. Node 1 decodes the message of node 3 and node 2 that of node 4. For the 2-slot protocol the achievable rates for the transmission of nodes 3 and 4 are

$$R_3 = \frac{1}{2} C\left(\frac{\left|\tilde{\mathbf{H}}_U\left[1,3\right]\right|^2}{\left|\tilde{\mathbf{H}}_U\left[1,2\right]\right|^2 + \left|\tilde{\mathbf{H}}_U\left[1,4\right]\right|^2 + R_{\tilde{n}_U}\left[1,1\right]} \right)$$
$$R_4 = \frac{1}{2} C\left(\frac{\left|\tilde{\mathbf{H}}_U\left[2,4\right]\right|^2}{\left|\tilde{\mathbf{H}}_U\left[2,1\right]\right|^2 + \left|\tilde{\mathbf{H}}_U\left[2,3\right]\right|^2 + R_{\tilde{n}_U}\left[2,2\right]} \right). \quad (10.10)$$

Note that nodes 1 and 2 subtract self-interference $\tilde{\mathbf{H}}_U\left[1,1\right]x_1$ and $H_U\left[2,4\right]x_2$ respectively. The HBS receives two signals from nodes 3 and 4 containing both x_1 and x_2, which are jointly processed. Let $H_B = \left[H_{B1} H_{B2}\right]$ where

$$H_{B1} = \begin{bmatrix} \alpha_5 h_{3,5} h_{5,1} & \alpha_5 h_{3,5} h_{5,2} \\ \alpha_6 h_{4,6} h_{6,1} & \alpha_6 h_{4,6} h_{6,2} \end{bmatrix}$$

$$H_{B2} = \begin{bmatrix} \alpha_5 h_{3,5} h_{5,3} & 0 \\ 0 & \alpha_6 h_{4,6} h_{6,4} \end{bmatrix}. \quad (10.11)$$

The sub-matrix H_{B2} represents self-interference for nodes 3 and 4 and therefore its effects can be cancelled. In consequence only H_{B1} affects the achievable rate of nodes 1 and 2 whose signals are jointly decoded by nodes 3 and 4. We assume that H_{B1} is fully known by the HBS. In the case of linear detection a beamforming matrix $W=[w_1, w_2]$, which is a function of H_{B1} representing the global channel state information (CSI), is designed by the HBS and applied to the received signals. $w_1, w_2 \in \mathrm{C}^{2\times 1}$ denote the beamforming vectors corresponding to the signals transmitted by nodes 1 and 2 respectively. The finally extracted signal can be expressed in vector form as

$$y_B = W y_B = W H_{B1} x_U + W n_B \tag{10.12}$$

where $x_U = [x_1, x_2]^T$. Let $H_{B1} = [h_1, h_2]$ where h_k corresponds to node k. The achievable rate for nodes $k=1,2$ is

$$R_k = \frac{1}{2} C\left(\frac{\left| w_k^T h_k \right|^2}{\left| w_k^T h_{n,n\neq k} \right|^2 + \left\| w_k^T \right\|^2 R_{\tilde{n}_B}[k,k]} \right) \tag{10.13}$$

where factors $\left| w_k^T h_{n,n\neq k} \right|^2$ and $\left\| w_k^T \right\|^2 R_{\tilde{n}_B}[k,k]$ correspond to inter-node interference and noise enhancement respectively, which both have a detrimental effect.

We assume that the HBS obtains perfect global CSI (matrix H_{B1}) and acts as a Network MIMO central unit. The beamforming matrix can be based on Zero-Forcing (ZF), where $W = H_{B1}^{\dagger}$, or the Minimum Mean Square Error (MMSE), where $W = \left(H_{B1}^H H_{B1} + R_B \right)^{-1} H_{B1}$. Detection can be improved further if it is performed in a successive fashion, i.e., the detected symbols are subtracted from the remaining received signal. This frees the signal from some interference components and can enhance the achieved capacity. The composite channel $H_{B1} = [h_1, h_2]$ is ordered so that $\|h_1\| \leq \|h_2\|$. The beamforming vector w_k corresponding to node k is the first row of matrix $W_k = H_k^{\dagger}$ for ZF and $W_k = \left(H_k^H H_k + R_B \right)^{-1} H_k^H$ for MMSE, where $H_k = [h_k, h_{k+1}]^T$. With successive interference cancellation (SIC), each node expreriences only interference from nodes with higher index. This results in improved performance compared with linear detection. The achievable sum-rate is

$$R_{AF} = \sum_{k=1}^{4} R_k. \tag{10.14}$$

3-slot AF

According to this protocol, in the first time slot MS and HBS nodes transmit their symbols and the received signal by the ABSs is given by (4). In the second time slot ABS 5 transmits with the amplification factor α_5 and ABS 6 remains silent. In the third time slot ABS 6 transmits with the amplification factor α_6 and ABS 5 remains silent. The employed amplification factors are given by (6).

The received signals by the MSs and the HBS antennas (vectors y_U and y_B respectively), accumulated in the second and third time slot, are as in (7). It should be noted that H_R, H_B are as in (5) and (8) respectively, where H_U is as follows

$$H_U = \begin{bmatrix} \alpha_5 h_{1,5} & 0 \\ 0 & \alpha_6 h_{2,6} \end{bmatrix}. \tag{10.15}$$

The noise covariances are

$$R_{\tilde{n}_U} = \mathrm{diag}\left\{\left|H_U[1,1]\right|^2 + 1, \left|H_U[2,2]\right|^2 + 1\right\}$$
$$R_{\tilde{n}_B} = \mathrm{diag}\left\{\left|H_B[1,1]\right|^2 + 1, \left|H_B[2,2]\right|^2 + 1\right\}. \quad (10.16)$$

The achievable rates for the transmission of nodes 3 and 4 are

$$R_3 = \frac{1}{3}C\left(\frac{\left|\tilde{\mathbf{H}}_U[1,3]\right|^2}{\left|\tilde{\mathbf{H}}_U[1,2]\right|^2 + R_{\tilde{n}_U}[1,1]}\right)$$
$$R_4 = \frac{1}{3}C\left(\frac{\left|\tilde{\mathbf{H}}_U[2,4]\right|^2}{\left|\tilde{\mathbf{H}}_U[2,1]\right|^2 + R_{\tilde{n}_U}[2,2]}\right). \quad (10.17)$$

The HBS receives in the second time slot a signal from node 3 and in the third time slot a signal from node 4. These signals are jointly processed in the third time slot with the use of Network MIMO techniques as above. Therefore achievable rate for nodes $k = 1,2$ is

$$R_k = \frac{1}{3}C\left(\frac{\left|w_k^T h_k\right|^2}{\left|w_k^T h_{n,n\neq k}\right|^2 + \left\|w_k^T\right\|^2 R_{\tilde{n}_B}[k,k]}\right). \quad (10.18)$$

The achievable rates can be enhanced with the application of SIC techniques as described above.

10.1.4 Numerical Results

For simplicity, we assume a symmetric interfering two-way relay channel; the wireless links of the access network, the backhaul network and the interfering links experience the same average SNR, i.e., $\overline{\gamma}_{1,5} = \overline{\gamma}_{5,1} = \overline{\gamma}_{2,6} = \overline{\gamma}_{6,2} = \overline{\gamma}_{AC}$, $\overline{\gamma}_{5,3} = \overline{\gamma}_{3,5} = \overline{\gamma}_{4,6} = \overline{\gamma}_{6,4} = \overline{\gamma}_{BH}$, and $\overline{\gamma}_{5,2} = \overline{\gamma}_{2,5} = \overline{\gamma}_{1,6} = \overline{\gamma}_{6,1} = \overline{\gamma}_I$.

Figure 10-2 plots the total AMSR versus the average SNR $\overline{\gamma}_I$ for the considered schemes when backhaul and access networks experience identical average SNR $\overline{\gamma}_{BH} = \overline{\gamma}_{AC} = 10\mathrm{dB}$ and Rayleigh fading, i.e., $\Gamma_{k,n}$: $\mathrm{NC}(0,1)$. As can be seen from Figure 10-2, in the low CCI regime ($\overline{\gamma}_I < 0\mathrm{dB}$) the 2-slot DF-XOR approach performs better. When CCI becomes dominant, the 2-slot AF scheme perform better as it effectively exploits interference through Network MIMO processing at the HBS. Amongst the AF schemes, the ones taking advantage of SIC are superior. Although the 3-slot schemes avoid some interference, they perform worse than those based on 2-slots as the pre-log penalty of $\frac{1}{3}$ is dominant in the considered scenario. The performance of the 4-slot DF-XOR scheme is not affected by CCI and serves as a baseline for comparisons. Figure 10-3 plots the AMSR for the downlink and uplink separately, for the 2-slot and 3-slot DF-XOR and the 2-slot AF-LMMSE scheme. Uplink rate is generally higher as the directional HBS antennas eliminate CCI in the second time slot. The AMSR deteriorates when CCI becomes stronger for all cases apart from the uplink of the AF scheme. The AMSR for the uplink of AF improves as $\overline{\gamma}_I$ increases because the HBS jointly processes the received signals by nodes 3 and 4 using Network MIMO techniques.

Figure 10-4 plots the total AMSR for the same schemes when the average SNR of the backhaul network is $\overline{\gamma}_{BH} = 20\mathrm{dB}$ and that of the access network is $\overline{\gamma}_{BH} = 10\mathrm{dB}$. This is justified by the fact that the backhaul network can be planned to have links of high quality as the positions of the ABSs relative to the HBS can be selected appropriately. As expected, the performance of all schemes improves when the quality

of backhaul links increases. Furthermore the AF protocols perform relatively better than the case of Figure 10-2.

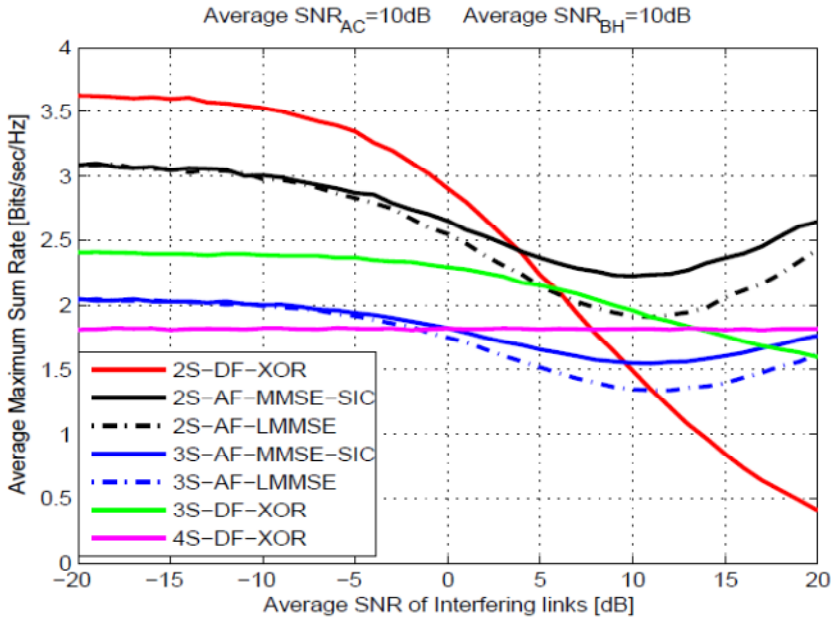

Figure 10-2 The total AMSR versus $\overline{\gamma}_I$ when $\overline{\gamma}_{BH} = \overline{\gamma}_{AC} = 10\text{dB}$.

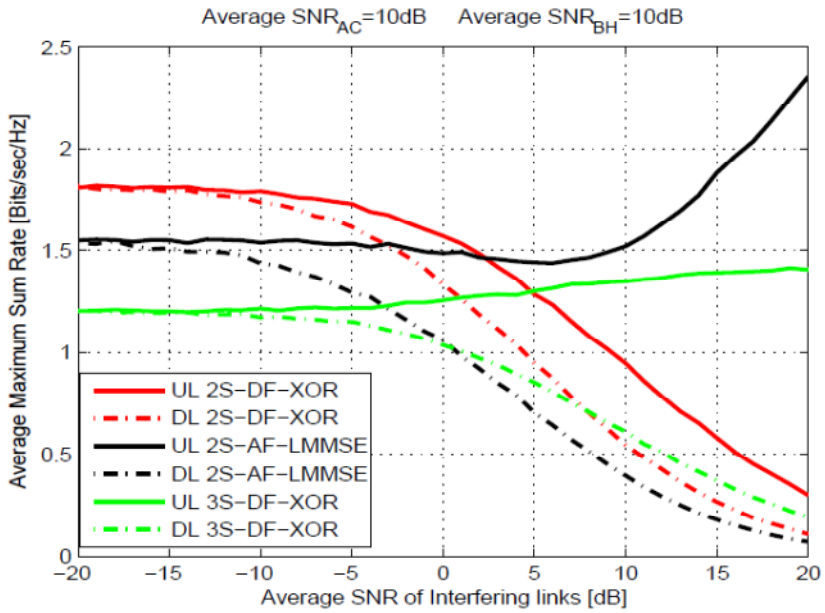

Figure 10-3 The AMSR of the uplink and downlink of 2S-DF-XOR, 3S-DF-XOR and 2S-AF-LMMSE versus $\overline{\gamma}_I$ when $\overline{\gamma}_{BH} = \overline{\gamma}_{AC} = 10\text{dB}$.

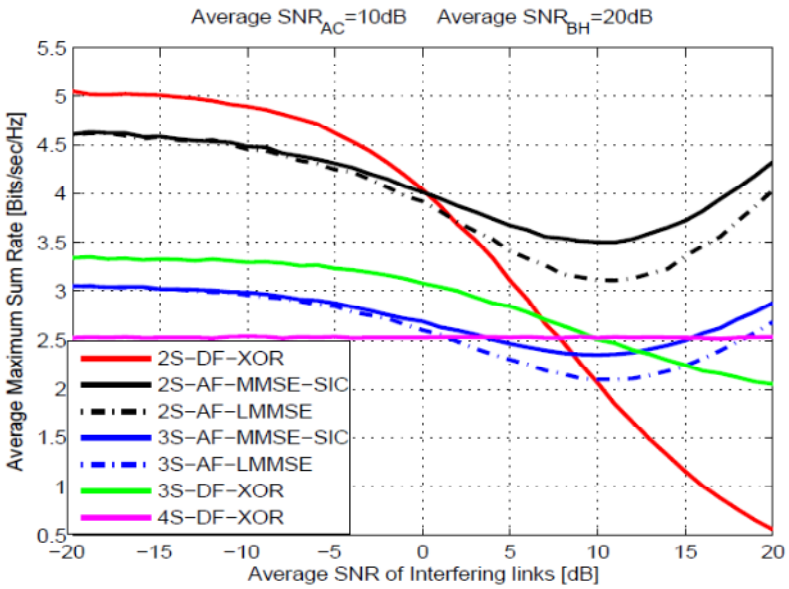

Figure 10-4 The total AMSR versus $\overline{\gamma}_I$ ***when*** $\overline{\gamma}_{BH} = 20\text{dB}$ ***and*** $\overline{\gamma}_{AC} = 10\text{dB}$.

10.2 Orthogonal sequence-based PLNC for hierarchical wireless network

10.2.1 System Model

Consider again a minimal HWN model (see Figure 10-5) which contains 2 MSs (nodes 1 and 2), 2 ABSs (nodes 5 and 6) and 1 HBS. (In respect of its communication with node 5, the HBS will be treated as the *node 3*; to communicate with node 6, HBS acts as *node 4*.). We assume that all nodes are equipped with an *omni-directional half-duplex antenna*. The links between the HBS and the ABSs are defined as the *backhaul network (BH)*, while the links between the ABSs and the MSs are defined as the *access network (AC)*. We also assume that the channel links of each node pair experiences flat fading. The channel gain between node *m* and *n* should obey

$$h_{m,n} = \Gamma_{m,n}\sqrt{\gamma_{m,n}} \tag{1.19}$$

where $\Gamma_{m,n}$ is the normalized fading coefficient. The quantity $\overline{\gamma}_{m,n}$ is the average signal-to-noise ratio (SNR) of the corresponding channel link. Assume that the received signals at each node are corrupted by circularly symmetric Additive Gaussian White Noise (AWGN) with variance N_0.

In Figure 10-9, from the perspective of the ABSs, we refer to the transmissions from MSs/HBS to ABSs as the *multiple access channel* (MAC*) phase* (the purple solid lines) in the HWN architecture, while the transmission from ABSs to MSs/HBS constitutes the *BC phase* (the green solid lines). In a perfect scenario, the two groups ({node 1-node 5-node 3} and {node 2-node 6-node 4}) should work independently without interfering with each other. However, in a real scenario, nodes 1 and 2 will receive/cause interference from/to nodes 6 and 5 respectively (see the blue dashed lines in Figure 10-5). In a conventional system, interference links cause degradation of system performance. This is because the interference signals are normally treated as noise when detecting the signals at the MAC phase. However, in our scheme, we will exploit the interference links in our HWN structure so that they can provide useful information which can improve system performance.

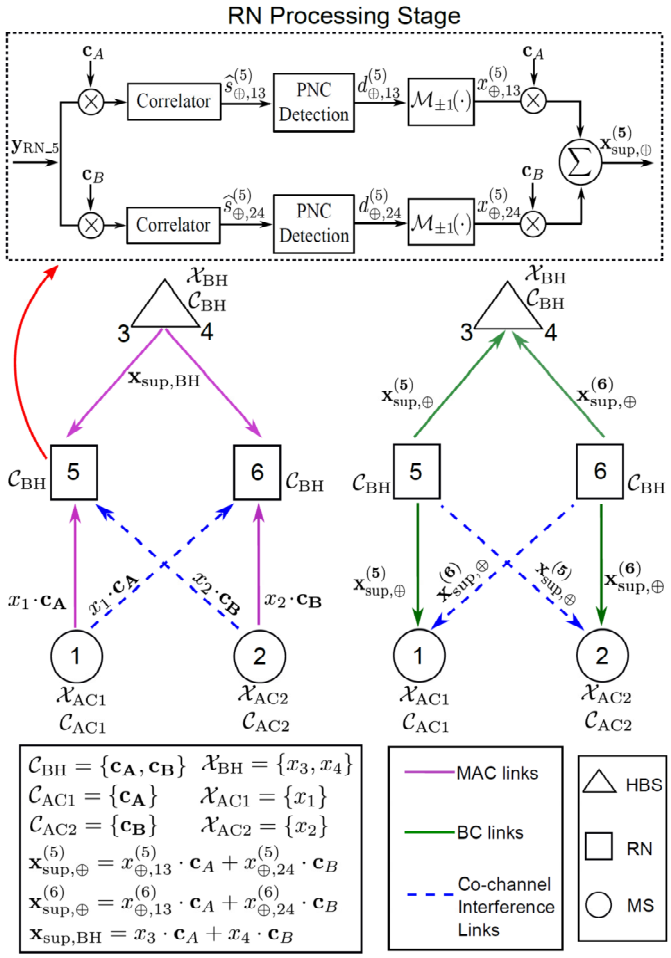

Figure 10-5 model of proposed scheme in a simple minimal HWN architecture

10.2.2 Description of the proposed scheme.

In the MAC phase, we expect the binary data d_1 / d_2 at node 1/2 to be exchanged with d_3 / d_4 at node 3/4. For simplicity, assume that each node employs BPSK modulation $\mathrm{M}_{\pm 1}(\cdot)$. Thus, each transmitted symbol with unit variance is obtained by: $x_i = \mathrm{M}_{\pm 1}(d_i)$, $i \in \{1,2,3,4\}$. The alphabets of transmitted symbols in AC can be defined as $\mathrm{X}_{\mathrm{AC1}} = \{x_1\}$ and $\mathrm{X}_{\mathrm{AC2}} = \{x_2\}$ for each MS, respectively. The alphabet of transmitted symbols for the HBS can be defined as $\mathrm{X}_{\mathrm{BH}} = \{x_3, x_4\}$ which refers to the available symbol alphabet in BH. Note that if all nodes want to transmit their signals simultaneously, severe interference is unavoidable. So instead of directly transmitting x_1, x_2 and $[x_3, x_4]^T$ in the MAC phase, we allocate a unique orthogonal code (signature sequence, SS) to each transmitted signal.

Suppose that each MS knows only its own SS. The alphabet of SSs for each MS is defined as $\mathrm{C}_{\mathrm{AC1}} = \{\mathbf{c}_A\}$ and $\mathrm{C}_{\mathrm{AC2}} = \{\mathbf{c}_B\}$. Then the spread signal for nodes 1 and 2 can be written as $x_1 \cdot \mathbf{c}_A$ and $x_2 \cdot \mathbf{c}_B$, respectively.

The HBS and ABSs own the global SS alphabet for both MSs, which then constitutes the available SS alphabet for the BH, defined as $\mathrm{C}_{\mathrm{BH}} = \{\mathbf{c}_A, \mathbf{c}_B\}$. Note that the HBS should allocate different SSs for symbols transmitted to different MSs. That is, to match the SS at node 1, the symbol x_3 should be spread as $x_3 \cdot \mathbf{c}_A$, and similarly x_4 should be $x_4 \cdot \mathbf{c}_B$. The two spread symbols are then superposed at the HBS:

$$\mathbf{x}_{\mathrm{sup,BH}} x = x_3 \cdot \mathbf{c}_A + x_4 \cdot \mathbf{c}_B \tag{10.20}$$

So in the 1st time-slot (the MAC phase), node 1/2 and node 3/4 simultaneously transmit their spread signals to node 5/6, respectively. In the meantime, the useful signals and interfering signals are naturally superimposed at the ABSs (nodes 5 and 6):

$$\begin{aligned}\mathbf{y}_{RN5} &= h_{3,5}\cdot\mathbf{x}_{\text{sup,BH}} + h_{1,5}\cdot x_1\cdot\mathbf{c}_A + h_{2,5}\cdot x_2\cdot\mathbf{c}_B + \mathbf{n}_{w5}\\ \mathbf{y}_{RN6} &= h_{4,6}\cdot\mathbf{x}_{\text{sup,BH}} + h_{1,6}\cdot x_1\cdot\mathbf{c}_A + h_{2,6}\cdot x_2\cdot\mathbf{c}_B + \mathbf{n}_{w6}\end{aligned} \tag{10.21}$$

where $\mathbf{n}_{wi} \sim \mathcal{CN}(0, N_0), i \in \{5,6\}$. Normally, x_2 and x_1 are treated as the interference signals for node 5 and node 6, respectively.

Due to the orthogonality of our selected spreading sequences, the despreading procedure can be simplified as the multiplication with the corresponding SS and passing through the parallel correlators which are shown in Figure 10-5. For *node 5*, the despreading pair $\hat{\mathbf{s}}_{\oplus}^{(5)} = \{\hat{s}_{\oplus,13}^{(5)}, \hat{s}_{\oplus,24}^{(5)}\}^T$ satisfies

$$\begin{aligned}\hat{s}_{\oplus,13}^{(5)} &= \frac{1}{N}\left(\mathbf{y}_{RN5}\cdot\mathbf{c}_A^H\right)\\ \hat{s}_{\oplus,24}^{(5)} &= \frac{1}{N}\left(\mathbf{y}_{RN5}\cdot\mathbf{c}_B^H\right)\end{aligned} \tag{10.22}$$

where $s_{\oplus,13}^{(5)} = h_{1,5}x_1 + h_{3,5}x_3$ is the superimposed signal for symbols x_1 and x_3; and $s_{\oplus,24}^{(5)} = h_{2,5}x_2 + h_{3,5}x_4$ is the superimposed signal for symbols x_2 and x_4. It is clear that $s_{\oplus,13}^{(5)}\mathbf{c}_A + s_{\oplus,24}^{(5)}\mathbf{c}_B = h_{3,5}\mathbf{x}_{\text{sup,BH}} + h_{1,5}x_1\mathbf{c}_A + h_{2,5}x_2\mathbf{c}_B$.

The PLNC detection follows the despreading procedure. Denoting the estimation of $s_{\oplus,pq}$ as $\tilde{s}_{\oplus,pq}$ (where $pq \in \{13,24\}$), the PLNC detection can be computed as follows:

$$\begin{aligned}\tilde{s}_{\oplus,13}^{(5)} &= \arg\min_{s_{\oplus,13}}\left\|\hat{s}_{\oplus,13}^{(5)} - (h_{1,5}x_1 + h_{3,5}x_3)\right\|\\ d_{\oplus,13}^{(5)} &= \text{mod}\left(\frac{\tilde{s}_{\oplus,13}^{(5)}}{2} - 1\right) = \hat{d}_1 \oplus \hat{d}_3\\ \tilde{s}_{\oplus,24}^{(5)} &= \arg\min_{s_{\oplus,24}}\left\|\hat{s}_{\oplus,24}^{(5)} - (h_{2,6}x_2 + h_{4,6}x_4)\right\|\\ d_{\oplus,24}^{(5)} &= \text{mod}\left(\frac{\tilde{s}_{\oplus,24}^{(5)}}{2} - 1\right) = \hat{d}_2 \oplus \hat{d}_4\end{aligned} \tag{10.23}$$

where $\text{mod}(\cdot)$ means the modulus operation.

Note that the despreading and PLNC detection procedure at node 6 is similar to (10.22) and (10.23) at node 5.

In accordance with the MAC phase, node 5 also employs the BPSK modulation $\mathrm{M}_{\pm 1}(\cdot)$ for the network coded data $d_{\oplus,13}^{(5)}$ and $d_{\oplus,24}^{(5)}$ to obtain the network coded symbols $x_{\oplus,13}^{(5)}$ and $x_{\oplus,24}^{(5)}$. In order to successfully distinguish each network coded symbol for each node, $x_{\oplus,13}^{(5)}$ and $x_{\oplus,24}^{(5)}$ are separately spread by SSs $\mathbf{c}_A$ and $\mathbf{c}_B$, and then are added together for transmission:

$$\mathbf{x}_{\text{sup},\oplus}^{(5)} = x_{\oplus,13}^{(5)}\cdot\mathbf{c}_A + x_{\oplus,24}^{(5)}\cdot\mathbf{c}_B \tag{10.24}$$

Note that the BC phase operation at node 6 is also similar to the above. The broadcast signal is then:

$$\mathbf{x}_{\text{sup},\oplus}^{(6)} = x_{\oplus,13}^{(6)}\cdot\mathbf{c}_A + x_{\oplus,24}^{(6)}\cdot\mathbf{c}_B \tag{10.25}$$

where $x_{\oplus,13}^{(6)}$ and $x_{\oplus,13}^{(6)}$ are node 6's version of network coded symbols. The similar forms in (10.24) and (10.25) for the broadcast signals and the independence of fading channels implies that *transmit diversity* is available. The received signals at MSs and HBS should be:

$$\begin{aligned}\mathbf{y}_{\text{MS\_1}} &= h_{5,1}\mathbf{x}_{\text{sup},\oplus}^{(5)} + h_{6,1}\mathbf{x}_{\text{sup},\oplus}^{(6)} + \mathbf{n}_{w1}\\ \mathbf{y}_{\text{MS\_2}} &= h_{5,2}\mathbf{x}_{\text{sup},\oplus}^{(5)} + h_{6,2}\mathbf{x}_{\text{sup},\oplus}^{(6)} + \mathbf{n}_{w2}\\ \mathbf{y}_{\text{HBS}} &= h_{5,3}\mathbf{x}_{\text{sup},\oplus}^{(5)} + h_{6,4}\mathbf{x}_{\text{sup},\oplus}^{(6)} + \mathbf{n}_{w34}\end{aligned} \tag{10.26}$$

where $n_{wi} \sim \mathcal{CN}(0, N_0), i \in \{1,2,34\}$. We notice that the combining is naturally implemented on the antenna of each node and the CSIs are unknown to the transmitters (ABSs). The equivalent SNRs at the receivers (MSs and HBS) is then:

$$\gamma_{1,\text{equv.}} = \frac{\left|2h_{5,1} + 2h_{6,1}\right|^2}{N_0}$$
$$\gamma_{2,\text{equv.}} = \frac{\left|2h_{5,2} + 2h_{6,2}\right|^2}{N_0} \quad (10.27)$$
$$\gamma_{34,\text{equv.}} = \frac{\left|2h_{5,3} + 2h_{6,4}\right|^2}{N_0}$$

10.2.3 Analysis of Sum-Rate

In this section, we focus on the alphabet-unconstrained cut-set bound capacity, in particular, the maximum average sum-rate in HWN for the proposed scheme.

Assuming the bandwidth is normalized to 1 Hz, such that a link m-to-n with SNR of $\gamma_{m,n}$ can reliably transfer up to:

$$C(\gamma_{m,n}) = \log_2(1+\gamma_{m,n}) \left[\text{bit/s}\right] \quad (10.28)$$

Sum-rate analysis of the proposed scheme

Neglecting for the moment the use of the SSs, and the interfering links, we suppose that the node $i, i \in \{5,6\}$ can exploit the set

$$\mathrm{D}_{13}(\hat{s}^{(i)}_{\oplus,13}) = \{(x_1^{(i)}, x_3^{(i)}) \mid (x_1^{(i)}, x_3^{(i)}, \hat{s}^{(i)}_{\oplus,13}) \text{is jointly typical}\}$$
$$\mathrm{D}_{24}(\hat{s}^{(i)}_{\oplus,24}) = \{(x_2^{(i)}, x_4^{(i)}) \mid (x_2^{(i)}, x_4^{(i)}, \hat{s}^{(i)}_{\oplus,24}) \text{is jointly typical}\} \quad (10.29)$$

together with the mapping function

$$\mathrm{M}_{\oplus,i} : \begin{cases} \hat{s}^{(i)}_{\oplus,13} \rightarrow d^{(i)}_{\oplus,13} \\ \hat{s}^{(i)}_{\oplus,24} \rightarrow d^{(i)}_{\oplus,24} \end{cases}, i \in \{5,6\} \quad (10.30)$$

where we advise readers to refer to [Cov06] for a precise definition of the concept of joint typicality (applied here to the triplets $(x_1^{(i)}, x_3^{(i)}, \hat{s}^{(i)}_{\oplus,13})$ and $(x_2^{(i)}, x_4^{(i)}, \hat{s}^{(i)}_{\oplus,24})$). Note that if we employed BPSK as above, the mapping function $\mathrm{M}_{\oplus,i}$ should satisfy (5). Here, for a more general scenario (arbitrary modulation scheme), we assume that the *exclusive law* [Aki09a] is achievable which allows the unambiguous detection of PLNC. The following results are upper bounds of the sum-rate of our proposed scheme based on this assumption.

Based on the above assumption, for each of the ABSs, the rate pair $\{R_1, R_3\}$ ($\{R_2, R_4\}$) which corresponds to the symbol pair $\{x_1, x_3\}$ ($\{x_2, x_4\}$) whose elements are expected to be exchanged with each other, is still upper bounded by the point-to-point capacity given the implementation of PLNC:

$$R_1^{(i)} = R_3^{(i)} \le \max\{I(s^{(i)}_{\oplus,13}; y_{\text{RN}\_i})\}$$
$$R_2^{(i)} = R_4^{(i)} \le \max\{I(s^{(i)}_{\oplus,24}; y_{\text{RN}\_i})\}, \; i \in \{5,6\} \quad (10.31)$$

where $s^{(i)}_{\oplus,13}$ and $s^{(i)}_{\oplus,24}$ $i \in \{5,6\}$ are the superimposed signals as previously defined.

Now we must consider the condition with SSs and interfering links. Considering node 5, we find that the despreading operation is actually implemented on the superimposed signals $s^{(5)}_{\oplus,13} = h_{1,5}x_1 + h_{3,5}x_3$ and $s^{(5)}_{\oplus,24} = h_{2,5}x_2 + h_{3,5}x_4$. This can be modelled as two virtual stations (VS 1 and 2) transmitting the superimposed signals with corresponding SS: $s^{(5)}_{\oplus,13} \cdot \mathbf{c}_A$ and $s^{(5)}_{\oplus,24} \cdot \mathbf{c}_B$ to node 5 in MAC phase which can be illustrated as in Figure 10-6.

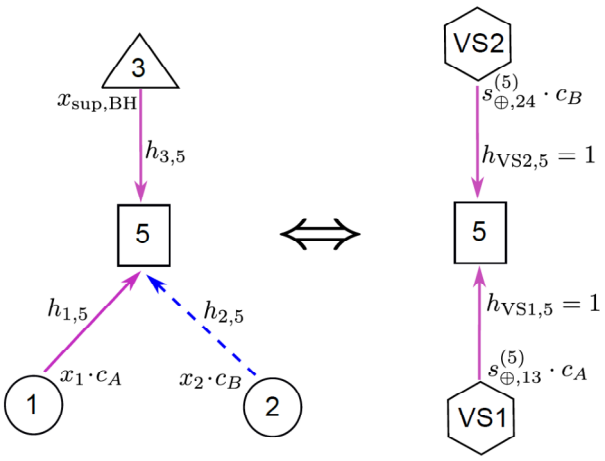

Figure 10-6 Equivalent model of multiple access phase from virtual stations to node 5 (similarly for node 6).

Hence the equivalent SNRs at node 5 should be $\gamma^{(5)}_{\text{VS1}} = \left|h_{1,5} + h_{3,5}\right|^2 / N_0$ for $s^{(5)}_{\oplus,13} = h_{1,5}x_1 + h_{3,5}x_3$ from VS 1 and $\gamma^{(5)}_{\text{VS2}} = \left|h_{2,5} + h_{3,5}\right|^2 / N_0$ for $s^{(5)}_{\oplus,13} = h_{1,5}x_1 + h_{3,5}x_3$ from VS 2. We treat interference as useful information. Note that we apply DS-CDMA (with orthogonal sequences) for each ABS. So the set of rates $\{R^{(5)}_{\text{VS1}}, R^{(5)}_{\text{VS2}}\}$ are subjected to the capacities of orthogonal code division multiple access channels [Erk98]. Hence the rate expressions should be:

$$\begin{aligned} R^{(5)}_{\text{VS1}} &\le \alpha^{(5)} C\left(\frac{\gamma^{(5)}_{\text{VS1}}}{\alpha^{(5)}}\right) \\ R^{(5)}_{\text{VS2}} &\le (1-\alpha^{(5)}) C\left(\frac{\gamma^{(5)}_{\text{VS2}}}{1-\alpha^{(5)}}\right) \end{aligned} \tag{10.32}$$

where, $\alpha^{(5)}$ denotes the fraction of the degrees of freedom to VS 1and $1-\alpha^{(5)}$ to VS 2.

In the above part, we analysed the rate constraints for node 5 and we have the same situation for node 6: there is also a virtual model in which VS 1 transmits $s^{(6)}_{\oplus,13} \cdot \mathbf{c}_A = (h_{1,6}x_1 + h_{4,6}x_3) \cdot \mathbf{c}_A$ and VS 2 transmits $s^{(6)}_{\oplus,24} \cdot \mathbf{c}_A = (h_{2,6}x_2 + h_{4,6}x_4) \cdot \mathbf{c}_B$, such that the rate constraints are:

$$\begin{aligned} R^{(6)}_{\text{VS1}} &\le \alpha^{(6)} C\left(\frac{\gamma^{(6)}_{\text{VS1}}}{\alpha^{(6)}}\right) \\ R^{(6)}_{\text{VS2}} &\le (1-\alpha^{(6)}) C\left(\frac{\gamma^{(6)}_{\text{VS1}}}{1-\alpha^{(6)}}\right) \end{aligned} \tag{10.33}$$

where $\alpha^{(6)}$ and $1-\alpha^{(6)}$ are also the fraction of the degrees of freedom to VS 1 and 2 respectively.

We know node 5/6 transmits symbol $\mathbf{x}^{(5)}_{\text{sup},\oplus} / \mathbf{x}^{(6)}_{\text{sup},\oplus}$ with variance 2 to HBS and MSs. This can be treated as a multiple antenna transmitter and a single antenna receiver (transmit diversity) for HBS and MSs. So the rate set for HBS and MSs in the BC phase should obey:

$$\begin{aligned} R_1 &\le C(\gamma_{1,\text{equv.}}) \\ R_2 &\le C(\gamma_{2,\text{equv.}}) \\ R_{34} &\le C(\gamma_{34,\text{equv.}}) \end{aligned} \tag{10.34}$$

The sum-rate is the total amount of information exchanged between MSs and HBS divided by the total time consumed in MAC and BC phase. Suppose that the transmission duration of MAC phase is M symbols. The sum-rate can be expressed as

$$R_{\text{Sum}} = \frac{R^{(5)}_{\text{VS1}} M + R^{(5)}_{\text{VS2}} M + R^{(6)}_{\text{VS1}} M + R^{(6)}_{\text{VS2}} M}{M\left[\frac{R_1}{R^{\text{BC}}_{\min}} + \frac{R_2}{R^{\text{BC}}_{\min}} + \frac{R_{34}}{R^{\text{BC}}_{\min}}\right]} \tag{10.35}$$

where, $R_{\min}^{\mathrm{BC}} = \min\{R_1, R_2, R_{34}\}$ denotes the minimum rate in the BC phase. The denominator of (10.35) denotes the total duration of both MAC and BC phases. It is clear that $R_{\min}^{\mathrm{BC}} = C_{\min}^{\mathrm{BC}}$ maximizes the sum-rate for any rate in the MAC phase. Making all rates achieve their corresponding capacities, (10.35) can be rewritten as

$$\begin{aligned} R_{\mathrm{Sum}} &= C_{\min}^{\mathrm{BC}} \frac{R_{\mathrm{VS1}}^{(5)} + R_{\mathrm{VS2}}^{(5)} + R_{\mathrm{VS1}}^{(6)} + R_{\mathrm{VS2}}^{(6)}}{\left[R_1 + R_2 + R_{34}\right]} \\ &= C_{\min}^{\mathrm{BC}} \frac{\left[\alpha^{(5)} C(\frac{\gamma_{\mathrm{VS1}}^{(5)}}{\alpha^{(5)}}) + (1-\alpha^{(5)}) C(\frac{\gamma_{\mathrm{VS2}}^{(5)}}{1-\alpha^{(5)}})\right] + \left[\alpha^{(6)} C(\frac{\gamma_{\mathrm{VS1}}^{(6)}}{\alpha^{(6)}}) + (1-\alpha^{(6)}) C(\frac{\gamma_{\mathrm{VS2}}^{(6)}}{1-\alpha^{(6)}})\right]}{C(\gamma_{1,\mathrm{equv.}}) + C(\gamma_{2,\mathrm{equv.}}) + C(\gamma_{34,\mathrm{equv.}})} \end{aligned} \tag{10.36}$$

where, we take $\alpha^{(5)} = 1/2$ and $\alpha^{(6)} = 1/2$ for VSs 1 and 2 to share the equal bandwidth.

Sum-rate analysis of TDMA based PLNC scheme

We choose the TDMA based PLNC scheme as the benchmark. In such a scheme, in the 1st time-slot, MS 1 and HBS simultaneously transmit symbols x_1 and x_3 to ABS 5. Then ABS 5 decodes the superimposed signal of x_1 and x_3 in the absence of CCI. In the 2nd time slot, ABS 5 broadcasts the network coded symbol $x_5 = x_1 \oplus x_3$ to MS 1 and HBS. In the 3rd time-slot, MS 2 and HBS transmit symbols x_2 and x_4 to ABS 6. Then ABS 6 decodes the superimposed signal of x_2 and x_4 also in the absence of CCI. In the 4th time slot, ABS 6 broadcasts the network coded symbol $x_6 = x_2 \oplus x_4$ to MS 2 and HBS. The sum-rate of such scheme can be calculated as

$$R_{\mathrm{Sum,TD}} = \beta \cdot \frac{MR_{15} + MR_{35}}{M\frac{R_{51}}{R_{\min,5}^{\mathrm{BC}}} + M\frac{R_{53}}{R_{\min,5}^{\mathrm{BC}}}} + (1-\beta) \cdot \frac{MR_{26} + MR_{46}}{M\frac{R_{62}}{R_{\min,6}^{\mathrm{BC}}} + M\frac{R_{64}}{R_{\min,6}^{\mathrm{BC}}}} \tag{10.37}$$

where $R_{\min,5}^{\mathrm{BC}} = \min\{R_{51}, R_{53}\}$ and $R_{\min,6}^{\mathrm{BC}} = \min\{R_{62}, R_{64}\}$ are the weakest transmission rates for ABSs in the BC phase. The quantity β denotes the time scheduling factor for the group of nodes 1, 5 and 3; and $1-\beta$ denotes that for the other group. Letting all rates achieve their corresponding capacities, (10.37) can be rewritten as

$$R_{\mathrm{Sum,TD}} = \beta \cdot C_{\min,5}^{\mathrm{BC}} \frac{C(\gamma_{15}) + C(\gamma_{35})}{C(\gamma_{51}) + C(\gamma_{53})} + (1-\beta) \cdot C_{\min,6}^{\mathrm{BC}} \frac{C(\gamma_{26}) + C(\gamma_{46})}{C(\gamma_{62}) + C(\gamma_{64})} \tag{10.38}$$

where we normally take $\beta = 1/2$ to let the two groups share equal time-slots to exchange their data.

Sum rate comparison between the two schemes

For simplicity, we consider a symmetric interfering case for the 2-way relay channel in which the channels of the AC, the BH, the and the CCI links experience the same average SNRs, i.e., $\gamma_{15} = \gamma_{51} = \gamma_{26} = \gamma_{62} = \gamma_{\mathrm{AC}}$, $\gamma_{35} = \gamma_{53} = \gamma_{46} = \gamma_{64} = \gamma_{\mathrm{BH}}$, and $\gamma_{25} = \gamma_{52} = \gamma_{16} = \gamma_{61} = \gamma_{\mathrm{CCI}}$.

Figure 10-7 shows the numerical results of average maximum sum rate versus the average CCI link SNR γ_{CCI} for the two schemes. In this simulation, we assume Rayleigh fading i.e, $\Gamma \sim \mathcal{CN}(0,1)$ and identical average SNRs for BH and AC links, i.e, $\gamma_{\mathrm{AC}} = \gamma_{\mathrm{BH}} = 10\mathrm{dB}$. In Figure 10-7L, we note that the TDMA based PLNC scheme is not affected by CCI and serves as a baseline. Since our proposed scheme takes advantage of the interfering signals as useful information, when the CCI links becomes strong, the sum rate increases. The interference signals are transformed to useful signals which moreover provide transmit diversity.

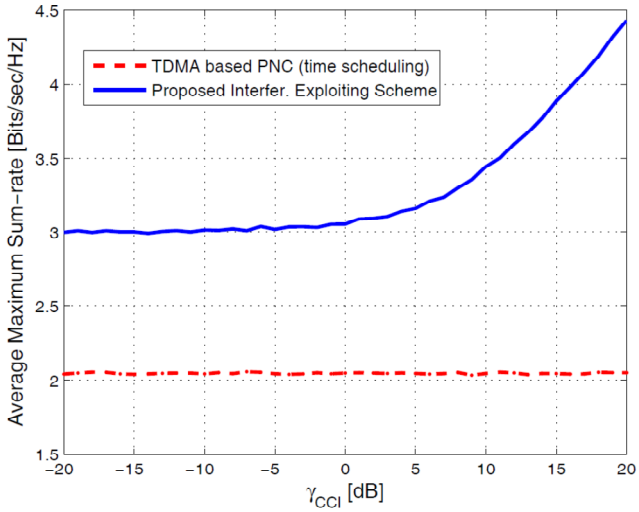

Figure 10-7 Comparison of Average Maximum Sum Rate between TDMA based PLNC and proposed scheme

10.2.4 Performance Evaluation

In this section, we evaluate the real performance (modulation-constraint) of the proposed scheme in terms of the normalized throughput (that is, the number of packets successfully transmitted per timeslot per user). In this simulation, we also consider the symmetric case for the 2-way relay channel in which $\gamma_{AC} = \gamma_{BH} = \gamma_{CCI}$. We assume that each link experiences a non-fading channel to give an upper bound of throughput, i.e. maximum throughput. We use the simplest 2nd order Hadamard Matrix to generate the orthogonal SS alphabet for MSs 1 and 2. In addition, we choose BPSK as the modulation scheme for each node. Unambiguous detection for BPSK modulated PLNC is implemented at the ABSs. The corresponding simulation results are shown in Figure 10-8.

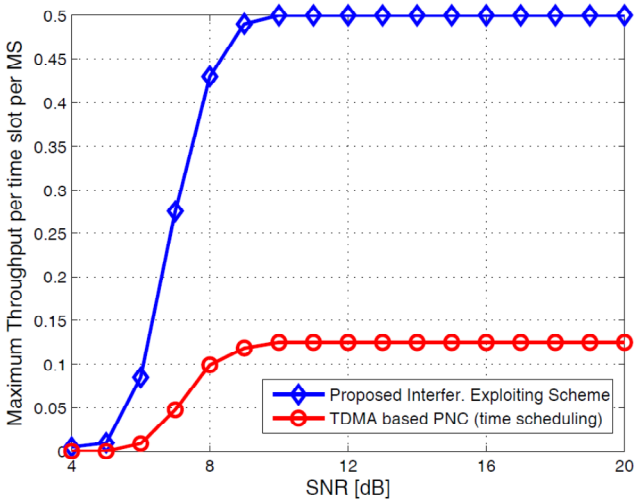

Figure 10-8 Comparison of maximum normalized throughput for MS

Based on Figure 10-8, it is clear that the performance of the proposed scheme outperforms the benchmark (time-scheduling scheme), there is a large improvement for the proposed scheme resulted from the reduced number of time-slots and the introduction of the transmit diversity.

10.3 Cooperative physical layer network coding for efficient backhaul transmission

Recently *wireless network coding* (an alternative term for *physical layer network coding* [Zha06]) has been introduced for wireless networks containing multiple nodes and multiple data flows. In particular the concept of *hierarchical decode and forward* (HDF) has been defined [Syk10]. The approach here is that an intermediate or relay node in a multihop wireless network which receives a superimposed combination of source symbols decodes and forwards some joint function of these symbols rather than either of the symbols alone. Typically this joint function is some linear operation on the Galois field containing the modulation constellation, a generalisation of the modulo-2 (XOR) function employed in the original physical layer network coding [Zha06]. This can then be combined at the destination with other information which may have come by a different route through the network to regenerate the original data symbols.

This section considers the application of this principle to uplink transmission in a hierarchical wireless network. We will show that it can have a similar effect to network MIMO in effectively eliminating interference between the ABSs, but does not increase the backhaul load. Here we consider a very small subset of the BuNGee network to demonstrate the principle, and restrict our attention to QPSK modulation, again for simplicity. In the next section we describe the network and system model, in section 10.3.2 we describe the network coding approach used at the ABSs, and in section 10.3.3 we determine the system throughput in terms of the mutual information, and give numerical results.

10.3.1 System model

For the purposes of illustration we use the simplest possible hierarchical network, referred to as the *minimal hierarchical network* in [Bur10], consisting of two terminals communicating with two ABSs and thence to a single hub, as illustrated in Figure 10-9. In this section we focus on the terminal-relay links, and assume that the relay-hub links are perfect, with unlimited signal to noise ratio, and mutually non-interfering. We assume that the links from each terminal to each ABS are subject to Rayleigh fading with channel gain from the i^{th} terminal to the j^{th} ABS given by h_{ji}, as shown in Figure 10-9. We assume that the direct link from the i^{th} terminal to the i^{th} ABS has unit mean square amplitude $\overline{|h_{ii}|^2} = 1, i = 1,2$, while what might be termed the "interfering link" has mean square amplitude a^2, $\overline{|h_{i,(2-i)}|^2} = a^2, i = 1,2$, where $1/a^2$ is defined as the *signal to interference ratio*.

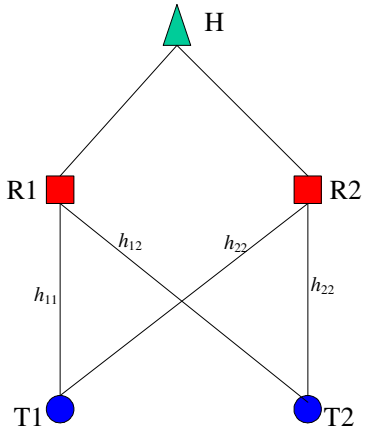

Figure 10-9 Minimal hierarchical network

If the transmitted symbol sequence at each terminal is represented by the vector $\mathbf{s}_i$, i =1,2, then the received signal at each ABS may be represented by:

$$\mathbf{r}_i = h_{i1}\mathbf{s}_1 + h_{i2}\mathbf{s}_2 + \mathbf{n}_i, i = 1,2 \tag{10.39}$$

where $\mathbf{n}_i$ is the vector of noise samples at ABS i. In this section we assume that hierarchical decode and forward processing [Syk10] is used at each ABS, in which what is decoded there is not necessarily either symbol sequence $\mathbf{s}_1$ or $\mathbf{s}_2$, but some sequence of symbols:

$$\mathbf{v}_i = \left\{ f_i\left(s_{11}, s_{21}\right), f_i\left(s_{12}, s_{22}\right), f_i\left(s_{13}, s_{23}\right)\ldots \right\} \tag{10.40}$$

where $f_i\left(x,y\right), i=1,2$ denotes a linear *mapping function*, in the Galois field sense, of the symbols *x*, *y*. (In the case of binary symbols, the XOR function commonly used for network coding is an example of such a function). The two ABSs then forward sequences $\mathbf{v}_1$ and $\mathbf{v}_2$ to the hub. The functions must be such that in combination they are unambiguously decodable, i.e:

$$\left(f_1\left(x,y\right), f_2\left(x,y\right)\right) = \left(f_1\left(x',y'\right), f_2\left(x',y'\right)\right) \text{iff } x=x' \,\&\, y=y' \tag{10.41}$$

This is equivalent to the *exclusive law* of [Syk10]; in the terms used in that paper, each function provides *complementary side information* (C-SI) for the other, to allow the original symbols to be decoded at the destination. We may then define a pair of single-valued functions such that:

$$x = g_1\left(f_1\left(x,y\right), f_2\left(x,y\right)\right); y = g_2\left(f_1\left(x,y\right), f_2\left(x,y\right)\right) \tag{10.42}$$

We assume that the states of all four channels between terminals and relays (i.e. the values $h_{ij}, i, j = 1,2$) are known to the relays and the hub. The mapping functions are then selected according to these channel states, firstly to ensure unambiguous decodability, and secondly to maximise the overall capacity. The details of these functions and the selection criteria are described in the next section for the case of QPSK.

10.3.2 Wireless Network Coding

We assume, as mentioned, that the mapping functions are linear in a Galois field sense: that is, that the symbols f_i, *x* and *y* are treated as members of an appropriate Galois field, and the symbol f_i returned is a linear function in the field of *x* and *y*:

$$f_i\left(x,y\right) = \alpha_i x + \beta_i y, i = 1,2 \tag{10.43}$$

where α_i and β_l are also members of the field and addition and multiplication are as defined within the field. Specifically the symbols are members of a binary extension field GF(2^q), and can be represented using binary words of length *q*: the constellation point labels. In this case the linear function can be represented in terms of multiplication by a binary matrix, using modulo-2 arithmetic. Multiplication by an element of GF(2^q) is represented by multiplication by a $q \times q$ matrix. Then:

$$f_i\left(x,y\right) \Leftrightarrow \mathbf{f}_i\left(\mathbf{x},\mathbf{y}\right) = \mathbf{A}_i\mathbf{x} + \mathbf{B}_i\mathbf{y} = \begin{bmatrix}\mathbf{A}_i & \mathbf{B}_i\end{bmatrix}\begin{bmatrix}\mathbf{x}\\ \mathbf{y}\end{bmatrix} = \mathbf{G}_i\begin{bmatrix}\mathbf{x}\\ \mathbf{y}\end{bmatrix}, i = 1,2 \tag{10.44}$$

where $\mathbf{f}_i$, **x**, and **y** are length *q* binary vectors representing the symbols.

Assuming perfect backhaul transmission, the data received at the hub can be represented as a composite vector:

$$\mathbf{f} = \begin{bmatrix}\mathbf{f}_1\\ \mathbf{f}_2\end{bmatrix} = \begin{bmatrix}\mathbf{A}_1 & \mathbf{B}_1\\ \mathbf{A}_2 & \mathbf{B}_2\end{bmatrix}\begin{bmatrix}\mathbf{s}_1\\ \mathbf{s}_2\end{bmatrix} = \begin{bmatrix}\mathbf{G}_1\\ \mathbf{G}_2\end{bmatrix}\begin{bmatrix}\mathbf{s}_1\\ \mathbf{s}_2\end{bmatrix} = \mathbf{G}\begin{bmatrix}\mathbf{s}_1\\ \mathbf{s}_2\end{bmatrix} \tag{10.45}$$

The invertibility condition of (10.41) is then fulfilled if **G** is invertible, i.e. if it is full rank. The inverse function is then given by multiplying by $\mathbf{G}^{-1}$.

Hence mapping functions at the relays, defined by $\mathbf{G}_1$ and $\mathbf{G}_2$, should be chosen first to ensure that the composite matrix **G** is full rank. Secondly they should be chosen according to the channel fading coefficients to maximise the total throughput. This can be determined by the mutual information of the constellations at the ABSs. However when the mapping function is applied it is the mutual information of the mapped constellation which is important. If the transmission rate of coded symbols from the source terminals is less than the minimum of these mutual informations at the two ABSs then the network coded symbols can be decoded without error at both ABSs, and given that the mappings at the two ABSs are jointly invertible this ensures that the original source data can be recovered at the hub.

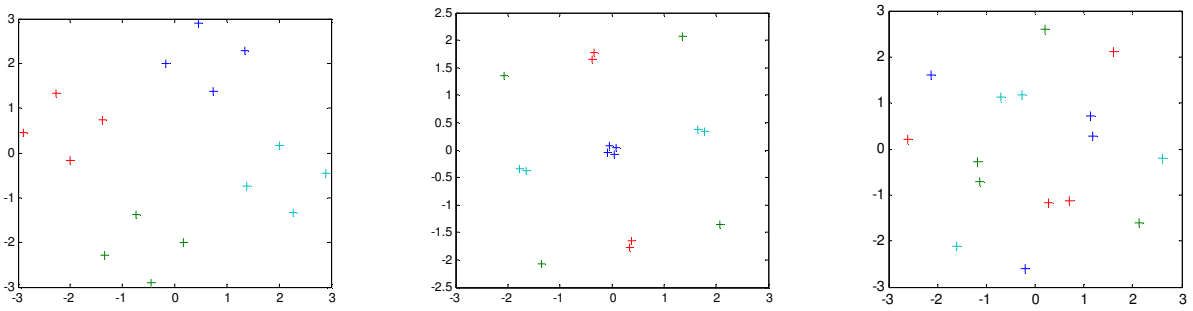

(a) (b) (c)

Figure 10-10 Mapped received constellations at ABS for different channel fading states, with QPSK signalling

Figure 10-10 shows typical received constellations at an ABS for different channel fading states, with QPSK signalling from the terminals. Appropriate mapping functions are applied at the ABS which assign different received points to different network coded symbols. The points corresponding to the same network coded symbol are plotted in the same colour in the figure.

The mutual information between the received signal and the network coded symbol, as represented by the colours of the constellation points, is affected by the equivocation of the received point with two or more different network coded symbols, which in Gaussian noise is determined by the distance of the received point from the each. This will be minimised if the minimum distance between any points of any two different network code symbols is maximised. The mapping should therefore be chosen to maximise this minimum distance by choosing the optimum clustering of received points into network code symbols.

In principle a search may be performed through all the possible pairs of mappings, corresponding to all the 2^{4q^2} binary matrices **G** to determine the full rank matrix which maximises the minimum distance over the received mapped constellations at both ABSs. This however would require a very large number of possible mappings to be examined. In practice we have found that several different mappings give the same minimum distance for a given set of channel fading coefficients, and in fact that a much reduced subset of the possible mappings is sufficient to ensure that an optimum mapping can always be found among them.

In fact all the mapping matrices used are made up of a combination of the 9 rows given Table 10-1. A mapping function consisting of one of these rows will divide the received constellation into two groups of 8 points. Hence at each ABS we must choose two of these rows which are linearly independent, both of which maximise the minimum distance between these groups of points. Then we must ensure that the rows chosen at the other ABS are also both linearly independent of the first two, ensuring that the complete matrix **G** is full rank. In some cases such a choice is not available which also simultaneously maximises minimum distance at both ABSs: in this case the choice is made which results in the largest minimum distance over the two ABSs.

Table 10-1 Rows of mapping matrices G

a	1	0	0	0
b	0	1	0	0
c	0	0	1	0
d	0	0	0	1
e	1	0	1	0
f	0	1	0	1
g	1	0	0	1
h	0	1	1	0
i	1	1	0	1

It is interesting to consider the effect of some of these mapping matrices. For example a matrix at one ABS made up of rows *a* and *b* would simply map according to the first terminal symbol, neglecting the other terminal. This would be optimum if one signal is much stronger than the other, as in the constellation

illustrated in Figure 10-10 (a). Similarly rows *c* and *d* would map according to the second terminal symbol. Rows *e* and *f* effectively form the XOR of the two bits of the constellation labels. This might be optimum in the case of the constellation of Figure 10-10(b); in some cases rows *g* and *h* may be optimum there (depending on the relative phase shift).

Note that in some cases, where symbols from both terminals are heavily attenuated at one ABS, it may be preferable to ignore that ABS, and instead decode both symbols at the other ABS and forward that to the destination. This case can also be treated as a special case of the network coding in which one of the $\mathbf{G}_i$'s is set to the unit matrix while the other is null, and selected when optimum in the same way as the others.

10.3.3 Numerical results for mutual information

The mutual information of the received signal and the network coded constellation:

$$I(S;R) = H(S|R) - H(S) \tag{10.46}$$

where:

$$H(S|R) = -\sum_S P(S) \int p(r|S) \log_2 \left(P(S|R) \right) dr \tag{10.47}$$

Using Bayes' theorem:

$$P(S|r) = \frac{p(r|S)P(S)}{p(r)} = \frac{p(r|S)P(S)}{\sum_S P(S)\, p(r|S)} \tag{10.48}$$

Then:

$$H(S|r) = -\sum_S P(S) \int p(r|S) \log_2 \left(\frac{p(r|S)P(S)}{\sum_{S'} P(S')\, p(r|S')} \right) dr \tag{10.49}$$

Let the network coded constellation consist of *M* clusters of *L* points each, each cluster corresponding to the same network coded symbol:

$$\begin{aligned} S &= \{S_1, \ldots S_m, \ldots S_M\} \\ S_m &= \{S_{m1}, \ldots S_{ml}, \ldots S_{mL}\} \end{aligned} \tag{10.50}$$

where the mapping of points to symbols is determined by the mapping matrix $\mathbf{G}_i$.

Then:

$$P(r|S_m) = \sum_{l=1}^{L} P(S_{ml})\, p(r|S_{ml}) \tag{10.51}$$

$$H(S|R) = -\sum_m P(S_m) \int p(r|S_{ml}) \log_2 \left(\frac{\sum_l P(S_{ml})\, p(r|S_{ml})}{\sum_{m'} \sum_{l'} P(S_{m'l'})\, p(r|S_{m'l'})} \right) dr \tag{10.52}$$

where the conditional pdf $p(r|S_{ml})$ is Gaussian. This can be evaluated numerically using Monte Carlo integration, given the constellation and hence the points corresponding to each S_{ml}. In addition the fading coefficients are assigned randomly and in each case the optimum pair of mapping functions is determined as described in the previous section. The total mutual information is assumed to be given by twice the minimum mutual information at the two ABSs (since source symbols may only be reliably decoded if both network coded symbols are successfully decoded at the ABSs). The simulation is then used to obtain the pdf of the throughput over the random fading, and hence a plot of outage probability against throughput.

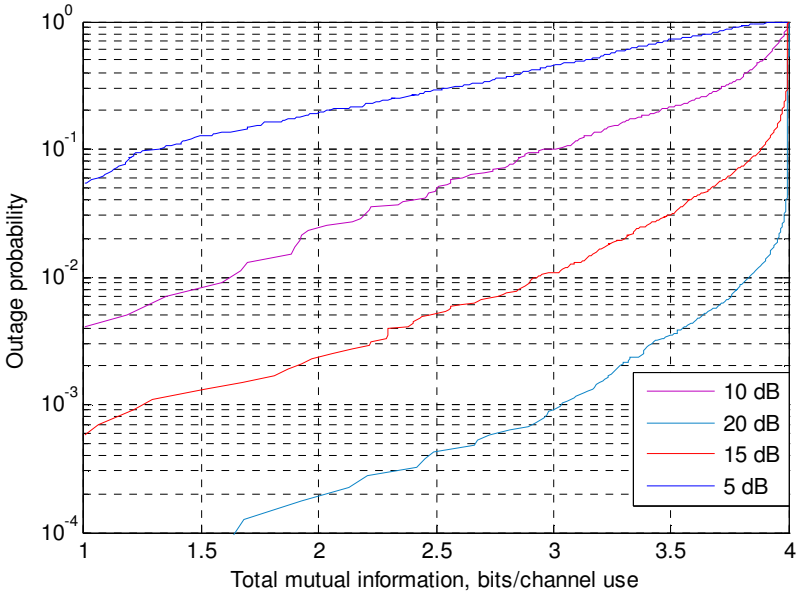

Figure 10-11 Outage probability* versus *throughput for network coded hierarchical network, SIR 0 dB, various SNR.

Figure 10-11 shows the resulting curves for the network coded system, with SNR as a parameter, and SIR 0 dB (that is, with average fading the same from each terminal to each ABS). We note that a diversity order of 2 is obtained, since at least selection diversity is available between the ABSs. As a baseline for comparison, the equivalent results for a conventional non-cooperative system, in which each ABS serves one terminal only, are shown in Figure 10-12. We note here that only first order diversity is obtained, and that outage capacity is much improved in the network coded case: for example for SNR 15 dB the 1% outage capacity is increased by a factor of more than 3.

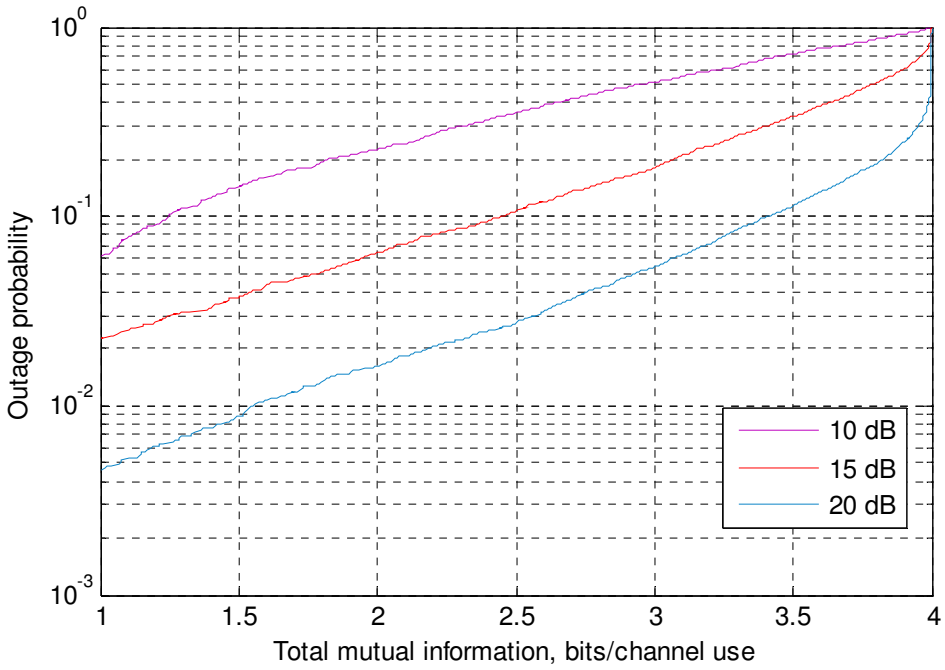

Figure 10-12 Outage* versus *throughput for non-cooperative system

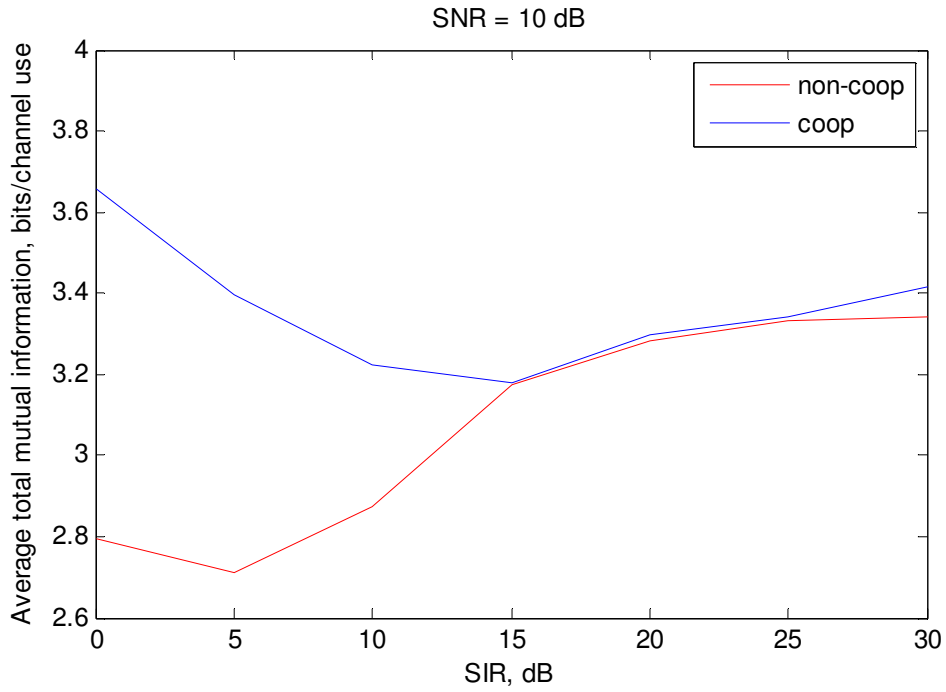

Figure 10-13 Average mutual information* versus *SIR

Figure 10-13 shows the average throughput for the two systems, this time plotted against SIR for SNR 10 dB. We note that while as a general rule for the non-cooperative system the throughput increases with SIR, as one might expect, for the cooperative system it in fact decreases. This is because the system exploits what would otherwise be interference in a non-cooperative system, in a way very similar to network MIMO. Note however that for relatively large SIR the two system throughput is very similar, since the advantages of cooperation are then negligible.

10.4 Fading correction scheme for PLNC

10.4.1 Simple Model of PLNC in TWR Channel

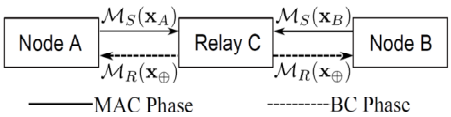

Figure 10-14 Simple model of PLNC in TWR Channel

The TWR channel consists of 2 nodes and 1 relay (Figure 10-14). PLNC allows 2 nodes using the same modulation scheme $\mathrm{M}_S(.)$ to transmit signal simultaneously in the MAC phase. The electromagnetic signals are superimposed and received by the relay, given by

$$\mathbf{y}_R = h_A\mathbf{s}_A + h_B\mathbf{s}_B + \mathbf{n}_R \tag{10.53}$$

where $\mathbf{s}_i = \mathrm{M}_S(\mathbf{x}_i), i \in \{A,B\}$ is the modulated symbol for each node, in particular, we assume that both nodes employ Gray mapped QPSK whose constellation has *unity energy* (thus, $s_i \in \mathscr{A}_4 \ \forall s_i \in \mathbf{s}_i$, where $\mathscr{A}_4$ is the QPSK alphabet). The codeword $\mathbf{x}_i$ is obtained by encoding the data word $\mathbf{d}_i, i \in \{A,B\}$. For QPSK, each symbol in codeword sequence can be represented as a 2-bit binary tuple, i.e., $x_i \in \mathrm{Z}_4, i \in \{A,B\}$ (where $\mathrm{Z}_q = \{0,1,...q-1\}$). We refer to the result of the bit-wise eXclusive-OR operation on x_A and x_B as the network coded symbol $x_\oplus$, i.e., $x_\oplus = x_A \oplus x_B$ which also takes the form of a 2-bit binary tuple. Both nodes are assumed to be memoryless uniform sources and they employ an identical codebook C. h_A and h_B are the

channel gains from nodes A and B to relay C, respectively. $\mathbf{n}_R$ is the complex Additive Gaussian White Noise (AWGN) with variance σ_w^2 per complex dimension. We substitute the *superimposed signal* $\mathbf{s}_\oplus = h_A\mathbf{s}_A + h_B\mathbf{s}_B$ into (1) to obtain $\mathbf{y}_R = \mathbf{s}_\oplus + \mathbf{n}_R$. The relay processes the received signal and forwards network coded data stream $\mathbf{x}_\oplus$ or its variations (quantized version etc.) with modulation scheme $\mathrm{M}_R(.)$ for the BC phase.

Normally, it is assumed that the *channel status information* (CSI) is perfectly known to the receiver side only, that is, to the relay only for the MAC phase and to the destination nodes only for the BC phase. We pay particular attention to the fading in MAC phase since there is no signal superimposition in BC phase and the fading can be well compensated for the nodes using perfectly known CSI (After channel compensation, the fading in BC phase would cause only a scaling effect at each node, which is the same as the case of point-to-point channel. So this is not our major focus). Thus, we can suppose that the BC phase is *non-fading*. For simplicity, it is also assumed that the relay transmits with the same power as both sources and the noise variance is again σ_w^2. The signal broadcasted by the relay is denoted as $\mathbf{s}_R$. The received signal at the nodes can thus be represented as

$$\mathbf{y}_i = \mathbf{s}_R + \mathbf{n}_i \tag{10.54}$$

where $\mathbf{n}_i$ is the complex AWGN at node i ($i \in \{A, B\}$).

10.4.2 Detailed Structure of Proposed Scheme

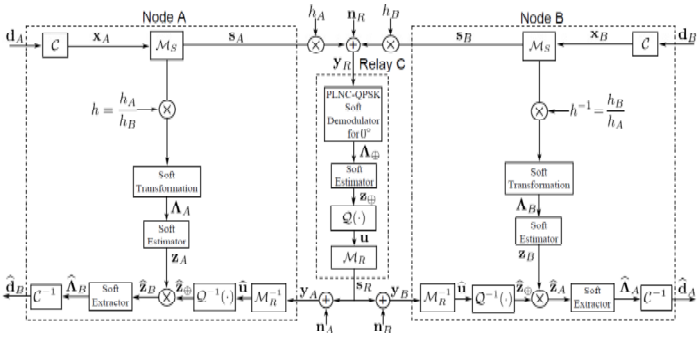

Figure 10-15 System diagram of proposed scheme

The block diagram of the proposed scheme is shown in Figure 2-2. Based on (10.54), we denote the relative fading factor as $h = h_A / h_B = re^{j\varphi}$ (r is the channel amplitude ratio and φ is the phase shift).

Generating network coded soft-bit

The reliability of the superimposed code is obtained by the designed PLNC-QPSK soft demodulator. Detecting the network coded symbol is based on the MAP (Maximum A Posteriori) principle. We use $x_{\oplus,n}(s_\oplus)$ to denote the *n*-th ($n \in \{1,2\}$) bit in the network coded symbol corresponding to the superimposed signal $s_\oplus$. The bit-wise network coded LLR (log-likelihood ratio) can be computed as

$$\Lambda_{\oplus,n} = \ln\left(\frac{p(x_{\oplus,n}(s_\oplus)=0 \mid y_R)}{p(x_{\oplus,n}(s_\oplus)=1 \mid y_R)}\right), n \in \{1,2\} \tag{10.55}$$

where, for each network coded bit $x_{\oplus,n}(s_\oplus)$, the alphabet of the superimposed signal, $\mathrm{S}_\oplus$,can be split into two parts: $S_n^{(0)}$ and $S_n^{(1)}$, which correspond to $x_{\oplus,n}(s_\oplus)=0$ and $x_{\oplus,n}(s_\oplus)=1$, given as: $S_n^{(0)} = \{s_\oplus \mid x_{\oplus,n}(s_\oplus)=0, s_\oplus \in \mathrm{S}_\oplus\}$ and $S_n^{(1)} = \{s_\oplus \mid x_{\oplus,n}(s_\oplus)=1, s_\oplus \in \mathrm{S}_\oplus\}$. (10.55) can thus be rewritten as

$$\Lambda_{\oplus,n} = \ln\left(\frac{\sum_{s_\oplus \in S_n^{(0)}} p(y_R \mid s_\oplus)P(s_\oplus)}{\sum_{s_\oplus \in S_n^{(1)}} p(y_R \mid s_\oplus)P(s_\oplus)}\right), n \in \{1,2\} \tag{10.56}$$

where $p(y_R \mid s_\oplus)$ is the conditional probability density function (PDF) of the received signal and $P(s_\oplus)$ is the prior probability. Both depend on the mapping strategy of the soft demodulator. Figure 10-15 illustrates the

PLNC superimposed constellation with 0° phase shift, i.e., $\mathrm{S}_{\oplus}\left(0^\circ\right)$ ($\mathrm{M}_{\oplus} \Rightarrow m, m \in \mathscr{A}_4$ represents the eXclusive-OR mapping of the superimposed signals onto the QPSK alphabet). Then $p(y_R \mid s_{\oplus})$ can be calculated as

$$p(y_R \mid s_{\oplus}) = \frac{1}{2\pi\sigma_w^2} \exp(-\frac{\left|y_R - s_{\oplus}\right|^2}{2\pi\sigma_w^2}),\ s_{\oplus} \in \mathrm{S}_{\oplus}\left(0^\circ\right) \tag{10.57}$$

Note that there is no adaptive-selection in our proposed scheme. Regardless of the channel parameters, the relay employs only one PLNC-QPSK soft demodulator, that corresponding to the superimposed constellation $\mathrm{S}_{\oplus}\left(0^\circ\right)$ with $\varphi = 0^\circ$ and $r = 1$. The network coded soft-bit can be calculated as

$$\mathbf{z}_{\oplus} = \tanh(\mathbf{\Lambda}_{\oplus} / 2) \tag{10.58}$$

where $\tanh(\cdot)$ is the hyperbolic tangent function. The soft-bit has several advantages compared with LLR:

1. the hyperbolic tangent domain has a fixed range [-1,+1] rather than $(-\infty, +\infty)$ for the logarithm domain;
2. the eXclusive-OR operation in hyperbolic tangent domain is simpler than that in logarithm domain;
3. the soft-bit is more effective than the LLR in power constrained scenarios.

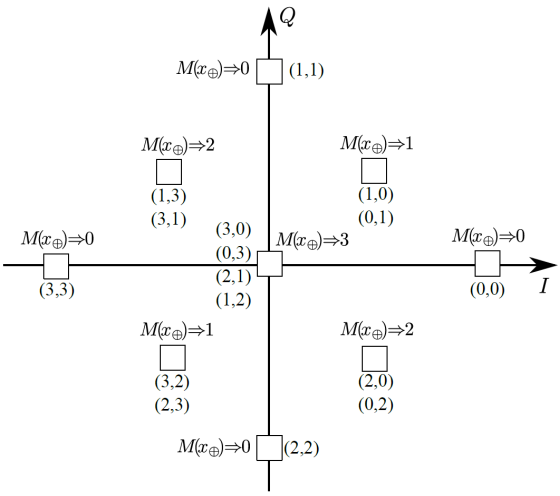

Figure 10-16 Superimposed constellation for $h = h_A / h_B = 1$

Robust Quantize-and-Forward for TWR fading channel

Note that directly transmitting analogue signal in digital communication systems is technically nontrivial. There are several quantize-and-forward strategies which have been proposed to overcome the weakness of broadcasting the analogue signal. In [Zei09] and [Win11], an information bottleneck method (IBM) is involved to quantize the LLR in the TWR channel. However, note that this scheme is designed for the AWGN channel and is not optimized for PLNC. In addition, our soft-bit correction scheme is applied on the soft-bit rather than the LLR level.

Consider that the amplitude of the soft-bit lies only within the range [-1,+1]. A big amplitude variation in the logarithm domain (for the LLR) transforms to only a small change in the hyperbolic tangent domain (for soft-bit). Inspired by this, we suggest that the mean-square error (MSE) optimal quantization (Lloyd [Llo82]-Max [Max60]) would be suitable for the soft-bit. The Lloyd-Max algorithm determines quantization levels based on minimizing the MSE for the input signal with a known distribution. So it is necessary to find out the statistical properties of the soft-bit to achieve the optimal quantization.

According to Bayes' principle, the PDF of the received signal can be expressed as

$$p_{Y_R}(y_R) = \sum_{s_{\oplus} \in \mathrm{S}_{\oplus}(0^\circ)} p(y_R \mid s_{\oplus}) P(s_{\oplus}) \tag{10.59}$$

The transformation for a function of a random variable [Zwi00] to calculate the PDF of network coded LLR can be expressed as

$$p_{\Lambda_{\oplus}}(\lambda) = p_{Y_R}(w(\lambda)) \left|\frac{dw(\lambda)}{d\lambda}\right| \tag{10.60}$$

where λ is the random variable for network coded LLR and $w(\lambda)$ is the inverse function of (10.56) for variable y_R. Based on (10.56), (10.59) and (10.60), the distribution of the network coded LLR can be calculated as

$$p_{\Lambda_\oplus}(\lambda)=\frac{2\exp\left(-\lambda-\cosh^{-1}(-\lambda+\frac{1}{\sigma_n^2})-\frac{1}{4}\sigma_n^2\cosh^{-1}(-\lambda+\frac{1}{\sigma_n^2})^2\right)\left(1+\exp(2\cosh^{-1}(-\lambda+\frac{1}{\sigma_n^2}))+2\exp(\cosh^{-1}(-\lambda+\frac{1}{\sigma_n^2}))\right)\sigma_n}{8\sqrt{\pi\exp(-2\lambda+\frac{2}{\sigma_n^2})}} \quad (10.61)$$

Note that because of the symmetry of the points on the superimposed constellation, both the 1st bit $\Lambda_{\oplus,1}$ and 2nd bit $\Lambda_{\oplus,2}$ obey the same distribution as (10.61). Similarly, the PDF of the soft-bit can also be calculated by the transformation for a function of a random variable:

$$p_{Z_\oplus}(z)=p_{\Lambda_\oplus}(h(z))\left|\frac{dh(z)}{dz}\right| \quad (10.62)$$

where z is the random variable for the soft-bit and $h(z)$ is the LLR extraction function, denoted as $h(z)=2\tanh^{-1}(z)$. The final PDF of the soft-bit thus can be derived as:

$$p_{Z_\oplus}(z)=\frac{2\exp\left(-2\tanh^{-1}(z)-\cosh^{-1}(-2\tanh^{-1}(z)+\frac{1}{\sigma_n^2})-\frac{1}{4}\sigma_n^2\cosh^{-1}(-2\tanh^{-1}(z)+\frac{1}{\sigma_n^2})^2\right)\left(1+\exp(2\cosh^{-1}(-2\tanh^{-1}(z)+\frac{1}{\sigma_n^2}))+2\exp(\cosh^{-1}(-2\tanh^{-1}(z)+\frac{1}{\sigma_n^2}))\right)\sigma_n}{4(1-z^2)\sqrt{\pi\exp(-4\tanh^{-1}(z)+\frac{2}{\sigma_n^2})}} \quad (10.63)$$

The theoretical analysis of the PDF (10.63) can be verified by *Monte-Carlo simulation*. Figure 10-17 illustrates the comparison between the theoretical and simulated PDF of the soft-bit. The consistency between the theoretical and simulated results is clear, which implies that based on our derived theoretical PDF, the optimum MSE quantization in the non-fading MAC phase can be achieved.

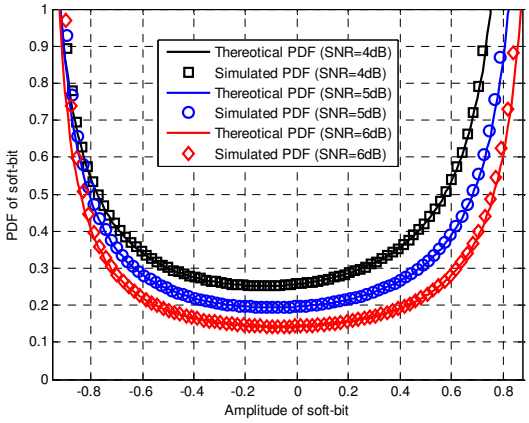

Figure 10-17 Comparison between theoretical and simulated PDF for soft-bit with different SNRs in non-fading MAC phase

Next, we need to check the robustness of our design in approaching the quantization in fading MAC phase. We assume that the two channel links in the MAC phase have same power: $E[|h_A|^2]=E[|h_B|^2]$ (where, $E[.]$ is the expectation function) to respect the symmetrical rates from A and B. We denote the average SNR in MAC phase as $E[|h_A|^2+|h_B|^2]/2\sigma_w^2$. An extreme scenario for relative fading factor is also considered, where the phase shift obeys: $\varphi \sim U(0^\circ,360^\circ)$. Figure 2-5 shows the comparison between PDF for soft-bit in the non-fading and fading MAC phase .

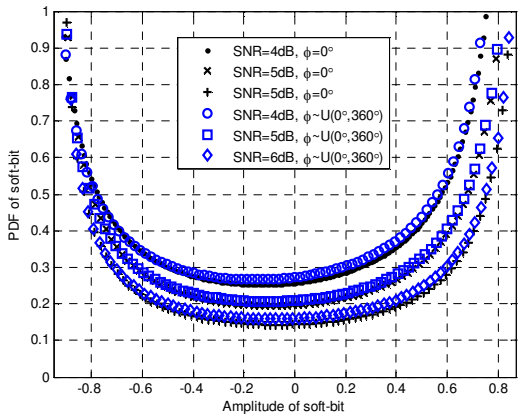

Figure 10-18 Comparison between simulated PDF for soft-bit in non-fading MAC phase and fading MAC phase with different SNRs

Based on Figure 10-18, it is clear that although the phase shift fading varies dramatically, the statistical properties of the soft-bit changes only slightly. This implies that our designed MSE quantization can be approximated in the fading MAC phase. But it is still not certain that this is a robust solution. So in the following parts of the paper, we successively measure the performance loss in terms of both MSE and mutual information (as shown in Figure 10-19 and 2-7, respectively).

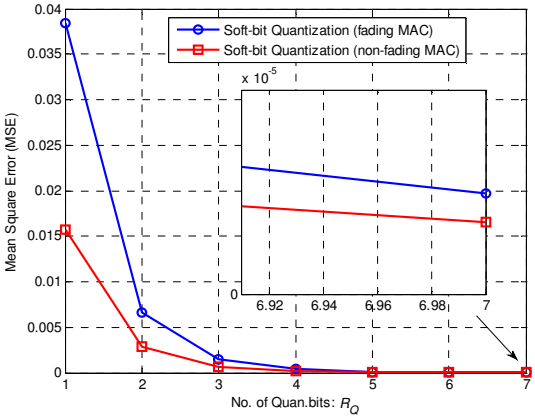

Figure 10-19 MSE vs. number of quantization bits when SNR=10dB

The designed MSE quantizer $\mathrm{Q}(\cdot)$ has 2^{R_Q} levels (R_Q is the number of quantization bits). If a soft-bit $z_{\oplus}$ is located within the quantization interval ℓ_u ($u \in \{0,1,...,2^{R_Q}-1\}$ is quantization index), the quantizer maps it to the reconstruction value $\hat{z}_{\oplus}$. This procedure can be described as

$$\mathrm{Q}(z_{\oplus}) = \hat{z}_{\oplus}, \; if \; z_{\oplus} \in \ell_u \tag{10.64}$$

where each quantization interval ℓ_u is iteratively calculated by the implementation of the Lloyd-Max algorithm.

In Figure 10-19, we set SNR equal to 10dB, obviously, the more quantization bits involved, the higher quantization precision can be provided. We observe that if the number of quantization bits $R_Q \geq 3$, the MSE for the fading MAC can achieve almost the same level as that for the non-fading case.

The mutual information loss ΔI can be measured as the difference between the unquantized and the quantized mutual information: $\Delta I = I_{unquant.} - I_{quant.}$. Here, the unquantized mutual information is the bit-wise mutual information between network coded bit and network coded LLR. In practice, this can be calculated by the ergodicity theorem [Hag04]

$$I_{unquant.} = I(\tilde{x}_{\oplus,k}; \Lambda_{\oplus,k}) \approx 1 - \frac{1}{K}\sum_{k=1}^{K} \log_2(1 + e^{-\tilde{x}_{\oplus,k} \cdot \Lambda_{\oplus,k}}) \tag{10.65}$$

where $K = \mathrm{length}(\mathbf{x}_{\oplus})$ and $k \in \{1,2...K\}$. As the binary antipodal signal for the network coded bit, $\tilde{x}_{\oplus,k}$ is defined in GF(2) with the elements {+1, -1} (where +1 represents the 'null' element). Note that for (10.65), a

long data sequence would guarantee the availability and precision of the measure of the mutual information even for a non-Gaussian or unknown distribution [Tuc02] (It is clear from (9) that the distribution of $\Lambda_{\oplus,k}$ is non-Gaussian). Moreover, by invoking the definition of fidelity in [Hag04] and [Tuc02]: $E[z_{\oplus}]=\frac{1}{K}\sum_{k=1}^{K}\tilde{x}_{\oplus,k}\cdot z_{\oplus,k}$, (10.65) can be rewritten as

$$I_{unquant.}\approx\frac{1}{K}\sum_{k=1}^{K}\log_2(1+\tilde{x}_{\oplus,k}\cdot z_{\oplus,k}) \tag{10.66}$$

Note that (10.66) is also not limited to the Gaussian distribution. Thus, the measure of the mutual information can be transformed to the soft-bit domain. Similarly, the quantized mutual information can be expressed as

$$I_{quant.}=I(\tilde{x}_{\oplus,k};\hat{\Lambda}_{\oplus,k})\approx\frac{1}{K}\sum_{k=1}^{K}\log_2(1+\tilde{x}_{\oplus,k}\cdot\hat{z}_{\oplus,k}) \tag{10.67}$$

where, $\hat{\Lambda}_{\oplus,k}$ is the recovered bit-wise network coded LLR, which is $\hat{\Lambda}_{\oplus,k}=2\tanh^{-1}(\hat{z}_{\oplus,k})$ and $\hat{z}_{\oplus,k}$ is the reconstruction value of soft-bit: $\hat{z}_{\oplus,k}=\mathrm{Q}^{-1}(u_k)$.

Figure 10-20 shows the comparison of the mutual information loss for quantization with different numbers of bits between the fading and non-fading MAC phase. Here, we choose 10^7 bits per frame and 10000 frames for *Monte-Carlo evaluation* of (10.66) and (10.67) to guarantee the precision. The simulation results imply that:

1. with $R_Q\geq 2$, the mutual information loss ΔI can decrease to an acceptable level ($<4\times10^{-2}$) for the quantization in both fading and non-fading MAC phase;
2. the performance degradation caused by the designed approximated quantization for TWR fading channel is small if the number of quantization bits $R_Q\geq 2$.

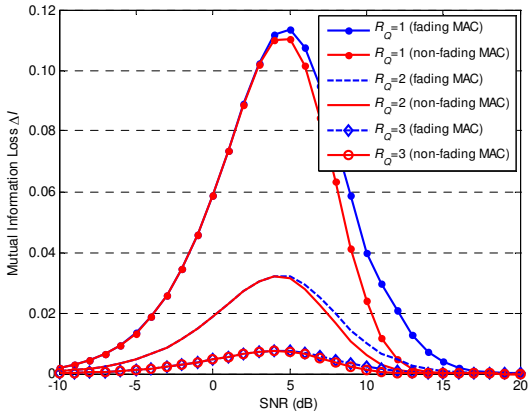

Figure 10-20 Comparison of bit-wise Mutual Information Loss ΔI .

Soft-bit fading correction at each node

In this sub-section, we explore the soft-bit fading correction at each node, which is based on the following principles

$$\begin{aligned}\hat{\mathbf{x}}_B&=[F(\mathbf{x}_A)\oplus\mathbf{x}_B]\oplus F(\mathbf{x}_A)\\ \hat{\mathbf{x}}_A&=[\mathbf{x}_A\oplus F'(\mathbf{x}_B)]\oplus F'(\mathbf{x}_B)\end{aligned} \tag{10.68}$$

where $F(.)$ represents the effect of the relative fading factor $h=h_A/h_B$ on the data stream from node A, and $F'(.)$ represents the effect of the reciprocal of the relative fading factor $h^{-1}=h_B/h_A$ on the data stream from node B. From node A's perspective, the data stream broadcast by the relay affected by fading can be represented as $F(\mathbf{x}_A)\oplus\mathbf{x}_B$ and from node B's perspective, it is $\mathbf{x}_A\oplus F'(\mathbf{x}_B)$. The corrected data at each node is denoted as $\hat{\mathbf{x}}_i, i\in\{A,B\}$. Note that we apply this principle at the level of the soft-bit. Unlike hard bits, the soft-bit contain reliability information rather than simply '1' or '0'. The following equations show the equivalent relationship between hard bits and soft-bit for the eXclusive-OR operation

$$\mathbf{x}_{\oplus} = \mathbf{x}_A \oplus \mathbf{x}_B \;\Leftrightarrow\; \mathbf{z}_{\oplus} = \mathbf{z}_A . \times \mathbf{z}_B \tag{10.69}$$

Note both '$\oplus$' and '$.\times$' are bit-wise operation.

Besides the principle for fading correction of the soft-bit, the *correction factor* is also important. The correction factor for node A then equals the relative fading factor $h = h_A / h_B$; for node B, it is the reciprocal of the relative fading factor $h^{-1} = h_B / h_A$. Note that the destination nodes do not know the relative fading factor. Thus we need to quantize the relative fading factor. Since we assume symmetric channel power for both channel links in MAC phase, only the phase shift needs to be quantized uniformly over unit circle. Here, we apply 8-bit quantization to ensure sufficient accuracy for the phase shift. The quantized relative fading factor is inserted in the payload of each frame.

For nodes A and B, the modulated signals will multiply the relative fading factor/its reciprocal, respectively. Next, the single user end-to-end QPSK soft demodulator is used to transform these faded signals into soft information $\mathbf{\Lambda}_A$ and $\mathbf{\Lambda}_B$. Then they are fed to the soft estimator to obtain their own soft-bit $\mathbf{z}_A$ and $\mathbf{z}_B$, which can be treated as the Complementary Side Information (C-SI) at each node. The C-SI contains the fading information which corresponds to that included in the network coded soft-bit. After recovering the network coded soft-bit $\hat{\mathbf{z}}_{\oplus}$, the fading correction at the soft-bit level can be expressed using the following equations. This is equivalent to the correction principle (10.68)

$$\hat{\mathbf{z}}_B = \hat{\mathbf{z}}_{\oplus} \times \mathbf{z}_A \;\text{ and }\; \hat{\mathbf{z}}_A = \hat{\mathbf{z}}_{\oplus} \times \mathbf{z}_B \tag{10.70}$$

where $\hat{\mathbf{z}}_i, i \in \{A, B\}$ represents the fading corrected soft-bit which can be extracted to obtain the corrected LLR ($\hat{\mathbf{\Lambda}}_i = 2\tanh^{-1}(\hat{\mathbf{z}}_i), i \in \{A, B\}$) for decoding. The mismatch caused by the fading between the data bits and parity bits can be removed by the soft-bit correction. Thus, the system can utilize the error-correction capability of the channel code.

Optimized mapping for UEP based Broadcasting

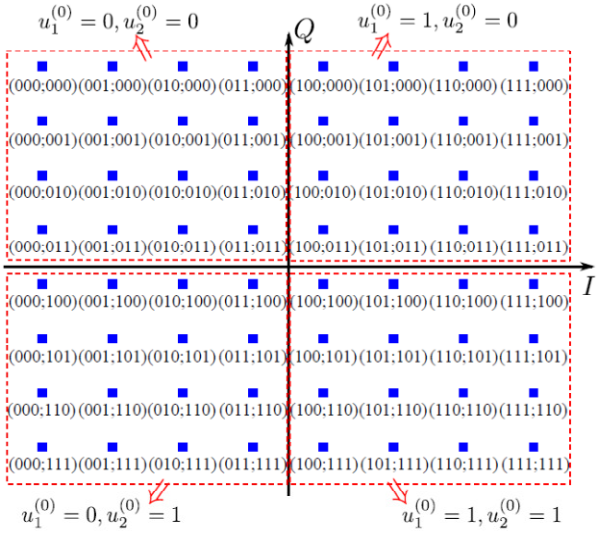

Figure 10-21 64QAM Mapping with UEP for broadcasted quantization indices

Note that each network coded symbol carries two soft-bits, each soft-bit is quantized separately. So there are two quantization indices associated with one network coded symbol. If we apply 2-bit quantization, a group of quantization indices corresponding to a specific network coded symbol can be represented by their binary form: $(u_1^{(0)}, u_1^{(1)}; u_2^{(0)}, u_2^{(1)})$, where $u_n^{(0)}$ and $u_n^{(1)}$ ($n \in \{1, 2\}$) represent the MSB (Most Significant Bit) and the LSB (Least Significant Bit) in binary representation of the index which corresponds to the *n*-th bit of the network coded symbol. Similarly, if 3-bit quantization is applied, the binary form for quantization indices can be represented as $(u_1^{(0)}, u_1^{(1)}, u_1^{(2)}; u_2^{(0)}, u_2^{(1)}, u_2^{(2)})$. In order to conserve bandwidth efficiency and without reducing throughput, we should keep the transmission rate equal for the MAC and BC phase. Thus the 16QAM and 64QAM need to be employed for 2-bit and 3-bit quantization. It is obvious that different bits in the quantization index have different importance. Note that the MSB of the quantization index determines the sign of the quantized soft-bit. If an error occurs in MSB, a sign error will occur which could lead to a serious

decision error. So the Gray mapping is not optimal. In [Zeg90], the authors use the *binary switching algorithm* (BSA) to find an optimal mapping to achieve unequal error protection (UEP) for LLR quantization. We test the availability of BSA and find that *the natural mapping gives the same results as using BSA*. In Figure 10-21, the optimal/natural mapping for 64QAM is illustrated. We can clearly observe that UEP for the bits with different significance is achieved.

10.4.3 Simulation Results

In this section, we evaluate the BER (bit error rate) performance of the proposed scheme. Both h_A and h_B are assumed to be frequency-flat, quasi-static *Rayleigh* fading channels. The length of the original data packet on each node is 5000 bits. Then the data packet is encoded by a rate 1/3 turbo code with generator polynomials: $(G_r, G) = (37, 21)_8$ (where G_r stands for the recursive code polynomial). The number of decoding iterations at the nodes is **18** for all simulations. The BER performance is measured at one of the nodes because of the symmetry of the TWR channel. The simulation scenario includes channel links from node to relay (MAC phase) and relay to node (BC phase). So the average SNR in the MAC phase as defined above is unsuitable here. Considering the bit-wise property of the soft-bit, we choose E_b/N_0 (Bit Energy to Noise Power Spectral Density Ratio) as the simulation parameter. Note that due to the symmetry of the TWR channel, the values of E_b/N_0 on MAC and BC phase are set to be equal. Figure 10-22 shows the corresponding simulation results.

In order to independently test the fade resistance capability of soft-bit correction, we introduce a perfect scenario in which the fading in MAC phase is set as described above but the BC phase is assumed to be undistorted (Suppose that the soft-bits are unquantized and perfectly received by each node). From Figure 10-22, we can see that, in such a scenario, the BER curve of the soft-bit correction scheme can rapidly converge to a low level compared with the scheme without soft-bit correction (In the case of without soft-bit correction, the relative fading causes the failure of the exclusive law and further leads to a mismatch between data bits and parity bits). It implies that the soft-bit correction could erase the fading effects on MAC phase and utilize the error-correction ability for channel codes.

To test the realistic performance, we separately choose 3-bit and 2-bit quantization for soft-bit correction (including the optimized mapping and a distorted BC phase). From Figure 10-22, it is clear that the performance of 3 bit quantization with optimized 64QAM mapping can closely approach the limit for soft-bit correction in a perfect scenario. And we can conclude that in the BC phase, the quantization error will be the dominant factor affecting performance, rather than the noise.

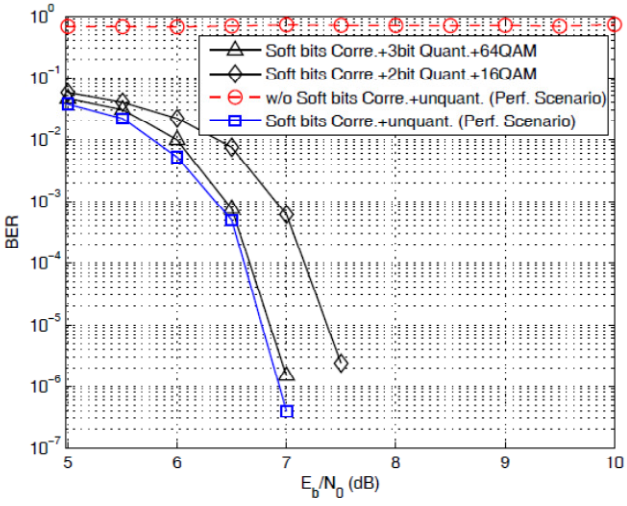

Figure 10-22 Comparison of BER performance

10.5 Conclusions

This section has considered the application of physical layer network coding to hierarchical wireless networks such as the BuNGee network architecture. It has shown that the concept of the two-way relay channel can be extended to such a network, which can be viewed as a series of interfering two-way relay networks, with the ABS taking the role of the relay. This implies that the backhaul and access segments of

the network can share the same channel, more readily allowing frequency re-use between the two segments. Two approaches have been investigated, based on amplify-and-forward and upon DS-CDMA decode-and-forward relaying: in both cases it has been shown that the 'interference' between the relay channels in the network can be exploited, to yield a form of network MIMO benefit. Note however that in contrast to network MIMO as described in section 8 the backhaul load is not increased by either of these approaches.

A further novel approach is also described in which the ABSs apply PLNC on the uplink (it can also be applied to the downlink) to combine the signals from two user terminals. We observe that this also can give rise to a network MIMO benefit, again without any increase in backhaul load.

A novel compress-and-forward approach is also described in which the ABS performs soft output detection, rather than full decoding, of the received signal, and forwards a quantised version of the soft output, allowing full decoding to be performed only at the destination. It is also shown how this approach can compensate for channel fading at the destination.

11. Conclusions

This report has described the work undertaken in Task 2.3 of BuNGee "Collaborative, Networked and Multibeam MIMO". While the original title of the report was to be "Final Report on Advanced MIMO and Interference Cancellation Techniques", the work has in fact focussed on MIMO techniques, including network MIMO, and wireless network coding, rather than interference cancellation explicitly. However throughout it considers the application of MIMO in the context of the BuNGee network architecture, and at many points it shows how signals from other parts of the network, conventionally regarded as "interference", can in fact be exploited in order to increase capacity. Such approaches in effect render interference cancellation obsolete, and can be regarded as an important advance in BuNGee.

As mentioned in the Introduction, the primary objective of the work has been to exploit advanced MIMO techniques to improve the capacity of the BuNGee network, in both its segments, access and backhaul. The in-band backhaul network in particular, being specific to BuNGee, has been a major focus. In particular the BuNGee multibeam antenna has provided a basis for the exploration of multi-beam assisted (MBA) MIMO techniques (section 5). It has been shown that this approach, employing joint beam processing at the HBS, can increase capacity by a factor of around 6 to 8 compared with conventional single beam processing, in which signals received by other beams are treated as interference. This is further increased by a further factor of nearly two by the use of dual polarisation on the backhaul links. These conclusions are largely unaffected by the effect of interference from other HBSs than the target. The work described here depends on channel modelling work carried out in Task T2.1, the conclusions of which are also summarised in the report (section 2).

The application of advanced MIMO to the access segment has also been addressed (section 8): specifically network-enabled MIMO has been investigated. This is shown to increase capacity by at least a factor of 4 compared to the baseline frequency-planning scheme used in BuNGee, because it enables the whole access segment bandwidth to be used by all ABSs. However this results potentially in a large increase in the backhaul load. It is to be noted that the millimetre-wave backhaul technology discussed in D2.4 would probably be able to support this backhaul load.

However, it has also been shown (section 10) that the application of physical layer network coding has the potential to provide similar benefits as network MIMO without giving rise to any increase in backhaul load. This also allows the resources of backhaul and access network to be more readily shared, helping to overcome the restrictions resulting from the duplexing constraint upon the ABSs.

Both access and backhaul link are assumed to use adaptive modulation and coding, and adaptive MIMO techniques, which requires precoding techniques, and the transfer of channel state information back to the transmitter. An approach has been developed (section 6) to greatly reduce (by a factor of around 2) the number of bits required for this feedback, and to design receivers which are robust to inaccurate CSI. This assumes linear detection: it is also shown (section 7) that a near maximum likelihood detector, implemented using iterative techniques, reduces the size of the precoder codebook required, and hence also reduces the CSI feedback overhead.

A further important function of the work in T2.3 was to support the system level simulation carried out in Task T4.1. To simplify link level simulation in such a simulator a simplified method for mapping from SINR to link throughput has been developed (section 3) , based on the Truncated Shannon Bound. This has also been extended to the MIMO case (section 4), and also to MBA-MIMO in the backhaul link (section 5.5). This has been used in T4.1 (see [BunD412]) to evaluate the benefits of MBA-MIMO, backing up the results given here for the degree of benefit obtained. Note that MBA-MIMO has also been tested in the BuNGee Live Test, demonstrating the ease of implementation and also supporting the simulation results on the gain available.

12. Bibliography

[3GP06] 3GPP TR 25.814 V7.1.0, “Physical layer aspects for evolved Universal Terrestrial Radio Access (UTRA) (Release 7)”, Sep. 2006

[3GP07] 3GPP TS 36.211 V8.0.0, “Evolved Universal Terrestrial Radio Access (E-UTRA); Physical channels and modulation (Release 8),” Sep. 2007.

[3GP10] 3GPP; Technical Specification Group Radio Access Networks, “LTE - Evolved Universal Terrestrial Radio Access (E-UTRA) Radio Frequency (RF) system scenarios,” 3GPP TR 36.942 version 9.0.1 Release 9, April 2010.

[Aki09a] T. Koike-Akino, P. Popovski, and V. Tarokh, "Optimized constellations for two-way wireless relaying with physical network coding", IEEE J. Sel. Areas Commun., vol. 27, pp. 773–787, June 2009.

[Aki09b] T. Koike-Akino, P. Popovski, and V. Tarokh, "Denoising strategy for convolutionally-coded bidirectional relaying," in Proc. IEEE Int. Conf. Comm. (ICC), Dresden, Germany, June 2009.

[Ala98] S. M. Alamouti, “A simple transmit diversity technique for wireless communications,” *IEEE Journal on Selected Areas in Communications*, vol. 16, no. 8, pp. 1451–1458, Oct. 1998.

[Bai08] I. J. Baik and S. Y. Chung, “Network coding for two-way relay channels using lattices,” in *Proc. IEEE Int’l Conference on Communications (ICC)*, Beijing, China, May 2008.

[Boc07] F. Boccardi, H. Huang, "Limited Downlink Network Coordination in Cellular Networks," IEEE 18th International Symposium on Personal, Indoor and Mobile Radio Communications, 2007. PIMRC 2007. pp.1-5, 3-7 Sept. 2007.

[Boy04] S. Boyd and L. Vandenberghe, *Convex optimization*.Cambridge University Press, 2004.

[Bri01] ten Brink, S. ``Convergence behavior of iteratively decoded parallel concatenated codes," Communications, IEEE Transactions on , vol.49, no.10, pp.1727-1737, Oct 2001.

[BunD21] BuNGee Project, Deliverable Report D2.1, “BuNGee Channel Models”, December 2011.

[BunD22] BuNGee Project, Deliverable Report D2.2, "Final Report on BuNGee Antenna" December 2011

[BunD24] BuNGee Project, Deliverable Report D2.4, “Comparative Analysis between Backhauling Technologies”, November 2011.

[BunD412] BuNGee Project, Deliverable Report D4.1.2 "Simulation Tool(s) and Simulation Results" June 2012

[Bur04] A. G. Burr, L. Zhang, and S. Hirst “Space-time signal processing for real-world channels” Euro-Microwave Conference, Amsterdam, October 2004

[Bur10] A. G. Burr, “Hierarchical Wireless Networks and Wireless Network Coding,” in *COST 2100 TD(10)12100*, Bologna, 2010.

[Bur12] Alister Burr, Agisilaos Papadogiannis and Tao Jiang “MIMO Truncated Shannon bound for system level capacity evaluation of wireless networks” *IEEE Wireless Communications and Networking Conference*, Paris, France, 31st March 2012

[Bur94] A. G. Burr, "Bounds and estimates of the uplink capacity of cellular systems," in *Vehicular Technology Conference, 1994 IEEE 44th*, Jun. 1994, pp. 1480-1484 vol.3.

[Cai10] G. Caire, N. Jindal, M. Kobayashi, and N. Ravindran, “Multiuser MIMO achievable rates with downlink training and channel state feedback,” IEEE Trans. on Information Theory, vol. 56, no. 6, pp. 2845–2866, Jun. 2010.

[Cha07] B. K. Chalise, S. Shahbazpanahi, A. Czylwik, and A. B. Gershman, “Robust downlink beamforming based on outage probability spacifications,” IEEE Trans. on Wireless Communications, vol. 6, no. 10, pp. 3498–3503, Oct. 2007.

[Cha08] C.-B. Chae, D. Mazzarese, N. Jindal, and R. W. Heath, “Coordinated beamforming with limited feedback in the MIMO broadcast channel,” *IEEE Journal on Selected Areas in Communications*, vol. 26, no. 8, pp. 1505–1515, Oct. 2008.

[Che09] Peng Chen; Wei Hong; Zhenqi Kuai; Junfeng Xu; Haiming Wang; Jixin Chen; Hongjun Tang; Jianyi Zhou; Ke Wu; , "A Multibeam Antenna Based on Substrate Integrated Waveguide Technology for MIMO Wireless Communications," IEEE Transactions on Antennas and Propagation, vol.57, no.6, pp.1813-1821, June 2009

[Chi97] M. Chiani, "Introducing erasures in decision-feedback equalization to reduce error propagation," *Communications, IEEE Transactions on,* vol. 45, pp. 757-760, July 1997.

[Cho02] R. L. Choi and R. D. Murch, “Transmit MMSE pre-rake pre-processing with simplified receivers for the downlink of MISO TDD-CDMA systems,” in Proc. IEEE Global Communications Conference, Nov. 2002, pp. 429–433.

[Cos83] M. Costa, “Writing on dirty paper,” IEEE Trans. on Information Theory, vol. 29, no. 3, pp. 439–441, May 1983.

[Cov06] T. M. Cover and J. A. Thomas, Elements of information theory, 2nd ed. New Jersey: Wiley-Interscience, 2006.

[Czy96] Czylwik, A., "Adaptive OFDM for wideband radio channels," Global Telecommunications Conference, 1996. GLOBECOM '96. 'Communications: The Key to Global Prosperity , vol.1, no., pp.713-718 vol.1, 18-22 Nov 1996

[Dai04] H. Dai, A. F. Molisch, H. V. Poor, ``Downlink capacity of interference-limited MIMO systems with joint detection" *IEEE Transactions on Wireless Communications*, vol. 3, No. 2, March 2004.

[Ede98] A. Edelman, T. A. Arias, and S. T. Smith, “The geometry of algorithms with orthogonality constraints,” *SIAM Journal on Matrix Analysis and Applications*, vol. 20, no. 2, pp. 303–353, Oct. 1998.

[Eln04] Elnaggar, M.S.; Safavi-Naeini, S.; Chaudhuri, S.K.; , "Simulation of the achievable indoor MIMO capacity by using an adaptive phased-array," IEEE Radio and Wireless Conference, 2004, pp. 155- 158,19-22 Sept. 2004;

[Erk98] E. Erkip and B. Aazhang “A Comparative Study of Multiple Accessing Schemes”, in Proc. IEEE Globecom, 1998

[Fos98] G. J. Foschini and M. J. Gans, “On limits of wireless communications in a fading environment when using multiple antennas,” *Wireless Personal Communications*, vol. 6, no. 3, pp. 311–335, Mar. 1998.

[Ges10] D. Gesbert, S. Hanly, H. Huang, S. Shamai, O. Simeone, Y. Wei, "Multi-Cell MIMO Cooperative Networks: A New Look at Interference," IEEE Journal on Selected Areas in Communications, , vol.28, no.9, pp.1380-1408, December 2010.

[Gol03] A. Goldsmith, S. Jafar, N. Jindal, and S. Vishwanath, “Capacity limits of MIMO channels,” *IEEE Journal on Selected Areas in Communications*, vol. 21, no. 5, pp. 684–702, Jun. 2003.

[Gol05] Andrea Goldsmith, Wireless Communications, Cambridge University Press, 2005, pp.127-129

[Gor00] Gore, D.A.; Nabar, R.U.; Paulraj, A., "Selecting an optimal set of transmit antennas for a low rank matrix channel," Acoustics, Speech, and Signal Processing, 2000. ICASSP '00. Proceedings. 2000 IEEE International Conference on , vol.5, no., pp.2785-2788 vol.5, 2000

[Gra05a] Grau, A.; Romeu, J.; De Flaviis, F.; , "On the diversity gain using a Butler matrix in fading MIMO environments," *IEEE/ACES International Conference on Wireless Communications and Applied Computational Electromagnetics*, 2005., pp. 478- 481, 3-7 April 2005

[Gra05b] Grau, A.; Romeu, J.; De Flaviis, F.; , "On the diversity gain using a Butler matrix in fading MIMO environments," *IEEE/ACES International Conference on Wireless Communications and Applied Computational Electromagnetics*, 2005. pp. 478- 481, 3-7 April 2005

[Gra05c] Grau, A.; Romeu, J.; Jofre, L.; De Flaviis, F.; , "On the MIMO capacity using a Butler matrix with circular arrays in fading indoor environments," IEEE Antennas and Propagation Society International Symposium, 2005, vol.2A, pp. 297-300 3-8 July 2005

[Gra06] Grau, A.; Romeu, J.; Blanch, S.; Jofre, L.; De Flaviis, F.; ,"Optimization of Linear Multielement Antennas for Selection Combining by Means of a Butler Matrix in Different MIMO Environments," IEEE Transactions on Antennas and Propagation, vol.54, no.11, pp.3251-3264, Nov. 2006

[Gun08] D. Gündüz, E. Tuncel, and J. Nayak, “Rate regions for the separated two-way relay channel,” in *Proc. 46th Annual Allerton Conf. on Comm., Control, and Computing*, Monticello, IL, September 2008.

[Guo05] D. Guo, S. Shamai, and S. Verdú, “Mutual information and minimum mean-square error in Gaussian channels,” *IEEE Trans. Information Theory*, vol. 51, no. 4, pp. 1261–1283, April 2005.

[Guo08] D. Guo, S. Shamai, and S. Verdú, “Estimation of non-Gaussian random variables in Gaussian noise: Properties of the MMSE,” in *Proc. IEEE Int’l Symposium on Information Theory*, June 2008, pp. 1083–1087.

[Hag04] J. Hagenauer, “The EXIT chart - Introduction to extrinsic information transferin iterative processing,” in Proc. European Signal Process. Conf., Vienna, pp. 1541-1548, Austria, 2004.

[Hea01a] Heath, R.W., Jr.; Sandhu, S.; Paulraj, A., "Antenna selection for spatial multiplexing systems with linear receivers," Communications Letters, IEEE , vol.5, no.4, pp.142-144, Apr 2001

[Hea01b] Heath, R.W., Jr.; Paulraj, A., "Antenna selection for spatial multiplexing systems based on minimum error rate," Communications, 2001. ICC 2001. IEEE International Conference on , vol.7, no., pp.2276-2280 vol.7, 2001

[Hea05] Heath, R.W., Jr.; Love, D.J., "Multimode antenna selection for spatial multiplexing systems with linear receivers," Signal Processing, IEEE Transactions on , vol.53, no.8, pp. 3042-3056, Aug. 2005

[Hea09] R.W. Heath, T.Wu, and A. C. K. Soong, "Progressive refinement of beamforming vectors for high-resolution limited feedback," *EURASIP Journal on Advances in Signal Processing*, pp. 1–13, 2009.

[Hol01] S. Holm, A. Austeng, K. Iranpour, and J. F. Hopperstad, Sparse sampling in array processing. Springer, formerly Kluwer Academic/Plenum Publishers, 2001, pp. 787–833.

[Hor85] R. A. Horn and C. R. Johnson, Eds., Matrix Analysis. Cambridge University Press, 1985.

[Hua06] K. Huang, B. Mondal, R. W. Heath, and J. G. Andrews, "Multi-antenna limited feedback for temporally correlated channels: feedback compression," in *Proc. IEEE Globecom'06*, Nov. 2006.

[Hua09] K. Huang, R. W. Heath, and J. G. Andrews, "Limited feedback beamforming over temporally-correlated channels," *IEEE Trans. on Signal Processing*, vol. 57, no. 5, pp. 1959–1975, May 2009.

[IEE05] IEEE Standard for Local and metropolitan area networks Part 16: Air Interface for Broadband Wireless Access Systems, IEEE Std. 802.16, 2005.

[IEE06] IEEE 802.16e-2005, "IEEE Standard for Local and metropolitan area networks Part 16: Air Interface for Fixed and Mobile Broadband Wireless Access Systems Amendment 2: Physical and Medium Access Control Layers for Combined Fixed and Mobile Operation in Licensed Bands and Corrigendum 1 ", Feb. 2006

[Inn09a] Innok, A.; Uthansakul, M.; Uthansakul, P.; , "Performance of MIMO capacity using angle domain processing realized by Butler matrix," *6th International Conference on Electrical Engineering/Electronics, Computer, Telecommunications and Information Technology, 2009. ECTI-CON 2009.* vol.2, pp.844-847, 6-9 May 2009

[Inn09b] Innok, A.; Uthansakul, M.; Uthansakul, P.; , "The enhancement of MIMO capacity using angle domain processing based on measured channels," Asia Pacific Microwave Conference, 2009. APMC 2009. pp.2172-2175, 7-10 Dec. 2009

[Ino09] T. Inoue and R. W. Heath, "Geodesic prediction for limited feedback multiuser MIMO systems in temporally correlated channels," in *Proc. IEEE Radio and Wireless Symposium*, Jan. 2009.

[Jan04] M. Jankiraman, Space-time codes and MIMO systems, Artech House on Demand, 2004.

[Jin07] S. Jing, D. N. C. Tse, B. J. Soriaga, J. Hou, J. E. Smee. E. R. Padovani, "Downlink Macro-Diversity in Cellular Networks," IEEE International Symposium on Information Theory, 2007. ISIT 2007. pp.1-5, 24-29 June 2007.

[Joh02] M. Joham, K. Kusume, M. H. Gzara, W. Utschick, and J. A. Nossek, "Transmit Wiener filter for the downlink of TDDDS-CDMA systems," in Proc. IEEE International Symposium on Spread-Spectrum Tech. & Appl., Sep. 2002.

[Joh05] M. Joham, W. Utschick, andJ. A. Nossek, "Linear transmit processing in MIMO communications systems." IEEE Transactions on Signal Processing, 53(8), 2700–2712. 2005.

[Kar09] N. E. Karoui, "Operator norm consistent estimation of large-dimensional sparse covariance matrices," Annals of Statistics, vol. 36, no. 6, pp. 2717–2756, Jan. 2009.

[Ker12] P. de Kerret, D. Gesbert, "Sparse precoding in multicell MIMO systems," 2012 IEEE Wireless Communications and Networking Conference (WCNC), pp.958-962, 1-4 April 2012.

[Kha08] S. Khattak, W. Rave, G. Fettweis, "Distributed Iterative Multiuser Detection through Base Station Cooperation," EURASIP Journal on Wireless Communications and Networking, vol. 2008, pp. 15, 2008.

[Kno06] R. Knopp, "Two-way radio networks with a star topology," in International Zurich Seminar on Communications (IZS 2006), Zurich, Switzerland, march 2006, pp. 154 –157.

[Kyo07] P. Kyosti, et al., "WINNER II channel models," European Commission, Deliverable IST-WINNER D1.1.2 ver 1.1, Sept. 2007

[Lev08] E. Levina, A. Rothman, and J. Zhu, "Sparse estimation of large covariance matrices via a nested lasso penalty," Annals of Applied Statistics, vol. 2, no. 1, pp. 245–263, Mar. 2008.

[Li11] P. Li, R. C. d. Lamare, and R. Fa, "Multiple Feedback Successive Interference Cancellation Detection for Multiuser MIMO Systems," *IEEE Transactions on Wireless Communications,* vol. 10, pp. 2434-2439, Aug. 2011.

[Li12] P. Li and R. C. d. Lamare, "Adaptive Decision-Feedback Detection With Constellation Constraints for MIMO Systems," *Vehicular Technology, IEEE Transactions on,* vol. 61, pp. 853-859, Feb. 2012.

[Liu11] J. Liu, M. Tao and Y. Xu, "Pseudo Exclusive-OR for LDPC coded two-way relay block fading channels", in Proc. IEEE Int. Conf. Comm. (ICC), Kyoto,Japan, June 2011.

[Llo82] S. Lloyd, “Least squares quantization in PCM,” IEEE Trans. Inform. Theory, vol. IT-28, pp. 129–137, 1982.

[Lov03] D. J. Love, R. W. Heath, and T. Strohmer, “Grassmannian beamforming for multiple-input multiple-output wireless systems,” *IEEE Trans. on Information Theory*, vol. 49, no. 10, pp. 2735–2747, Oct. 2003.

[Loz06] A. Lozano, A. M. Tulino, and S. Verdú, “Optimum power allocation for parallel Gaussian channels with arbitrary input distributions,” *IEEE Trans. Information Theory*, vol. 52, no. 7, pp. 3033–3051, July 2006.

[Mad94] U. Madhow, M. L Honig, ``MMSE interference suppression for direct-sequence spread-spectrum CDMA," *IEEE Transactions on Communications*, vol.42, no.12, pp.3178-3188, Dec 199.

[Mad94] U. Madhow, M. L Honig, ``MMSE interference suppression for direct-sequence spread-spectrum CDMA," IEEE Transactions on Communications, vol.42, no.12, pp.3178-3188, Dec 1994.

[Mag02] J. R. Magnus and H. Neudecker, Matrix Differential Calculus with Applications in Statistics and Econometrics, 3rd ed. Wiley, 2002.

[Mar08] I. Maric, R. Dabora, and A. Goldsmith, “On the capacity of the interference channel with a relay,” in Proc. International Symposium on Information Theory (ISIT 2008), Toronto, Canada, july 2008, pp. 554–558.

[Mar09] F. Marvasti, A. Amini, F. Haddadi, M. Soltanolkotabi, B. H. Khalaj, A. Aldroubi, S. Holm, S. Sanei, and J. Chambers, “A unified approach to sparse signal processing,” submitted, Feb. 2009.

[Max60] J. Max, “Quantizing for minimum distortion,” IEEE Trans. Inform. Theory, vol. IT-6, pp. 7–12, 1960.

[May06] T. Mayer, H. Jenkac, and J. Hagenauer, "Turbo base-station cooperation for intercell interference cancellation,” IEEE International Conference on Communications, vol. 11, pp. 4977 – 4982. June 2006.

[Mol03] Molisch, A.F.; Zhang, X.; Kung, S.Y.; Zhang, J.; , "DFT-based hybrid antenna selection schemes for spatially correlated MIMO channels," 14th IEEE Symposium on Personal, Indoor and Mobile Radio Communications, 2003. PIMRC 2003, vol.2, pp. 1119- 1123 vol.2, 7-10 Sept. 2003

[Nab02] R. U. Nabar, H. Bolcskei, V. Erceg, D. Gesbert, and A. J. Paulraj, “Performance of multiantenna signaling techniques in the presence of polarization diversity,” IEEE Transactions on Signal Processing, vol. 50, no. 10, pp. 2553–2562, 2002.

[Nam10] W. Nam, S.-Y. Chung, and Y. H. Lee, “Capacity of the Gaussian two-way relay channel to within 1/2 bit,” *IEEE Trans. on Information Theory*, 2010, to appear. [Online]. Available: http://arxiv.org/abs/0902.2438

[Nar07] K. Narayanan, M. P. Wilson, and A. Sprintson, “Joint physical layer coding and network coding for bi-directional relaying,” in *Proc. 45th Annual Allerton Conference on Communication, Control, and Computing*, Monticello, IL, September 2007.

[Nee93] F. Neeser and J. Massey, “Proper complex random processes with applications to information theory,” *IEEE Trans. on Information Theory*, vol. 39, no. 4, pp. 1293–1302, April 1993.

[Pal03] D. P. Palomar, J. M. Cioffi, and M. A. Lagunas, “Joint Tx-Rx beamforming design for multicarrier MIMO channels: a unified framework for convex optimization,” *IEEE Trans. on Signal Processing*, vol. 51, no. 9, pp. 2381–2401, Sep. 2003.

[Pan07] T. Pande, D. J. Love, and J. V. Krogmeier, “Reduced feedback MIMOOFDM precoding and antenna selection,” *IEEE Trans. on Signal Processing*, vol. 55, no. 5, pp. 2284–2293, May 2007.

[Pap08] A. Papadogiannis, D. Gesbert, E. Hardouin, E., "A Dynamic Clustering Approach in Wireless Networks with Multi-Cell Cooperative Processing," IEEE International Conference on Communications, 2008. ICC '08., vol., no., pp.4033-4037, 19-23 May 2008.

[Pay09a] M. Payaró and D. P. Palomar, “On optimal precoding in linear vector Gaussian channels with arbitrary input distribution,” in *Proc. IEEE International Symposium on Information Theory (ISIT’09)*, Jul. 2009.

[Pay09b] M. Payaró and D. P. Palomar, “Hessian and concavity of mutual information, differential entropy, and entropy power in linear vector Gaussian channels,” *IEEE Trans. on Information Theory*, vol. 55, no. 8, pp. 3613 – 3628, Aug. 2009, (see also the extended version in arXiv:0903.1945).

[Pen04] X. Pennec, P. Fillard, and N. Ayache, “A Riemannian framework for tensor computing,” *International Journal of Computer Vision*, vol. 66, no. 1, pp. 41–66, Jan. 2006, a preliminary version appeared as INRIA Research Report 5255, July 2004.

[Ran05] B. Rankov and A. Wittneben, “Spectral efficient signaling for half-duplex relay channels,” in *Proc. 39th Asilomar Conference on Signals, Systems, and Computers*, Pacific Grove, CA, November 2005.

[Roh06] J. C. Roh and B. D. Rao, “Design and analysis of MIMO spatial multiplexing systems with quantized feedback,” *IEEE Trans. on Signal Processing*, vol. 54, no. 8, pp. 2874–2886, Aug. 2006.

[Roh07] J. C. Roh and B. D. Rao, “Efficient feedback methods for MIMO channels based on parameterization,” *IEEE Trans. on Wireless Communications*, vol. 6, no. 1, pp. 282–292, Jan. 2007.

[Ros08] Rose, M.R.C.; Suaidi, M.K.; Aziz, M.Z.A.A.; Kadir, M.F.A.; Misman, D.; Shah, M.S.R.M.; Rahim, M.K.A.; , "Analysis of Angle Diversity in MIMO Channel," 6th National Conference on Telecommunication Technologies 2008 and 2008 2nd Malaysia Conference on Photonics. NCTT-MCP 2008. pp.110-112, 26-28 Aug. 2008;

[Sac09] D. Sacristán-Murga and A. Pascual-Iserte, “Differential feedback of MIMO channel correlation matrices based on geodesic curves,” in Proc. IEEE Int. Conf. Acoust., Speech, Signal Process, Apr. 2009, pp. 2553–2556.

[Sac10] D. Sacristán-Murga and A. Pascual-Iserte, “Differential feedback of MIMO channel Gram matrices based on geodesic curves,” IEEE Trans. on Wireless Communications, vol. 9, no. 12, pp. 3714–3727, Dec. 2010.

[Sac10b] D. Sacristán-Murga and A. Pascual-Iserte, “Differential feedback of channel Gram matrices for block diagonalized multiuser MIMO systems,” in Proc. IEEE Intl. Conf. on Communications, May 2010, pp. 1–5.

[Sac12] D. Sacristán-Murga, M. Payaró, and A. Pascual-Iserte, “Transceiver design framework for multiuser MIMO-OFDM broadcast systems with channel Gram matrix feedback,” accepted for publication in IEEE Trans. on Wireless Communications, January 2012.

[Sam01] H. Sampath, “Linear Precoding and decoding for Multiple Input Multiple Output (MIMO) Wireless Channels”, Ph.D. Thesis, Stanford, April 2001

[Sch08] C. Schnurr, S. Stanczak, and T. J. Oechtering, “Coding theorems for the restricted half-duplex two-way relay channel with joint decoding,” in *Proc. IEEE Int’l Symp. on Information Theory*, Toronto, Canada, July 2008.

[Sel02] Sellathurai, M.; Haykin, S., ``Turbo-BLAST for wireless communications: theory and experiments," Signal Processing, IEEE Transactions on , vol.50, no.10, pp. 2538-2546, Oct 2002

[Shi07] S. Shi, M. Schubert, and H. Boche, “Downlink MMSE transceiver optimization for multiuser MIMO systems: duality and sum-MSE minimization,” IEEE Trans. on Signal Processing, vol. 55, no. 11, pp. 5436–5446, Nov. 2007.

[Spe04] Q. H. Spencer, A. L. Swindlehurst, and M. Haardt, “Zero-forcing methods for downlink spatial multiplexing in multiuser MIMO channels,” *IEEE Trans. on Signal Processing*, vol. 52, no. 2, pp. 461–471, Feb. 2004.

[Sud04] Sudarshan, P.; Mehta, N.B.; Molisch, A.F.; Jin Zhang; , "Spatial diversity and channel statistics-based RF-baseband co-design for antenna selection," IEEE 60th Vehicular Technology Conference, 2004. VTC2004-Fall. 2004, vol.3, no., pp. 1658- 1662 Vol. 3, 26-29 Sept. 2004

[Sun09] H. Sung, S. Lee, and I. Lee, “Generalized channel inversion methods for multiuser MIMO systems,” IEEE Trans. On Communications, vol. 57, no. 11, pp. 3489–3499, Nov. 2009.

[Syk10] J. Sykora and A. Burr, “Hierarchical alphabet and parametric channel constrained capacity regions for HDF strategy in parametric wireless 2-WRC,” in *IEEE Wireless Commun. Network. Conf. (WCNC),*, Sydney, April 2010.

[Tal07] M. Talih, “Geodesic Markov chains on covariance matrices,” Statistical and Applied Mathematical Sciences Institute, Tech. Rep., Mar. 2007.

[Tar99] V. Tarokh, H. Jafharkani, and A. R. Calderbank, “Space-time block codes from orthogonal designs,” *IEEE Trans. on Information Theory*, vol. 45, no. 5, pp. 1456–1467, Jul. 1999.

[Tel99] I. E. Telatar, “Capacity of multi-antenna Gaussian channels,” *European Trans. On Telecommunications*, vol. 10, no. 6, pp. 585–595, Nov. 1999.

[Ten04] A. Tenenbaum and R. S. Adve, “Joint multiuser transmit-receive optimization using linear processing,” in Proc. IEEE Intl. Conf. on Communications, Jul. 2004, pp. 588–592.

[Tuc02] M. Tuchler, S. ten Brink, and J. Hagenauer, “Measures for tracing convergence of iterative decoding algorithms,” in Proc. 4th IEEE/ITG Conf. on Source and Channel Coding, Berlin, Germany, pp. 53–60, Jan 2002.

[Tun06] E. Tuncel, “Slepian-Wolf coding over broadcast channels,” *IEEE Trans. on Information Theory*, vol. 52, no. 4, pp. 1469–1482, April 2006.

[Ven07] S. Venkatesan, "Coordinating Base Stations for Greater Uplink Spectral Efficiency in a Cellular Network," Personal, IEEE 18th International Symposium on Indoor and Mobile Radio Communications, 2007. PIMRC 2007. , vol., no., pp.1-5, 3-7 Sept. 2007.

[Ver02] S. Verdú, “Spectral efficiency in the wideband regime,” *IEEE Trans. on Information Theory*, vol. 48, no. 6, pp. 1319–1343, June 2002.

[Ver98] S. Verdu, Multiuser Detection, Cambridge University Press,1998, pp. 288-369

[Vuc09] N. Vucic, H. Boche, and S. Shi, “Robust transceiver optimization in downlink multiuser MIMO systems,” IEEE Trans. on Signal Processing, vol. 57, no. 9, pp. 3576–3587, Sep. 2009.

[Wan10] J. Wang and D. P. Palomar, “Robust MMSE precoding in MIMO channels with pre-fixed receivers,” IEEE Trans. on Signal Processing, vol. 58, no. 11, pp. 5802–5818, Nov. 2010.

[Wan99] X. Wang and H.V. Poor, “Iterative (Turbo) soft interference cancellation and decoding for coded CDMA,” IEEE Transactions on Communications, vol. 47, no. 7,pp. 1046-1061, 1999.

[Win11] A. Winkelbauer, G. Matz "Soft-Information-Based Joint Network-Channel Coding for the Two-Way Relay Channel", in Proc. IEEE International Symposium on Network Coding (NetCod), Beijing , China, July, 2011.

[Wol98] Wolniansky, P.W.; Foschini, G.J.; Golden, G.D.; Valenzuela, R.A., "V-BLAST: an architecture for realizing very high data rates over the rich-scattering wireless channel," Signals, Systems, and Electronics, 1998. ISSSE 98. 1998 URSI International Symposium on , vol., no., pp.295-300, 29 Sep-2 Oct 1998

[Xia09] Y. Xiao, W. Miao, M. Zhao, S. Zhou, and J. Wang, “Limited-feedback modified block diagonalization for multiuser MIMO downlink with timevarying channels,” in *Proc. IEEE ICC’09*, Jun. 2009.

[Yan07] J. Yang and D. B. Williams, “Transmission subspace tracking for MIMO systems with low-rate feedback,” *IEEE Trans. on Communications*, vol. 55, no. 8, pp. 1629–1639, Aug. 2007.

[Yil11] E. Yilmaz, R. Knopp, and D. Gesbert, “Interference Two-Way Relay Channel with Three End-nodes,” in Proc. IEEE International Symposium on Information Theory (ISIT 2011), St. Petersburg, Russia, Aug. 2011.

[Yli07] Ylitalo, J.; , "Double-Directional Beamforming MIMO: A Simulation Study," IEEE 65th Vehicular Technology Conference, 2007. VTC2007-Spring. pp.2063-2067, 22-25 April 2007

[Zeg90] K. Zeger and A. Gersho, “Pseudo-gray coding,” IEEE Trans. Comm., vol. 38, no. 12, pp. 2147–2158, Dec. 1990.

[Zei09] G. Zeitler, R. Koetter, G. Bauch, and J.Widmer, "On Quantizer Design for Soft Values in the Multiple-Access Relay Channel," in Proc. IEEE International Conference on Communications (ICC 2009), Dresden, Germany, June 2009, p. 1548-1552

[Zha06] S. Zhang, S. C. Liew, and P. K. Lam, “Physical layer network coding,” in Proc. MobiCom’06, pp. 358–365, 2006.

[Zhu02] Xu Zhu; Murch, R.D., "Performance analysis of maximum likelihood detection in a MIMO antenna system," Communications, IEEE Transactions on , vol.50, no.2, pp.187-191, Feb 2002

[Zwi00] D. Zwillinger and S. Kokoska, Standard probability and Statistics tables and Formulae, Chapman & Hall/CRC, 2000

13. Release History

This page is used to follow the deliverable production. All release numbers prior to the submission to EC should be numbered 0.x.x

Release 1.0.0 is the first official version; Release 1.0.1 can include editorial changes; Release 1.1.0 includes small technical changes; Release 2.0.0 is a document significantly modified.

The rows including release numbers for non-official versions shall be deleted when the document is submitted to EC.

Please give details in the table below about successive releases:

Release number	Date	Comments	Dissemination of this release (task level, WP/SP level, Project Office Manager, Steering Committee, etc)
0.1	15-04-12	Outline version, AGB	
0.3	17-05-12	Incorporates sects 6 and 9 from CTTC (MP,AI)	
0.5	25-06-12	Incorporates all remaining sections from UOY (AP, YW, CL, PL, DF)	
0.6	27-06-12	Final draft version	
1.0.0	29-06-12		Document submitted to EC